COLLECTED PAPERS

ON

COHERENT OPTO-ELECTRONICS

January 1982-May 1985

Associate Professor

Motoichi OHTSU

TOKYO INSTITUTE OF TECHNOLOGY

INTERNATIONAL COOPERATION CENTER

FOR SCIENCE AND TECHNOLOGY

2-12-1, O-okayama, Meguro-ku,

Tokyo 152, JAPAN

各位殿

これは大津元一が１９８２年1月より１９８５年５月まで東京工業大学理工学国際交流センターに在職中に行なった研究をまとめた論文集です。　いずれも未熟な論文ばかりですが御査納頂ければ幸いです。現在、下記へ配置換となっておりますが今後共、御指導御鞭達の程宜しく御願い申し上げます。

現在の所属　：　東京工業大学　総合理工学研究科　物理情報工学専攻
住所　（〒２２７）　横浜市緑区長津田４２５９
電話　０４５－９２２－１１１１　内線２５２６

PREFACE

This is a research review on coherent opto-electronics by Assoc. Prof. M. Ohtsu, Tokyo Institute of Technology. It contains copies of technical papers published while he belonged to the International Cooperation Center for Science and Technology (Jan. 1982 - May 1985). M. Ohtsu wishes to thank Prof. T. Yanagisawa , Director of International Cooperation Center, for his encouragement during these works.

MEMBERS

Associate Professor

Motoichi OHTSU (Ph. D.)[a)]

Graduate Students (Master Course)

Yoshihiro OTSUKA (B. S.)[b)]

Shinichi KOTAJIMA (B. S.)[c)]

Satohiko ARAKI (B. S.)

Katsuhiko KUBOKI (B. S.)

Minoru HASHIMOTO (B. S.)

Noboru TABUCHI (B. S.)

Tetsuya MIYAZAKI (B. S.)

Undergraduate Students

Hiroki KOTANI[d)]

Haruo TAGAWA[e)]

Hiroshi YUKINARI[f)]

Kazu NANBO[g)]

Satoshi HASEGAWA[h)]

Hidetaka OZAWA[h)]

Takumi OZAWA[h)]

Toshihiko OUCHI

Masahiro SEGAMI

Visiting Researchers

Budi Pardono PARIMIN[i)]

Akio OSAKI[j)]

a) Presently with Graduate School at Nagatsuta, Tokyo Institute of Technology.

b) Presently with NTT.

c) Presently with NEC.

d) Presently with SONY.

e) Presently with MATSUSHITA TSUSHIN Co..

f) Presently with NISSAN CAR Co..

g) Presently with NEC.

h) Presently with graduate school in Tokyo Inst. Tech..

i) Permanent address : LIPI-LFN, Bandung, Indonesia

j) Permanent address : Precision Engineering Res. Lab., HITACHI.

LIST OF PAPERS

[I] IMPROVEMENTS IN COHERENCE OF LASERS

(a) Journal Papers

Vol. 26, No. 4, April 1985, pp. L256 - L258,
[pp. 27 - 29]

[7] T. Kunikane, M. Ohtsu, T. Nakamura and T. Tako : "A Simple Technique for Obtaining a Stable Frequency Sweep in a Waveguide CO_2 Laser", Jpn. J. Appl. Phys., Vol. 23, No.5, May 1984, pp. 600 - 605 [pp. 30 - 35]

[8] I. Siio, A. Kusnowo, M. Ohtsu and T. Tako : "A Frequency Stabilized Laser System for High Resolution Spectroscopy Using Stark Spectrum", J. Jpn. Soc. of Spectro., Vol. 33, No. 3, 1984, pp. 172 - 178 (in Japanese) [pp. 36 - 42]

[9] T. Nakamura, M. Ohtsu and T. Tako : "Frequency Stabilization and Sweep for a Waveguide CO_2 Laser by Using Stark Absorption Lines", J. Jpn. Soc. of Spectro., Vol. 34, No. 1, 1985, pp.23 - 28 (in Japanese) [pp. 43 - 48]

(b) International Conferences

[1] M. Ohtsu, H. Tsuchida and T. Tako : "Frequency Stabilization of AlGaAs Lasers", 6B - 2, 36th Annual Frequency Control Symposium, 2 - 4 June 1982, Philadelphia, USA
[pp. 49 - 59]

[2] M. Ohtsu : "Frequency Control of Semiconductor Lasers and Its Application to Metrology", Proc. of International Conf. Lasers'83, 12 - 16 Dec. 1983, San Fransisco, USA, pp. 85 - 92 (Invited Paper) [pp. 60 - 67]

[3] M. Ohtsu : "Linewidth Reduction of a Semiconductor Laser by Electrical Feedback", ThZ5, Postdeadline Paper, Conference

semiconductor lasers", Appl. Phys. Lett., 46(2), 15 Jan. 1985, pp. 108 - 110 [pp. 95 - 97]

[7] M. Ohtsu, Y. Otsuka, A. Osaki and Y. Teramachi : "Analysis of Mode Hopping Phenomena in a 1.5 μm InGaAsP Laser", Rev. of Laser Eng., Vol. 13, No. 5, May 1985, pp. 416 - 425 (in Japanese) [pp. 98 - 107]

(b) International Conferences

[1] Y. Teramachi, Y. Otsuka and M. Ohtsu : "Precise Experimental and Theoretical Approach to Analyze and Reduce Mode-Hopping Noise in Semiconductor Lasers for Optical Applications", B4 - 2, The 13th Congress of the International Commissionfor Optics, 20 - 24 August, 1984, Sapporo, Japan [pp. 108 - 109]

[III] Applications

(a) Journal Papers

[1] M. Ohtsu, H. Kotani and H. Tagawa : "Spectral Measurements of NH_3 and H_2O for Pollutant Gas Monitoring by 1.5 μm InGaAsP/InP Lasers", Jpn. J. Appl. Phys., Vol. 22, No. 10, Oct. 1983, pp. 1553 - 1557 [pp. 110 - 114]

[2] K. Fukuoka, M. Ohtsu and T. Tako : "Accurate Wavelength Measurementsof the Absorption Lines in H_2O Vapor by a 0.8 μm AlGaAs Laser", Jpn. J. Appl. Phys., Vol. 23, No. 2, Feb.

1984, pp. L117 - L120 [pp. 115 - 118]

(b) International Conferences

[1] M. Ohtsu, M. Hashimoto and H. Ozawa : "A Highly Stabilized Semiconductor Laser and Its Application to Optically Pumped Rb Atomic Clock", 10B - 5, 39th Annual Frequency Control Symposium , 29 - 31, May 1985, Philadelphia, USA [pp. 119 - 129]

[IV] Reviews

[1] M. Ohtsu and T. Tako : "Spectroscopic Technique to Improve the Stability and Reproducibility of Laser Frequencies", J. Jpn. Soc. of Spectro., Vol. 32, No. 5, 1983, pp. 305 - 317 (in Japanese) [pp.130 - 142]

[2] T. Tako, M. Ohtsu and H. Tsuchida : "Frequency Stabilization of Semiconductor Lasers", Monthly J. Jpn. Soc. Appl. Phys., Vol. 52, No. 5, 1983, pp. 407 - 411 (in Japanese) [pp. 143 - 147]

[3] M. Ohtsu : "Overlook on Optics in 1983, Japan - Lasers", J. Optics, Vol. 13, No. 2, 1984, pp. 102 - 104 (in Japanese) [pp. 148 - 150]

[4] M. Ohtsu : "Techniques for Stabilizing Laser Frequencies", J. IEE of Jpn., Vol. 104, No. 9, Sept. 1984, pp. 803 - 805 (in Japanese) [pp. 151 - 155]

[5] M. Ohtsu : " Noises in Lasers ", Physics Monthly, Vol. 6, No. 5, May 1985, pp. 297 - 303 (in Japanese)

[pp. 156 - 162]

[V] Oral Presentations in Domestic Conferences

[1] Nat. Conv. Rec. of Jpn. Appl. Phys. 26 papers

[2] IECE Jpn., Tech. Group Meeting, OQE 8 papers

[3] Ridar Symposium 4 papers

[VI] Books

[1] Excitation of Lasers (Section 4.2 of " Laser Handbook ", Ed. by C. Yamanaka, Ohm-sha, 1982, in Japanese)

[2] Light Control and Noise in Semiconductor Lasers (Chapter 9 of " Semiconductor Lasers and Active Integrated Optics ", Ed. by Y. Suematsu, Ohm-sha, 1984, in Japanese)

[VII] Awards

[1] Award from The Japanese Society of Applied Physics (to the paper entitled " Frequency Stabilization of a He - ^{22}Ne Laser by Intracavity Polarization Spectroscopy of CH_4 " puplished in Jpn. J. Appl. Phys., Vol. 20, No. 9, Sept. 1981, pp. 1701 - 1707) , 28 Sept. 1982

[2] Issac Koga Gold Medal from International Union of Radio Science (URSI) , 28 Aug. 1984, at XXIst General Assembly, Florence, Italy

JAPANESE JOURNAL OF APPLIED PHYSICS
VOL. 21, NO. 9, SEPTEMBER, 1982 pp. L561–L563

Frequency Stabilization of AlGaAs Semiconductor Laser Based on the ^{85}Rb-D_2 Line

Hidemi TSUCHIDA, Motoichi OHTSU,† Toshiharu TAKO,
Naimu KURAMOCHI and Nobunori OURA

Research Laboratory of Precision Machinery and Electronics,
†International Cooperation Center for Science and Technology,
Tokyo Institute of Technology, 4259 Nagatsuta-cho, Midori-ku, Yokohama, Kanagawa 227

(Received July 6, 1982; accepted for publication August 21, 1982)

The frequency of an AlGaAs semiconductor laser was stabilized by using the linear absorption spectrum of the ^{85}Rb-D_2 line. By controlling the injection current, the frequency stability of $3.0\times10^{-10}\geqq\sigma\geqq1.4\times10^{-12}$ was obtained for $10\,\text{ms}\leqq\tau\leqq500\,\text{s}$. First observation of the saturated absorption spectrum of the ^{85}Rb-D_2 line is demonstrated, which can be used as a frequency reference to improve the frequency stability.

§1. Introduction

There have been several reports on the frequency stabilization of semiconductor lasers, by using a Fabry-Perot interferometer,[1-7] and by using atomic or molecular absorption lines,[8-10] as frequency references. In the previous work,[10] the frequency of an AlGaAs semiconductor laser was stabilized by using the linear absorption spectrum of water vapor in the (2, 1, 1) vibration-rotation band as a frequency reference. By controlling the injection current, the frequency stability of $1.9\times10^{-9}\geqq\sigma\geqq1.1\times10^{-11}$ was obtained for $10\,\text{ms}\leqq\tau\leqq500\,\text{s}$, where σ and τ represent the square root of the Allan variance and the integration time, respectively. In that case, however, the stability was limited mainly by the signal-to-noise ratio of the signals of the frequency reference, which was caused by the weak absorption of water vapor in this band. Therefore, in order to obtain higher frequency stability, it is necessary to increase the signal-to-noise ratio of the signals, i.e., to use stronger absorption lines. In addition, it is also necessary to use narrower spectra, such as saturated absorption spectra.

In this paper, the authors report the frequency stabilization of an AlGaAs semiconductor laser based on the ^{85}Rb–D_2 line ($\lambda=780.0$ nm), which has a strong absorption. First, the laser frequency was stabilized by using the linear absorption spectrum, which is described in §2. In §3, first observation of the saturated absorption spectrum of the ^{85}Rb–D_2 line is demonstrated to improve the frequency stability. It is expected that Rb-stabilized lasers can be used as optical pumping sources for Rb atomic frequency standards to improve the short-term frequency stability.[11]

§2. Frequency Stabilization of the AlGaAs Laser

The experiments were carried out in an underground tunnel for long-distance interferometry with temperature fluctuations within 0.1°C/day. An AlGaAs laser[12] oscillating near the ^{85}Rb–D_2 line ($\lambda=780.0$ nm) was selected and mounted on a copper plate which was attached to a thermoelectric cooler. The threshold current of the laser was about 48 mA. Laser frequency was roughly tuned by changing the temperature. The fine tuning of the frequency was achieved by adjusting the injection current.

An absorption cell of 6 cm length was used at room temperature. This cell did not contain any buffer gases and the corresponding vapor pressure was about 10^{-5} Torr. The Doppler width of ^{85}Rb at $\lambda=780$ nm was about 500 MHz.

The laser beam was focused on an APD after passing through the cell. The laser frequency was modulated by modulating the injection current and the output signals from the APD were synchronously detected with a lock-in amplifier. The output signals from the amplifier were fed to the current source for the laser. The servo-controller for the laser consisted of an integrator, a low pass filter (−7 dB/decade), a proportional amplifier and a differentiator.[6] Laser frequency stability was estimated from the error signals for the frequency stabilization.

Figure 1 shows the linear absorption spectrum of the ^{85}Rb–D_2 line obtained by sweeping the injection current. In this figure, T represents the temperature at the copper plate on which the laser was mounted. The upper trace represents the spectral profile. Lines A and B correspond to the transitions from the hyperfine levels with $F=2$ and 3 in the lower level $5^2S_{1/2}$, respectively; distance between the lines is about 3 GHz. The upper level $5^2P_{3/2}$ has four hyperfine levels with $F=1$, 2, 3 and 4, but they are not resolved in this figure due to Doppler broadening. The lower traces represent the first derivative used as a frequency discriminator. The modulation frequency and the modulation amplitude of the injection current are $f_m=50$ kHz and $i_m=20\,\mu A_{p-p}$, respectively, which corresponds to the frequency deviation of about 20 MHz_{p-p}. The peak-to-peak widths of lines A and B are 530 MHz and 640 MHz, respectively. Laser frequency was locked to line B in this experiment.

Figure 2 shows the time dependence of the fluctuations of laser frequency. The upper trace corresponds to the free-running laser. Frequency varied about 200 MHz during a period of 10 min, caused mainly by the temperature change in the active region. The lower trace corresponds to the stabilized laser. The frequency fluctuations were reduced to less than 100 kHz, which are less than those of the free-running laser by three orders of magnitude.

Figure 3 shows the square root of the Allan variance

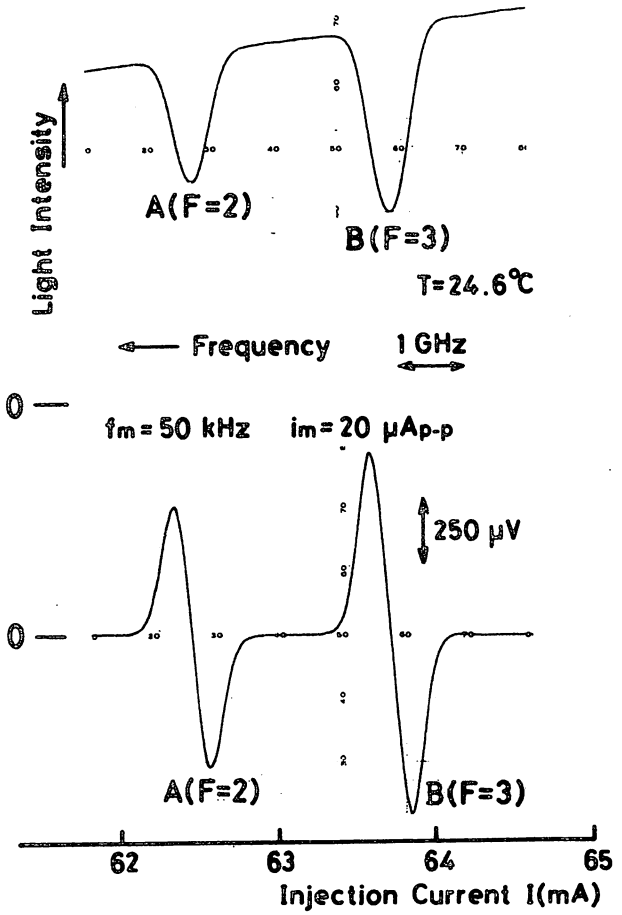

Fig. 1. Linear absorption spectrum of the ^{85}Rb-D_2 line obtained by sweeping the injection current. The upper and lower traces represent the spectral profile and its first derivative, respectively. Lines A and B correspond to the transitions from the hyperfine levels with $F=2$ and 3 in the lower level $5^2S_{1/2}$, respectively.

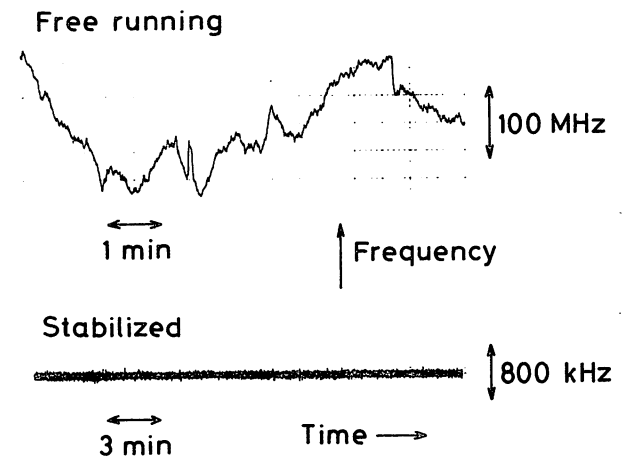

Fig. 2. Time dependence of the frequency fluctuations. Upper and the lower traces correspond to the free-running and the stabilized lasers, respectively.

σ^2 of the frequency fluctuations. In this figure, τ and N represent the integration time and the number of data, respectively. Curve A represents the frequency stability of the free-running laser, which corresponds to the upper trace in Fig. 2. The value of σ on this curve is nearly proportional to $\tau^{1/2}$ for $\tau>0.3$ s, which was caused by the thermal drift of the laser frequency. Minimum value on curve A is

$$\sigma_{\min}=2.8\times10^{-9} \text{ at } \tau=0.3 \text{ s}, \quad (1)$$

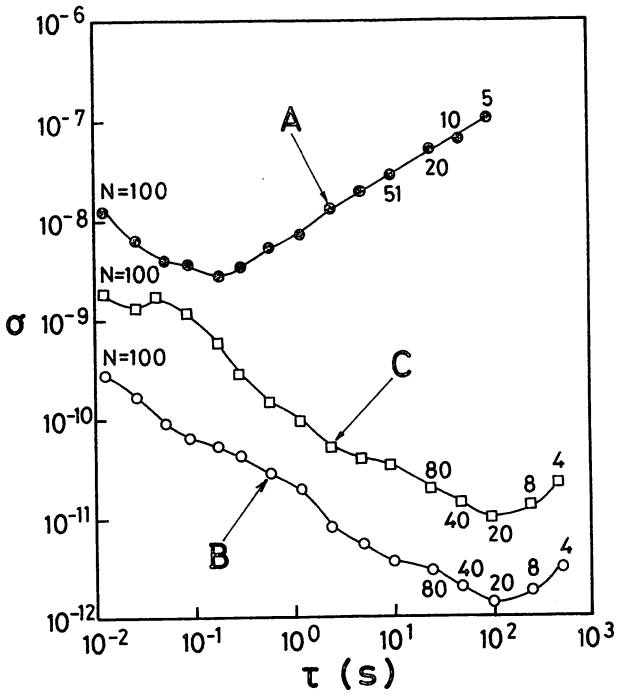

Fig. 3. Square root of the Allan variance σ^2 of the frequency fluctuations, where τ and N represent the integration time and number of data, respectively. A(●): Frequency stability of the free-running laser. B(○): Frequency stability obtained by using the absorption spectrum of water vapor (curve A in Fig. 4 of ref. 10).

and the stability is better than 1.1×10^{-7} for 10 ms$\leqq\tau\leqq$100 s. Curve B in Fig. 3 represents the frequency stability of the stabilized laser, which corresponds to the lower trace in Fig. 2. The value of σ on this curve is nearly proportional to $\tau^{-1/2}$. The minimum value on curve B is

$$\sigma_{\min}=1.4\times10^{-12} \text{ at } \tau=100 \text{ s}, \quad (2)$$

and the stability is better than 3.0×10^{-10} for 10 ms$\leqq\tau\leqq$500 s. It can be seen that the long-term stability is improved by five orders of magnitude. Curve C in Fig. 3 represents the frequency stability obtained by using the absorption spectrum of water vapor in the previous work (curve A in Fig. 4 of ref. 10). The values of σ on curve B are about ten times smaller than those on curve C at each value of τ in this figure. These improvements are attributed to the increased signal-to-noise ratio of the signals of the frequency reference. Similar stability can be expected if the ^{85}Rb–D_1 line ($\lambda=794.8$ nm) is used as a frequency reference.

§3. Observation of the Saturated Absorption Spectrum

The saturated absorption spectrum of the ^{85}Rb–D_2 line was observed to improve frequency stability, which also improves frequency reproducibility. The laser beam was collimated by an objective lens and passed through the cell as a strong saturating beam. A small protion of the transmitted beam was reflected back into the cell by a mirror as a weak probe beam and was detected with the APD.

Figure 4 shows the saturated absorption spectrum obtained by sweeping the injection current. The upper and the lower traces represent the spectral profile and its first derivative, respectively. The modulation parameters

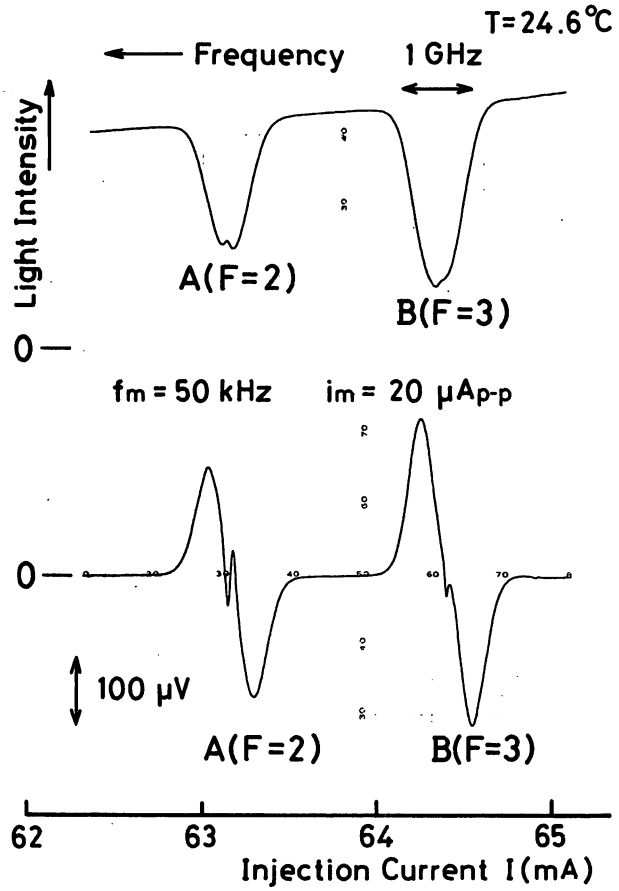

Fig. 4. Saturated absorption spectrum of the ^{85}Rb-D_2 line obtained by sweeping the injection current. Upper and lower traces represent the spectral profile and its first derivative, respectively.

for the injection current were the same as in Fig. 1. Since six transitions are allowed between the lower and the upper levels ($5^2S_{1/2}$, $F=2\rightarrow 5^2P_{3/2}$, $F=1$, 2 and 3, $5^2S_{1/2}$, $F=3\rightarrow 5^2P_{3/2}$, $F=2$, 3 and 4), six saturated absorption lines and six cross-resonance lines should be observed on the Doppler broadened profiles. However, only two lines can be seen in this figure. The cause for this discrepancy is not clear at present and is still under investigation. One of the possible explanations is that the light intensity inside the cell was not adequate, that is, it was so strong as to induce power broadening, or it was too weak to produce complete saturation. The width of the saturated absorption line on the Doppler broadened profile A is about 53 MHz, which is consistent with the value estimated from the radiative lifetime of the upper level $5^2P_{3/2}$ ($\tau=27.0$ ns).[13] Further experiments are now in progress to use the saturated absorption spectrum as a frequency reference to improve frequency stability.

§4. Conclusion

In the present work, the frequency of an AlGaAs semiconductor laser was stabilized by using the linear absorption spectrum of the ^{85}Rb–D_2 line. By controlling the injection current, the following frequency stability was obtained for 10 ms$\leqq\tau\leqq$500 s:

$$3.0\times10^{-10}\geqq\sigma\geqq1.4\times10^{-12}. \quad (3)$$

Furthermore, the first observation of the saturated absorption spectrum of the ^{85}Rb–D_2 line was demonstrated and the spectral width obtained here was 53 MHz.

Acknowledgements

The authors would like to express their thanks to Drs. M. Nakamura and K. Aiki of Hitachi, Ltd. for support of the experiment.

This work was partially supported by a Grant-in-Aid for Scientific Research from the Ministry of Education, Science and Culture of Japan.

References

1) Yu A. Bykovskii, V. L. Velichanskii, I. G. Goncharov and V. A. Masrov: Sov. Phys.-Semicond. **4** (1970) 580.
2) J. L. Picque and S. Roizen: Appl. Phys. Lett. **27** (1975) 340.
3) T. Okoshi and K. Kikuchi: Electron. Lett. **16** (1980) 179.
4) F. Favre and D. Le Guen: Electron. Lett. **16** (1980) 709.
5) H. Tsuchida, S. Sanpei, M. Ohtsu and T. Tako: Jpn. J. Appl. phys. **19** (1980) L721.
6) H. Tsuchida, M. Ohtsu and T. Taok: Jpn. J. Appl. Phys. **20** (1981) L403.
7) H. Tsuchida, M. Ohtsu and T. Tako: Trans. Inst. Electron. & Commun. Eng. Jpn. **E-65** (1982) 65.
8) M. Ohi: Jpn. J. Appl. Phys. **19** (1980) L541.
9) T. Yabuzaki, T. Ibaragi, H. Hori, M. Kitano and T. Ogawa: Jpn. J. Appl. Phys. **20** (1981) L451.
10) H. Tsuchida, M. Ohtsu and T. Tako: Jpn. J. Appl. Phys. **21** (1982) L1.
11) L. L. Lewis and M. Feldman: Proc. 35th Annual Symposium Frequency Control, 1981 Philadelphia, Pa., p. 612.
12) T. Kajimura, T. Kuroda, S. Yamashita, M. Nakamura and J. Umeda: Appl. Opt. **18** (1979) 1812.
13) J. K. Link: J. Opt. Soc. Am. **56** (1966) 1195.

JAPANESE JOURNAL OF APPLIED PHYSICS
VOL. 22, No. 4, APRIL, 1983 pp. L258–L260

Frequency Stabilization of AlGaAs Semiconductor Lasers with External Grating Feedback

Seiichi SAMPEI*, Hidemi TSUCHIDA, Motoichi OHTSU† and Toshiharu TAKO

Research Laboratory of Precision Machinery and Electronics,
†International Cooperation Center for Science and Technology,
Tokyo Institute of Technology,
4259 Nagatsuta-cho, Midori-ku, Yokohama, Kanagawa 227

(Received February 18, 1983; accepted for publication March 19, 1983)

The frequency of AlGaAs semiconductor lasers with external grating feedback has been locked to a Fabry-Perot interferometer by controlling the external cavity length with a PZT. The lasers were tunable over a wavelength range of 3.0~4.5 nm. The frequency stability of $8.0\times10^{-10}\geqq\sigma_y\geqq3.2\times10^{-12}$ was obtained for $1\text{ ms}\leqq\tau\leqq100\text{ s}$.

§1. Introduction

Frequency-stabilized semiconductor lasers[1-5] are very useful light sources for such applications as precise metrology, high resolution spectroscopy, coherent optical transmission systems[6] and so on. Frequency stabilities as high as 10^{-12} have been obtained by controlling the injection current.[3,5]

In addition to high frequency stability, a wide wavelength tunability of lasers is also desirable for the above applications. In semiconductor lasers, wavelength tuning is generally achieved by changing the temperature (0.2~0.3 nm/°C for AlGaAs lasers). However, this method has a disadvantage in that a large temperature variation is required in order to obtain the wide tuning range, which influences the lifetime of lasers significantly. For instance, a tuning range of 5 nm corresponds to a temperature variation of about 20°C.

Another method to obtain a wide tuning range is the use of an external cavity configuration. With this method, a single longitudinal mode oscillation was obtained over a wavelength range as wide as 10 nm.[7-10] An external grating[7-10] or intracavity etalons with the combination of an external mirror[11] can be used as frequency selective elements. The external cavity configuration is also attractive for the purpose of spectral linewidth reduction. The spectral linewidths obtained with this method were less than 100 kHz,[10,12-15] which were narrower than those of solitary lasers by two orders of magnitude.

In this paper the authors report the simultaneous achievement of high frequency stability and wide wavelength tunability in AlGaAs semiconductor lasers with external grating feedback. The wavelength of the lasers is tuned by the grating, and then the frequency is stabilized by controlling the external cavity length with a piezoelectric transducer (PZT). A Fabry-Perot interferometer is used as a frequency reference.

§2. Experimental Procedure

Figure 1 shows the experimental setup. A channeld substrate planar (CSP) laser[16] ($I_{th}=62$ mA, $\lambda=776$ nm) and a transverse junction stripe (TJS) laser[17] ($I_{th}=22$ mA, $\lambda=840$ nm) were used. In order to obtain a wider tuning range, it is necessary to increase the optical feedback ratio.[10] For this purpose, the reflectivity of the front facet of the TJS laser was reduced to about 0.14 by evaporating a SiO film onto it.

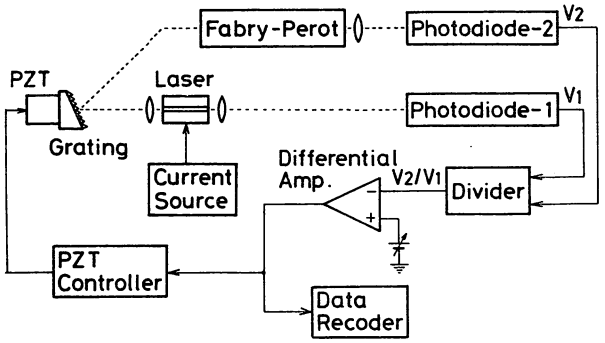

Fig. 1. The experimental setup.

The experiments were carried out in an underground tunnel for long distance interferometry. Since the temperature in the tunnel was stable within 0.1°C/day, no special techniques were employed for controlling the temperature of the heat sink on which the lasers were mounted.

The laser beam was collimated by AR-coated objective lenses. An external diffraction grating had 750 nm blaze wavelength, 13° blaze angle and 1.67 μm groove pitch and was mounted in a Littrow configuration. The junction plane of the lasers was parallel to the grating rulings and the first order diffracted beam was reflected back into the lasers. Laser wavelength was tuned by rotating the grating. The grating was mounted on a PZT to precisely control the external cavity length. To reduce the influences of the ambient temperature fluctuation and mechanical vibration, the lasers, objective lenses and grating were rigidly mounted on Invar rods.

The oscillation mode spectrum and the frequency tuning characteristics of the lasers were analyzed using a Fabry-Perot interferometer. The interferometer has a free spectral range of 10 GHz and a finesse of about 20.

The interferometer was also used as a reference for

*Present address: Radio Research Laboratory, 4-2-1 Nukui-Kitamachi, Koganei-shi, Tokyo 184

frequency stabilization. The zeroth order diffracted beam from the grating was detected with a Si photodiode (PD)-2 after passing through the interferometer. The output beam from the rear facet was directly detected with a PD-1. Output signal from the PD-2 was divided by that from the PD-1 to eliminate the intensity fluctuation of the lasers. The output signal from the divider was compared with a reference voltage and then fed to the PZT controller. The servo-controller for the PZT consisted of a proportional amplifier, an integrator, a low pass filter (−7dB/decade), and a differentiator.[18] Frequency stability was estimated from the error signals for stabilization.

§3. Experimental Results and Discussion

The wavelength tuning ranges obtained by rotating the grating were about 4.5 nm and 3.0 nm for the CSP and TJS lasers, respectively. The tuning range of the TJS laser was narrower. This fact indicates that the feedback ratio was higher in the CSP laser than in the TJS laser in spite of the lower facet reflectivity of the latter. The cause for this discrepancy can be attributed to the smaller active region of the TJS laser. The other characteristics such as frequency tuning and frequency stability were almost the same for the two lasers. In this section, the experimental results for the CSP laser are presented.

A stable single longitudinal mode oscillation was observed for 8 cm $\leqq L \leqq$ 10 cm and for $1.03 \leqq I/I_{th} \leqq 1.1$, where L, I and I_{th} represent the external cavity length, the injection current and the threshold current with optical feedback, respectively.

The rate of the laser frequency change by the injection current was −0.3 GHz/mA (−2.65 GHz/mA for the laser without optical feedback). The continuous tuning range was about 0.2 GHz due to the frequency jump phenomena.[14,19] On the other hand, a wider continuous tuning range of about 1.5 GHz was obtained by sweeping the external cavity length with the PZT. For this reason, PZT control was employed for frequency stabilization.

Seventeen longitudinal modes were independently selected by rotating the grating, which corresponds to the wavelength range of about 4.5 nm. However, continuous tuning could not be achieved due to the longitudinal mode hopping. In order to overcome this difficulty, it is necessary to reduce the facet reflectivity.[10] Frequency stabilization and frequency stability measurement were carried out for six longitudinal modes within this wavelength range. The frequency stability was almost independent of the selected mode for both cases of free-running and stabilized operation.

Figure 2 shows the typical results for the frequency stabilities, where σ_y, τ and N represent the square root of the Allan variance, the integration time and the number of data, respectively. Measurements were carried out for 1 ms $\leqq \tau \leqq$ 100 s.

Curve A corresponds to the free-running laser without optical feedback. The value of σ_y increases with increasing τ mainly due to the thermal drift.

Curve B in Fig. 2 corresponds to the free-running laser with optical feedback. By comparing curves A and B, it can be seen that the stability of the laser with optical feedback is better than that without feedback by an order of magnitude

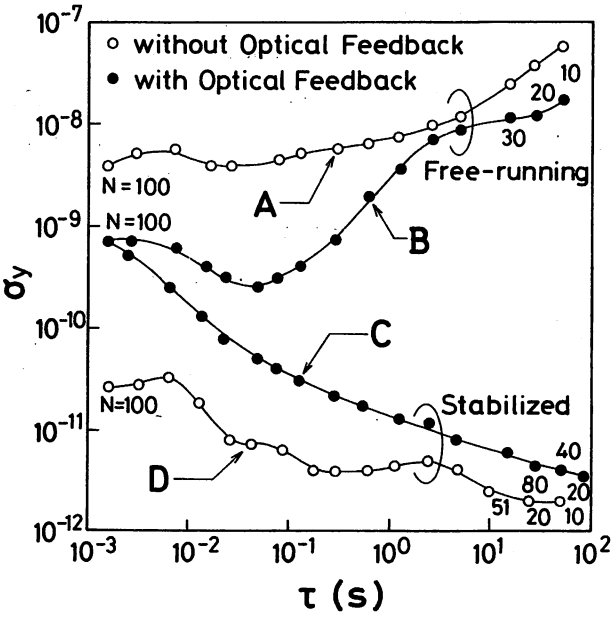

Fig. 2. Typical results for the frequency stabilities, where σ_y, τ and N represent the square root of the Allan variance, the integration time and the number of data, respectively. Curves A and B correspond to free-running lasers without and with optical feedback, respectively. Curves C and D correspond to stabilized lasers with and without optical feedback, respectively. Curves C and D are obtained by controlling the PZT and the injection current, respectively.

for 1 ms $< \tau <$ 1 s. This difference is attributed to the suppression effect of the frequency deviation in external cavity configuration.[14,19]

Curve C in Fig. 2 corresponds to the stabilized laser with optical feedback. The minimum value on this curve is

$$\sigma_y = 3.2 \times 10^{-12} \quad \text{at} \quad \tau = 100\ \text{s}, \tag{1}$$

and the stability is better than 8.0×10^{-10}. The value of σ_y on curve C for $\tau > 1$ s does not represent exactly the frequency stability of the laser, because the stability of the interferometer itself is not high enough in this time region.[1] It is interpreted as representing the frequency traceability of the laser to the interferometer. But such a stability can be expected if stable frequency references such as atomic or molecular absorption lines are used. Vibration-rotation spectra of water vapor,[4] ^{85}Rb-D_2 line,[5] or Cs-D_2 line[20] can be used in the near infrared region. By comparing curves A, B and C, it can be seen that the stability is improved by more than one order of magnitude.

Curve D in Fig. 2 corresponds to the stabilized laser without optical feedback. The laser is locked to the interferometer by controlling the injection current.[3] The value of σ_y on this curve is about ten times smaller than that on the curve C for $\tau < 1$ s. The cause for this is that the response time of the injection current is faster than that of the PZT. Therefore, the short-term stability of the stabilized laser with optical feedback (curve C) was limited by the response time of the PZT.

Further experiments are now in progress to increase the tuning range and to improve the short-term ($\tau < 1$ s) stability. The results will be reported later.

§4. Conclusion

In the present work, high frequency stability and wide wavelength tunability were achieved simultaneously in

AlGaAs semiconductor lasers with external grating feedback. The frequency stability obtained here was

$$8.0\times10^{-10}\geqq\sigma_y\geqq3.2\times10^{-12} \quad (2)$$

for 1 ms$\leqq\tau\leqq$100 s. Single longitudinal mode oscillations were obtained over the wavelength range of 3.0$\sim$4.5 nm.

Acknowledgements

The authors would like to express their thanks to Drs. M. Nakamura, K. Aiki (Hitachi, Ltd.), W. Susaki and S. Takamiya (Mitsubishi Electric Corp.) for support in the experiment. They also appreciate valuable discussions with Prof. K. Iga and Dr. K. Kishino of their Institute.

This work was partially supported by a Grant-in-Aid for Scientific Research from the Ministry of Education, Science and Culture of Japan.

References

1) H. Tsuchida, S. Sanpei, M. Ohtsu and T. Tako: Jpn. J. Appl. Phys. **19** (1980) L721.
2) H. Tsuchida, M. Ohtsu and T. Tako: Jpn. J. Appl. Phys. **20** (1981) L403.
3) H. Tsuchida, M. Ohtsu and T. Tako: Trans. Inst. Electron. & Commun. Eng. Jpn. **E-65** (1982) 65.
4) H. Tsuchida, M. Ohtsu and T. Tako: Jpn. J. Appl. Phys. **21** (1982) L1.
5) H. Tsuchida, M. Ohtsu, T. Tako, N. Kuramochi and N. Oura: Jpn. J. Appl. Phys. **21** (1982) L561.
6) Y. Yamamoto and T. Kimura: IEEE J. Quantum Electron. **QE-17** (1981) 919.
7) R. Ludeke and E. P. Harris: Appl. Phys. Lett. **20** (1972) 499.
8) H. Heckscher and J. A. Rossi: Appl. Opt. **14** (1975) 94.
9) M. Ito and T. Kimura: IEEE J. Quantum Electron. **QE-16** (1980) 69.
10) M. W. Fleming and A. Mooradian: IEEE J. Quantum Electron. **QE-17** (1981) 44.
11) C. Voumard: Opt. Lett. **1** (1977) 61.
12) K. Kikuchi and T. Okoshi: Electron. Lett. **18** (1982) 10.
13) L. Goldberg, H. F. Taylor, A. Dandridge, J. F. Weller and R. O. Miles: IEEE J. Quantum Electron. **QE-18** (1982) 555.
14) S. Saito, O. Nilsson and Y. Yamamoto: IEEE J. Quantum Electron. **QE-18** (1982) 961.
15) F. Favre, D. Le Guen and J. C. Simon: IEEE J. Quantum Electron. **QE-18** (1982) 1712.
16) T. Kajimura, T. Kuroda, S. Yamashita, M. Nakamura and J. Umeda: Appl. Opt. **18** (1979) 1812.
17) W. Susaki, T. Tanaka, H. Kan and M. Ishii: IEEE J. Quantum Electron. **QE-13** (1977) 587.
18) M. Ohtsu, S. Katsuragi and T. Tako: IEEE J. Quantum Electron. **QE-17** (1981) 1100.
19) R. Lang and K. Kobayashi: IEEE J. Quantum Electron. **QE-16** (1980) 347.
20) T. Yabuzaki, A. Ibaragi, H. Hori, M. Kitano and T. Ogawa: Jpn. J. Appl. Phys. **20** (1981) L451.

JAPANESE JOURNAL OF APPLIED PHYSICS
VOL. 22, NO. 7, JULY, 1983 pp. 1157–1166

Estimation of the Ultimate Frequency Stability of Semiconductor Lasers

Motoichi OHTSU, Hiroyuki FUKADA,† Toshiharu TAKO† and Hidemi TSUCHIDA†

International Cooperation Center for Science and Technology, Tokyo Institute of Technology, 2-12-1 O-okayama, Meguro-ku, Tokyo 152
†*Research Laboratory of Precision Machinery and Electronics, Tokyo Institute of Technology, 4259 Nagatsuta-cho, Midori-ku, Yokohama, Kanagawa 227*

(Received February 14, 1983; accepted for publication April 23, 1983)

The frequency stabilities of 0.8 μm AlGaAs lasers were estimated by using the Allan variance as a measure of the stability. The contributions of the quantum noise (the spontaneous emission, carrier, and current noise) and additional noise (current source noise and temperature noise) are given. The highest frequency stability of the free-running laser was estimated to be 6.3×10^{-11} at an integration time of 0.1 s. It is shown that the frequency stability of the stabilized laser is limited by the quantum noise. The estimated results were compared with the experimental results and with the estimated stability of 3.39 μm He–^{22}Ne lasers. The derivations of the spectral width from the frequency stability are also given. The narrowest limit of the spectral width was estimated to be 5.5 MHz (HWHM) for $I/I_{th}=1.3$, while the corresponding experimental result was 6.2 MHz for a channeled-substrate planar (CSP)-type laser.

§1. Introduction

The spectral properties of semiconductor lasers have been greatly improved as a result of the demands of the optical communication industry. When these lasers are used in new applications such as laser gyroscopes, air pollution monitoring, and high-speed coherent communication, better frequency stability will be required. Theoretical and experimental studies have recently been done on spectral width,[1,2] AM and FM noise,[3,4] and frequency stabilization[5–9] with these applications in mind.

In the present paper, the frequency stability limits of 0.8 μm AlGaAs lasers are estimated for the Fourier frequency range up to 1 GHz, i.e., an integration time of more than 1 ns, to obtain one of the guidelines for designing new lasers with better frequency stability for new applications. The estimated results are compared with experimental results and with the frequency stability of a gas laser. Estimations of the spectral width from the frequency stability are also given.

§2. Noise Sources Limiting Frequency Stability

In this chapter, several kinds of noise source and their contributions to the frequency stability are discussed. Before going into this discussion, the definitions of the measures for frequency stability are given.

If the electric field of the laser is expressed as

$$E(t)=(A_0+a(t))\cdot\exp\left[i\{2\pi\nu_0 t+\varphi(t)\}\right]+\text{c.c.}, \tag{1}$$

its instantaneous frequency is given by

$$\nu(t)=\nu_0+\frac{\mathrm{d}\varphi}{\mathrm{d}t}\Big/2\pi\equiv\nu_0+\delta\nu(t), \tag{2}$$

where A_0 and $a(t)$ are the amplitude and its fluctuations, ν_0 is the optical frequency, $\varphi(t)$ and $\delta\nu(t)$ are the fluctuating phase and frequency, and c.c. means the complex conjugate. The normalized fluctuating frequency can then be defined by

$$y(t)\equiv\delta\nu(t)/\nu_0=\frac{\mathrm{d}\varphi}{\mathrm{d}t}\Big/2\pi\nu_0, \tag{3}$$

and its autocorrelation function is expressed as

$$R_y(\tau)=\langle y(t)y(t+\tau)\rangle=\lim_{T\to\infty}\frac{1}{T}\int_{-T/2}^{T/2}y(t)y(t+\tau)\,\mathrm{d}t, \tag{4}$$

where $\langle\ \rangle$ represents the time average as shown by the right-hand side of this equation. The one-sided power spectral density is calculated from this autocorrelation function using the following Fourier integral:

$$S_y(f)=4\int_0^\infty R_y(\tau)\cos(2\pi f\tau)\,\mathrm{d}\tau \tag{5}$$

This power spectral density is a popular measure which is used to represent the characteristics of the frequency fluctuations in the Fourier frequency domain. An alternative measure which is also widely used is the Allan variance.[10] This is defined by

$$\sigma_y^2(\tau)\equiv\lim_{N\to\infty}\frac{1}{N-1}\sum_{k=1}^{N-1}\frac{(\bar{y}_{k+1}-\bar{y}_k)^2}{2}, \tag{6}$$

where $\bar{y}_k$ is the value averaged over the integration time τ as given by

$$\left.\begin{aligned}&\bar{y}_k\equiv\frac{1}{\tau}\int_{t_k}^{t_k+\tau}y(t)\,\mathrm{d}t,\\&t_{k+1}=t_k+\tau\qquad(k=1,2,3,\cdots)\end{aligned}\right\}. \tag{7}$$

The Allan variance can be used to represent the characteristics of the frequency fluctuations in the time domain. It is used particularly widely in the field of frequency standards such as cesium atomic clocks, hydrogen masers, and frequency-stabilized lasers. Because this measure has several practical advantages in representing the frequency stability, it has been commonly used to represent the

frequency stability since 1966.[11,12]

Considering the historical situation, the frequency stability discussed in this paper will be represented by the Allan variance for convenience in comparing our results with experimental results on the frequency stability and with other kinds of laser. The conversion from $S_y(f)$ to $\sigma_y^2(\tau)$ is given by

$$\sigma_y^2(\tau)=2\int_0^\infty S_y(f)\frac{\sin^4(\pi f\tau)}{(\pi f\tau)^2}\,df. \tag{8}$$

As a special case, when $S_y(f)$ is proportional to f^M (M; integer, $-2\leqq M\leqq 2$), the mutual conversion between the two is readily carried out, and is shown in Table A(I) in Appendix A. Using eq. (8) or Table A(I), the frequency stability limited by several noise sources can be expressed by the Allan variance. Since 0.8 μm channeled-substrate planar (CSP)-type lasers[13] were used in these experiments, numerical values of the parameters for these lasers are used for the estimations described in this paper.

2.1 *Free-running lasers*

2.1.1 *Spontaneous emission noise*

One fundamental type of quantum noise is due to spontaneous emission. The frequency fluctuations induced by this phenomenon can be discussed by Langevin's method of formulation.[14,15] In eq. (1), the fluctuating component is expressed as

$$\tilde{E}(t)=(A_0+a(t))\exp[i\varphi(t)], \tag{9}$$

which can be assumed to vary far slower than $\exp(i2\pi\nu_0 t)$. Langevin's equation for $\tilde{E}(t)$ is given by

$$\frac{d\tilde{E}}{dt}+(\gamma-\alpha_0+\beta_0\tilde{E}\tilde{E}^*)\tilde{E}=\Gamma(t), \tag{10}$$

where α_0 is the small signal gain, $\beta_0 EE^*$ is the saturated gain, and γ is the cavity loss of the laser. $\Gamma(t)$ represents Langevin's force, which gives the fluctuations due to spontaneous emission. By substituting eq. (9) into eq. (10), following equation is obtained for the phase $\varphi(t)$:

$$A_0\frac{d\varphi}{dt}=\Gamma_i(t), \tag{11}$$

where $\Gamma_i(t)$ is the imaginary part of $\Gamma(t)$. By using eq. (11), the second-order moment for phase fluctuations within the integration time τ can be calculated as

$$\langle\delta\varphi^2\rangle=\frac{1}{A_0^2}\int_t^{t+\tau}\int_t^{t+\tau}\Gamma_i(t')\Gamma_i(t'')\,dt'\,dt''. \tag{12}$$

As $\Gamma(t)$ represents the quantum noise due to spontaneous emission, it can be considered to be composed of pulses with widths narrower than the value of the time constant $(\alpha_0-\gamma)^{-1}$ of the laser oscillation, and can be expressed as

$$\langle\Gamma_i(t)\Gamma_i(t+\tau)\rangle=\delta(\tau)\gamma h\nu_0 n_{sp}, \tag{13}$$

where $\delta(\tau)$ is the delta function. The spontaneous emission factor n_{sp} is given by[2]

$$n_{sp}=\{1-\exp[(h\nu_0+E_{Fv}-E_{Fc})/kT]\}^{-1}, \tag{14}$$

where E_{Fc} and E_{Fv} are the conduction-band and valence-band quasi-Fermi levels, k is Boltzmann's constant, and T is the temperature. From eqs. (12), (13), and (14), one obtains

$$\langle\delta\varphi^2\rangle=\frac{2\gamma^2 h\nu_0 n_{sp}}{P}\tau, \tag{15}$$

where P represents the intracavity power of the laser, given by

$$P=2\gamma A_0^2. \tag{16}$$

As the Allan variance $\sigma_y^2(\tau)$ corresponds to the second-order moment for frequency fluctuations $\langle\delta\nu^2\rangle/\nu_0^2$, it can be derived from eq. (15), and is expressed as

$$\sigma_y^2(\tau)=\langle\delta\nu^2\rangle/\nu_0^2=\frac{\langle\delta\varphi^2\rangle}{(2\pi\tau)^2}\Big/\nu_0^2 =\frac{2\Gamma_c^2 h n_{sp}}{\nu_0 P}\frac{1}{\tau}, \tag{17}$$

where Γ_c represents the cavity linewidth (HWHM), which is given by

$$\Gamma_c=\gamma/2\pi. \tag{18}$$

Furthermore, the cavity linewidth Γ_c and the intracavity power P can be expressed as

$$\left.\begin{aligned}&\Gamma_c=c(\alpha_i L-\ln R)/4\pi nL\\ &P=P_0\left[(\ln R-\alpha_i L)/\ln\sqrt{R}\right]\end{aligned}\right\}, \tag{19}$$

where c is the speed of light, α_i is the mode loss coefficient, L is the cavity length, n is the refractive index, R is the facet reflectivity, and P_0 is the single-ended output power of the laser. Substitution of eq. (19) into eq. (17) gives

$$\sigma_y^2(\tau)=\frac{h}{16\pi^2\nu_0 P_0}\left(\frac{c}{nL}\right)^2(\ln R-\alpha_i L)(\ln R)n_{sp}\cdot\frac{1}{\tau}. \tag{20}$$

The following numerical values are used for calculation:

$$\left.\begin{aligned}&\nu_0=3.75\times10^{14}\ \text{Hz},\ P_0=3.0\ \text{mW},\ n=3.5,\\ &L=300\ \mu\text{m},\ R=0.3,\ \alpha_i=80\ \text{cm}^{-1},\ n_{sp}=2^{2)}\end{aligned}\right\}. \tag{21}$$

The value of P_0 shown above is for $I/I_{th}=1.3$ in the CSP-type laser used in the experiments, where I and I_{th} are the injected current and its threshold value, respectively. The value of α_i was derived by measuring the slope of the injected current-output power curve of the CSP-type laser. These values give the following result:

$$\sigma_y^2(\tau)=2.6\times10^{-24}\tau^{-1}. \tag{22}$$

The result is shown by curve A in Fig. 1.

2.1.2 *Carrier noise and current noise*

Other types of quantum noise specific to semiconductor lasers are due to carrier and junction current fluctuations. As the power spectral densities of the frequency fluctuations by these types of noise have been given by Yamamoto *et al.*,[3,4] the values of the Allan variance due to the noise will be derived here using their results and eq. (8).

The carrier noise is due to quantum mechanical fluctuations by spontaneous emission. The power spectral density of the frequency fluctuations $\delta\nu(t)$ by this phenomenon for a CSP-type laser of $L=900$ μm can be expressed as (Fig. 16 of ref. 4)

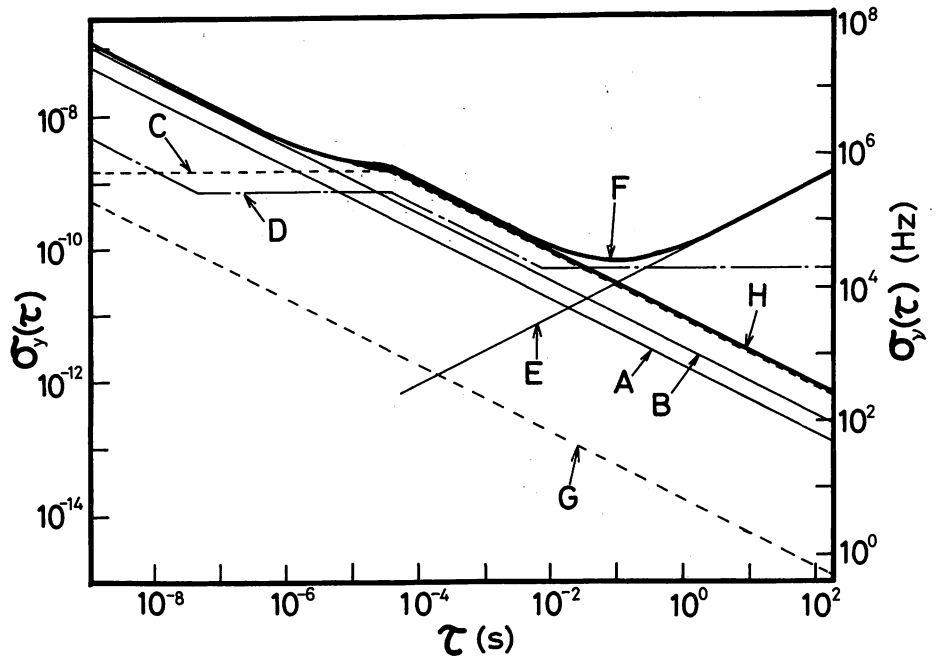

Fig. 1. Calculated results of the square root of the Allan variance $\sigma_y^2(\tau)$ of the frequency fluctuations for 0.8 μm AlGaAs lasers. A; spontaneous emission noise (eq. (22)). B; carrier noise (eq. (25)). C; current noise (eq. (28)). D; current source noise (eq. (37)). E; temperature noise (eq. (41)). F; free-running laser (sum of eqs. (22), (25), (28), (37), and (41)). G; tentative result for frequency-stabilized lasers (eq. (47)). H; frequency-stabilized laser (sum of eqs. (22), (25), and (28)).

$$S_v(f)=7.0\times 10^{5}\quad (\mathrm{Hz}) \tag{23}$$

for $I/I_{th}=1.3$. This power spectral density $S_v(f)$ has a resonant peak at the Fourier frequency f_r of about a few GHz, and this is specific to semiconductor lasers.[4] The frequency stability around this resonant peak is rather complicated because the integral of eq. (8) does not converge to a finite value. Further study is now in progress to overcome this difficulty, and the results will be published elsewhere. In the present work, however, the stability for $f<1$ GHz, i.e., $\tau>1\times 10^{-9}$ s, is discussed as the first step of the study. The power spectral density for $y(t)$ is given by $S_v(f)/\nu_0^2$, and its Allan variance can be derived by using eqs. (8) and (23). It is expressed as

$$\sigma_y^2(\tau)=2.5\times 10^{-24}\tau^{-1}. \tag{24}$$

As this carrier noise is originally induced by the spontaneous emission, the dependence of $\sigma_y^2(\tau)$ on the cavity length L is the same as that of the spontaneous emission,[3] which is shown by eq. (2). Therefore, the value of $\sigma_y^2(\tau)$ for $L=300$ μm due to the carrier noise can be estimated from eqs. (20) and (24), and is given by

$$\sigma_y^2(\tau)=9.7\times 10^{-24}\tau^{-1}. \tag{25}$$

The current noise is due to the fluctuations of the injected current caused by the quantum mechanical fluctuations of the carrier density described above, and the corresponding power spectral density of $S_v(f)$ for $L=900$ μm can be expressed as (Fig. 16 of ref. 4):

$$S_v(f)=\begin{cases}5.0\times 10^{6}\ (\mathrm{Hz}) & (f<1\times 10^{4}\ \mathrm{Hz})\\ 5.0\times 10^{10}f^{-1}\ (\mathrm{Hz}) & (f\geqq 1\times 10^{4}\ \mathrm{Hz}).\end{cases} \tag{26}$$

The value of $S_v(f)$ decreases with increasing Fourier frequency f for $f\geqq 10$ kHz because the induced temperature fluctuations of the laser cannot follow the high-frequency component of the current fluctuations. The Allan variance due to this noise source can be derived from eqs. (8) and (26):

$$\sigma_y^2(\tau)=\begin{cases}4.9\times 10^{-19} & (\tau<1\times 10^{-4}\ \mathrm{s})\\ 1.8\times 10^{-23}\tau^{-1} & (\tau\geqq 1\times 10^{-4}\ \mathrm{s}).\end{cases} \tag{27}$$

As this current noise is also from the spontaneous emission,[3] the dependence of $\sigma_y^2(\tau)$ of eq. (27) on the cavity length L is the same as that of eq. (20). Therefore, the value of $\sigma_y^2(\tau)$ for $L=300$ μm due to the current noise can be estimated from eqs. (20) and (27), and is expressed as

$$\sigma_y^2(\tau)=\begin{cases}1.9\times 10^{-18} & (\tau<1\times 10^{-4}\ \mathrm{s})\\ 6.9\times 10^{-23}\tau^{-1} & (\tau\geqq 1\times 10^{-4}\ \mathrm{s}).\end{cases} \tag{28}$$

The results given by eqs. (25) and (28) are shown in Fig. 1.

2.1.3 *Current source noise*

The frequency fluctuations described in 2.1.1 and 2.1.2 are due to quantum mechanical phenomena, and the noise sources are therefore intrinsic to semiconductor lasers. Additional noise sources should be investigated when the lasers are used in practice. One of these additional noise sources is the regulated current supply used in the experiment. Figure 2 shows a schematic diagram of a typical regulated current supply. As shown by this figure, the regulated current supply is generally composed of active electronic devices such as transistors and operational amplifiers. Thus the output current fluctuations depend on the noise characteristics of these active devices. The power spectral density of the voltage fluctuations of typical operational amplifiers can be expressed as

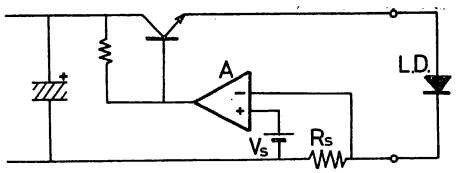

Fig. 2. Schematic explanation of a typical regulated current supply. A; low-noise operational amplifier. V_s; reference voltage. R_s; resistor for current monitoring. L.D.; semiconductor laser.

$$S_V(f)=\begin{cases} V_n^2 f_c/f & (f<f_c) \\ V_n^2 & (f\geqq f_c) \end{cases} \quad (\mathrm{V^2/Hz}), \tag{29}$$

i.e., the noise characteristics are dominated by the $1/f$ noise for $f<f_c$, and by the thermal noise for $f\geqq f_c$. As an example, typical values of V_n and f_c for the low-noise monolithic JFET-input operational amplifier LF356 are 15 nV and 50 Hz, respectively.[16] Since the output current is monitored by the reference resistor R_s in the current supply in Fig. 2, the power spectral density of the current fluctuations is given by

$$S_I(f)=S_V(f)/R_s^2 \quad (\mathrm{A^2/Hz}). \tag{30}$$

Its Allan variance is derived from eqs. (8), (29), and (30), and is expressed as

$$\sigma_I^2(\tau)=\begin{cases} \frac{1}{2}(V_n/R_s)^2\tau^{-1} & (\tau<f_c^{-1}) \\ (2\ln 2)(V_n/R_s)^2 f_c & (\tau\geqq f_c^{-1}) \end{cases} \quad (\mathrm{A^2}). \tag{31}$$

Figure 3 shows the calculated and experimental results of the spuare root of $\sigma_I^2(\tau)$. Curve A represents the calculated result derived from eq. (31), where R_s of 25 Ω was used for the calculation as the value actually employed in the experiments. The experimental curve B has a bump at around τ of 1×10^{-2} s. This bump is due to the ripple from the AC power supply with the frequency of 50 Hz and its second harmonics, 100 Hz. Except for this bump, approximate agreement can be seen between the two curves. Curve A in Fig. 3 or eq. (31) can be thought to represent the lowest limit of the current fluctuations attainable by modern low-noise electronic circuit design techniques.

The fluctuations of carrier density and temperature are induced by this current noise, and these in turn induce the laser frequency fluctuations. The induced laser frequency change is given by[17]

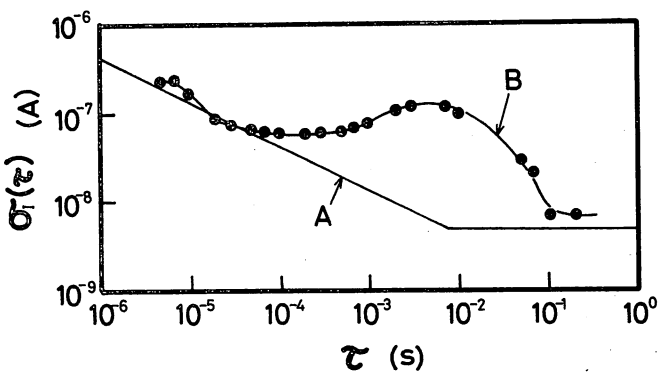

Fig. 3. Square root of the Allan variance of the current fluctuations. A; calculated results for $R_s=25\,\Omega$ (eq. (31)). B; experimental results for regulated current supply used in experiments of Fig. 5.

$$\delta\nu/\nu_0=-A\frac{1}{n}\delta N_c-(\alpha_T+\beta_T)\delta T, \tag{32}$$

where A is the refractive index change due to unit change in the carrier density, δN_c is the change in the carrier density, α_T is the temperature coefficient of the cavity length, β_T is that of the refractive index, and δT is the temperature change. The change in the carrier density due to the current can be expressed as

$$\frac{dN_c}{dI}=\frac{\partial N_c}{\partial I}+\frac{\partial N_c}{\partial T}\frac{dT}{dI}. \tag{33}$$

The first term of the right-hand side of this equation represents the direct modulation by the current, and the second term is the thermally-induced change in the carrier density. The relation between $\delta\nu$ and δI is obtained from eqs. (32) and (33), and is expressed as

$$\delta\nu/\nu_0=-\left[A\frac{1}{n}\frac{\partial N_c}{\partial I}+\left\{A\frac{1}{n}\frac{\partial N_c}{\partial T}+(\alpha_T+\beta_T)\right\}\frac{dT}{dI}\right]\delta I. \tag{34}$$

The value of the quantity in the square brackets [ ] in this equation, i.e., the proportional constant between the change in the injected current and that of the laser frequency, has been obtained experimentally.[18,19] Figure 4 shows the relation between the square of this proportional constant and the frequency of the injected current, obtained from the experimental results reported by the authors (Fig. 3 of ref. 19). If this experimental value, represented by curve A in Fig. 4, is approximated by curve B for simplicity, its value, represented by $H(f)$, can be expressed as

$$H(f)=\begin{cases} 1.3\times10^{25} & (f<1\times10^4\ \mathrm{Hz}) \\ 1.3\times10^{29}f^{-1} & (1\times10^4\ \mathrm{Hz}\leqq f<8\times10^6\ \mathrm{Hz}) \\ & (\mathrm{Hz^2/A^2}) \\ 1.7\times10^{22} & (f\geqq8\times10^6\ \mathrm{Hz}) \end{cases}. \tag{35}$$

In this equation, the thermal effect, i.e., the term in curly brackets { } in eq. (34), gives the main contribution for $f<1\times10^{-4}$ Hz, and the value of $H(f)$ decreases with increasing frequency for $f\geqq1\times10^4$ Hz. This feature is consistent with that of eq. (26) in 2.1.2. For $f\geqq8\times10^6$ Hz, only the effect of direct modulation of the carrier density, i.e., the first term in eq. (34), contributes to $H(f)$. As mentioned in 2.1.2, the effect of this direct modulation also gives a resonant peak to $H(f)$ at the Fourier frequency f_r of about a few GHz.[18] However, in the discussion for $f<1$ GHz ($\tau>1\times10^{-9}$ s) in this paper, eq. (35) can be safely used. By

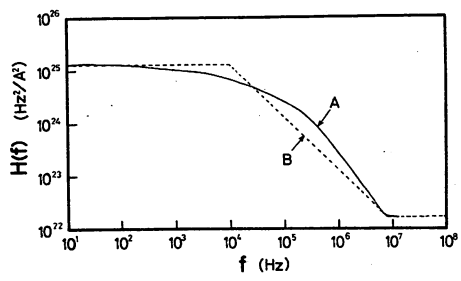

Fig. 4. Square of the coefficient of the laser frequency change due to the injected current, where f is the frequency of the injected current. A; experimental results obtained by authors (Fig. 3 of ref. 19). B; curve fitted to curve A to estimate frequency stability (eq. (35)).

using eq. (35) with eqs. (29) and (30), the power spectral density $S_y(f)$ is expressed as

$$S_y(f)=\frac{1}{\nu_0^2}H(f)\cdot S_I(f). \tag{36}$$

The Allan variance $\sigma_y^2(\tau)$ is then derived from eqs. (8) and (36). On substituting the numerical values given above, this is expressed as

$$\sigma_y^2(\tau)=\begin{cases} 2.2\times10^{-26}\tau^{-1} & (\tau<1.25\times10^{-7}\ \mathrm{s}) \\ 4.6\times10^{-19} & (1.25\times10^{-7}\ \mathrm{s}\leqq\tau<1\times10^{-4}\ \mathrm{s}) \\ 1.7\times10^{-23}\tau^{-1} & (1\times10^{-4}\ \mathrm{s}\leqq\tau<2\times10^{-2}\ \mathrm{s}) \\ 2.3\times10^{-21} & (\tau\geqq2\times10^{-2}\ \mathrm{s}) \end{cases}. \tag{37}$$

This result is shown in Fig. 1.

2.1.4 *Temperature noise*

Noise due to temperature fluctuations should also be discussed when the laser is used in practice. As the laser is usually fixed on a heat sink and its temperature is controlled electronically, its residual temperature fluctuations induce the laser frequency fluctuations. Several techniques for temperature stabilization have been developed recently, and the temperature fluctuations have been reduced to as low as 1×10^{-6} K.[20] One typical example of such a precise temperature control is reported in ref. 21, where the temperature of a stable quartz oscillator was stabilized by using a Pt resistor as a sensor and its temperature fluctuations were measured. Figure 8 of ref. 21 gives the following value of the power spectral density of the temperature fluctuations:

$$S_T(f)=3.0\times10^{-13}f^{-2} \qquad (\mathrm{K^2/Hz}). \tag{38}$$

To estimate the frequency stability limits, this value can be used as the lowest limit of the temperature fluctuations attainable by modern temperature control techniques. As given by eq. (34), the laser frequency change produced by a temperature change is given by

$$\delta\nu/\nu_0=-\left[A\frac{1}{n}\frac{\partial N_c}{\partial T}+(\alpha_T+\beta_T)\right]\delta T. \tag{39}$$

The value of the quantity $\nu_0[An^{-1}(\partial N_c/\partial T)+(\alpha_T+\beta_T)]$ in this equation, i.e., the temperature coefficient of the frequency change, has been measured as 25 GHz/K for CSP-type lasers.[22] On using this value, the power spectral density $S_y(f)$ is given by

$$S_y(f)=(2.5\times10^{10}/\nu_0)^2S_T(f). \tag{40}$$

The Allan variance, $\sigma_y^2(\tau)$, is then derived from eqs. (8), (38), and (40), and is expressed as

$$\sigma_y^2(\tau)=8.8\times10^{-21}\tau. \tag{41}$$

This result is shown in Fig. 1.

As random fluctuations are induced in the frequency of a free-running laser by the noise sources described in 2.1.1–2.1.4, its Allan variance is expressed as the sum of the values given by eqs. (22), (25), (28), (37), and (41). This is shown by curve F in Fig. 1. It can be seen from this figure that the minimum value of $\sigma_y^2(\tau)$ attainable by a free-running laser is

$$\sigma_y^2(\tau)=4.0\times10^{-21} \quad \text{at} \quad \tau=1\times10^{-1}\ \mathrm{s}, \tag{42}$$

or its square root is

$$\sigma_y(\tau)=6.3\times10^{-11} \quad \text{at} \quad \tau=1\times10^{-1}\ \mathrm{s}. \tag{43}$$

2.2 *Frequency-stabilized lasers*

The laser frequency can be stabilized to the appropriate frequency references by servo-controlling electronic circuits. Several atomic and molecular spectra as well as a stable Fabry-Perot interferometer have been successfully used as the frequency references for 0.8 μm AlGaAs lasers.[6-9] Among these references, the linear absorption spectra in H_2O vapor will be generally used as the references for 0.8 μm AlGaAs lasers because a great number of vibration-rotation spectra of the $(\nu_1, \nu_2, \nu_3)=(2, 1, 1)$ band are widely distributed in the 0.8 μm region, and, therefore, almost all the AlGaAs lasers can be tuned to at least one of these spectra even if they exhibit mode hopping.[7] For this reason, these spectra are employed as the most popular frequency references in the present discussion.

General discussions of the frequency stability of a stabilized laser have been given by Shimoda.[23] According to Shimoda's theory (eq. (19) of ref. 23), the minimum frequency fluctuations detectable by the servo-controlling system are expressed as

$$\delta\nu/\nu_0=2.1\left(\frac{u}{c}\right)\sqrt{P_n/P_i}, \tag{44}$$

where u is the most probable velocity of the H_2O molecule, and P_i is the laser power incident on the detector. The noise power of the detector P_n is given by

$$P_n=FkTB+(h\nu_0/\eta)B, \tag{45}$$

where B is the bandwidth, kT the thermal noise energy, $h\nu_0$ the photon energy, F the noise figure, and η the quantum efficiency, When an ideal detector is used ($F=\eta=1$), the Allan variance of the frequency fluctuations is given by eqs. (44) and (45), and is expressed as

$$\sigma_y^2(\tau)=(\delta\nu/\nu_0)^2=1.1\left(\frac{u}{c}\right)^2\frac{kT+h\nu_0}{P_i}\cdot\frac{1}{\tau}, \tag{46}$$

where τ is the integration time of the phase-sensitive detector, given by $\tau=1/4B$. For $u=520$ m/s, $c=3\times10^8$ m/s, $k=1.38\times10^{-23}$ J/K, $T=293$ K, and $P_i=3.0$ mW, the value of $\sigma_y^2(\tau)$ of eq. (46) is

$$\sigma_y^2(\tau)=2.8\times10^{-28}\tau^{-1}. \tag{47}$$

This result is shown in Fig. 1 together with that of the free-running laser. It can be seen that this value is smaller than those of eqs. (22), (25), and (28), i.e., those due to the types of quantum noise given in 2.1.1 and 2.1.2. This troublesome fact does not mean that the quantum noise is reduced as low as that of eq. (47) by the frequency stabilization. It means that the frequency fluctuations reduced by the frequency stabilization are only those due to additional noise such as the current source noise and temperature noise, which are usually far larger than those of eqs. (37) and (41) under actual experimental conditions. Therefore, even though the frequency stability is improved by the stabilization, it is limited by the quantum noise. That is, the frequency stability of the stabilized laser is actually described not by

eq. (47), but by the sum of eqs. (22), (25), and (28), which can be approximately represented as follows:

$$\sigma_y^2(\tau)=\begin{cases}1.2\times10^{-23}\tau^{-1} & (\tau<5\times10^{-6}\text{ s})\\ 8.1\times10^{-23}\tau^{-1} & (\tau>5\times10^{-6}\text{ s}).\end{cases} \quad (48)$$

This result is shown by curve H in Fig. 1.

§3. Comparison with the Experimental Results

Figure 5 shows the experimental results of the square root of the Allan variance for CSP-type lasers with a cavity length of 300 μm. Curves A_1, A_2, B_1, and B_2 represent the results previously reported by the authors.[7-9] Curves A_1 and B_1 represent the results for free-running lasers, while curves A_2 and B_2 are for frequency-stabilized lasers. By comparing these curves and the results of Fig. 1, it can be seen that the frequency stability of a free-running laser is limited by the temperature noise for $\tau\geqq3\times10^{-1}$ s. If the frequency is stabilized, this additional noise is reduced and the stability is improved until it is limited by the quantum noise; it can be seen that the values of curve B_2 closely approach the quantum noise level represented by curve F.

Curve C represents the measurements of the present work to find the stability of the free-running laser for $5\times10^{-6}\text{ s}\leqq\tau\leqq1\times10^{-2}$ s. The data were accumulated by using an auto-digitizer S210 (by Autonics Co. Ltd.,) with a sampling time of 1 μs. The other signal processing procedures were almost the same as the previous ones [6-9]. The bump at around $\tau=1\times10^{-2}$ s is due to the ripple from the power supplies of the experimental apparatus, as with curve B of Fig. 3. Except for this bump, the Allan variance of curve C has a constant value of

$$\sigma_y^2(\tau)=4.9\times10^{-17}. \quad (49)$$

By comparing Figs. 1, 3, and this curve, it can be seen that the frequency stability of the free-running laser for $5\times10^{-6}\text{ s}\leqq\tau\leqq1\times10^{-2}$ s is limited mainly by the current source noise. It can also be seen that the extrapolated line from curve C approaches curve E, where the frequency stability is limited by the quantum noise, i.e., the spontaneous emission and carrier noise.

In this quantum-noise-limited region of τ, the frequency stability can be estimated from the experimental results by Yamamoto *et al.*[4] According to their results (Fig. 16 of ref. 4), the power spectral density of $S_v(t)$ of a CSP-type laser 900 μm in length is expressed as

$$S_v(f)=1.0\times10^6\text{ (Hz)}\quad(1\times10^7\text{ Hz}\leqq f\leqq1\times10^9\text{ Hz}) \quad (50)$$

for $I/I_{th}=1.3$. By using this value and eq. (8), the Allan variance is given by

$$\sigma_y^2(\tau)=3.6\times10^{-24}\tau^{-1}\quad(1\times10^{-9}\text{ s}\leqq\tau\leqq1\times10^{-7}\text{ s}). \quad (51)$$

As the spontaneous emission noise and the carrier noise contribute to this value, it is given by the sum of $\sigma_y^2(\tau)$ due to these types of noise. As was described in 2.1.2, the dependence of the value of $\sigma_y^2(\tau)$ due to the carrier noise on the cavity length L is the same as that due to the spontaneous emission, given by eq. (20). Therefore, the value of $\sigma_y^2(\tau)$ for a CSP-type laser with $L=300$ μm is given by eqs. (20) and (51), and is expressed as

$$\sigma_y^2(\tau)=1.4\times10^{-23}\tau^{-1}\quad(1\times10^{-9}\text{ s}\leqq\tau\leqq1\times10^{-7}\text{ s}). \quad (52)$$

This result is represented by curve D in Fig. 5.

The extrapolation of curve D intersects that of curve C at $\tau=2.9\times10^{-7}$ s. It can be seen from this figure that no improvements in the stability for $\tau<2.9\times10^{-7}$ s can be expected even if the frequency is stabilized, because the stability of the free-running laser in this region of τ is already dominanted by the quantum noise, i.e., the spontaneous emission and the carrier noise. The frequency stabilization suppresses the fluctuations due to the temperature noise to as low as the quantum-noise-limited values for $\tau\geqq3\times10^{-1}$ s, as shown by curve B_2 in Fig. 5. Therefore, one of the problems remaining to be solved

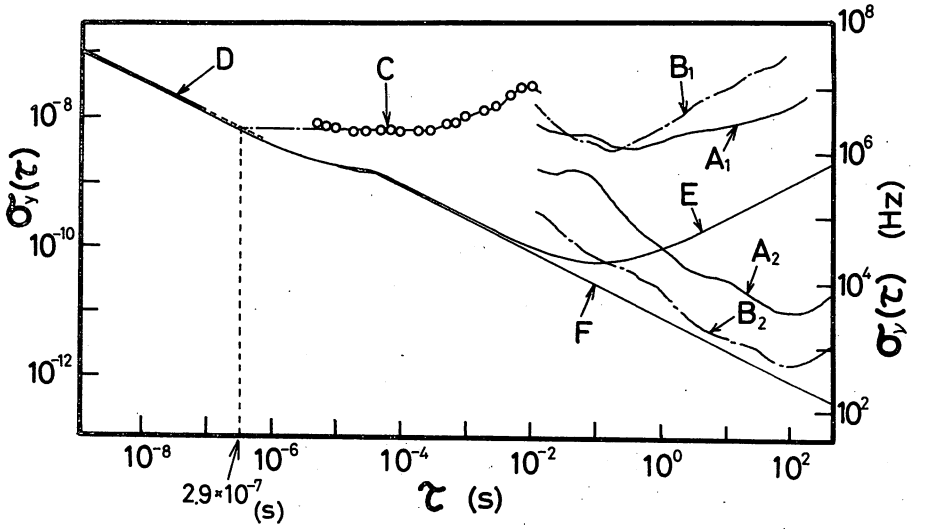

Fig. 5. Experimental results of the square root of the Allan variance of the frequency fluctuations of CSP-type lasers. A_1, B_1; experimental results of free-running lasers.[7,9] A_2, B_2; experimental results of frequency-stabilized lasers using absorption spectrum in H_2O vapor,[7] and ^{85}Rb–D_2 line,[9] respectively. C; experimental results of free-running laser measured in present work for $5\times10^{-6}\text{ s}\leqq\tau\leqq1\times10^{-2}$ s. D; experimental results of free-running laser estimated from results obtained by Yamamoto *et al.*[4] for $1\times10^{-9}\text{ s}\leqq\tau\leqq1\times10^{-7}$ s (eq. (52)). E; calculated results for free-running laser (curves F in Fig. 1). F; calculated result for frequency-stabilized lasers (curves H in Fig. 1).

concerning the frequency stabilization is to improve the stability for $2.9\times10^{-7}\,\mathrm{s}\leqq3\times10^{-1}\,\mathrm{s}$ until the Allan variance approaches the quantum-noise-limited value, where it is limited by the current source noise in actual systems.

As a reference, the 3.39 μm He–^{22}Ne laser is an appropriate example for comparison with semiconductor lasers because the oscillating characteristics and frequency stabilization have been fully reported as well as its use as a highly-accurate unified standard of both length and time.[24-31] The estimated frequency stability limit of the 3.39 μm He–^{22}Ne laser is shown in Fig. 6. Derivations of the results in this figure are described in Appendix B. By comparing Figs. 1 and 6, it can be seen that the contribution of the spontaneous emission to the He–^{22}Ne laser, for example, is far lower than that to the semiconductor laser. The ratio of the value of eq. (B.3) to that of eq. (22) is 2.3×10^{-8}.

In experimental tests on the frequency stabilization of the 3.39 μm He–^{22}Ne laser, a frequency stability as high as

$$\sigma_y^2(\tau)=1.0\times10^{-26}\ \text{at}\ \tau=10\,\mathrm{s} \tag{53}$$

has been obtained.[28]

§4. Estimation of the Spectral Width

In this chapter, several calculations are carried out to estimate the spectral width of the laser from its frequency stability. If it is assumed that the normalized amplitude fluctuations $a(t)/A_0$ is negligible compared with the normalized frequency fluctuations $y(t)$ in eqs. (1) and (3), the autocorrelation function of the electric field of eq. (1) is give by [15]

$$\begin{aligned}R_E(\tau)&=\langle\exp\left[\mathrm{i}\{2\pi\nu_0\tau+\varphi(t+\tau)-\varphi(t)\}\right]\rangle\\&=\langle\exp\left[\mathrm{i}\{2\pi\nu_0\tau+\delta\varphi(\tau)\}\right]\rangle.\end{aligned} \tag{54}$$

Since $\langle\delta\varphi(\tau)\rangle=0$, this can be expressed as

$$\begin{aligned}R_E(\tau)&=\exp\left(\mathrm{i}2\pi\nu_0\tau\right)\cdot\left[1-\frac{1}{2}\langle\delta\varphi^2\rangle+\cdots\right]\\&\cong\exp\left[\mathrm{i}2\pi\nu_0\tau-\langle\delta\varphi^2\rangle/2\right]\\&=\exp\left[\mathrm{i}2\pi\nu_0\tau-2(\pi\nu_0\tau)^2\sigma_y^2(\tau)\right]\end{aligned} \tag{55}$$

for small values of τ, where the relation $\langle\delta\varphi^2\rangle=(2\pi\nu_0\tau)^2\sigma_y^2(\tau)$ is used, as in eq. (17). Thus the spectral line shape can be derived from the Fourier transform of eq. (55), and is given by

$$I(\nu)=4\int_0^\infty R_E(\tau)\cdot\cos\left(2\pi\nu\tau\right)\mathrm{d}\tau, \tag{56}$$

and the spectral width is estimated from this line shape.

As an example, eqs. (55) and (56) are applied for the case in which the Allan variance is inversely proportional to τ as follows:

$$\sigma_y^2(\tau)=a\tau^{-1}. \tag{57}$$

In this case, the following Lorentzian spectral line shape can be readily derived from eqs. (55), (56), and (57).

$$|I(\nu)|^2=\frac{1}{\pi^2}\frac{1}{(\nu-\nu_0)^2+(\Delta\nu)^2}, \tag{58}$$

where the spectral width (HWHM) is

$$\Delta\nu=\pi\nu_0^2a. \tag{59}$$

In this calculation, only the values of $\sigma_y^2(\tau)$ for an integration time τ shorter than about 1×10^{-6} s are required, as in the numerical example shown below. This is because $R_E(\tau)$ for $\tau<1\times10^{-6}$ s contribute mainly to the Fourier integral of eq. (56). Therefore, eqs. (58) and (59) are also valid for the free-running laser in Fig. 1 (curve F) because the values of $\sigma_y^2(\tau)$ for $\tau<1\times10^{-6}$ s are given by the sum of those given by the spontaneous emission and carrier noise, which are inversely proportional to τ. By defining the quantity K as the ratio of the value of the carrier noise to that of the spontaneous emission, the width of the Lorentzian spectrum for the free-running laser is derived from eqs. (20), (57), and (59), and is expressed as

$$\Delta\nu=\frac{h\nu_0}{16\pi P_0}\left(\frac{c}{nL}\right)^2(\ln R-\alpha_1L)(\ln R)n_{sp}(1+K). \tag{60}$$

This is exactly the same as the result of the modified Schawlow-Townes theory given by Welford and Mooradian,[2] where the quantity K is represented by β^2, corresponding to α^2 in Henry's paper.[33] Since the quantity α or β was introduced to explain the additional spectral broadening by the fluctuations in the carrier density due to the spontaneous emission,[2,33] it corresponds to K, which represents the contribution of the carrier noise in 2.1.2 in the present paper. The agreement between eq. (60) with the previously-reported result shows the validity of the present formulations. The quantity α or β also represents the ratio of the change in the real part of the complex refractive index of the active layer to the change in the imaginary part due to the spontaneous emission, which depends on the working conditions of the lasers. The reported values of α or β fall between 3 and 6,[2,33] while that estimated from eqs. (22) and (25) is about 1.9. The cause of this diifference is now being investigated. Following these formulations, the narrowest limit of the spectral width can be estimated from eqs. (22), (25), (57), and (59), and is given by

$$\Delta\nu=5.5\times10^6\ (\mathrm{Hz})\quad(\mathrm{HWHM}) \tag{61}$$

for $I/I_{th}=1.3$.

On the other hand, the actual spectral width for a CSP-type laser with $L=300$ μm can also be derived by using the

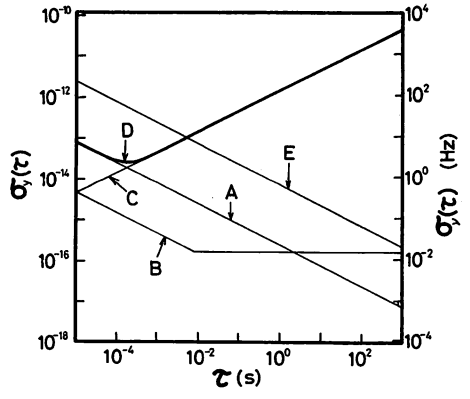

Fig. 6. Calculated results of the square root of the Allan variance of the frequency fluctuations for 3.39 μm He–^{22}Ne lasers. A; quantum noise (eq. (B.3)). B; current source noise (eq. (B.7). C; temperature noise (eq. (B.9)). D; free-running laser (sum of eqs. (B.3), (B.7), and (B.9)). E; frequency-stabilized laser using saturated absorption spectrum in CH_4 as frequency reference (eq. (B.12)).

experimental results shown in Fig. 5. The value of $R_E(\tau)$ for $\tau < 2.9 \times 10^{-7}$ s is determined by the Allan variance of curve D, and that for $\tau \geqq 2.9 \times 10^{-7}$ s is determined by the Allan variance of curve C. Thus it is seen that the value of $R_E(\tau)$ decreases monotonically with increasing τ, and at $\tau = 2.9 \times 10^{-7}$ s, its value is exp (−11) from eqs. (49), (52), and (55). This small value means that the Allan variance of curve C makes little contribution to $R_E(\tau)$, and it is almost wholly determined by that of curve D, i.e., by the spontaneous emission and the carrier noise. Thus it can easily be shown from eqs. (52), (57), and (59) that the spectral line shape is the Lorentzian with the spectral width of

$$\Delta\nu = 6.2 \times 10^6 \text{ (Hz)} \quad \text{(HWHM)} \tag{62}$$

for $I/I_{th} = 1.3$. This experimental result is consistent with the results of the measurements using a high-resolution Fabry-Perot interferometer.[1)]

As was pointed out in 2.1.2, the power spectral density $S_y(f)$ due to the carrier noise has a resonant peak at the Fourier frequency f_r of about a few GHz.[4, 8)] It can easily be seen that this resonant peak induces the modulation in the laser frequency, and an infinite number of low-intensity FM sidebands are generated at the frequency $\nu_0 \pm nf_r$, where $n = 1, 2, 3, \cdots$. Since the values of f_r are far larger than those of $\Delta\nu$ in eqs. (61) and (62), the strong optical carrier frequency component at ν_0 and weak FM sidebands at $\nu_0 \pm nf_r$ are well separated from each other in the frequency domain, which means that this frequency modulation does not cause any drastic line broadening in the spectrum of the optical carrier frequency component at ν_0. Therefore, the effect of this resonant peak in the carrier noise does not have to be considered in estimating the spectral width of the laser, and eqs. (61) and (62) can be safely used as the results of the estimated spectral width.

Further studies are now in progress to investigate the effect of this resonant peak on the spectral line shape by considering more detailed features of the resonant peak in the carrier noise.

§5. Summary

The frequency stability limits of 0.8 μm AlGaAs lasers for $\tau > 1 \times 10^{-9}$ s were estimated by using the Allan variance as a measure of the stability. The contributions of the quantum noise, i.e., the spontaneous emission noise, carrier noise, and current noise, were obtained. As additional noise, the current source noise and temperature noise were also discussed. The minimum of the square root of the Allan variance of the free-running laser, given by the superposition of the contributions from all of these different types of noise, was estimated to be

$$\sigma_y(\tau) = 6.3 \times 10^{-11} \text{ at } \tau = 1 \times 10^{-1} \text{ s}. \tag{63}$$

This value can be interpreted as the highest frequency stability limit of the free-running laser. It was also shown that the frequency stability of the stabilized laser is limited by the quantum noise, and is expressed as

$$\sigma_y(\tau) = \begin{cases} 3.5 \times 10^{-12} \tau^{-1/2} & (\tau < 5 \times 10^{-6} \text{ s}) \\ 9.0 \times 10^{-12} \tau^{-1/2} & (\tau > 5 \times 10^{-6} \text{ s}). \end{cases} \tag{64}$$

These estimated results were compared with the experimental results and with the frequency stability of 3.39 μm He−^{22}Ne lasers. Furthermore, the narrowest limit of the spectral width of the laser oscillation (HWHM) was estimated to be 5.5 MHz for $I/I_{th} = 1.3$ by using the estimated value of the frequency stability of the free-running laser. By using the experimental results of the frequency stability, the spectral width of the actual CSP-type laser was found to be 6.2 MHz for $I/I_{th} = 1.3$.

The results obtained in this study can also be used to estimate the frequency stabilities of other kinds of semiconductor laser such as 1.3 μm or 1.5 μm InGaAsP/InP lasers.

Acknowledgements

The authors would like to express their thanks to Drs. M. Nakamura and K. Aiki of Hitachi Ltd. for their support with the experiments, and to Drs. Y. Yamamoto and T. Mukai of NTT for showing them the galley proofs of their papers. They also wish to thank Prof. Y. Suematsu of their Institute for his encouragement in this study. They are also indebted to Dr. Y. Teramachi and Mr. M. Asada of their Institute for helpful discussions.

Appendix A

When the one-sided power spectral density $S_y(f)$ is proportional to f^M (M; integer, $-2 \leqq M \leqq 2$), the following table for the mutual conversion between $S_y(f)$ and $\sigma_y^2(\tau)$ can be obtained from eq. (8).[11, 12)]

Table A(I). Relation between $S_y(f)$ and $\sigma_y^2(\tau)$.[11, 12)]

M	$S_y(f)$	$\sigma_y^2(\tau)$
2	$h_2 f^2$ (*) ($2\pi f_h \tau \gg 1$)	$h_2 \cdot \frac{3f_h}{(2\pi)^2} \cdot \tau^{-2}$
1	$h_1 \cdot f^1$ (*) ($2\pi f_h \tau \gg 1$)	$h_1 \frac{1}{(2\pi)^2}\left[\frac{9}{2} + 3\ln(2\pi f_h \tau) - \ln 2\right] \cdot \tau^{-2}$
0	$h_0 \cdot f^0$	$\frac{1}{2} h_0 \cdot \tau^{-1}$
−1	$h_{-1} \cdot f^{-1}$	$(2 \cdot \ln 2) h_{-1} \cdot \tau^0$
−2	$h_{-2} \cdot f^{-2}$	$\frac{(2\pi)^2}{6} h_{-2} \cdot \tau^1$

(*) A low-pass filter with a cutoff frequency of f_h was used.

Appendix B: Frequency Stability of 3.39 μm He−^{22}Ne Lasers

B.1 *Free-running lasers*

B.1.1 *Spontaneous emission noise*

The quantum noise for frequency fluctuations of gas lasers would be due to the spontaneous emission only. Following the discussion of 2.1.1, the Allan variance due to this noise is given by eq. (17). In the gas laser, the quantities Γ_c, P, and n_{sp} in this equation are expressed as

$$\left.\begin{aligned} \Gamma_c &= \frac{c(1-R)}{4\pi L\sqrt{R}} \\ P &= \frac{P_0}{1-R} \\ n_{sp} &= \frac{N_2}{(N_2 - N_1)_{th}} \end{aligned}\right\}, \tag{B.1}$$

where N_1 is the population of the lower level of the laser transition, N_2 is that of the upper level, and $(N_2 - N_1)_{th}$ is

the threshold value of the population inversion. By using eqs. (17), (B.1) and the following values

$$\left.\begin{array}{l} \nu_0 = 8.85 \times 10^{13}\ \text{Hz},\ R = 0.95,\ n_{sp} = 2 \\ P_0 = 0.23\ \text{mW},\ L = 0.4\ \text{m} \end{array}\right\}, \tag{B.2}$$

the value of the Allan variance is found to be

$$\sigma_y^2(\tau) = 6.1 \times 10^{-32} \tau^{-1}. \tag{B.3}$$

This result is shown in Fig. 6 in the text.

B.1.2 *Current source noise*

In addition to the quantum noise source discussed in B.1.1, one of the additional sources investigated is the one from the regulated current supply used for the discuarge tube. The gas laser frequency is expressed as

$$\nu = \frac{\nu_G \Gamma_c + \nu_c \Gamma_G}{\Gamma_c + \Gamma_G}, \tag{B.4}$$

where ν_c is the resonance frequency of the cavity, ν_G is the center frequency of the gain curve, and Γ_G is the width (HWHM) of the gain curve. As the discharge current noise induces fluctuations $\delta\nu_G$ in the center frequency of the gain curve, the fluctuations of the laser frequency $\delta\nu$ are given by

$$\delta\nu = \frac{\Gamma_c}{\Gamma_G} \delta\nu_G, \tag{B.5}$$

where the relation $\Gamma_G \gg \Gamma_c$ is used with eq. (B.4). The change in the center frequency of the gain curve due to the discharge current has been measured as -1.4 GHz/A for the 3.39 μm He–^{22}Ne laser.[32] By considering that the current fluctuations can be reduced to as low as that of eq. (31) or curve A in Fig. 3, the Allan variance $\sigma_y^2(\tau)$ due to this current source noise is obtained from eqs. (31), (B.5), and the above value of the current shift, and is expressed as

$$\sigma_y^2(\tau) = \begin{cases} 9.8 \times 10^{17} (\Gamma_c V_n / \Gamma_G R_s \nu_0)^2 \tau^{-1} & (\tau < f_c^{-1}) \\ 2.7 \times 10^{18} (\Gamma_c V_n / \Gamma_G R_s \nu_0)^2 f_c & (\tau \geqq f_c^{-1}). \end{cases} \tag{B.6}$$

Again using $V_n = 15\ \text{nV}/\sqrt{\text{Hz}}$, $f_c = 50$ Hz, $R_s = 25\ \Omega$, and $\Gamma_G = 1.4$ GHz,

$$\sigma_y^2(\tau) = \begin{cases} 2.2 \times 10^{-34} \tau^{-1} & (\tau < 2 \times 10^{-2}\ \text{s}) \\ 3.0 \times 10^{-32} & (\tau \geqq 2 \times 10^{-2}\ \text{s}). \end{cases} \tag{B.7}$$

This result is shown in Fig. 6.

In actual lasers, however, fluctuations in the discharge current also induce plasma instabilities in the discharge tube, which induce further frequency fluctuations.[30] Since these fluctuations depend on experimental conditions such as the structure of the discharge tube, gas pressure, and so on, and there are no quantitative theories concerning these, the frequency fluctuations due to this phenomenon are not discussed here. This topic is a problem remaining to be solved for gas lasers.

B.1.3 *Temperature noise*

Another additional noise source examined is the temperature fluctuations. Here, it is assumed that the temperature fluctuations of the laser cavity are reduced to as low as that of eq. (38) by installing the laser in a thermobath. As a thermal change in the cavity length induces a change in the resonant frequency ν_c in eq. (B.4), the power spectral density of the laser frequency fluctuations is given by

$$S_y(f) = \kappa^2 S_T(f), \tag{B.8}$$

where eqs. (38), (B.4), and the relation $\Gamma_G \gg \Gamma_c$ are used. The quantity κ in this equation represents the temperature coefficient of the expansion of the spacer used to define the cavity legth. For $\kappa = 1 \times 10^{-6}\ \text{K}^{-1}$, the Allan variance $\sigma_y^2(\tau)$ is obtained from eqs. (8) and (B.8), and is expressed as

$$\sigma_y^2(\tau) = 2.0 \times 10^{-24} \tau, \tag{B.9}$$

which is shown in Fig. 6.

In the actual experimental setup, fluctuations larger than that by eq. (B.9) would be induced because the self-heating by the discharge tube must induce further temperature fluctuations in the thermobath.

The Allan variance for the free-running laser is given by the sum of eqs (B.3), (B.7), and (B.9), and is shown in Fig. 6. The minimum of the Allan variance of the free-running laser is

$$\sigma_y^2(\tau) = 7.0 \times 10^{-28} \text{ at } \tau = 2 \times 10^{-4}\ \text{s}, \tag{B.10}$$

or its square root is

$$\sigma_y(\tau) = 2.7 \times 10^{-14} \text{ at } \tau = 2 \times 10^{-4}\ \text{s}. \tag{B.11}$$

B.2 *Frequency-stabilized lasers*

To stabilize the frequency of the 3.39 μm He–^{22}Ne laser, a saturated absorption spectrum in CH_4 has been successfully used as a frequency reference by installing an absorption cell of CH_4 inside the cavity. The frequency stability of this stabilized laser has been estimated in Shimoda's paper (eq. (30) of ref. 23) for the same operating conditions as given by eq. (B.2), and is expressed as

$$\sigma_y^2(\tau) = 5.5 \times 10^{-29} \tau^{-1}. \tag{B.12}$$

This result is shown in Fig. 6. It can be seen that this value is larger than that of the quantum-noise-limited value of eq. (B.3). This relation is contrary to that of the semiconductor laser, and it means that the frequency stability of the stabilized laser is given by eq. (B.12) itself but does not reach the quantum-noise-limited value of eq. (B.3).

References

1) T. Takakura, K. Iga and T. Tako: Jpn. J. Appl. Phys., **19** (1980) L725.
2) D. Welford and A. Mooradian: Appl. Phys. Lett. **40** (1982) 865.
3) Y. Yamamoto: IEEE J. Quantum Electron., **QE-19** (1983) 34.
4) Y. Yamamoto, S. Saito and T. Mukai: IEEE J. Quantum Electrons., **QE-19** (1983) 47.
5) H. Tsuchida, S. Sanpei, M. Ohtsu and T. Tako: Jpn. J. Appl. Phys., **19** (1980) L721.
6) H. Tsuchida, M. Ohtsu and T. Tako: Jpn. J. Appl. Phys., **20** (1981) L403.
7) H. Tsuchida, M. Ohtsu and T. Tako: Jpn. J. Appl. Phys., **21** (1982) L1.
8) H. Tsuchida, M. Ohtsu and T. Tako: Trans. IECE Jpn, **E65** (1982) 65.
9) H. Tsuchida, M. Ohtsu, T. Tako, N. Kuramochi and N. Oura: Jpn. J. Appl. Phys., **21** (1982) L561.
10) D. Allan: Proc. IEEE, **54** (1966) 221.
11) J. A. Barnes, A. R. Chi, L. S. Cutler, D. J. Healey, D. B. Leeson, T. E. McGunigal, J. A. Mullen, Jr., W. L. Smith, R. Sydnor, R. F. C. Vessot and G. M. R. Winkler: "*Characterization of Frequency*

Stability" NBS Technical Note 394. US Government Printing Office, Washinton D.C., Oct., 1970.
12) J. A. Barnes, A. R. Chi, L. S. Cutler, D. J. Healey, D. B. Leeson, T. E. McGunigal, J. A. Mullen, Jr., W. L. Smith, R. L. Sydnor, R. F. C. Vessot and G. M. R. Winkler: IEEE Trans. Instrum. Meas., **MI-20** (1971) 105.
13) K. Aiki, M. Nakamura, T. Kuroda, J. Umeda, R. Ito, N. Chinone and M. Maeda: IEEE J. Quantum Electron., **QE-14** (1978) 89.
14) V. Koreman: Phys. Rev. Lett. **14** (1965) 293.
15) K. Shimoda, T. Yajima, Y. Ueda, T. Shimizu and T. Kasuya: *Quantum Electronics* (Syokabo, Tokyo, 1972) Chapter 4 [in Japanese].
16) *Linear Databook*, National Semiconductor Corp., Santa Clara, 1980.
17) M. Ito and T. Kimura: IEEE J. Quantum Electron., **QE-16** (1980) 910.
18) S. Kobayashi and T. Kimura: IEEE J. Quantum Electron., **QE-18** (1982) 575.
19) H. Tsuchida, T. Tako and M. Ohtsu: Jpn. J. Appl. Phys., **22** (1983) L19.
20) Z. Priel: J. Phys. E. Sci. Instrum., **11** (1978) 27.
21) Y. Noguchi, Y. Teramachi and T. Musha: Jpn. J. Appl. Phys., **21** (1982) 61.
22) *Hitachi Laser Diode Application Manual* (1978).
23) K. Shimoda: Jpn. J. Appl. Phys., **12** (1973) 246.
24) A. L. Bloom, W. E. Bell and R. C. Rempel: Appl. Opt., **2** (1963) 317.
25) J. L. Hall: IEEE J. Quantum Electron., **QE-4** (1968) 638.
26) R. L. Barger and J. L. Hall: Phys. Rev. Lett., **22** (1969) 4.
27) T. Tako, M. Ohi, Y. Akimoto, A. Sugiyama and K. Shimoda: Jpn. J. Appl. Phys., **9** (1970) 1535.
28) H. Hellwing, H. E. Bell and J. C. Bergquist: J. Appl. Phys., **43** (1972) 450.
29) K. Shimoda: Jpn. J. Appl. Phys., **12** (1973) 1393.
30) M. Ohi and Y. Akimoto: Jpn. J. Appl. Phys., **15** (1976) 1853.
31) M. Ohtsu, S. Ohta and T. Tako: Jpn. J. Appl. Phys., **20** (1981) 1701.
32) M. Ohi: Jpn. J. Appl. Phys., **12** (1973) 1377.
33) C. Henry: IEEE J. Quantum Electron., **QE-18** (1982) 259.

JAPANESE JOURNAL OF APPLIED PHYSICS
VOL. 23, NO. 6, JUNE, 1984 pp. 760–764

Derivation of the Spectral Width of a 0.8 μm AlGaAs Laser Considering 1/f Noise*

Motoichi OHTSU and Shinichi KOTAJIMA

International Cooperation Center for Science and Technology, Tokyo Institute of Technology, 2-12-1, O-okayama, Meguro-ku, Tokyo 152

(Received November 10, 1983; accepted for publication March 24, 1984)

The spectral profile of a CSP-type 0.8 μm AlGaAs laser and its spectral width (FWHM) were estimated from experimental results on the lasers FM noise at room temperature. The power-independent spectral width was also derived from the recently-reported power-independent $1/f$ noise. The result was 2.0 MHz, which agrees well with previous experimental results. The power-dependent width $\Delta\nu$ was also derived as 2.0 MHz $< \Delta\nu \leqq$ 8.8 MHz for $0 < (I/I_{th} - 1)^{-1} \leqq 7$, where I and I_{th} represent the injection current and its threshold value, respectively.

§1. Introduction

Since the spectral properties of semiconductor lasers have become greatly improved, a number of application using these lasers as light sources, such as optical communications, optical disk systems, fiber gyroscopes etc., have been investigated. However, a narrower spectral width is required for these applications, especially in coherent optical communications, and several basic experimental studies have been done on measuring and narrowing the spectral width of these lasers.[1-4]

One of these studies was by Welford and Mooradian,[1] who discovered the power-independent spectral width in 0.8 μm AlGaAs lasers, an effect which cannot be explained by the Schawlow-Townes' formula. They attributed it to carrier density fluctuations in the devices. As well as this, a power-independent $1/f$ noise in the frequency fluctuations of semiconductor lasers has recently been observed by Kikuchi and Okoshi,[5] and this is also caused by carrier density fluctuations, as pointed out in ref. 1.

In this paper, a relation between the spectral width of 0.8 μm AlGaAs lasers and the laser power, i.e., the injection current, is presented, using the authors' experimental results on FM noise and those on the power-independent $1/f$ noise by Kikuchi and Okoshi.[5] From these results, the value of the power-independent spectral width is estimated and the deviation from the Schawlow-Townes' formula[6] is reported.

§2. Measurement of FM Noise

There are several ways of measuring the spectral width of semiconductor lasers, e.g., by using a high-finesse Fabry-Perot interferometer,[2] by the delayed self-heterodyne technique,[3] and so on. However, these methods have the common problem, i.e., extra spectral broadening or narrowing is induced if the reflected light wave comes back into the laser cavity from the mirror surface of the interferometer or the ends of the optical fibers employed in the measurements. These reflected waves must be completely suppressed for accurate measurements of the intrinsic spectral width. In this study, a technique which is free from the effects of reflected light waves was employed. In the method, FM noise is measured by a tilted Fabry-Perot interferometer. The spectral profile and spectral width are then derived from the experimental results on the FM noise by taking a Fourier transformation.

Figure 1 shows the experimental setup for measuring the power spectral density of the frequency fluctuations. A single-mode, CSP-type AlGaAs laser with a cavity length of 300 μm was used. The laser was mounted on a heat sink consisting of a copper block, and its temperature was stabilized to within ±0.01 K at room temperature by using a Peltier element. A low-noise d.c. current source was used to drive the laser. The noise of this source, induced from the low-noise operational amplifier used, was measured and found to be as low as the theoretical limits.[7] The optical isolator was composed of a Fresnel prism and a Glan-Thompson prism, while the Fabry-Perot interferometer consisted of a rigid cylindrical rod of fused silica with multilayered films coated on both ends, and had a free spectral range of 3.4 GHz with a finesse of about 30. The linear part of the slope of the transmission spectrum of this interferometer was used as a frequency discriminator. However, the slope of this linear part, and the finesse of the interferometer, do not have to be large enough for FM noise measurements, because the sensitivity of the measurements can be maintained at a high enough level by appropriately increasing the gain of the preamplifiers for the detectors, even if the finesse is low. The finesse can therefore be reduced by slightly tilting the optical axis of

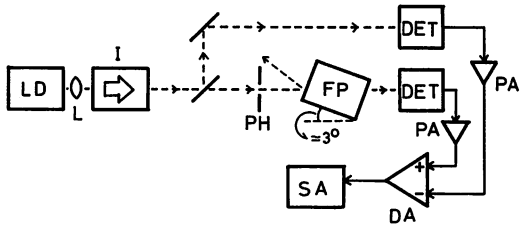

Fig. 1. Experimental setup for FM noise measurements. LD: 0.8 μm AlGaAs laser (CSP-type). L: AR-coated collimator lens. I: Optical isolator. FP: Fabry-Perot interferometer. PH: Pinhole. PA: Preamplifier. DA: Differential amplifier. SA: Spectrum analyzer.

*This work was presented orally at the Meeting on Opto-quantum Electronics, Inst. Electron. & Commun. Eng., Jpn, October, 1983 (paper number OQE83-67).

the interferometer from the direction of propagation of the laser beam. The effect of the reflected wave can be suppressed by this configuration, which is the main advantage of the present method. The angle of tilt was 3 degrees, and the distance between the interferometer and the laser was about 30 cm.

Figure 2 shows the experimental results on the power spectral density $S_y(f)$ of the frequency fluctuations at a temperature of 293 K. Here, $y=\delta\nu(t)/\nu_0$, where $\delta\nu(t)$ and ν_0 represent the temporal fluctuations and stationary value of the laser frequency, respectively. The figure shows the results for 1 MHz$\leqq f \leqq$20 MHz. For $f<1$ MHz, the value of $S_y(f)$ increased with decreasing f because of the slow thermal expansion of the laser cavity. As this expansion gives only the drift of the center frequency of the laser spectrum, it does not have to be considered in estimating the spectral width. Measurements for $f>20$ MHz were not carried out because the bandwidth of the preamplifier for the Si-avalanche photodiode was 20 MHz. However, since $S_y(f)$ is known to take a constant value for $f>$ several mega herz,[7] the value of $S_y(f)$ for $f>20$ MHz can be estimated by extrapolating the curves in Fig. 2. $S_y(f)$ also shows a resonant peak at a Fourier frequency f_r (a few giga herz) because of fluctuations in the carrier density.[8] This resonant peak induces modulation in the laser frequency, and an infinite number of low-intensity FM sidebands are generated at the frequency $\nu_0 \pm nf_r$, where $n=1, 2, 3, \cdots$. Since the value of f_r is far larger than that of the spectral width of the laser oscillation, the strong optical carrier frequency component at ν_0 and weak FM sidebands at $\nu_0 \pm nf_r$ are well separated from each other in the frequency domain. This means that this frequency modulation does not induce any line broadening in the spectrum of the optical carrier frequency at ν_0. Therefore, we can say that the spectral width is determined not by this sharp resonant peak but by a broad-band white noise as shown in Fig. 2. The effects of this resonant peak are also briefly described in ref. 7.

The magnitude of the white noise in Fig. 2, due to the intrinsic quantum noise, is inversely proportional to the injection current I when the laser is operated with a single longitudinal mode.[7,8] Therefore, $S_y(f)$ can be expressed as

$$S_y(f)=A_0\cdot(I/I_{th}-1)^{-1} \quad (\mathrm{Hz}^{-1}), \tag{1}$$

where I_{th} and A_0 represent the threshold value of the injection current and a proportional constant, respectively. The measured value of I_{th} was 53 mA at a temperature of 293 K. Figure 3 shows the relation between $S_y(f)$ and $(I/I_{th}-1)^{-1}$ for $f=10$ MHz and 18 MHz, these values being extracted from Fig. 2 to determine the value of A_0 in eq. (1). It can be seen that the parts for $(I/I_{th}-1)^{-1}>8.3$ on these curves do not follow eq. (1). This is probably due to the extra frequency fluctuations caused by the longitudinal-mode competition phenomenon because of the multimode oscillation around the threshold current. However, the parts for $(I/I_{th}-1)^{-1}<5.9$, where the single-longitudinal mode oscillation can be realized, follow eq. (1) well. Therefore, the value of A_0 should be determined from the results for $(I/I_{th}-1)^{-1}<5.9$ in Figs. 2 and 3. It is then given by

$$A_0=2.8\times10^{-24} \quad (\mathrm{Hz}^{-1}). \tag{2}$$

As described above, one should be careful to avoid using the values of the FM noise in the multimode oscillation region when the value of the proportional constant A_0 is derived. If these data are used, the proportional constant is overestimated. In the present experiment, the intensities of the satellite longitudinal mode were less than 1% of the main mode in the region $(I/I_{th}-1)^{-1}>8.3$. Extra FM noise can be induced even by such weak satellite modes, and the deviation from the linear relation of eq. (1) can be seen in this region.

The results of FM noise measurements are also reported in refs. 5 and 8. However, the derivation of the spectral width from the measured values of the FM noise is not presented in these papers. The detailed relation between the magnitude of the noise and $(I/I_{th}-1)^{-1}$, and the experimental details for removing the effect of reflected light are not described in these papers, either. In the present paper, however, the spectral width will be estimated, in the next section, using the experimental results on FM noise

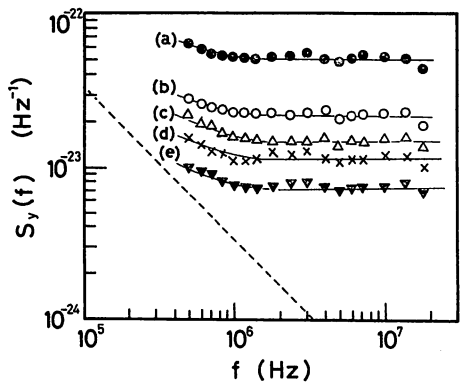

Fig. 2. Experimental results on power spectral density $S_y(f)$ of FM noise for several values of injection current (solid curves) at 293 K, where $(I/I_{th}-1)^{-1}=11.1$ (a), 8.3(b), 5.9 (c), 4.2(d), and 2.9 (e). The measured value of I_{th} was 53 mA. The broken line represents the $1/f$ noise reported by Kikuchi *et al.*[5]

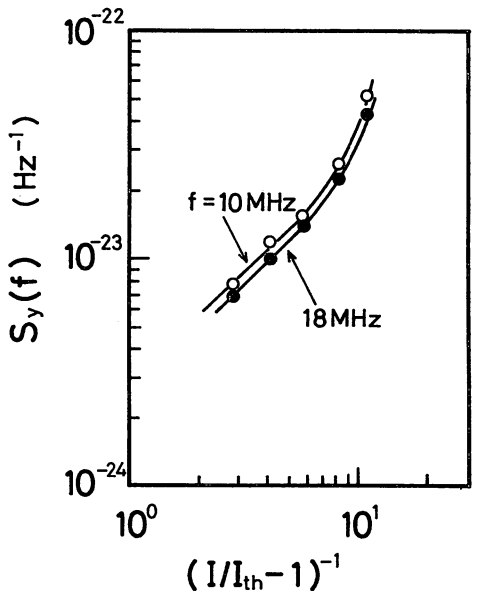

Fig. 3. Relation between $S_y(f)$ and $(I/I_{th}-1)^{-1}$ at $f=10$ and 18 MHz, extracted from Fig. 2.

measurements. For this purpose, accurate measurements of the FM noise, free from reflected light, were carried out using a tilted Fabry-Perot interferometer, and a linear relation between the noise magnitude and $(I/I_{th}-1)^{-1}$ was found.

As the frequency fluctuations depend on $(I/I_{th}-1)^{-1}$, the spectral width may be expected to depend on $(I/I_{th}-1)^{-1}$ as well. This corresponds to the well-known Schawlow-Townes' formula.[6] However, it has recently been reported that the power-independent $1/f$ noise can also exist in the frequency fluctuations,[5] and is given by

$$S_\nu(f)=A_1\cdot f^{-1}\quad (\mathrm{Hz}^{-1}), \tag{3}$$

where

$$A_1=3.4\times 10^{-18}. \tag{4}$$

Therefore, the actual power spectral density should be given by the sum of eqs. (1) and (3). In the next section, the spectral profile of the laser oscillation and its spectral width are estimated from the power spectral density of the frequency fluctuations, which is given by the sum of eqs. (1) and (3).

§3. Derivations of the Spectral Profile and Spectral Width

In this section, the sectral profile $I(\nu)$ and its width $\Delta\nu$ (full width at half-maximum) are derived when $S_\nu(f)$ is expressed as

$$S_\nu(f)=A_0\cdot(I/I_{th}-1)^{-1}+A_1\cdot f^{-1}\quad (\mathrm{Hz}^{-1}), \tag{5}$$

which is the sum of eqs. (1) and (3) in §2.

When $S_\nu(f)$ is given by eq. (5), the Allan variance $\sigma_y^2(\tau)$, which is an alternative measure of frequency fluctuations in the time domain, is expressed as[7,9]

$$\sigma_y^2(\tau)=\frac{1}{2}\{A_0\cdot(I/I_{th}-1)^{-1}\}\cdot\tau^{-1}+(2\ln 2)\cdot A_1\equiv a_0\cdot\tau^{-1}+a_1, \tag{6}$$

where τ represents the integration time of the measurements, and the following conversion formula from $S_\nu(f)$ to $\sigma_y^2(\tau)$ was used[7,9]:

$$\sigma_y^2(\tau)=2\int_0^\infty S_\nu(f)\cdot\frac{\sin^4(\pi f\tau)}{(\pi f\tau)^2}\cdot \mathrm{d}f. \tag{7}*$$

The autocorrelation function $R_E(\tau)$ of the electric field $E(t)$ of a laser can be expressed by using $\sigma_y^2(\tau)$, which is given by (eq. (55) of ref. 7)

$$\begin{aligned}R_E(\tau)&=\langle E(t)\cdot E^*(t+\tau)\rangle/\langle E(t)\cdot E^*(t)\rangle=\exp\{\mathrm{i}\cdot 2\pi\nu_0\tau-2(\pi\nu_0\tau)^2\cdot\sigma_y^2(\tau)\}\\&=\exp\{\mathrm{i}\cdot 2\pi\nu_0\tau-2(\pi\nu_0)^2\cdot(a_0\tau+a_1\tau^2)\},\end{aligned} \tag{8}*$$

where i is the unit of an imaginary number, $\langle\ \rangle$ represents the time average, and * represents the complex conjugate, respectively. The Fourier transformation of this autocorrelation function gives the spectral profile $I(\nu)$:

$$I(\nu)=\int_0^\infty R_E(\tau)\cdot\exp(-\mathrm{i}2\pi\nu\tau)\cdot\mathrm{d}\tau+\mathrm{c.c.}=\int_0^\infty\exp\{\mathrm{i}\cdot 2\pi(\nu_0-\nu)\tau-2(\pi\nu_0)^2\cdot(a_0\tau+a_1\tau^2)\}\cdot\mathrm{d}\tau+\mathrm{c.c.}, \tag{9}$$

where ν and c.c. represent the Fourier frequency and the complex conjugate of the first term, respectively. This equation can be transformed to

$$I(\nu)=\frac{1}{\sqrt{2(\pi\nu_0)^2a_1}}\int_0^\infty\exp(\mathrm{i}\cdot 2\zeta x-x^2)\cdot\mathrm{d}x+\mathrm{c.c.}\equiv\frac{1}{\pi\nu_0\sqrt{2a_1}}\cdot\mathrm{Im}\,[Z(\zeta)], \tag{10}$$

where

$$\begin{aligned}x&\equiv\sqrt{2(\pi\nu_0)^2a_1}\cdot\tau\\\zeta&\equiv\frac{\nu_0-\nu}{\sqrt{2\nu_0^2a_1}}+\mathrm{i}\cdot\frac{\pi\nu_0a_0}{\sqrt{2a_1}}\end{aligned}\quad, \tag{11}$$

and $Z(\zeta)$ is the complex function known as the "Plasma Dispersion Function" whose value was presented in a numerical table by Fried and Conte.[12] Im $[Z(\zeta)]$ represents its imaginary part. It should be noted again that a_0 and a_1 in eqs. (10) and (11) correspond to the first and second terms in eqs. (5) and (6), respectively. The solid curves of Fig. 4 show the spectral profile $I(\nu)$ for several values of the injection current calculated from eq. (10). As a reference, the broken curves represent the Lorentzian spectral profiles using the first term of eqs. (5) and (6) only, which corresponds to the result obtained using Schawlow-Townes' formula. It can be seen that the spectral shape is

*In several papers, e.g., ref. (10), $R_E(\tau)$ is expressed not by using eq. (7), but by the following integral:

$$\int_0^\infty S_\nu(f)\frac{\sin^2(\pi f\tau)}{(\pi f\tau)^2}\mathrm{d}f$$

However, it should be pointed out here that the expression for $R_E(\tau)$ in the present paper is more accurate than that determined using this integral, especially when nonstationary fluctuation processes, e.g., flicker noise ($S_\nu(f)\propto f^{-1}$) and random walk ($S_\nu(f)\propto f^{-2}$), exist in the relevant noise properties. For further details on this discussion, see, for example, refs. 9 and 11. Extensive experimental and theoretical studies on this topic have been carried out in the field of frequency control and metrology in quartz oscillators, atomic clocks, hydrogen masers, and gas lasers.

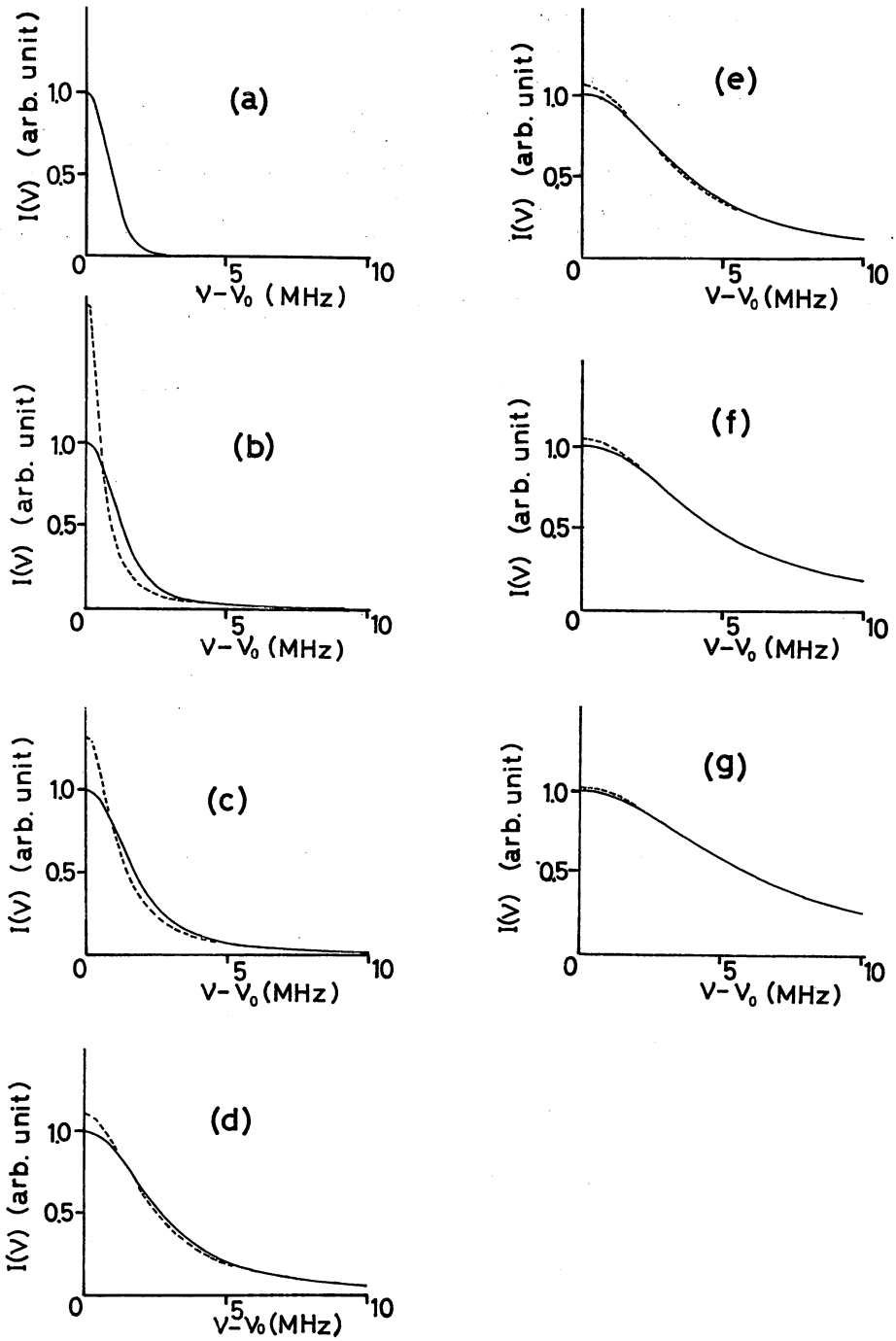

Fig. 4. Calculated spectral shapes for several values of $(I/I_{th}-1)^{-1}$. The broken curves represent the Lorentzian line shapes obtained by neglecting the $1/f$ noise in eq. (5). Here, $(I/I_{th}-1)^{-1}=0$ (a), 0.9 (b), 1.9 (c), 3.7 (d), 5.6 (e), 7.5 (f), and 9.3 (g).

considerably deformed from the Lorentzian when $(I/I_{th}-1)^{-1}\cong 0$, owing to the effect of the $1/f$ noise.

Figure 5 shows the relation between the spectral width and $(I/I_{th}-1)^{-1}$. The broken line in this figure represents the result derived by considering the white noise, i.e., the first term of eqs. (5) and (6), only. Therefore, this line corresponds to the result given by Schawlow-Townes' formula. The solid curve represents the result obtained by adding the $1/f$ noise to this white noise, i.e., using the second terms of eqs. (5) and (6) also. The power-independent spectral width on this curve, i.e., the value of $\Delta\nu$ at $(I/I_{th}-1)^{-1}=0$, is 2.0 MHz, as induced by $1/f$ noise. This value is almost equal to the experimental results by Welford and Mooradian (1.9 MHz at 273 K).[1] On the other hand, the power-dependent spectral width, i.e., the value of $\Delta\nu$ for $(I/I_{th}-1)^{-1}\neq 0$, takes the following value:

$$2.0\ \text{MHz}<\Delta\nu\leqq 8.8\ \text{MHz} \quad \text{for } 0<(I/I_{th}-1)^{-1}\leqq 7. \tag{12}$$

The result of eq. (12) is considered sufficiently reliable, because it was derived from careful measurements of FM noise which were free from the effects of reflected light, and is consistent with previously-reported spectral width measurements.[2,8]

From the results in Fig. 5, it is concluded that one origin of the power-independent spectral width is the $1/f$ noise of

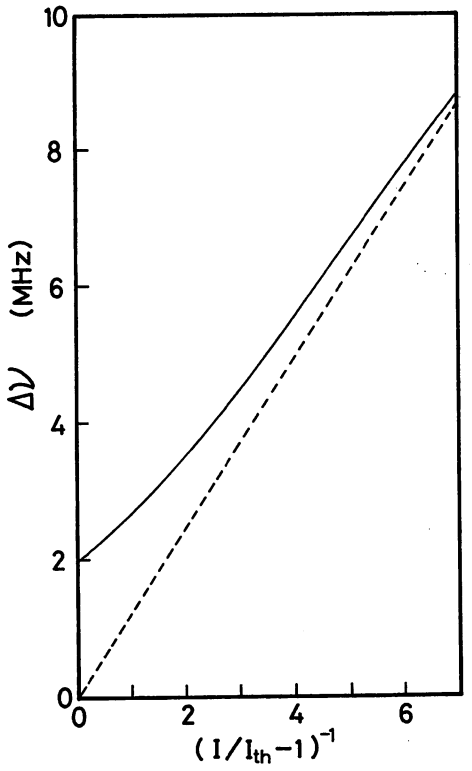

Fig. 5. Relation between spectral width $\Delta\nu$ (full width at half-maximum) and $(I/I_{th}-1)^{-1}$. The solid curve shows the present result, while the broken line shows the results obtained when the $1/f$ noise is neglected in eq. (5).

frequency fluctuations. This is quite plausible, because the $1/f$ noise of several quantities, e.g., current fluctuations, is commonly observed in a variety of semiconductor devices.[13] We can also conclude that the power-dependent spectral width has a value lower than ten MHz for $(I/I_{th}-1)^{-1} \leqq 7$, as shown by eq. (12).

§4. Summaries

The spectral profile of a 0.8 μm AlGaAs laser and its spectral width were derived from FM noise measurements. The existence of a power-independent spectral width was demonstrated by adding the recently-reported $1/f$ noise to the white noise in the frequency fluctuations. The value of the power-independent width was 2.0 MHz (FWHM), and the power-dependent width was $2.0\ \text{MHz} < \Delta\nu \leqq 8.8\ \text{MHz}$ for $0 < (I/I_{th}-1)^{-1} \leqq 7$.

Acknowledgements

We would like to express our thanks to Dr. M. Nakamura of Hitachi Ltd. for his support with the experiments, and to Dr. K. Kikuchi of the University of Tokyo for his valuable comments. We also wish to thank Profs. T. Tako and Y. Suematsu of our institute for their encouragement during this work.

References

1) D. Welford and A. Mooradian: Appl. Phys. Lett. **40** (1982) 560.
2) T. Takakura, K. Iga and T. Tako: Jpn. J. Appl. Phys. **19** (1980) L725.
3) T. Okoshi, K. Kikuchi and A. Nakayama: Electron. Lett. **16** (1980) 630.
4) F. Fabre, D. L. Guen and J. C. Simon: IEEE J. Quantum Electron. **QE-18** (1982) 1712.
5) K. Kikuchi and T. Okoshi: Electron. Lett. **19** (1983) 812.
6) A. L. Schawlow and C. H. Townes: Phys. Rev. **112** (1958) 1940.
7) M. Ohtsu, H. Fukada, T. Tako and H. Tsuchida: Jpn. J. Appl. Phys. **22** (1983) 1157.
8) Y. Yamamoto, S. Saito and T. Mukai: IEEE J. Quantum Electron. **QE-19** (1983) 47.
9) J. A. Barnes, A. R. Chi, L. S. Cutler, D. J. Healey, D. B. Lesson, T. E. McGunigal, J. A. Mullen, Jr., W. L. Smith, R. L. Sydner, R. F. C. Vessot and G. M. R. Winkler: IEEE Trans. Instrum. Meas. **MI-20** (1971) 105.
10) Y. Yamamoto: IEEE J. Quantum Electron. **QE-19** (1983) 34.
11) P. Kartaschoff: *Frequency and Time* (Academic Press, New York, 1978) Chapter 2.
12) B. D. Fried and S. D. Conte: *The Plasma Dispersion Function* (Academic Press, New York, 1961).
13) T. J. Boem, H. R. Bilger and J. L. Tandon: *Proc. the Symposium on 1/f Fluctuations* (Institute of Electrical Engineers of Japan, Tokyo, 1977) p. 62.

[Note added in proof]

On the same date this paper was received, a letter on the relation between $1/f$ noise and spectral width was published (M. J. O'Mahony and I. D. Henning: Electron. Lett. **19** (1983) 1000). However, the theoretical discussion in this letter is more approximate, and the deviation from the Schawlow-Townes' formula is not discussed.

論　文

UDC 621.375.826.038.825.5:621.316.726.078:681.323

半導体レーザの周波数の計算機制御

非会員　岡崎　博之[†*]　　正　員　大津　元一[††]　　正　員　田幸　敏治[†]

Frequency Control of Semiconductor Lasers Using a Microcomputer

Hiroyuki OKAZAKI[†*], *Nonmember*, Motoichi OHTSU[††] *and* Toshiharu TAKO[†], *Members*

あらまし　半導体レーザの周波数は注入電流制御により高い安定度が得られる．本研究は，ファブリ・ペロー干渉計の共鳴周波数を基準としたAlGaAs・DH レーザの周波数の安定化を行うのに，その制御系に計算機を組み入れ，レーザ周波数安定度実時間測定装置で安定度を評価しながら，制御変数を自動的に最適化することを試みた．

その結果，手動で制御系を設定した場合にくらべて，半桁程度安定度が向上し，積分時間1～10sにおいて2×10^{-12}の安定度を得た．また，レーザに外乱が加わり，安定度が劣化した場合，制御変数が補正され，100s 程度で安定度が回復することが確かめられた．この手法により，レーザが異なり，また環境条件が異なっても自動的に最適安定化が実現され，また，気体レーザなどの他のレーザにも適用できる．

1. まえがき

半導体レーザを高分解分光や精密計測，そして現在研究が進められているコヒーレント光通信[(1)]の光源として用いようとすると，レーザ光のスペクトル幅と共に発振周波数の安定度が問題となる．半導体レーザの周波数は，温度および電流の変化に対して非常に敏感で，例えば本研究で使用したAlGaAs レーザの場合，温度に対して－20 GHz／K，電流に対して（－3～－7）GHz／mA の割合で変化する．このためフリーランニング状態の半導体は周波数が大きく変動し，スペクトル線幅程度の安定度（数MHz）を得るためには，周波数の安定化，すなわち外部からの周波数制御が必要になる．

半導体レーザの発振周波数を安定化するには，レーザ周波数を基準周波数（例えば，原子・分子の吸収線やファブリ・ペロー干渉計）と比較し，その差に比例した信号をレーザ系にフィードバックすることによって実現できる．その周波数制御には温度および電流が用いられるが，取扱いの容易さ，応答速度の速さや高い安定度が得られる点で，一般に電流制御が用いられる[(2),(3)]．そしてレーザ周波数の安定度を見ながら制御変数（例えば，利得や帯域）を手動で調整し，最適値を見出すことが行なわれてきた．しかしながら，レーザが異なると高い安定度を得るための最適の制御変数の値が変化することがあり，また，レーザ系に外乱が加わった際に，最適条件から外れて周波数安定度の劣化をひきおこすことがある．

そこで，本研究では制御系に計算機を組み入れ，安定度を実時間で測定しながら制御変数を最適値に設定するよう制御することにより，

(i)　高い周波数安定度の実現

(ii)　外乱による安定度劣化の補正

を計った．

レーザの種類によって周波数基準や制御系は異なるであろうが，そのような場合でもこの計算機を用いたシステムは応用可能である．

2. 実験装置

本実験で使用した半導体レーザはAlGaAs のCSP（Channeled Substrated Planar）レーザ[(4)]で，発振波長は$\lambda=0.78\ \mu$mである．また，周波数基準として用いたファブリ・ペロー干渉計は溶融石英製で，反射率$R=90\%$，厚さ$d=10$mm で自由スペクトル域

†東京工業大学精密研究所，横浜市
Research Laboratory of Precision Machinery and Electronics, Tokyo Institute of Technology, Yokohama-shi, 227 Japan
††東京工業大学理工学国際交流センター
International Cooperation Center for Science and Technology, Tokyo Institute of Technology, Tokyo, 152 Japan
*現在，横河ヒューレット・パッカード株式会社

は10GHzである．

2.1 光学系

半導体レーザの周波数安定化の系を図1に示す．周波数基準としては，半導体レーザや波長可変レーザに対して一般的なファブリ・ペロー干渉計を用いた．半導体レーザから出るレーザ光は広がるため，無反射コーティングされたレンズによって平行ビームとなるよう調整する．無反射コーティングは，レーザに反射光が戻ることによるレーザ発振の不安定化を防止するために必要である．次いでビームスプリッタ（BS）によって2つのビームに分け，一方はフォトダイオードで直接受光しレーザ出力に比例した信号V_2を得，もう一方はファブリ・ペロー干渉計を透過後，レンズとピンホールによって干渉縞の中心部分のみをフォトダイオードで受光しV_1を得る．干渉縞の強度（$=V_1$）はレーザの発振周波数によって変化するだけでなく，レーザ出力によっても変化する．このため，干渉縞強度V_1をレーザ出力V_2で割り算することによって，周波数変動のみに対応した信号V_o（$=V_1/V_2$）が得られる．レーザを注入電流によって発振周波数を変化させたときの割り算器（Divider）の出力V_oを図2に示す．

V_oは，このままでは制御信号とはならないので，一定電圧V_s（$\sim V_{o\,max}/2$）と差動アンプにより比較している．これによって図2のP点が0Vとなる信号が得られ，この時の周波数ν_0からの周波数変動の様子が符号付きの電圧信号V_e（$=V_o-V_s$）によって示される．

2.2 周波数安定度とその測定系

本論文では，周波数安定度をアラン分散$\sigma^2(\tau)$によって評価しており，その定義式を以下に示す．

$$\sigma^2(\tau)=\sum_{k=1}^{N-1}\frac{\overline{y}_{k+1}(\tau)-\overline{y}_k(\tau)}{2(N-1)}$$

τ：積分時間

N：データ数

y：周波数変動

$$\nu(t)=\nu_0\{1+y(t)\}$$

$$\overline{y}_k(\tau)=\frac{1}{\tau}\int_{t_k}^{t_k+\tau}y(t)\,dt$$

アラン分散を実時間で測定するための装置[5]（ARPS）は本研究室で製作されており，積分時間τとデータ数Nを入力することにより，$\tau=10^{-3}$から10^2sまでの時間領域の安定度が測定可能となっている．

更に，制御用計算機とのインターフェイスにより，ARPSは全て制御用計算機を使って動作できる．これによって，常に必要とする積分時間τにおけるデータ数Nの周波数安定度をモニターできる．測定に要する時間は，殆どがデータ収集に要する時間（$\tau\times N$）で占められており，これが非常に大きいと，安定度の変化に対して素早い対応が困難となる．このため積分時間τの大きな時間領域（1s以上）では，データ数Nを30以下にすることによって，測定時間を短縮するようにした．

2.3 レーザ周波数制御装置

本研究で用いた，制御装置の構成を図3に示す．制御方式は比例＋積分のPI制御を用いた．当初，比例と積分制御の両方を計算機を用いて行うことを試みたが，計算機の実行速度が遅くなり（1ms以上），制御周波数帯域が500Hz以下となってしまうことが明らかとなり，比例制御は従来からのアナログ増幅器を用

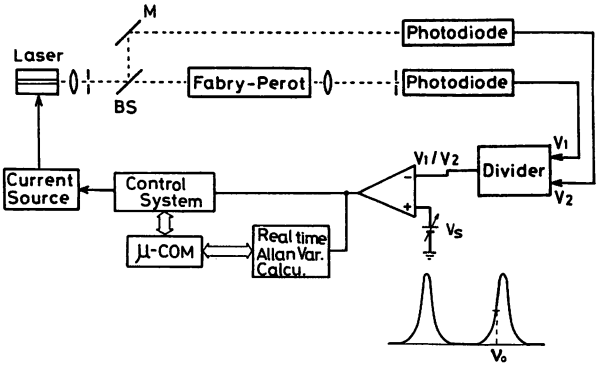

図1 Fabry-Perot干渉計を用いた半導体レーザの周波数安定化システム
Fig.1－Laser diode frequency stabilization system using a Fabry-Perot interferometer.

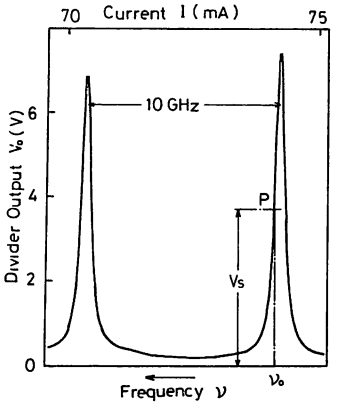

図2 Fabry-Perot干渉計の透過特性
Fig.2－Fabry-Perot transmission curve.

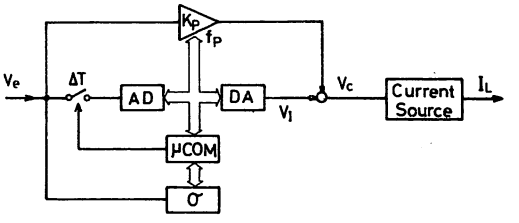

図3　計算機制御系
Fig.3－Microcomputer control system for the laser diode frequency stabilization.

いることにした．積分制御は，制御帯域が低いところにあるため，計算機を用いて行った．

基準周波数 ν_0 との差に比例した誤差信号 V_e は，制御用入力信号としてだけでなく周波数安定度の解析用の信号としても用いられる．

積分制御信号 V_I は誤差信号 V_e を時間間隔 ΔT 毎にアナログ／ディジタル（A／D）変換し，このディジタル信号 V_e' を計算機により式(1)で示す処理を行い積分信号 V_I' を求め，これをディジタル／アナログ（D／A）変換することで得ている．

$$V_I'(t_n)=K_I\cdot 2^{-12}\sum_{i}^{n}V_e'(t_i) \qquad (1)$$

ただし，$\Delta T=t_i-t_{i-1}$ である．

処理速度の向上を図るため，積分を単純加算で近似した．このとき，$K_I=1$ において，A／D変換後の計算機処理時間，つまり入出力間の時間遅れは約 200 μs であった．従って，V_e のサンプリング間隔 ΔT は 200 μs 以上で設定可能となる．ここで，ΔT はタイマー ICを用いることによって設定している．また，式(1)の K_I は，積分ゲインであり，計算時間を長くしないよう 2^n（$n=0, 1, 2, \cdots, 7$）の値に限定した．また，2^{-12} という係数は，次のディジタル／アナログ（D／A）変換によって出力されるアナログ信号の大きさが適当となるように決めた値である．

ここで，A／D変換器は 12 ビット分解能で，変換時間は約 20 μs，±5 Vの入力レンジである．またD／A変換器は 16 ビット分解能で，変換時間は約 35 μs，±5 V の出力レンジである．

比例制御用に用いた，アナログ・アンプは抵抗やコンデンサの組み合わせを計算機で決定でき，これによって比例ゲイン K_p と周波数帯域 F_p を変えられる．比例ゲイン K_p は 1.0 から 5.0 まで約 0.3 毎に 16 段階に設定可能で，また周波数帯域は，0.3，1，3，8 kHz と 4 段階に設定できる．積分制御を行うためのプログラムはアセンブリ言語で書かれており，タイマーによって時間 ΔT 毎に，このプログラムが起動され積分動作を行うようにした．

レーザ周波数安定化のための様々なプログラムは主にベーシックで書き，ここで，モニターした周波数安定度を調べ，その結果に応じて各制御パラメータを調整するようにした．

3．制御変数と周波数安定度

周波数安定度の向上を計るためには，上に述べた 4 つの制御変数の内でどれが有効に働くか，そしてそれはどの程度の値であるかを予め知っておくことは重要である．そこで，計算機による制御変数の自動調整を行う前に，各々の制御変数と周波数安定度の関係を測定した．

最初に比例ゲイン K_p と周波数安定度の関係を図 4 に示す．積分制御の影響を極力小さくするため，積分ゲイン $K_I=2^0$，サンプリング間隔 $\Delta T=3$ ms に設定した．積分時間 $\tau=1$ ms では，周波数安定度 σ は比例ゲイン K_p との間に明らかな関係は見られない．$\tau=30$，300 ms においては，K_p が 1 から 4.5 まで変化する間に周波数安定度は K_p と共に向上していることが分かる．更に，$\tau=3$ ms 以上でも同様なことが観測されており，比例ゲイン K_p は $\tau\geqq 3$ ms において有効な制御変数となる．

また，比例ゲイン K_p を 4.5 以上とすると制御系が発振気味で不安定な状態となるため，長時間の安定化が困難となるので，比例ゲイン K_p は 4.5 以下で調整する必要がある．

次に，積分ゲイン K_I と周波数安定度の関係を図 5 に示す．比例制御の影響を小さくするために比例ゲイン $K_p=1$ に設定した．積分制御では，τ の大きな値での周波数安定度の向上を狙っており，ここでは，$\tau=300$ ms 以上で積分ゲインが周波数安定度の向上に効果があることが分かる．

また，積分ゲイン K_I を 2^7 まで高めると周波数安定度が低下してしまい，K_I は 2^7 以下で調整する必要がある．

比例カットオフ周波数 F_p，サンプリング間隔 ΔT に対しても同様に周波数安定度を観測したが，$F_p\geqq 1$ kHz，ΔT は 0.6～2.0 ms において大きな変化は見られなかった．従って，F_p や ΔT は安定度向上のための制御変数としては有効ではなく，一定値に保っておいて良いことが分かった．

以上より，周波数安定度を向上させるのに有効な制

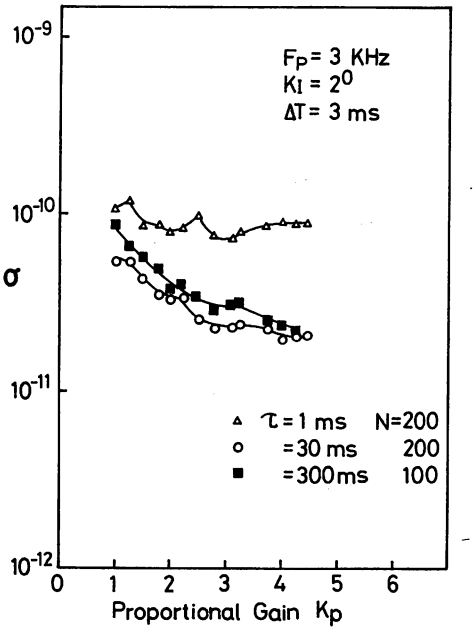

図4 比例ゲイン-周波数安定度特性
Fig.4- Frequency stability vs. propotional gain.

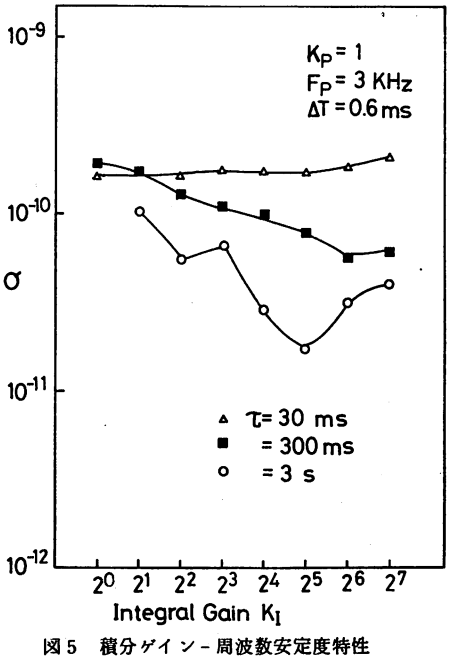

図5 積分ゲイン-周波数安定度特性
Fig.5-Frequency stability vs. integral gain.

御変数は，比例ゲインK_pと積分ゲインK_Iであることが分かり，今回の実験では，$K_p \leqq 4.5$，$K_I \leqq 2^6$で各制御変数の調整を行えばよい．

4. 最適安定化

4.1 周波数の高安定度の追求

レーザを使用する測定では，高安定度が必要な積分時間τの範囲が，それぞれの測定に対して異なってくる．

最初に特定の積分時間τにおける安定度向上を計る実験を行った．$\tau=9$ ms，$N=200$で周波数安定度を測定し，その安定度向上の様子を測定開始からの時間を横軸にプロットした．これを図6に示す．制御変数の初期値は，$K_p=1$，$K_I=2^0$，$\Delta T=1$ msとした．ここでは比例ゲインK_pのみ自動調整を行っている．測定開始から約20秒後には到達可能な安定度を実現している．また，これから比例カットオフ周波数F_pは1 kHz以上必要であることが分かる．

次に，τを2 msから6 sの間で設定し，この時間域における周波数安定度の向上を計った．これを図7に示す．Aの曲線は測定開始時の周波数安定度であり，このときの制御変数は$K_p=1$，$F_p=3$ kHz，$K_I=2^0$，$\Delta T=1$ msとした．K_p，K_Iについて自動調整を行うことにより，Bの曲線の周波数安定度を得ることができた．この場合には，一回のデータ収集に約5分の時間を要するため，実際に使用する場合には，マニュアルでの調整後，自動調整に移行すると良いであろう．

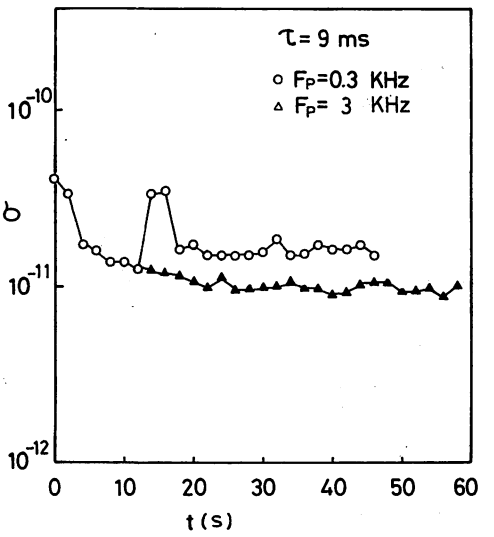

図6 周波数安定度の時間推移
Fig.6- Frequency stability characteristics from the beginning of control.

4.2 外乱による安定度劣化の補償

レーザによる計測中に外乱が入り，周波数安定度の

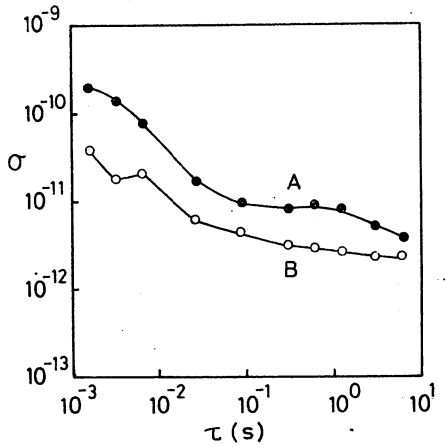

図7　周波数の最適安定化　Aは手動調整，Bは最適安定化を行ったときの周波数安定度
Fig.7－Frequency stability obtained by manual control A and by optimal control B.

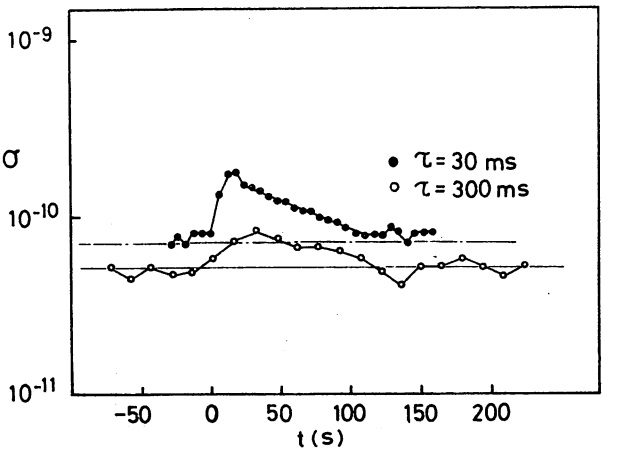

図8　外乱による安定度劣化を補償した場合の周波数安定度の変化
Fig.8－Frequency stability characteristics when the laser system was disturbed by noise.

低下が生じた場合，これが測定精度に影響するとなると，何らかの方法で周波数安定度を元の値に戻すことが必要となる．そこで，制御変数を自動調整することによって，外乱が加わった際にも周波数安定度を一定に保つ実験を行った．この結果を図8に示す．

外乱としてはノイズ発生器を用い，$1/f$ ノイズをレーザの電源に加えることにより周波数変動を与えることにした．ノイズを加える以前の制御変数の値は，$K_p=2$，$F_p=3$ kHz，$K_I=2^0$，$\Delta T=2$ ms とした．測定は，$\tau=30$ ms と 300 ms について行い，$t=0$ でノイズを加え，それぞれ鎖線と実線で示された周波数安定度を保つように K_p を自動調整している．ノイズを加えてから100秒程度で安定は回復していることが分かる．この回復時間が長いのは，K_p の調整時の変化分が0.3と小さいことと，更に，安全度の回復を確認するための手続きに手間取るためであり，この時間は適当な方法により短くすることができると考えられる．

5. むすび

半導体レーザの周波数を，ファブリ・ペロー干渉計の共鳴周波数を基準として安定化することを行った．その制御系に計算機を組み入れ周波数安定度を実時間で測定しながら制御変数を最適値に設定するよう自動化することによって，手動で固定設定した場合に比較して，半桁程度の安定度向上が見られ，$\tau=1\sim10$ s において 2×10^{-12} 程度の安定度が得られた．

また外乱がレーザ系に加わり，安定度が劣化した場合，制御変数が補正され100秒前後で安定度を回復することができた．

以上のように計算機を制御系に用いることによって，レーザ周波数を様々の設定条件で最適安定化を行うことが可能となった．本研究は半導体レーザを対象としたが，他の種類のレーザに対しても容易に応用が可能である．

謝辞　本研究に御援助いただいた日立製作所，中村道治博士，相本国男博士に深く感謝します．

また，本研究に関して御討論いただいた東工大精研岸野克己博士，土田英実氏に深く感謝します．

文　献

(1) Yamamoto, Y. and Kimura, T. : "Coherent Optical Fiber Transmission Systems", IEEE J. Quantum Electron, QE-17, pp.919-935 (1981).
(2) Tsuchida, H., Ohtsu, M. and Tako, T. : "Frequency Stabilization of AlGaAs DH Lasers", Jpn. J. Appl. Phys., 20, pp.L403-406 (1981).
(3) Tsuchida, H., Ohtsu, M. and Tako, T. : "Improvements in the Short-Term Frequency Stability of AlGaAs DH Laser", Trans. IECE Japan, E65, pp.65-66 (1982).
(4) Kajimura, T., Kuroda, T., Yamashita, S., Nakamura, M. and Umeda, J. : "Transverse-mode stabilized $Ga_{1-x}Al_xAs$ visible diode lasers", Appl. Opt., 18, pp.1812-1815 (1979).
(5) 椎尾，大津，田幸："レーザ周波数安定度の実時間測定装置の試作"，信学論 (C)，J64-C, 1, pp.204-208 (昭56-01).

（昭和59年3月26日受付）

JAPANESE JOURNAL OF APPLIED PHYSICS
VOL. 24, NO. 4, APRIL, 1985 pp. L256-L258

Linewidth Reduction of a 1.5 μm InGaAsP Laser by Electrical Feedback*

Motoichi OHTSU and Shinichi KOTAJIMA

International Cooperation Center for Science and Technology,
Tokyo Institute of Technology,
2-12-1, O-okayama, Meguro-ku, Tokyo 152

(Received February 13, 1985; accepted for publication March 23, 1985)

An electrical feedback technique was proposed for stable reduction of the spectral linewidth of a 1.5 μm InGaAsP laser (DFB type). By controlling the injection current with a servo control circuit of 0.5 kHz~0.8 GHz bandwidth, the linewidth was reduced by more than five times that of the free running laser. The minimum value obtained here was 2 MHz. Attainable minimum value, which was limited by the shot noise of the detector, was estimated as being 1.0×10^{-6} times that of the value given by the modified Schawlow-Townes formula.

§1. Introduction

A narrower spectral linewidth of a semiconductor laser is required for applications of coherent optical communication, optical heterodyne measurements, and so on. For example, a linewidth narrower than 1 MHz is essential to reduce the bit error rate as low as 10^{-9} in a PSK heterodyne optical communication system.[1] Several techniques for reducing the linewidth for these applications have been reported. On of them is to increase the cavity Q factor by using an external mirror or an optical fiber. This has been called an optical feedback technique[2,3] and makes use of the injection of the light reflected into the laser from the external mirror or optical fiber. For example, the linewidth of an AlGaAs laser has been reduced to 30 kHz by connecting an optical fiber to the laser.[3] However, this technique presents several problems, e.g., the linewidth can be temporally varied by phase fluctuations of the reflected light which are induced by the mechanical vibration of the external mirror or thermal extension of the optical fiber. Furthermore, oscillation characteristics sometimes become very unstable as a result of these phase fluctuations. To overcome these difficulties, the authors propose here a simpler and more stable technique, and electrical feedback for reducing the FM noises and the linewidth of a 1.5 μm InGaAsP laser by controlling the injection current. The authors have already succeeded in improving the stability of the line center frequency by controlling the injection current with a servo control bandwidth of about 1 MHz.[4] It is expected that the linewidth can also be reduced if the bandwidth of this servo control is sufficiently expanded.

Quite recently, Saito *et al.*[5] reported that the FM noise of a 0.8 μm AlGaAs laser can be reduced to a value of less than the one limited by the spontaneous emission by the application of electrical feedback. This means that the linewidth can also be stably reduced to a value less than that given by the modified Schawlow-Townes formula.[6] This makes electrical feedback a more promising technique than optical feedback. For the electrical feedback, Saito *et al.* detected the FM noise of a slave laser by heterodyning it with a stabilized master laser;[5] however, the attainable minimum linewidth of the slave laser is limited by the linewidth of the master laser. Therefore, the linewidth reduction of the master laser would also be required for further reduction of the linewidth of the slave laser, making the system more complex.

In the present study, a Fabry-Perot interferometer was employed for FM noise detection to make the control system simpler and more stable.

This letter reports the first successful results of linewidth reduction for a 1.5 μm InGaAsP laser by the electrical feedback technique. This mode can be used as a potential coherent light source for many applications.

§2. Experimental Apparatus

A distributed feedback-type InGaAsP laser at 1.5 μm was used.[7] Reproducible measurements were carried out with this laser because a single longitudinal mode oscillation was guaranteed for a wide range of injection current or output power. Figure 1 shows the experimental apparatus. D.C. current was injected to the laser by a low noise current source with current fluctuations of 0.6 $nA/\sqrt{Hz}$. Temperature fluctuations of the heat sink for the laser were reduced to 0.05 K at 293 K. The laser light was transmitted through a Fabry-Perot interferometer which worked as a frequency discriminator for servo control. This interferometer was made of a cylindrical rod of fused silica of 5 mm thick with dielectric multilayers

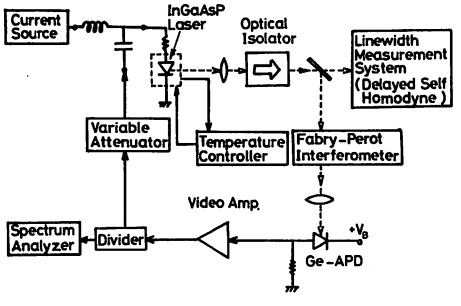

Fig. 1. Experimental apparatus.

*Read at 45th Meeting of the Japan Society of Applied Physics, Okayama, October, 1984

coated on both ends; reflectivity of the layers was 80%. The intensity fluctuations of the transmitted light, which were proportional to the FM noise of the laser, were detected by a Ge-avalanche photodiode (APD), and its output signal was negatively fed back to the injection current after being amplified by a video amplifier and a variable attenuator. Bandwidth of the Ge-APD was 0~0.8 GHz. The gain and bandwidth of the video amplifier were 60 dB and 0.5 KHz~1.0 GHz, respectively. The attenuation and bandwidth of the variable attenuator were −40 dB~0 dB and 0~18 GHz, respectively. These values imply that the bandwidth of the servo control was 0.5 kHz~0.8GHz. The distance between Ge-APD and the laser was kept as short as possible by directly connecting each component of the control circuit (the Ge-APD, video amplifier, variable attenuator, and so on) without using any coaxial cables between them. By this configuration, the resultant time delay around the feedback loop was reduced to 10 ns. Furthermore, these components were carefully shielded to reduce the electromagnetically induced noises.

The FM noise of the laser was monitored by a spectrum analyzer, and the spectral line shape was observed by the delayed self-homodyne technique[8] using a single mode fiber 1.5 km long.

§3. Experimental Results and Discussion

Figure 2 shows the relation between the power spectral density of the FM noise and the attenuation of the variable attenuator. FM noise intensity was reduced within the frequency range of the bandwidth of the servo control by decreasing the attenuation of the variable attenuator, i.e., by increasing the gain of the servo control. When the attenuation was 0 dB, the FM noise intensity was minimum, being limited by the noise from the Ge-APD. The linewidth measurements were done under this feedback condition. Figure 3 shows the spectral line shapes for the free running and feedback conditions; the linewidth reduction by the feedback can be clearly seen. The spectral line shape showed none of the temporal fluctuations which have sometimes been observed in the optical feedback technique. Figure 4 shows the relation between linewidth, output power, and injection current normalized to its threshold value. The linewidth of the free running laser was measured as larger than about 10 MHz. When compared with this value, the effect of the electrical feedback was notable, that is, the linewidth was reduced by more than five times that of the free running laser, and the minimum value obtained was 2 MHz. This approaches the value required for the PSK heterodyne optical communication system mentioned in §1. The results obtained here show that the present simple technique is quite effective for linewidth reduction. Further reduction can be expected by improving the finesse of the Fabry-Perot interferometer and by reducing noise from the detector.

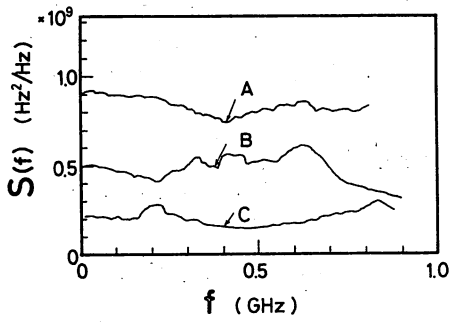

Fig. 2. Relation between power spectral density of the FM noise of the laser and attenuation of the variable attenuator. Here, $(I/I_{th}-1)^{-1}=1.0$, where I and I_{th} are the injection current and its threshold value, respectively. I_{th} was 30.2 mA at 293 K. The attenuations were −40 dB (A), −10 dB (B), and 0 dB (C).

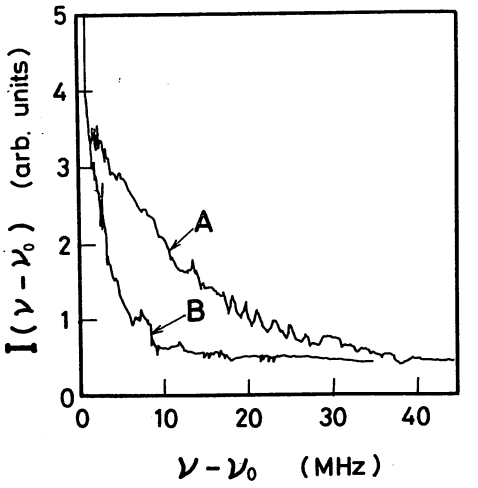

Fig. 3. Spectral line shapes $I(\nu-\nu_0)$ for the free running (A) and feedback (B) conditions, where $(I/I_{th}-1)^{-1}=0.67$. For the curve B, attenuation of the variable attenuator was 0 dB. A sharp peak at 0 Hz represents the zero beat signal from the spectrum analyzer.

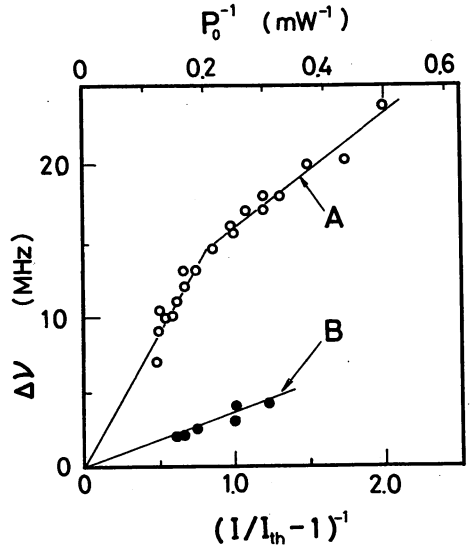

Fig. 4. Relation between the linewidth $\Delta\nu$ (full width at half maximum), ouput power P_o, and normalized injection current I/I_{th}. The curves A and B represent the results for the free running and feedback conditions, respectively.

For further improvements in this technique, the attainable minimum linewidth is roughly estimated in the following. If the claim for the heterodyning method given by Saito *et al.*[5] (see §1) is applied to the present method of FM noise detection, such noise can be reduced to that limited by the shot noise of the detector used for the servo control. This value for a 0.8 μm AlGaAs laser

has already been estimated by the authors (eq. (46) of ref. 4). If the numerical values for a 1.5 μm InGaAsP laser are substituted into it, the value of the FM noise, limited by the shot noise of the detector, is given by

$$\sigma_{y1}^2(\tau)=1.5\times10^{-28}\cdot\tau^{-1}, \quad (1)$$

where $\sigma_{y1}^2(\tau)$ and τ are the Allan variance for the frequency fluctuations[9] and the integration time for the fluctuation measurements, respectively. The value of the FM noise for a 0.8 μm AlGaAs laser, limited by the spontaneous emission, has also been derived (sum of eqs. (22), (25) and (28) of ref. 4). Using the numerical values for the 1.5 μm InGaAsP laser, this is given by

$$\sigma_{y2}^2(\tau)=1.5\times10^{-22}\cdot\tau^{-1}. \quad (2)$$

The ratio between these two values is

$$\sigma_{y1}^2(\tau)/\sigma_{y2}^2(\tau)=1.0\times10^{-6}. \quad (3)$$

Since it has been pointed out that the linewidth is proportional to the Allan variance of the FM noise,[4,9,10] it is estimated from eq. (3) that the linewidth can be reduced by 1.0×10^{-6} times that of the value limited by the spontaneous emission, i.e., the value given by the modified Schawlow-Townes formula. The implication is that, in an ideal case, the electrical feedback can make it possible to realize a linewidth narrorwer than 1 kHz, which can be very attractive for several applications.

Further experiments and theoretical work are now in progress and will be published elsewhere.

§4. Summary

With electrical feedback, the linewidth of the 1.5 μm InGaAsP laser was reduced to more than five times less than that of the free running laser; the minimum value obtained was 2 MHz. The spectral line shape showed no temporal fluctuations. The attainable minimum linewidth by this feedback was roughly estimated at 1.0×10^{-6} times that of the value given by the modified Schawlow-Townes formula. It can thus be concluded that this electrical feedback is quite effective in reducing linewidth.

Acknowledgements

The authors would like to express their thanks to Drs. T. Yamamoto and S. Akiba of KDD Research and Development Laboratories for valuable discussions on the DFB laser, and to Dr. Y. Yamamoto of NTT for his valuable discussion and showing them the galley proof of his paper (ref. 5.) They also wish to thank Prof. Y. Suematsu of their institute for his encouragement during this work.

References

1) K. Kikuchi, T. Okoshi, M. Nagamatsu and N. Henmi: Electron. Lett. **19** (1983) 417
2) S. Saito and Y. Yamamoto: Electron. Lett. **17** (1981) 325
3) F. Fabre, D. Le Guen and J. C. Simon: IEEE J. Quantum Electron. **QE-18** (1982) 1712
4) M. Ohtsu, H. Fukada, T. Tako and H. Tsuchida: Jpn. J. Appl. Phys. **22** (1983) 1157
5) S. Saito, O, Nilsson and Y. Yamamoto: Appl. Phys. Lett. **46** (1985) 3
6) D. Welford and A. Mooradian: Appl. Phys. Lett. **40** (1982) 865
7) S. Akiba, K. Utaka, K. Sakai and Y. Matsushima: IEEE J. Quantum Electron. **QE-19** (1983) 1052
8) T. Okoshi, K. Kikuchi and A. Nakayama: Electron. Lett. **16** (1980) 630
9) D. Allan: Proc. IEEE **54** (1966) 221
10) M. Ohtsu and S. Kotajima: Jpn. J. Appl. Phys. **23** (1984) 760

JAPANESE JOURNAL OF APPLIED PHYSICS
VOL. 23, NO. 5, MAY, 1984 pp. 600–605

A Simple Technique for Obtaining a Stable Frequency Sweep in a Waveguide CO_2 Laser

Tatsuro KUNIKANE,* Motoichi OHTSU,† Takuo NAKAMURA and Toshiharu TAKO

Research Laboratory of Precision Machinery and Electronics, Tokyo Institute of Technology, 4259 Nagatsuta-cho, Midori-ku, Yokohama, Kanagawa 227
†International Cooperation Center for Science and Technology, Tokyo Institute of Technology, 2-12-1, O-okayama, Meguro-ku, Tokyo 152

(Received September 13, 1983; accepted for publication February 25, 1984)

A simple technique for obtaining a stable frequency sweep in a waveguide-type CO_2 laser is described. The laser was compact, and contained a Stark cell inside its cavity, and the Stark spectrum in NH_2D was observed in the frequency range at the 10.6 μm P(20) laser transition. The frequency of the laser was stabilized at the center of the inverted Lamb dip in one of the Stark components, and a stability as high as 2.1×10^{-11} was obtained at an integration time τ of 250 s. The stabilized laser frequency was swept by slowly varying the d.c. electric field applied to the NH_2D molecules. It was swept for the whole frequency range of the single longitudinal-mode oscillation (195 MHz) while maintaining a traceability to the center frequency of the inverted Lamb dip of as high as $5.5 \times 10^{-10} \cdot \tau^{-1/2}$ for $1\,s \leqq \tau \leqq 100\,s$.

§1. Introduction

Many types of gas laser are in use as coherent light sources for optical measurements. Infrared CO_2 lasers in the 10 μm region are the most popular of these, and they are employed in high-resolution laser spectroscopy, pollutant gas monitoring and so on. However, to improve the accuracy of such measurements, the laser frequencies should be stabilized. It is especially important in spectroscopic measurements for the laser frequencies to be tunable over a wide frequency range in a sufficiently stable manner, while the laser maintains its single longitudinal-mode oscillation. One of the best types of laser for use as such a broad-band frequency-variable CO_2 laser is the waveguide-type,[1] because the spectral width of its gain curve is considerably pressure-broadened by its high-pressure operation. A pressure of as high as 50–300 Torr is usually employed in this type of laser, and this value is more than ten times as high as that of a conventional, d.c. discharge-excited CO_2 laser.[2] Furthermore, the waveguide laser has a wider longitudinal-mode frequency interval, and its single longigudinal-mode oscillation has a wider frequency range than that of a conventional CO_2 laser because of the short cavity length of the waveguide type. Thus the waveguide CO_2 laser promises to be an efficient frequency-variable laser. However, its frequency stability has not yet been quantitatively evaluated. Up to now, most efforts have been directed toward how to increase the output power and the efficiency.[3] Recently, a preliminary result on the frequency stabilization of such a laser was reported, with the Stark component of NH_2D in an external absorption cell being used as a frequency reference.[4] Meanwhile, Herlemont *et al.* have observed several saturated absorption spectra in CH_3Br using an intracavity absorption cell and a free-running waveguide CO_2 laser.[5]

In the present study, a simple technique for obtaining a stable frequency sweep in a waveguide CO_2 laser was developed by using the intracavity saturated absorption spectral components, i.e., the inverted Lamb dips, in NH_2D, as frequency references. First, the laser frequency was stabilized to a Stark component of NH_2D. For this purpose, the absorption cell for NH_2D was installed inside the cavity so as to make the whole system sufficiently compact and to obtain the inverted Lamb dip in NH_2D to be used as a frequency reference. Second, was locked to the Stark component and slowly swept.

More accurate techniques than that described here for obtaining a stable frequency sweep in CO_2 lasers, have previonsly been reported, e.g., using a frequency-offset locking technique,[6,7] which has been used for ultrahigh-resolution laser spectroscopy. However, compared with the latter technique, the one described here is simpler, because no auxiliary lasers or fast photodiodes are required, and furthermore, the apparatus is more compact. As a result, the present technique can be used to develop stable light sources for practical coherent optical measurements such as pollutant gas monitoring, and so on.

§2. Experimental Apparatus

Figure 1 shows the experimental apparatus. For power calibration, the laser output was detected by a conventional power meter. For frequency stabilization, it was detected by an $LiTaO_3$ pyroelectric detector (Eltec-Model 420) with a response time shorter than 1 ns, and its output signal was amplified by a lock-in amplifier. A folded-type laser cavity, originally designed by Hotta *et al.*,[8] was employed. It consisted of a grating (G) and two mirrors (M_1 and M_2). The cavity length, i.e., the distance between G and M_1 along the optical axis, was 640 mm. The grating G, 150 lines/mm, was driven by a stepping motor to select each branch of CO_2 laser oscillation with high reproducibility. The reflectivity of the flat output mirror M_1 was 90%. This mirror was placed about 2 or 3 mm from the end of the waveguide. The reflectivity and radius of curvature R

*Present address: Fujitsu Co. Limited, Kamiodanaka, Kawasaki, Kanagawa 211.

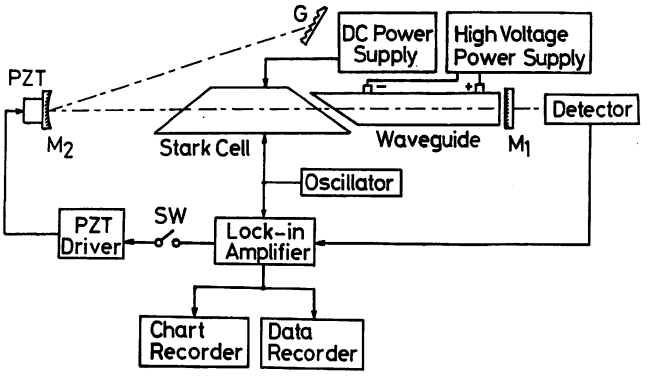

Fig. 1. Experimental apparatus. M_1 : flat output mirror with reflectivity of 90%. M_2: concave mirror. The radius of curvature R and the reflectivity were 400 mm and 100%, respectively. G: 150 lines/mm grating.

The cavity length of the laser was 640 mm, and the distance between M_2 and G, as well as between M_2 and the Brewster window of the waveguide, was fixed at $R/2$ (=200 mm). The switch SW was turned on when the laser frequency was stabilized.

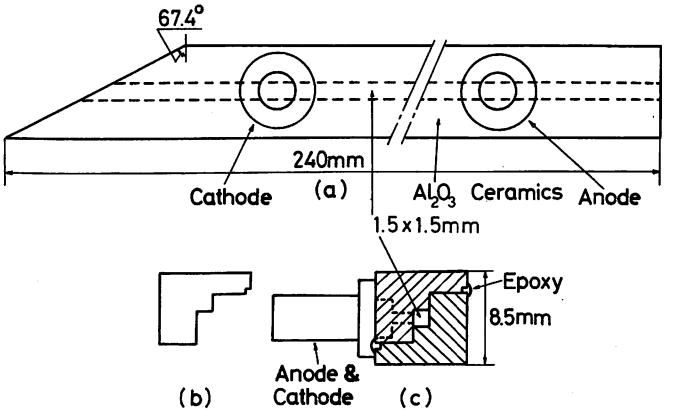

Fig. 2. Schematic of hollow waveguide made of Al_2O_3 ceramic. (a) The left hand end of the waveguide was cut at the Brewster angle for a ZnSe plate. (b), (c) Cross-section of ceramics. Two ceramics with the cross section of (b) were fixed together with epoxy adhesive to produce the hollow waveguide (c).

of the concave mirror M_2 were 100% and 400 mm, respectively. Mirror M_2 was mounted on a piezoelectric transducer (PZT) for fine tuning and stabilization of the laser frequency. The distance between M_2 and G, as well as that between M_2 and the left-hand side of the waveguide, was fixed to $R/2$ (=200 mm) to keep the coupling efficiency of the laser beam high enough at the end of the waveguide.[9] The free space between the mirror M_2 and the waveguide was used for the absorption cell for NH_2D.

Figure 2 shows a hollow waveguide made of Al_2O_3 ceramics, originally designed by Hotta.[10] It is 240 mm in length, and a ZnSe plate is fixed on the left-hand end of the waveguide at the Brewster angle. The other end is open to the enclosed space which is filled with the laser gases, and faces mirror M_1.

The cross-section of the waveguide is shown in Figs. 2(b) and (c). The two Al_2O_3 ceramic rods shown in Fig. 2(b) were joined with epoxy adhesive to form the waveguide shown in Fig. 2(c). The surface of the inner wall of the waveguide was polished to a flatness of 0.5 μm, and two hollow copper electrodes were fixed on the waveguide and used for d.c. discharge. The diameter and length of these electrodes were 3.5 mm and 11 mm, respectively.

In order to obtain stable oscillation of the laser, the waveguide must be supported rigidly in the cavity and the cavity mirrors must be accurately adjusted. In the present configuration, accurate optical adjustment of mirror M_1 is rather difficult owing to the position of the mirror, which is very close to the end of the waveguide. To overcome this difficulty, the accurate mechanism shown in Fig. 3 was developed. The waveguide was buried in a heat sink consisting of a brass block and was fixed to the flange A. Tap water was then passed through a hole bored in the heat sink for temperature stabilization. The heat sink was fixed on the Invar rods used as the cavity spacers, while flange A was connected to flange B. Flange B was connected to flange C by a flexible bellows. Mirror M_1 was mounted at the end of the pipe on flange D, which was also connected to flange C.

Two accurate adjusting screws F on flange C were used to connect flanges C and E, and also for optical alignment of M_1. Mirror M_1 and the waveguide are mechanically isolated by the flexible bellows, so optical alignment of these components can be carried out independently. This

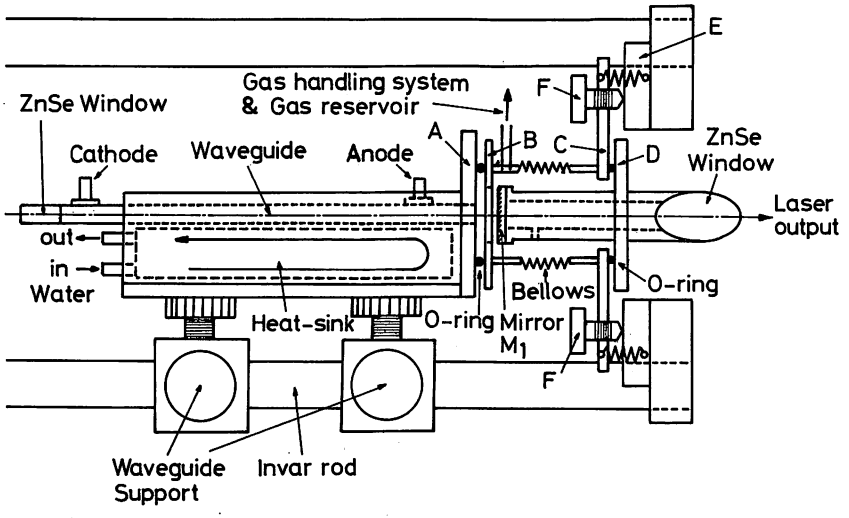

Fig. 3. Schematic diagram for optical alignments of waveguide and mirror M_1. A, B, C, D, E: Flanges. F: Accurate adjusting screws.

mechanism permits stable and reproducible optical alignment of the cavity. Flanges A and B, as well as C and D, were connected with each other via O-rings so that laser gases were confined inside the waveguide, bellows, and the pipe on flange D. This enclosed volume was connected to the gas handling system and a gas reservoir 200 cm^3 in volume through a capillary tube.

A mixture of CO_2, Xe, N_2, and He gase was employed as the laser gas, and the total pressure P_T was empirically adjusted between 50 and 75 Torr so as to give a low noise output. The fractional gas pressures were adjusted so that $0.20 \leqq f_{CO_2} \leqq 0.24$, $f_{Xe} \cong 0.05$, $0 \leqq f_{N_2} \leqq 0.10$, $0.65 \leqq f_{Ne} \leqq 0.71$, respectively, where $f_{CO_2} + f_{Xe} + f_{N_2} + f_{He} = 1.00$. The d.c. discharge current i_d was adjusted within the range $3.5\ mA \leqq i_d \leqq 4.0\ mA$.

Figure 4 shows the Stark electrode for the absorption gas used as a frequency reference for stabilization. The electrode was made of a glass plate 15 mm in thickness, and its surface was polished to a flatness of 0.05 μm. Thin films of Cr and Au were coated in succession on the shaded portion in Fig. 4. Two glass plates, prepared as above, were fixed together using three 00-class block gauges 3 mm in thickness as spacers, and two ZnSe plates were fixed on both ends of the glass plates at the Brewster angle. With this configuration, these two glass plates could be operated not only as a pair of Stark electrodes but also as the wall of the Stark cell. As the spot size of the laser beam inside the Stark cell was only about 1 mm, no insertion loss was produced when the cell was installed inside the cavity.

§3. Experimental Results and Discussions

3.1 *Oscillating properties of the free-running laser*

Prior to the frequency stabilization, several oscillating properties of the free-running laser were measured without the Stark cell in the cavity.

Figure 5 shows the output power of each branch obtained by rotating the grating G. Each power was measured by a conventional power meter. The experimental conditions were the same as those of Fig. 1 except that the Stark cell was removed and the feedback loop was open. Here, $P_T = 61$ Torr, $f_{CO_2} = 0.21$, $f_{Xe} = 0.05$, $f_{N_2} = 0.08$, $f_{He} = 0.66$, and $i_d = 4$ mA. Oscillations of thirteen R branches and eighteen P branches were obtained at the 10.6 μm region (the transition between the $00^0 1$ and $10^0 0$ levels), while eight R and P branches were oscillated in the 9.6 μm region (the transition between the $00^0 1$ and $02^0 0$ levels). The power drift of the laser output of each branch was measured as less than 1% in 10 minutes, which confirms that stable oscillation was obtained. Figure 6 shows the tuning curve of the P(20) branch of the 10.6 μm region

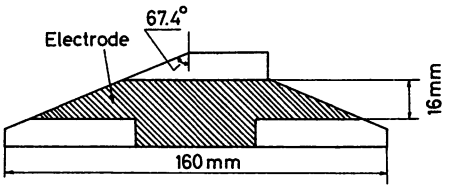

Fig. 4. Stark electrode also used as wall of absorption cell. The electrode was made of a glass plate 15 mm thick, whose surface was polished to a flatness of 0.05 μm. Thin films of Cr and Au were coated in succession onto the shaded portion of the figure.

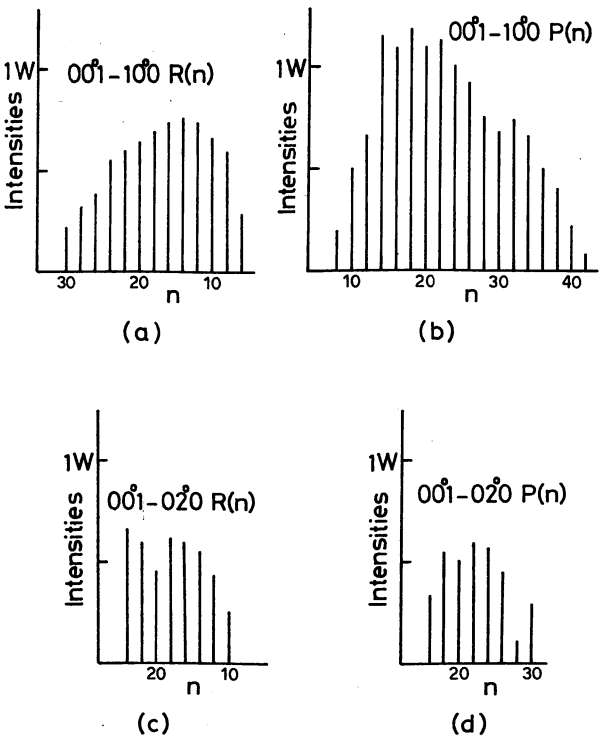

Fig. 5. Output powers of each branch of laser oscillation. The R(n) and P(n) branches on the 10.6 μm transitions between the $00^0 1$ and $10^0 0$ levels are shown by (a) and (b). Those of the 9.6 μm transition between the $00^0 1$ and $02^0 0$ levels are shown by (c) and (d), respectively. Here, the values of n are given on the abscissa of each figure in order of increasing oscillation wavelength. $P_T = 61$ Torr, $f_{CO_2} = 0.21$, $f_{Xe} = 0.05$, $f_{N_2} = 0.08$, $f_{He} = 0.66$, and $i_d = 4$ mA.

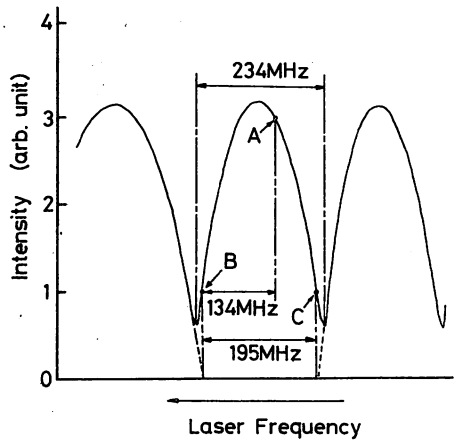

Fig. 6. Tuning curve of P (20) branch at 10.6 μm. $P_T = 52$ Torr, $f_{CO_2} = 0.24$, $f_{Xe} = 0.05$, $f_{N_2} = 0$, $f_{He} = 0.71$, and $i_d = 3.6$ mA. The values of these parameters were fixed in the remaining parts of this study. The longitudinal-mode frequency interval was 234 MHz. By extrapolating the tails of the tuning curve to the abscissa, it was estimated that the single longitudinal-mode oscillation was obtained within the frequency range of 195 MHz on the tuning curve. Point A represents the starting point of the frequency sweep of the laser in Fig. 11, while points B and C represent both ends of the range of the single longitudinal-mode oscillation.

measured by sweeping the d.c. voltage of the PZT on which mirror M_2 was mounted. Here, $P_T = 52$ Torr, $f_{CO_2} = 0.24$, $f_{Xe} = 0.05$, $f_{N_2} = 0$, $f_{He} = 0.71$, and $i_d = 3.6$ mA, respectively, and a pyroelectric detector was employed for this measurement. These experimental conditions were kept the same in the remaining part of this study. The smooth curve in this

figure is evidence for the fact that stable, low-noise oscillation was actually obtained. As the cavity length was 640 mm, the corresponding longitudinal-mode frequency interval was 234 MHz. Here, two longitudinal modes were simultaneously oscillated around the tails of the tuning curve, because the spectral width of the gain curve was larger than this longitudinal mode frequency interval because of the pressure-broadening phenomenon. The existence of this two-mode oscillation can easily be confirmed because the tails of the tuning curve do not cross the abscissa in this figure. Extrapolation of the curve th the abscissa gives an estimate of the frequency range of the single longitudinal-mode oscillation, about 195 MHz, as shown in the figure. The two ends of the frequency range of the single longitudinal-mode oscillation, about 195 MHz, as shown in the figure. The two ends of the frequency range of the single longitudinal-mode oscillation are given by points B and C in the figure. In §3.3, a stable frequency sweep within this frequency range will be described.

3.2 *Measurements of intracavity Stark components in* NH_2D

In this study, Stark components in NH_2D were employed as frequency references for the stabilization of the laser frequency. NH_3 and ND_3 were mixed at equal pressure to give NH_2D. It is well known that about 45% of a mixture of these low-pressure gases converts spontaneously into NH_2D at room temperature.[11] As the transition frequency between the $(1_a5_{0,5})$ and $(0_a4_{0,4})$ levels in NH_2D is only about 1.7 GHz lower than the center frequency of the 10.6 μm P(20) laser transition, and as the energy of the lower level, i.e., $(0_a4_{0,4})$, suffers the Stark shift, this spectral line can easily be tuned to the P(20) branch by applying an electric field to the NH_2D molecules. The magnitude of the Stark shift of the transition frequency can be expressed as

$$\delta = -2042 + 0.143 \cdot |M| \cdot E \quad \text{(MHz)}, \qquad (1)$$

where E represents the amplitude of the applied electric field expressed in V/cm.[4] The quantity M is the component of the rotational quantum number of the $(0_a4_{0,4})$ level in NH_2D in the direction of the Stark electric field vector. The selection rule for the transition is given by $\Delta M = \pm 1$ because the direction of the electric field vector was set perpendicular to that of the electric field vector of the laser oscillation in the cavity configuration of Fig. 1.

After the Stark cell had been installed in the cavity, linear absorption spectral components on NH_2D were measured. Figure 7 shows their derivative shapes. They were measured by sweeping the d.c. electric field, whose value is shown along the abscissa. An a.c. electric field of 167 V/cm (peak-to-peak value), with a frequency of 5 kHz, was superimposed on this d.c. electric field, and the output signal from the pyroelectric detector was amplified by a lock-in amplifier. The time constant τ_L of the output stage of the lock-in amplifier was kept at 3 ms throughout this study. The total pressure of the NH_3 and ND_3 mixture was 80 mTorr. In Fig. 7, the components for $|M| = 2$, 3, and 4 are shown. The small dips appearing on the top or bottom of these derivative signals are the inverted Lamb dips, and these are indicated by arrows in the figure. However, these

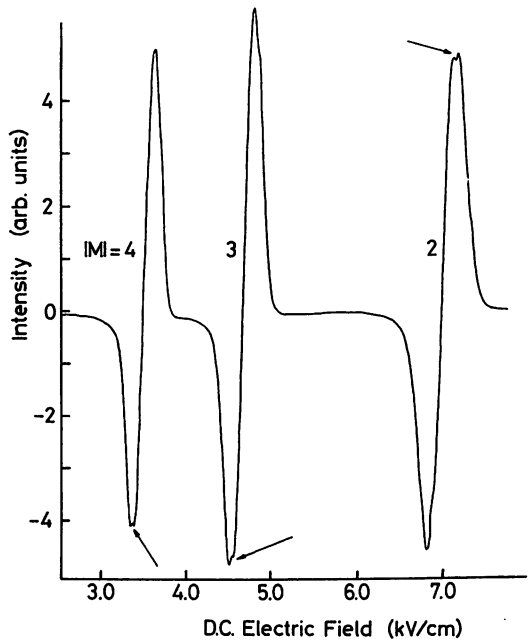

Fig. 7. Derivative signals of linear absorption spectra of NH_2D in intracavity absorption cell, measured by P (20) branch at 10.6 μm of laser oscillation. The pressure of the NH_3 and ND_3 mixture was 80 mTorr, and the peak-to-peak value of the amplitude of the a.c. electric field was 167 V/cm. The three signals correspond to $|M| = 2$, 3, and 4, respectively, and were measured by sweeping the d.c. electric field applied to the NH_2D molecules while keeping the PZT voltage at a constant value. The small dips indicated by the three arrows represent the inverted Lamb dips.

dips are not clearly seen because the amplitude of the a.c. electric field was too large, i.e., the value of 167 V/cm (peak-to-peak value) corresponds to the maximum frequency deviations of 47.8 MHz, 71.6 MHz, and 95.5 MHz, for $|M| = 2$, 3, and 4, respectively (see eq. (1)). The amplitude of the a.c. electric field was thus decreased to 16.7 V/cm (peak-to-peak value) to show up these dips more clearly and the result is given in Fig. 8. Here, the spectral shape for $|M| = 4$ is shown, for which the value of 16.7 V/cm corresponds to the maximum frequency deviation of 9.6 MHz. A sharp dispersive line shape can be seen at the center of the derivative of the linear absorption spectrum, and this represents the derivative of the inverted Lamb dip. Its half-width at half-maximum (HWHM) was measured as 5 MHz by assuming that it had a Lorentzian line shape. The value of the HWHM decreased as the amplitude of the a.c. electric field and the gas pressure decreased. The minimum value of the HWHM obtained here was 4 MHz, and this would be limited by the transit-time broadening, power broadening, the temporal and spatial fluctuation of the applied electric field, etc. However, no full quantitative estimations have yet been made.

3.3 *Stabilization and continuous sweep of the laser frequency*

As the first step, frequency stabilization of the laser oscillation in the P (20) branch at 10.6 μm was tried using the inverted Lamb dip of $|M| = 4$ as a frequency reference. For this experiment, the total pressure of the NH_3 and ND_3 mixture was kept at 70 mTorr, while the other experimental conditions were the same as in Fig. 8. After

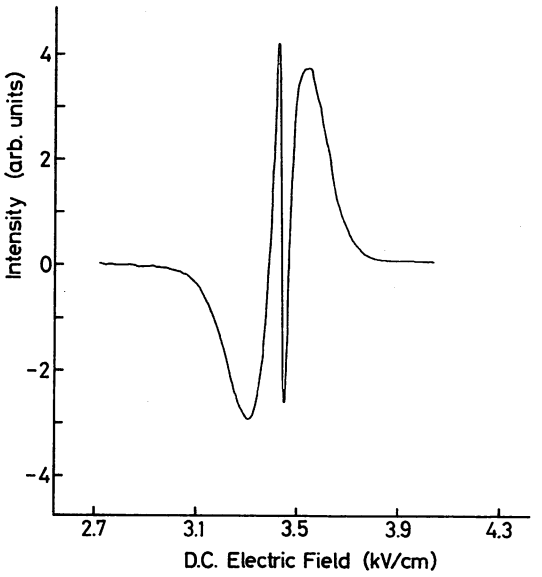

Fig. 8. Derivative of inverted Lamb dip clearly appearing at center of derivative of linear absorption spectral shape. This spectral shape is for $|M|=4$. The peak-to-peak value of the amplitude of the a.c. electric field was 16.7 V/cm, when the other experimental conditions were the same as those of Fig. 7. The HWHM of this dip was measured as 5 MHz.

the feedback loop was closed, the laser frequency was locked to the center of the inverted Lamb dip in NH_2D by using the linear part of the derivative of this dip as a frequency discriminator and by controlling the PZT voltage applied to the cavity mirror M_2. The PID servo-control technique was employed to control the PZT voltage.[7] The response time of this servo-control system was limited by the time constant τ_L of the lock-in amplifier to a value of 3 ms. Figure 9 shows the temporal fluctuations of the stabilized laser frequency. It can be seen that the frequency fluctuations were reduced to as low as 125 kHz by the stabilization. To evaluate the frequency stability more quantitatively, the Allan variance σ^2 of the frequency fluctuations[10] was measured; the output signals from the lock-in amplifier were recorded on a data recorder and the value of σ^2 was calculated from these recorded signals by using a micro-computer after analog-to-digital conversion. Figure 10 shows the square root of σ^2, where τ and N represent the integration time and number of data, respectively. Curve A represents the result for the stabilized laser, while curve B is for the free-running laser. These curves represent the laser frequency traceability σ_{tr} to the center frequency of the inverted Lamb dip in NH_2D. The

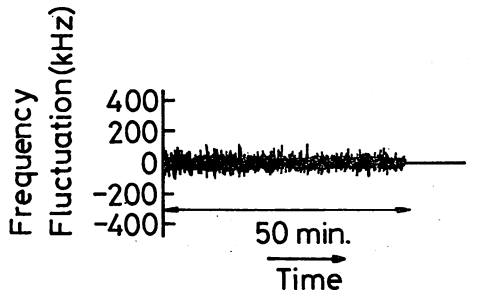

Fig. 9. Temporal frequency fluctuations of P (20) branch at 10.6 μm of laser oscillation, which was stabilized to center frequency of inverted Lamb dip of $|M|=4$ in NH_2D.

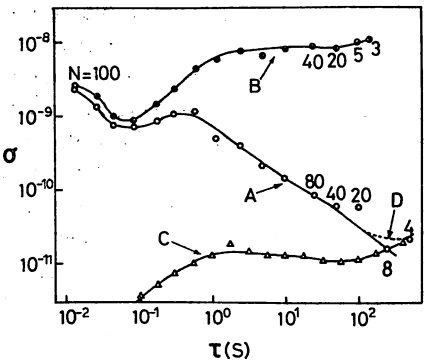

Fig. 10. Square root of Allan variance σ^2 for frequency fluctuations. Here, τ and N represent the integration time and number of data, respectively. Curves A and B are the frequency traceability σ_{tr} of the stabilized and free running laser to the center frequency of the inverted Lamb dip in NH_2D, respectively. Curve C represents the stability $\sigma_{st,i}$ of the center frequency of the inverted Lamb dip in NH_2D, as estimated from the temporal fluctuations of the Stark electric field. Curve D is the laser frequency stability σ_{st}, estimated using the results of curves A, C, and eq. (2).

value of σ_{tr} on curve A decreases with increasing τ for $\tau \geqq 1$ s, which means that the thermal drift of the cavity length was compensated by the stabilization. In the range $\tau < 0.1$ s, however, no distinct differences can be seen between the values of the two curves. This is because the overall noise characteristics of the servo-control system for stabilization are governed not only by the laser frequency fluctuations but also by the noise of the pyroelectric detector for $\tau < 1.0$ s. A higher frequency stability can be expected to be obtained by employing a detector with lower noise. The laser frequency stability σ_{st}^2 is given by the sum of the traceability σ_{tr}^2 and the frequency stability of the center frequency of the inverted Lamb dip $\sigma_{st,i}^2$, i.e.,

$$\sigma_{st}^2 = \sigma_{tr}^2 + \sigma_{st,i}^2. \tag{2}$$

Curve C represents the value of $\sigma_{st,i}$, which was estimated from the temporal fluctuations of the Stark electric field. Curve D shows the laser frequency stability σ_{st} obtained by using the results of curves A, C, and eq. (2). This curve can be approximately expressed as

$$\sigma_{st} = 5.5 \times 10^{-10} \cdot \tau^{-1/2} \text{ for } 1 \text{ s} \leqq \tau \leqq 100 \text{ s}, \tag{3}$$

and gives the minimum value of 2.1×10^{-11} at $\tau = 250$ s. A further decrease in this minimum value can be expected by improving the stability of the high-voltage power supply for the Stark electric field.

As the second step, a stable laser frequency sweep was tried by slowly varying the d.c. electric field applied to the NH_2D molecules, with the frequency locked to the center of the inverted Lamb dip in NH_2D. The result is given in Fig. 11. This figure shows the relation between the d.c. electric field and the d.c. voltage applied to the PZT for the cavity mirror M_2. The former was proportional to the center frequency of the inverted Lamb dip, and the latter to the laser frequency locked to it. The ordinate is marked in units of the laser frequency shift (MHz) of the laser oscillation instead of that of the PZT voltage. The time required for this sweep was about 10 s. A smoother curve would be obtained by increasing this time, because the sigularities on the curve are due to the slow response of

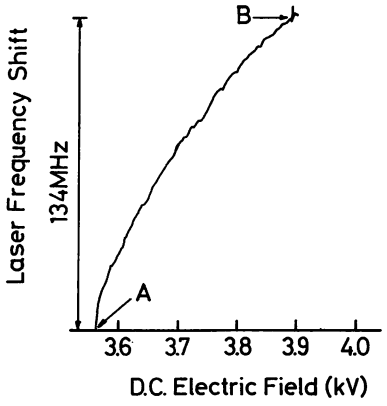

Fig. 11. Result of a continuous sweep of laser frequency by slowly varying the d.c. electric field applied to the NH_2D molecules. This was done by keeping the laser frequency locked to the inverted Lamb dip in NH_2D. The abscissa represents the value of the d.c. electric field, while the ordinate corresponds to the laser frequency shift derived from the PZT voltage applied to mirror M_2.

Points A and B in this figure represent the interval of the frequency sweep, and correspond to points A and B on the tuning curve of Fig. 6.

PZT to the large excursions of the applied voltage. The deviation from the linear shape of the curve in this figure is due to the nonlinear response of the PZT expansion.

Point A in this figure represents the values of the d.c. electric field and the locked laser frequency when the sweep was started. On increasing the d.c. electric field, the locked laser frequency also increased until it reached point B in the figure. The range of the locked frequency excursion is shown as being 134 MHz. These points correspond to points A and B of Fig. 6, respectively. That is, the laser frequency was initially located at around the center of the tuning curve, and by the frequency sweep, it reached the end of the higher-frequency side of the single longitudinal-mode oscillation region. It was also possible to sweep down to the end of the lower-frequency side of this region, shown by point C in Fig. 6. These results confirm that the laser frequency can be swept over the whole range of single longitudinal-mode oscillation of the 10.6 μm P (20) laser transition, i.e., 195 MHz, while it is locked to the inverted Lamb dip in NH_2D. When the sweep time was longer than 10 s, it was confirmed that the laser frequency traceability σ_{tr} was almost equal to the result of curve A in Fig. 10, i.e.,

$$\sigma_{tr} = 5.5 \times 10^{-10} \cdot \tau^{-1/2} \text{ for } 1\,\text{s} \leqq \tau \leqq 100\,\text{s}. \quad (4)$$

This high traceability means that the laser frequency was tightly locked to the center frequency of the inverted Lamb dip in NH_2D even though this center frequency was slowly swept. A higher frequency traceability can be produced by expanding the bandwidth of the servo-control system. The laser frequency stability σ_{st} can also be estimated by analyzing the stability $\sigma_{st,i}$ of the swept frequency of the inverted Lamb dip. A full quantitative analysis of this stability is now in progress. However, it can be said from the fluctuation measurements of the Stark electric field that no distinctive deteriorations in the stability $\sigma_{st,i}$ were seen, even though the inverted Lamb dip was slowly swept. Therefore it can be concluded that the laser frequency stability σ_{st} was maintained approximately as high as that of curve D in Fig. 10 when the laser frequency was slowly swept.

A shorter cavity length and a lower-noise detector are required in order to expand the range of the frequency sweep and to obtain a higher frequency stability, respectively. If other molecules are employed, the present technique can also be used to stabilize the laser frequency of other oscillation branches.

§4. Summaries

A simple technique for obtaining a stable frequency sweep in a waveguide-type CO_2 laser is presented. It has several practical applications, such as pollutant gas monitoring. The laser is compact and has an absorption cell inside its cavity. The Stark components of NH_2D in this absorption cell were observed in the frequency range at the 10.6 μm P (20) laser transition. The laser frequency was stabilized at the center of the inverted Lamb dip in one of these NH_2D Stark components, and the resulting stability was as high as 2.1×10^{-11} at an integration time τ of 250 s.

The stabilized laser frequency was then swept by slowly ecules, while the laser frequency was locked to the spectrum. It could be swept over the whole frequency range of rum. It could be swept over the whole frequency range of the single longitudinal-mode oscillation, about 195 MHz. When the laser frequency was slowly swept by this technique, its traceability to the center frequency of the inverted Lamb dip was maintained as high as $5.5 \times 10^{-10} \cdot \tau^{-1/2}$ for $1\,\text{s} \leqq \tau \leqq 100\,\text{s}$.

Further experiments are now in progress to improve the performance of this laser system.

Acknowledgements

The authors would like to express their thanks to Mr. K. Hotta of Nippon Electric Co. for his valuable advice on laser design. They also wish to thank Drs. E. Sakuma and M. Ohi of the National Research Laboratory of Metrology for providing technical support. This work was partially supported by a Grant-in-Aid for Scientific Research from the Ministry of Education, Science and Culture.

References

1) T. J. Bridges, E. G. Burkhardt and P. W. Smith: Appl. Phys. Lett. **20** (1972) 403.
2) C. K. N. Patel: Phys. Rev. Lett. **13** (1964) 617.
3) J. J. Degnan: Appl. Phys. **11** (1976) 1.
4) T. A. Nussmeien and R. L. Abrams: Appl. Phys. Lett. **25** (1974) 615.
5) F. Herlemont, J. Fleury, J. Lemaire and J. Demaison: J. Chem. Phys. **76** (1982) 4705.
6) Ch. Borde, M. Ouhayoun, A. van Lerberghe, C. Salomon and S. Avriller: *Laser Spectroscopy IV* eds. H. Walther and K. W. Rothe, *Springer Series in Optical Sciences*, Vol. 21 (Springer-verlag, Berlin, 1979) p. 142.
7) M. Ohtsu, S. Katsuragi and T. Tako: IEEE J. Quantum Electron., **QE-17** (1981) 1100.
8) K. Hotta, K. Inoue and K. Washio: *Proc. Conf. Lasers and Electro-Optic Systems, 1978, San Diego* (Opt. Soc. Am., Washingtion, 1978) ThAA4.
9) R. L. Abrams: IEEE J. Quantum Electron. **QE-8** (1972) 838.
10) K. Hotta: Submitted to Japan Patent 15716 (1979).
11) A. R. Johnston and R. D. Melville, Jr.: Appl. Phys. Lett. **19** (1971) 503.
12) D. W. Allan: Proc. IEEE **54** (1966) 2.

報 文 2

シュタルクスペクトルを用いた高分解能分光用周波数安定化レーザー

椎尾 一郎*, アヌン・クスノボ*†, 大津 元一**, 田幸 敏治*

* 東京工業大学精密工学研究所 横浜市緑区長津田 4259 (〒227)
** 東京工業大学理工学国際交流センター 東京都目黒区大岡山 2-12-1 (〒152)

(1984年3月9日受理)

A Frequency Stabilized Laser System for High Resolution Spectroscopy Using Stark Spectrum

Itiro SIIO*, Anung KUSNOWO*†, Motoichi OHTSU**
and Toshiharu TAKO*

* Research Laboratory of Precision Machinery and Electronics, Tokyo Institute of Technolgy, 4259 Nagatsuta-cho Midori-ku, Yokohama, Kanagawa 227
** International Cooperation Center for Science and Technology, Tokyo Institute of Technology, O-Okayama Meguro-ku, Tokyo 152

(Received March 9, 1984)

An offset-locked He-Xe laser system for high resolution spectroscopy on H_2CO at 3.51 μm, was constructed using a Stark shifted line. In this offset-locked laser system, a local oscillator laser which is necessary in conventional system can be eliminated, because reference laser is locked at offset-frequency. The frequency stability and tunable range of this system is $\sigma=8.8\times10^{-14}$ (at $\tau=10$ s) and 12 MHz, respectively, where σ is the square root of Allan variance and τ is the sampling time. The performance of this offset-locked laser system satisfied the requirement for a light source of ultra-high resolution spectroscopy.

The pressure broadening coefficient of H_2CO was measured to be 56±7 kHz/mTorr, using present system.

Stark coefficient of H_2CO at 3.51 μm was precisely measured using beat frequency between two stabilized He-Xe lasers. The electric dipole moment at $v_5=1$ excited vibrational state was measured to be 2.288±0.005 D.

1. はじめに

周波数の安定化制御を行わない気体レーザーの周波数安定度は，共振器長の熱膨張による変動等の原因で，10^{-7}～10^{-6} 程度である．一方，飽和分光法等によりドップラー幅を除去した赤外高分解能分光では分解能が 10^{-8} から 10^{-10} [1] に達するので，分光用光源レーザーの周波数安定化が必要となる．また，光源レーザーの周波数は測定対象のスペクトルの範囲で精密に掃引可能であることが必要である．

周波数が安定で波長可変のレーザーを実現する方法の

† National Institute for Physics, Indonesian Institute of Sciences Kompleks Lipi, Jalan Cisitu, Bandung, Indonesia.

一つはシュタルク効果などにより周波数掃引可能な原子・分子の吸収線を周波数基準としてレーザーの周波数安定化を行うことである[2),3)]．しかし，この安定化レーザーを分光光源に応用出来るのは，周波数基準の吸収線が測定対象のスペクトル範囲を掃引可能な場合に限られる．

精密な分光用光源レーザーを実現するもう一つの方法はオフセットロックレーザーの手法である．特に3台のレーザーから成るオフセットロックレーザーシステムを用いる事で，原理的には任意の測定対象スペクトルを安定に周波数掃引する事が出来る[1),4),5)]．この方法を Fig. 1 (a) に示す．図中の3台のレーザーは上からそれぞれ，掃引レーザー，局部発振レーザー，基準レーザーの働きをする．基準レーザーは測定対象の吸収線を基準として周波数安定化される．次に局部発振レーザーは基準レーザーとのビート周波数と基準発振器の周波数を位相比較して，基準レーザーに対して Δf だけ異なる周波数に周波数オフセットロックされる．更に，掃引レーザーは局部発振レーザーに対して周波数オフセットロックされ，測定対象の吸収線を中心に精密に周波数掃引される．この方法では，ゼロビート時の注入同期によるレーザーゆらぎを防ぐため2台目の局部発振レーザーが必要となる．

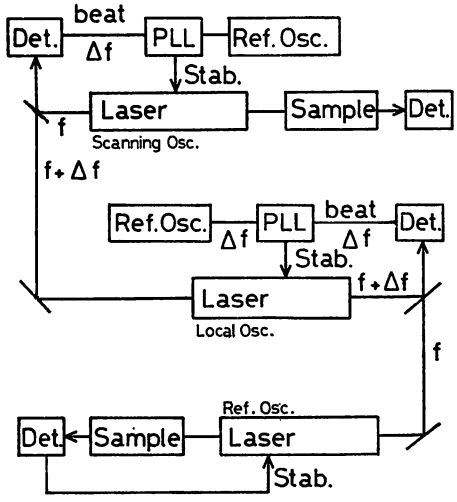

Fig. 1 (a) Conventional offset-locked laser system. The reference laser is stabilized using the inverted Lamb dip in H_2CO.

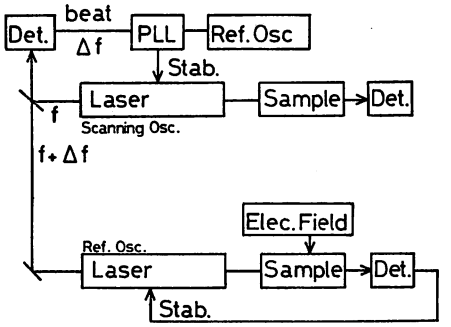

Fig. 1 (b) Proposed offset-locked laser system. The reference laser is stabilized to Stark shifted line.

ところが，Fig. 1 (b) に示すように基準レーザーを測定対象吸収線のシュタルク分裂した吸収線により安定化することにより，2台のレーザーで精密分光用光源レーザーを構成することが出来る．本論文では H_2CO の 3.51 μm 吸収線の精密分光用オフセットロックレーザーシステムを，シュタルク効果により 12.7 MHz シフトした H_2CO の吸収線を基準とした H-Xe レーザーを用いて製作した．また，この吸収線のシュタルク係数の精密測定についても述べる．

2. 性能の目標

本研究では H_2CO の 3.51 μm 吸収線の精密な高分解能分光測定のための分光用光源としてシュタルクシフトを用いたオフセットロックレーザーシステムを製作した．本装置に必要とされる性能は次の2点である．

(1) 周波数安定度

測定対象である H_2CO の飽和吸収スペクトル線の全幅 (FWHM) は約 500 kHz である．これを精密に測定するためには少くとも 10 kHz 程度の掃引きざみで測定することになる．また超微細構造[6),7)]の影響を観測する場合は 1k Hz 程度の掃引きざみが必要である．このためレーザーの安定度は測定時間程度の積分時間において 10^{-11} (~1 kHz) から 10^{-12} (~100 Hz) 程度である必要がある．一方，積分制御された安定化レーザーの安定度は積分時間の $-1/2$ 乗から -1 乗に比例する傾向があるため測定時間を長くする方が有利である．しかし吸収セルやシュタルク電場の安定度などを考えると，一回の測定の所要時間は 10^{3} s 程度以下が適当である．この場合周波数掃引の1きざみ当りの測定時間は 1 s のオーダーである．このため前述の安定度は 1 s から 10^{3} s の測定時間の範囲で達成されることが必要である．すなわち本装置には $1\,\mathrm{s} \leq \tau \leq 10^{3}\,\mathrm{s}$ において $\sigma \leq 10^{-11}$ から $\sigma \leq 10^{-12}$ の周波数安定度が要求される．

(2) 周波数掃引特性

前述のように測定対象のスペクトル線全幅が約 500 kHz であることから本装置は吸収線を含む周波数領域で 2 MHz 程度掃引幅を持つことが必要である．

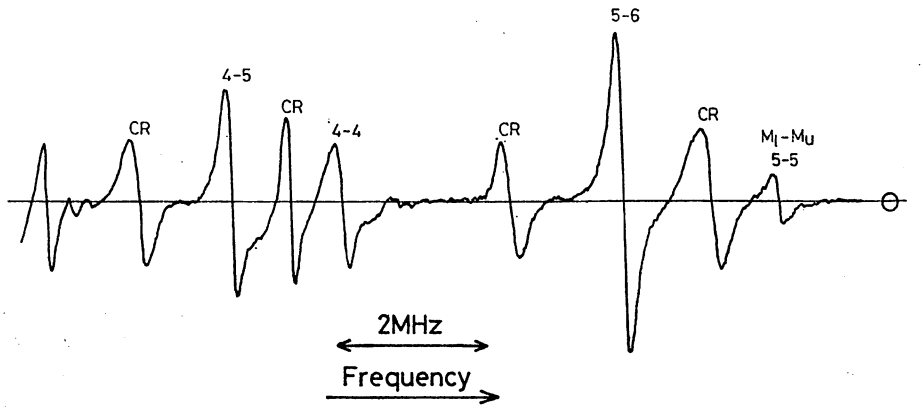

Fig. 2 Derivative signal of Stark components of H_2CO.

そこで，以上の性能を達成することを目標としてオフセットロックレーザーシステムを製作した．

3. 基準レーザー

本装置の基準レーザーは，H_2CO の 3.51 μm 吸収線の高分解能シュタルクスペクトル[8]を周波数基準として安定化した He-Xe レーザーである．この吸収線は $6_{0,6}$ $(v_5=1)\leftarrow 5_{1,5}$ $(v=0)$ 振動回転遷移によるものであり，飽和吸収分光法によって初めて観測される程度の2次の弱いシュタルク効果を示す．He-Xe レーザーにより観測した H_2CO の高分解能シュタルクスペクトルを Fig. 2 に示す．これはレーザー共振器内に長さ 33cm，間隔 6.5 mm のシュタルク電極を内蔵した H_2CO 吸収セルを設置して反転ラムくぼみを測定した結果である．印加電場は 4.6155±0.0001 kV/cm であり，シュタルク変調の目的で 3 kHz，40 Vp.p. の正弦波電圧を重畳した．H_2CO の圧力は 5 mTorr でスペクトルの半値全幅は約 430 kHz である．図中で吸収線に付された記号は帰属の結果を示す．すなわち数値は下準位及び上準位の M の値の絶対値 $|M_l|$, $|M_u|$ を示し，記号 CR は飽和吸収分光に特有の交叉共鳴の吸収線を示す．基準レーザーはこのうち $|M_l|=5$, $|M_u|=6$ の吸収線の直線部分を周波数弁別信号として用いて共振器ミラーを PID（比例，積分，微分）制御して安定化された．これは比例制御に加えて長期及び短期の安定度の改善のために積分器及び微分器を併用する制御である[4]．この吸収線のシュタルク係数は 597 kHz/(kV/cm)^2 であるので，基準レーザーは H_2CO の 3.51 μm 吸収線に対して 12.72 MHz 高周波側に安定化される．

基準レーザーの周波数安定度は制御系の誤差信号から得られる結果すなわち吸収線への追従度と，シュタルク電場の安定度の二乗和の平方根として求めた．後者は印加電圧の安定度と電極スペーサーの温度変化による膨張を測定して算出した．Fig. 3 にこれらの結果をアラン分散の平方根 σ で示す．積分時間 $\tau>10$ s の安定度はシュタルク電場のゆらぎのため 10^{-13} 程度に制限される．基準レーザーの周波数安定度は $\tau=10$ s において $\sigma=8.6\times10^{-14}$ である．

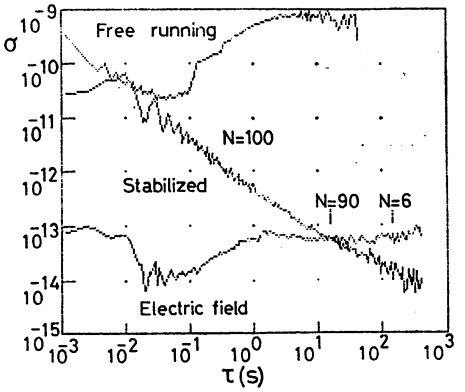

Fig. 3 Frequency stability of the reference laser as measured by Allan variance.

4. シュタルク係数の精密測定

シュタルクスペクトル安定化 He-Xe レーザーをオフセットロックレーザーシステムの基準レーザーとして使用するためには，シュタルク係数が正確に測定されている必要がある．そこで Fig. 4 に示すシュタルク係数の精密測定の実験装置によって測定を行った．これは2台の H_2CO 安定化 He-Xe レーザーを用いて，1台を零電場の吸収線に，他の1台をシュタルクスペクトルの吸収線に安定化する．2台のレーザーのビート信号を周波数

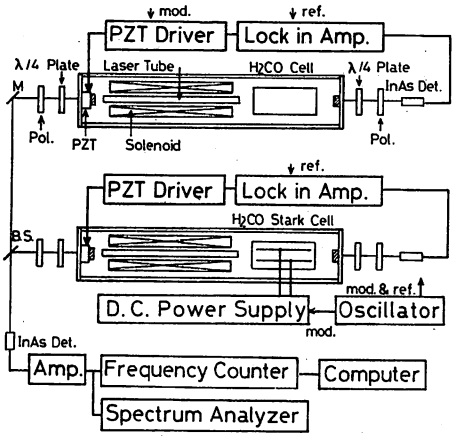

Fig. 4 Experimental set-up for precise measurement of Stark coefficient of H_2CO, using two He-Xe lasers which are stabilized to a Stark shifted line and a zero field absorption line, respectively.

カウンタで計測して，マイクロコンピュータで統計処理して，シュタルク係数を精密に測定する．H_2CO の零電場の吸収線に安定化した He-Xe レーザーの周波数安定度は $\tau \leq 1$s ではシュタルクスペクトル安定化レーザーの安定度とほぼ同じ結果となる．$\tau \geq 1$s ではシュタルク電場のゆらぎの影響を受けない零電場吸収線安定化レーザーの方が良い安定度となり，$\tau=10$s では $\sigma=4.0\times10^{-14}$ である．ビート周波数測定時間は，2台のレーザーの安定度が良い結果を示す 1s から 100s の範囲とした．

シュタルク係数の測定結果と，H_2CO の分子定数[9)~12)]から求めた計算値[8)]を Table 1 に示す．測定結果は計算値と良く一致した．なお係数の大きい2つの吸収線で計算値と一致しないのはビート測定系の周波数特性が原因である．係数の測定誤差の原因には電場の誤差，ビート周波数のばらつき，吸収線信号の零点に対する非対称性が考えられる．これらの値はビート周波数に換算してそれぞれ 0.5kHz, 1kHz, 20kHz であり，吸収線信号の非対称性が誤差の主要因である．

Table 1 A list of Stark coefficients of H_2CO absorption lines at 3.51 μm. Calculated values are computed using molecular constants in refs. (9), (10), (11) and (12).

Line $\lvert M_l\rvert-\lvert M_u\rvert$	Frequency Shift (kHz)	Electric field (kV/cm)	Stark coef. (kHz/(kV/cm)^2) Obs.	Calc.
5-5	14390±20	4.6155±1	676±1	684
cross res.	13531±20	4.6155±1	635±1	641
5-6	12716±20	4.6155±1	597±1	597
cross res.	11040±20	4.6155±1	518±1	518
4-4	9026±20	4.6155±1	421±1	423
cross res.	8281±20	4.6155±1	389±1	388
4-5	7518±20	4.6155±1	353±1	352

この測定結果から $v_5=1$ の振動励起状態の電気双極子モーメント μ_A を求めたところ

$$\mu_A(v_5=1)=2.288\pm0.005\,\mathrm{D}$$

を得た．これは従来の測定値である $\mu_A(v_5=1)=2.2844\pm0.0047$D[12)] と同じ精度の結果であり誤差範囲内で一致した．

5. 掃引レーザー

Fig. 5 に本研究で製作した H_2CO 分子の精密分光用オフセットロックレーザーシステムを示す．2台の He-Xe レーザーは基準レーザー及び掃引レーザーである．基準レーザーは先に述べた H_2CO のシュタルクスペクトル安定化 He-Xe レーザーで，H_2CO の 3.51 μm 吸収線に対して 12.7MHz 高周波側に安定化されている．掃引レーザーは周波数オフセットロックレーザーである．すなわち基準レーザーとのビート信号を検出し，ビート周波数が水晶発振器を基準とした周波数シンセサイザーの周波数値に一致するように制御されている．ここ

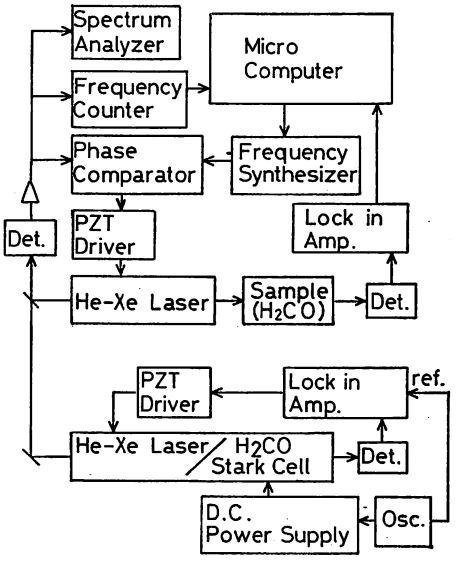

Fig. 5 Block diagram of the He-Xe offset-locked laser system for high resolution spectroscopy on H_2CO at 3.51 μm.

で周波数シンセサイザーの周波数を掃引すれば，掃引レーザーは基準レーザーと同程度の安定度を保ちつつ周波数掃引される．基準レーザーのシュタルクシフト量である 12.72 MHz を含む周波数範囲で掃引レーザーを周波数掃引すれば，H_2CO の 3.51 μm 吸収線の精密分光測定が可能である．

周波数オフセットロックでビート周波数を誤差信号に変換する方法として，周波数－電圧変換，位相－電圧変換などがある．本装置では2台のレーザーのビート周波数を 1/10 分周して周波数シンセサイザの周波数と位相比較して，これを誤差信号として掃引レーザー共振器ミラーを PID 制御した．位相比較器は 12 bit 2進カウンタが2組，加算器，12 bit D/A 変換器で構成される．2組の2進カウンタはそれぞれ比較すべき周波数信号を計数して，この計数値の差，すなわち位相差が加算器と D/A 変換器により電圧に変換される．周波数オフセットロックの方法を用いるときに問題となる点は2台のレーザーのビート周波数の変動が大きい場合，ビート信号と周波数シンセサイザーの信号の位相差が大きくなり，位相比較器のダイナミックレンジを超えてしまうことである．ここで用いた位相比較器は 12 bit カウンタを用いているので，位相余裕度は $2\pi\times2^{12}$ rad すなわち 4×10^3 Hz·s である．一方 He-Xe レーザーのフリーランニングの安定度は $\tau\leq1$ s では $\sigma\leq10^{-9}$ すなわち 10^5 Hz である．ビート信号は 1/10 分周した後に位相比較しているのでゆらぎは 10^4 Hz となるが，制御系の応答速度は 0.1 s より充分速いのでこの位相比較器の余裕度を超える事はない．このため周波数オフセットロックを安定に行うことが可能である．

掃引レーザーの周波数の設定，掃引及びモニターと，分光信号のデータ処理のためにマイクロコンピュータが用いられる．マイクロコンピュータの第1の役割は掃引レーザーの周波数の設定と掃引である．周波数シンセサイザの設定をマイクロコンピュータで制御する事により，掃引の開始と終了の周波数値，掃引のきざみ及び掃引の1きざみ当りの停留時間を任意にプログラムすることができる．マイクロコンピュータの第2の役割は掃引レーザーの周波数のモニターである．周波数シンセサイザの周波数値を新しい値に設定した後，掃引レーザーが正しい値に安定するまで 0.1 s～1 s 程度必要である．これは周波数シンセサイザとレーザーの制御系の応答時間が原因である．分光測定の際はこの不安定な過渡時期を避けなければならない．そこでビート周波数を周波数カウンタで計数し，マイクロコンピュータでモニターして，レーザー周波数掃引時の周波数の過渡時期を避けて分光測定するプログラムを開発した．マイクロコンピュータの第3の役割は掃引レーザーによる分光測定結果のデータ処理である．分光測定結果を 12 bit A/D 変換器でマイクロコンピュータに取り込み，信号の積分やその結果得られる離散的な測定データの数値処理を行う．

6. 性能の評価

本装置の周波数安定度と周波数掃引特性の性能を測定評価したところ以下の結果を得た．

位相比較器の出力電圧から測定した掃引レーザーの基準レーザーに対する追従度を Fig. 6 に示す．ここでは2台のレーザーのビート周波数が 11 MHz となるように周波数オフセットロックしている．掃引レーザーの追従度は $\tau=10$ s で $\sigma=2.0\times10^{-14}$ である．この図に示すように掃引レーザーの追従度が基準レーザーの安定度より良い結果を示しているので，掃引レーザーは基準レーザーに対して良好に追従していると言える．掃引レーザーの真の安定度は，基準レーザーの安定度との2乗和の平方根となり，$\tau=10$s で $\sigma=8.8\times10^{-14}$ である．これは前述の周波数安定度の目標値を満足している．

周波数掃引特性はビート周波数を分周して周波数－電圧変換器で電圧に変換して X-T レコーダーにより測定した．Fig. 7 は掃引レーザーを基準レーザーに対して低周波側に 11 MHz から 14 MHz 掃引した例である．掃引は 100 kHz きざみで行い，各周波数値の停留時間は 4 s とした．停留時間内に分光測定用ロックインアンプ出力は 1000 個採取され積分される．この測定はレーザー周波数の掃引に伴う周波数の過渡時期を避けて行われる．本装置の掃引可能範囲は基準レーザーに対して 2 MHz から －14 MHz である．これは前述の周波数掃引

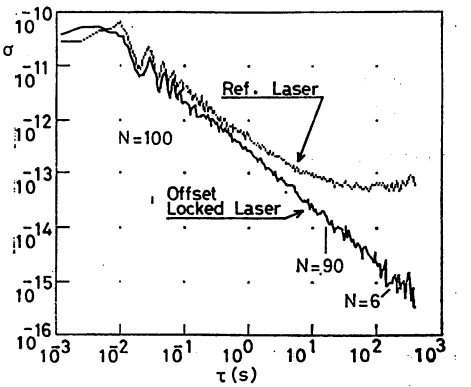

Fig. 6 Frequency traceability of the scanning laser to the reference laser as measured by Allan variance.

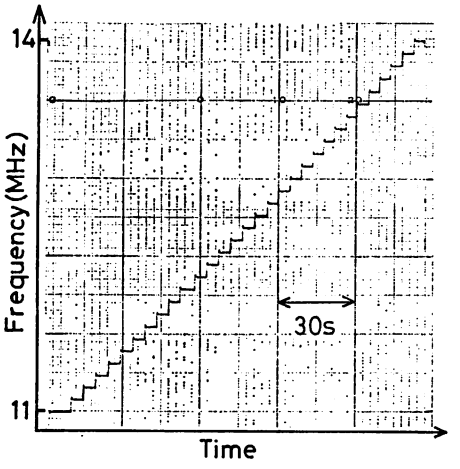

Fig. 7 An example of computer aided frequency scanning at 100 kHz interval.

特性の目標を満足している．掃引の下限は周波数シンセサイザの周波数レンジの制限に因るものであり，2 MHz 未満の掃引にはここでレンジ設定スイッチを切り換える必要がある．しかし H_2CO の精密分光装置として用いる場合この周波数領域の掃引はあまり意味が無い．一方，掃引範囲の上限 (14 MHz) を超えるとビート信号が小さくなり周波数オフセットが外れ易くなる．従って現在の結果より周波数可変範囲を広げるには，ビート検出の光軸合せを更に厳密に行い，光波面を一致させる必要がある．

7. H_2CO の飽和吸収線の精密測定

H_2CO の 3.51 μm 飽和吸収線（反転ラムくぼみ）の測定は，従来周波数安定化されていない He-Xe レーザーを用いていたので，信号の S/N 比，周波数軸の精度などの問題のために吸収線の形の評価や線幅の精密な測定が困難であった．そこで本研究で開発したオフセットロックレーザーシステムを用いて吸収線の精密測定を行った．

反転ラムくぼみを測定するために掃引レーザーの共振器中に H_2CO の吸収セルを設置した．掃引レーザーの出力光は 1 kHz のチョッパで強度変調してロックインアンプで同期検波した．Fig. 8 に精密測定された 4.9 m Torr 圧の H_2CO の飽和吸収線を示す．周波数の掃引は基準レーザーに対して −11 MHz から −14 MHz の範囲で 50 kHz きざみで行った．各周波数値における停留時間は 2 s でこの期間に 500 個の測定値を積分した．縦軸は図のフルスケールがロックインアンプ入力の 6.7 μV

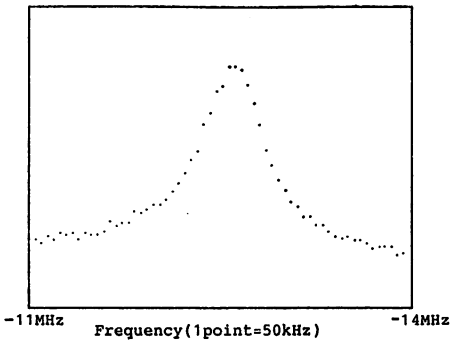

Fig. 8 Profile of the H_2CO absorption line observed by the offset-locked laser system.

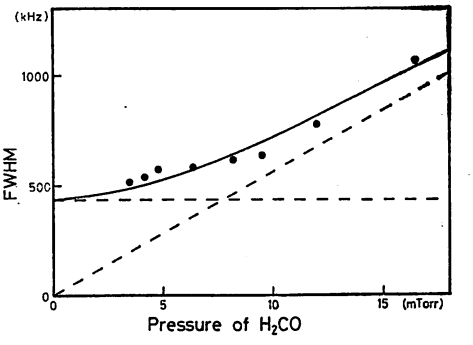

Fig. 9 Pressure dependence of FWHM of the inverted Lamb dip of H_2CO (circles). Lines show the result of curve fitting using the method of least squares.

に相当する．数 100 μV の強力なレーザー光をバックグラウンドとした微弱な反転ラムくぼみ信号が本装置により良い S/N 比で測定された．また横軸の周波数値は正確かつ線形であるので吸収線の形を正確に評価することが可能である．

Fig. 9 は本装置による H_2CO の圧力広がりの測定結果である．この結果から圧力に比例しない全幅は約 500 kHz であるが，これはパワー広がりによる値[13]と同じ程度であるので，これが原因であると考えられる．図の測定値から最小二乗法で圧力広がりの係数を求めたところ，反転ラムくぼみの全幅 $\Delta\nu_f$ は

$$\Delta\nu_f^2=\{(56\pm7)\cdot P_{H_2CO}\}^2+\{444\pm30\}^2 \quad (\mathrm{kHz}^2)$$

と近似できた．ただし P_{H_2CO} は H_2CO の圧力で単位は mTorr である．ここで得られた圧力広がりの係数 56 ±7 kHz/mTorr は，周波数安定化されていない He-Xe レーザーによる従来の測定結果[13]の HWHM に対する 155±31 kHz/Pa すなわち FWHM に対する 41.3±8.3

kHz/mTorr に比べて少し大きい値となった.

8. まとめと今後の展望

本論文では測定対象吸収線のシュタルク分裂スペクトルを用いたオフセットロックレーザーシステムを提案した. これは, 従来3台のレーザーを必要としていたオフセットロックレーザーシステムを2台のレーザーで構成するものである. そして H_2CO の 3.51 μm 吸収線の精密な高分解能分光測定を目的としたオフセットロックレーザーシステムを試作した. また基準レーザーの周波数値の測定のために, H_2CO の 3.51 μm 吸収線のシュタルク係数の精密測定を行った.

試作したオフセットロックレーザーシステムは H_2CO の精密な高分解能分光測定に必要な周波数安定度と周波数掃引特性を有している. またマイクロコンピュータ制御により正確な自動掃引と分光データ処理が行われる.

次に, 本装置を用いて H_2CO の反転ラムくぼみの精密測定を行い, 圧力広がりの係数を求めた.

本装置は周波数安定度が $\tau \gtrsim 1$ s で $\sigma \lesssim 10^{-12}$ ($\lesssim$100 Hz) であるので, 数 10 kHz の超微細構造の分解能を目標とする H_2CO の将来の高分解能分光用光源として充分使用可能である. また本論文で提案したオフセットロックレーザーシステムの方法は, H_2CO 以外の分子に対してもシュタルク分裂スペクトルが観測されれば適用可能である.

文 献

1) J.L. Hall and C. Bordé: Phys. Rev. Lett. **30**, 1101 (1973).
2) T.A. Nussmeier and R.L. Abrams: Appl. Phys. Lett. **25**, 615 (1974).
3) T. Kunikane, M. Otsu, T. Nakamura and T. Tako: Jpn. J. Appl. Phys.
4) M. Otsu, S. Katsuragi and T. Tako: IEEE **QE-17**, 1100 (1981).
5) J.L. Hall, C.J. Bordé and K. Uehara: Phys. Rev. Lett. **37**, 1339 (1976).
6) P. Thaddeus, L.C. Krisher and J.H.N. Loubser: J. Chem. Phys. **40**, 257 (1964).
7) B. Fabricant, D. Krieger and J.S. Muenter: J. Chem. Phys. **67**, 1576 (1977).
8) I. Siio, M. Ohtsu and T. Tako: Jpn. J. Appl. Phys. **21**, 813 (1982).
9) F.Y. Chu, S.M. Freund, J.W.C. Johns and T. Oka: J. Mol. Spectrosc. **48**, 328 (1973).
10) M. Allegrini, J.W.C. Johns and A.R.W. McKellar: J. Mol. Spectrosc. **66**, 69 (1977).
11) B. Fabricant, D. Krieger and J.S. Muenter: J. Chem. Phys. **67**, 1576 (1977).
12) M. Allegrini, J.W.C. Johns and A.R.W. McKellar: J. Mol. Spectrosc. **67**, 476 (1977).
13) M. Ohtsu and T. Tako: J. Appl. Phys. **50**, 599 (1979).

報　文 2

シュタルク吸収線による導波路型 CO_2 レーザーの周波数安定化と掃引

中村　拓男*，大津　元一**，田幸　敏治*

*東京工業大学精密工学研究所，横浜市緑区長津田町4259(〒 227)
**東京工業大学理工学国際交流センター，東京都目黒区大岡山2-12-1(〒 152)

(1984年12月11日受理)

Frequency Stabilization and Sweep for a Waveguide CO_2 Laser by Using Stark Absorption Lines

Takuo NAKAMURA*, Motoichi OHTSU** and Toshiharu TAKO*

*Research Laboratory of Precision Machinery and Electronics, Tokyo Institute of Technology. 4259 Nagatsuta-cho, Midori-ku, Yokohama, Kanagawa 227
**International Cooperation Center for Science and Technology, Tokyo Institute of Technology. 2-12-1, O-Okayama, Meguro-ku, Tokyo 152

(Received December 11, 1984)

A waveguide-type CO_2 laser was constructed, whose frequencies were stabilized and simultaneously swept by using Stark shifts of molecular spectral lines. The frequency of the laser was stabilized at the center of the inverted Lamb dip of a Stark line of NH_2D, and the frequency stability obtained was 1×10^{-11} at the integration time of 250s. This stability was kept when the laser frequency was then swept by slowly varying Stark electric field applied to NH_2D. The swept range was as wide as the free spectral range of the cavity (340 MHz).

1. 序　論

導波路型 CO_2 レーザーはその発振波長 9 μm 帯及び 10 μm 帯において数多くの発振ブランチがあり，また導波路に封入された媒質ガスの圧力を高くできるため，圧力広がりにより各発振ブランチの発振周波数の可変幅をドップラー幅より大きくすることができ，しかも小型で高出力なので，他の CO_2 レーザーに比べ分光用光源として有利である．導波路型 CO_2 レーザーを高分解能レーザー分光用光源として用いるにはレーザー周波数の安定化が必要である．高い周波数安定度を得るためには適当な分子ガスの飽和吸収線を用いるのがよい方法であるが，導波路型レーザーの広い周波数可変範囲をいかすにはレーザー周波数が安定化され，かつ周波数が可変であることが望ましい．この条件に合う周波数安定化法としては周波数オフセットロック法が提案されている[1]．これは周波数が安定化された周波数基準となるレーザーともう一台のレーザーとの周波数差を光ビートを用いて一定となるように制御するもので，非常に高い安定度が得られる．しかし，この方法はレーザーが二台必要であり，また光ビートを処理するために数百 MHz～数 GHz で安定に動作する信号処理系が必要なため，導波路型レーザーの小型軽量という特徴をいかせず，信号処理系の製作に高度の技術を必要とする．これらに対し筆者らは

既にレーザーが一台ですみ構造も比較的単純で信号処理系も低周波のものですむ簡便で実用的な方法を考案した[2]．すなわち，導波路型 CO_2 レーザーの共振器内にシュタルクセルを設置してレーザーの周波数を分子ガスのシュタルク吸収線に安定化することにより，周波数が高度に安定化され，かつ周波数が広範囲にわたり連続的に変化できるレーザーを試作した．本研究ではこれにひきつづきレーザーの構造を改良し，周波数安定度及び周波数可変範囲を向上させることを試みたので，これらの結果につき報告する．

2. 導波型 CO_2 レーザーの構成

Fig. 1 に試作したレーザーの構成を示す．共振器は回折格子，レンズ，導波路及び出力取出し用ミラーから構成される．レンズを用いた共振器を採用したのは，共振器内部にシュタルクセルを設置するスペースを確保し，かつできる限り共振器長を短かくして自由スペクトル域を広げ，レーザーの周波数可変幅を大きくするためである．この結果，従来の折返し型共振器[2]の共振器長640 mmに対し441 mmと短くすることができた．以下に共振器の各部分を説明する．

Fig. 2 に導波路の構造を示す．この構造は堀田ら[3]によるもので，その断面を(b),(c)に示す．(b)に示す角材

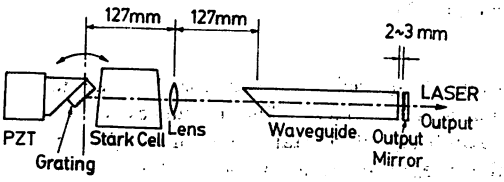

Fig. 1 Cavity configuration of the laser. A grating and a PZT are supported by a rotation stage.

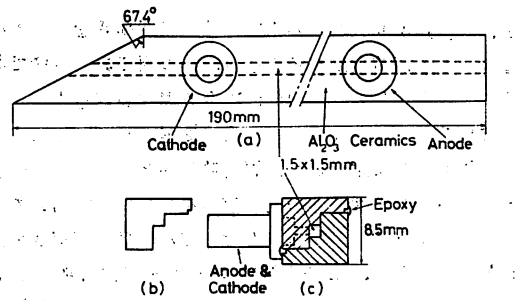

Fig. 2 (a) Schematic diagram of the hollow waveguide made of Al_2O_3 ceramics. (b), (c) Cross sectional view of the ceramics.

を二個真空用接着剤で(c)のように接着し，銅製の電極を取付け，ブリュースター角に切断された(a)の左端にZuSe の窓材を取り付け中空の導波路とした．導波路の内壁は表面精度 1 μm 以下で研摩されている．導波路は放電による温度上昇より生じる利得の低下を防ぐため，Fig. 3 に示す様に黄銅製のヒートシンクの中に埋め込まれ，水道水をヒートシンク内部に循環させて冷却している．出力取出し鏡 M_1 は反射率97%の平面鏡で Fig. 3 に示す様に導波路右端より 2～3 mmのところに置かれている．図中のフランジA～Dとマイクロメーターヘッド F は鏡 M_1 の光軸調整を行なう部分である．

Fig. 4 に回折格子とその回転機構を示す．用いた回折格子の刻線数は 150本/mm，ブレーズ波長は 10.6 μm である．回折格子はレーザー周波数を制御するため PZT に取付けられているが，レーザー周波数の安定化の際，PZT の伸縮による反作用を PZT を支える回転台が受ける．この力に対して回転台の軸が振動するのを極力小さくするため，回転台は Fig. 5 に示す様に回転軸を51mm

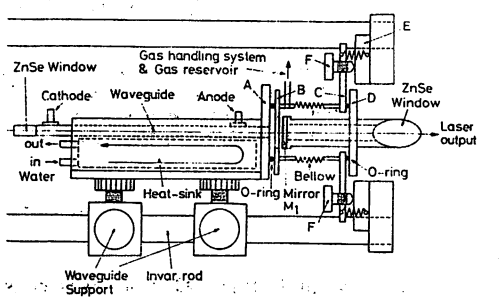

Fig. 3 Schematic diagram for the heat sink and optical alignments of waveguide and output mirror M_1.

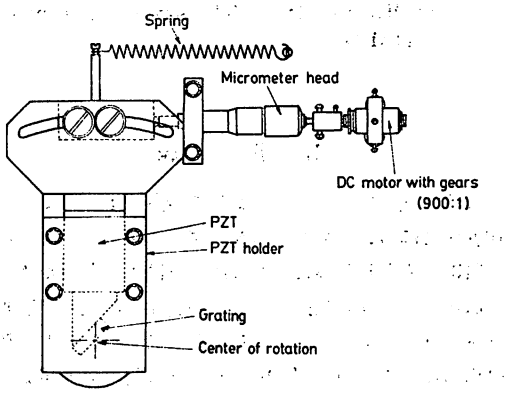

Fig. 4 Top view of the rotation stage, which supports the PZT. The d. c. motor is used to smoothly change the grating angle.

間隔の二個のアンギュラー玉軸受で支える方式とし充分な剛性を得，回転軸の振動をできる限り小さくした．回折格子の向きは Fig. 4 の減速ギアー付き DC モーターにより滑らかに変えることができ，容易に発振ブランチを選択することができる．

レンズは反尉防止膜付の ZnSe製で焦点距離は127mmである．Fig. 1 に示す様に回折格子とレンズとの距離及び導波路左端とレンズとの距離をレンズの焦点距離と等しくした．この配置では，導波路左端より出たレーザー光はレンズと回折格子を経て再び導波路端に同じ波面となって戻り，導波路左端における結合損失が非常に小さくなる．

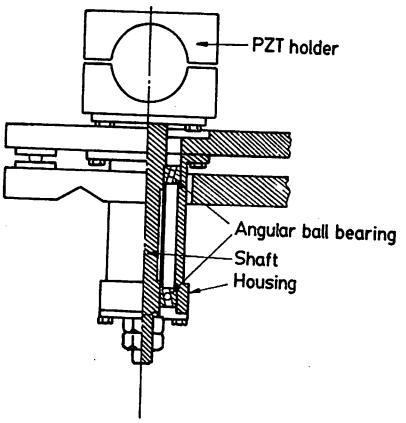

Fig. 5 Schematic diagram for the rotation shaft supported by two angular ball bearings separated by 51 mm.

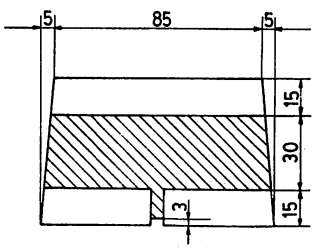

Fig. 6 A stark electrode made of a glass plate. Thin films of Cr and Au are coated onto the shaded portion.

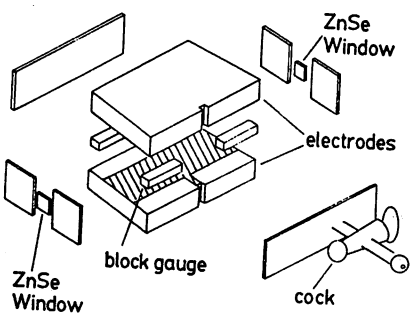

Fig. 7 Illustration for the Stark cell assembly.

吸収ガスを封入するシュタルクセルは，レーザー装置全体を小型にし，さらに容易に飽和吸収信号を得るために Fig. 1に示す様に共振器内部に設置した．セルの電極の形状を Fig. 6 に示す．BK-7ガラス製で厚さは15 mm，表面を 0.1 μm の精度で研摩し，斜線の部分にクロムと金を順次蒸着して電極とした．セルは Fig. 7に示す様にシュタルク電極が真空容器の壁を兼ねる構造とし，両端には反射防止膜付の ZnSe 製窓材を光軸に対し 5 度傾けて取り付けた．電極スペーサーの厚さは 6 mm，0 級の鋼鉄製ブロックゲージを用いた．

3. レーザーの発振特性

Fig. 8, Fig. 9 に製作したレーザーの発振特性を示す．レーザー光の強度の安定性，周波数の可変範囲及び発振強度の大きさの三つの特性の兼ね合いから経験的に，媒質ガスの全圧を 71 Torr，媒質ガスの分圧比を $CO_2 : Xe : He : N_2 = 1 : 0.25 : 3.9 : 0.75$，放電電流は 3 mA とした．この節以降の測定はすべてこの条件下で行なわれた．Fig. 8 はレーザーの各発振線の最大発振強度である．10 μm 帯 P ブランチでは16本，R ブランチでは15本，9 μm 帯 P ブランチでは 9 本，R ブランチでは 6 本の発振が得られた．Fig. 9 は 10 μm 帯 P (20) 線の

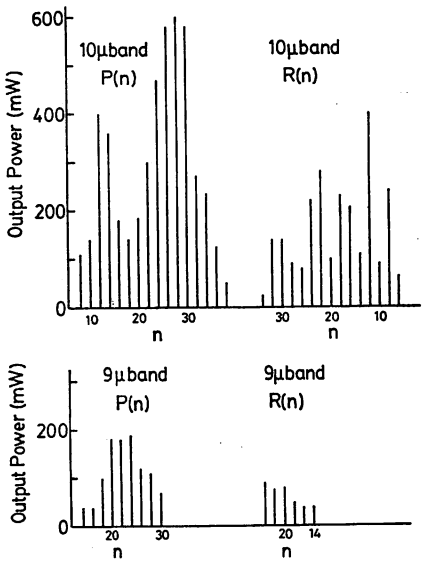

Fig. 8 Output powers of laser lines when the laser oscillation was tuned to each line.

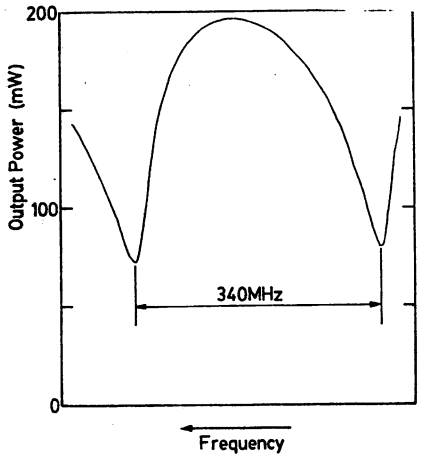

Fig. 9 Tuning curve of the P (20) line at 10.6 μm. The free spectral range was 340 MHz.

同調曲線で，横軸はレーザーの周波数に対応する PZT に印加した電圧，縦軸はレーザーの発振強度である．P (20)線ではレーザーは共振器の自由スペクトル域の全域で発振し，周波数可変幅は 340 MHz となった．同調曲線は滑らかであり，シュタルクセルの挿入によるレーザービームの乱れがなく雑音の少ない安定な発振が得られたことを示している．

4. NH_2D のシュタルクスペクトル

シュタルクスペクトルを周波数基準として用い，高精度の周波数安定化を実現するために，本研究では NH_2D の吸収線 $(0_a, 4_{04})-(1_a, 5_{05})$, $(0_a, 4_{04})-(1_s, 5_{14})$, $(0_s, 4_{14})-(1_a, 5_{24})$ の三本のシュタルクスペクトルを用いた．これらの周波数はそれぞれ CO_2 レーザーの 10 μm 帯 P(20), P(14), R(12) 線の周波数に近接している．

Fig. 10 に吸収線のエネルギー準位図を示す．吸収線の下準位 $(0_a, 4_{04})$ と $(0_s, 4_{14})$ とはわずか 644 MHz しか離れていないため近接効果[4]により高電界において二次のシュタルクシフトに比して充分に大きな一次のシュタルクシフトが得られる．両準位は電界の増加に伴い互いに反発する方向へシフトし，一次のシュタルク係数は $1.45\times10^3|M|$[Hz/(V/m)] (M：磁気量子数 $M=-4, -3, \ldots, 0, \ldots 3, 4$)[4] と大きな値となるので比較的低電界で発振線の発振周波数領域内に吸収線を同調できる．

Fig. 11 に NH_2D のシュタルクスペクトルを測定するために用いた測定系を示す．図中の Detector は液体窒素で冷却したバッテリー駆動の HgCdTe 光検出器を用いた．シュタルクセル用の高圧電源の長期的な電圧のドリフトは 200 s 間で 5×10^{-7} 程度，電圧の可変範囲は0.5

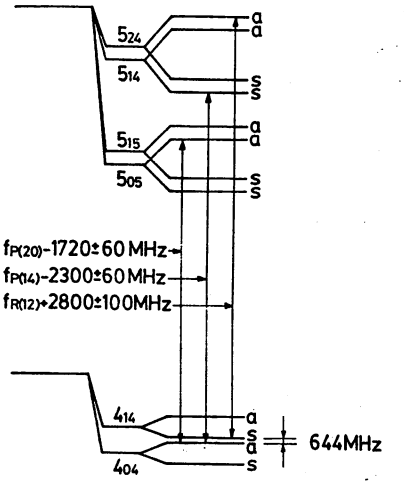

Fig. 10 Energy levels of NH_2D. Three transitions shown by arrows were used for the frequency stabilization.

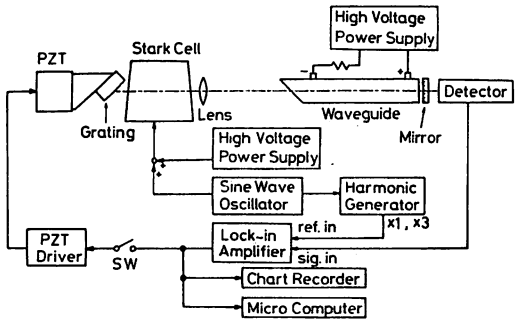

Fig. 11 Experimental set up for measuring absorption lines and the frequency stabilization.

～6 kV であり，電圧は 0.05 V/s から 50 V/s の速度で掃引することができる．吸収線の検出にはシュタルク変調法を用いた．シュタルク電界に 5 kHz の正弦波状の電界を重畳し，光検出器の出力信号をロックインアンプを用いてその三次の高調波成分を同期検波し，吸収スペクトルの三次微分信号を得た．シュタルクセルに封入する NH_2D は NH_3 と ND_3 を混合することにより得られる．NH_3 と ND_3 の圧力比を 1：1 とし，全圧を50 mTorr として用いた．

Fig. 12 に 10 μm 帯 P(20)線で測定した NH_2D の飽和吸収線 $(0_a, 4_{04})-(1_a, 5_{05})$ の三次微分曲線を示す．飽和吸収線の半値全幅は 15 MHz となり，圧力広がりから予想される幅(約 3 MHz)[5]よりも大きい．この幅はレーザーの発振強度と吸収ガスの圧力を変えても変化しないことから，シュタルク電極の歪みにより幅が広がってい

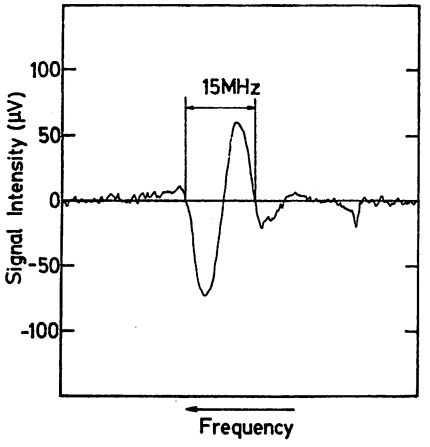

Fig. 12 The third derivative signal of the saturated absorption line of NH_2D measured by the lasing P (20) line at 10.6 μm.

ることがわかった．原因はシュタルク電極が真空容器の壁を兼ねているので，大気圧により電極に歪みが生じたためと思われる．他の二本の吸収線についても同様の測定を行ない，ほぼ同様の結果を得た．すなわち，半値全幅の値は $(0_a,4_{04})-(1_s,5_{14})$ については 17 MHz，$(0_s,4_{14})-(1_a,5_{24})$ については 18 MHz であった．

5. 周波数の安定化

まず，シュタルク電圧の値を調節することにより CO_2 レーザーの発振線の中央に NH_2D の飽和吸収線を同調して固定し，レーザーの周波数を飽和吸収線の三次微分信号の中心周波数に安定化して，レーザーの周波数安定度を測定した．飽和吸収線の三次微分信号を周波数弁別曲線として用い，Fig. 11 のスイッチ SW を閉じて周波数の制御ループを形成し，制御を行なった．制御法として PID[6]制御を用いた．

Fig. 13 に 10 μm 帯 P(20)線の発振周波数を NH_2D の飽和吸収線 $(0_a,4_{04})-(1_a,5_{05})$ に安定化した際の周波数安定度を示す．吸収ガスの圧力とレーザーの発振条件は前出の通りである．安定度はロックインアンプより出力される周波数の誤差信号より得た．図の縦軸は周波数安定度を表わすアラン分散の平方根 σ，横軸は積分時間 τ である．周波数安定度は $\tau=250$ s において 1×10^{-11} が得られ，フリーラニング時に比べ $\tau=1$ s において一桁，$\tau=100$ s において三桁，安定度の向上がみられた．他の二本の吸収線においてもほぼ同様の結果が得られた．また，この値は既報の値 5.5×10^{-11}($\tau=250$ s) よりもよいことが確認された．

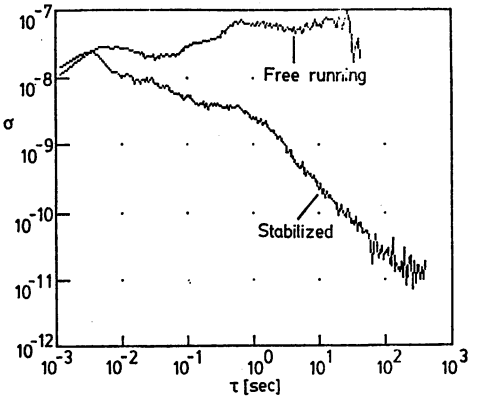

Fig. 13 Frequency stability of the laser. σ is the square root of Allan variance and τ is the integration time.

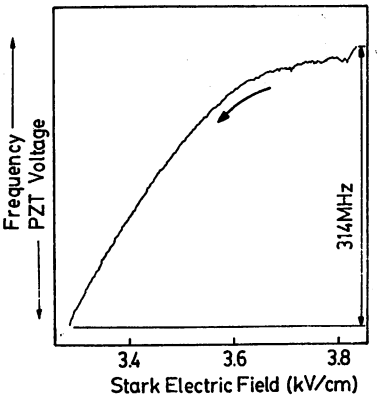

Fig. 14 Result of a continuous sweep of the laser frequency; the abssisa represents the d. c. Stark electric field, and the ordinate the PZT voltage.

6. 周波数掃引

Fig. 14 に 10 μm 帯 P(20)線でのレーザーの周波数掃引の様子を示す．図の横軸はシュタルク電界である．縦軸は PZT に印加した電圧であり，これは掃引されるレーザー周波数の値に対応している．また，図中の矢印は周波数掃引の方向を示す．レーザー周波数の掃引速度は 1 s 当り 0.5 MHz とした．図よりレーザーの周波数が飽和吸収線の三次微分の中心周波数に安定化されたまま飽和吸収線のシュタルクシフトに追従し，周波数が掃引されていることがわかる．曲線上に細かな凹凸があるのは PZT のヒステリシスによるものである．周波数掃引可能な周波数幅は10 μm 帯 P(20)線で314 MHz であった．これは既報の値 195 MHz[2]より大きい値になっており，

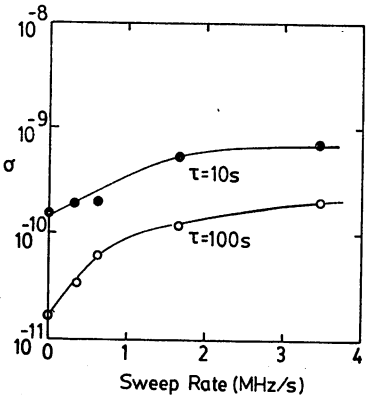

Fig. 15 Dependence of the frequency traceability on the sweeping rate.

性能の向上が確認できる．また，今回あらたに10 μm 帯 P (14),R (12) ブランチについても周波数掃引ができ，その範囲はそれぞれ113 MHz,164 MHz であった．

P(20)線ではレーザーの自由スペクトル域 (340 MHz) のほぼ全域で周波数の掃引が可能だが，P (14),R (12) ではレーザーの光強度不足のため自由スペクトル域の全域での発振が得られず可変範囲が制限された．これは，導波路形状と媒質ガスの最適化，導波路の冷却等により改善されると思われる．

Fig. 15 に掃引中のレーザー周波数の飽和吸収線の中心周波数に対するレーザー周波数の追従度と掃引速度との関係を示す．図の縦軸は追従度であり，積分時間は10s及び100sとした．この図より掃引速度が約0.1 MHz以下ならば追従度が劣化しないことが確認できる．これは，この範囲では周波数安定化のための積分制御が十分に効いているためと考えられる．

7. まとめ

本研究では，シュタルクセルを共振器内部に設置し，レンズを用い，PZT を回転台で支えた構造の導波路型 CO_2 レーザーを試作し，この周波数の安定化及び周波数の安定な掃引を行なう技術を開発した．試作したレーザーは10 μm 帯及び9 μm 帯において計46本の線で発振が得られ，10 μm 帯の P(20),P(14)及び R(12)ブランチにおいて NH_2D の飽和吸収線にレーザー周波数を安定化し，積分時間250 s において 1×10^{-11} の安定度が得られた．NH_2D のシュタルクシフトを利用してレーザーの周波数を吸収線に安定化したまま掃引した．その掃引範囲は10 μm 帯 P(20),P(14),R(12) の各線でそれぞれ314 MHz,113 MHz,164 MHz となった．これらの値は既報の結果[2]よりすぐれていることが確認できた．上の三本の線の他に，CH_3Cl[7],CH_3Br,CH_3F,NH_3,NF_3,$C_2H_4F_4$[8],$C_2H_2F_2$,PF_5 などの吸収ガスを用いれば，9μ, 10 μm 帯の多くの発振線で周波数の安定化と掃引が可能であると考えられる．

本研究の一部は文部省科学研究費補助金試験研究(2)の援助を受けた．

References

1) Ch. Borde, M. Ouhayoun, A. Van Lerberghe, C. Salmon and S. Avriller: *Laser Spectroscopy* IV eds. H. Walter and K. W. Rothe, Springer Series in Optical Sciences, Vol. 21 (Springer-verlag, Berlin, 1979) p. 142.
2) T. Kunikane, M. Ohtsu, T. Nakamura and T. Tako: Jpn. J. Appl. Phys., **23** 600 (1984).
3) K. Hotta, K. Inoue and K. Washio: *Proc. Conf. Lasers and Electro-Optics Systems*, 1978, San Diego(Opt. Soc. Am. Washington, 1978 Th AA 4).
4) C. H. Townes and A. L. Schawlow: *Microwave Spectroscopy*. (McGraw-Hill, New York, 1955).
5) A. R. Johnston and R. D. S. Melville, Jr.: Appl. Phys. Lett. **19** 503 (1972).
6) M. Ohtsu, S. Katsuragi and T. Tako: IEEE J. Quantum Electron. **QE-17** 1100 (1981).
7) F. Shimizu: J. Phys. Soc. of Japan **38** 1106 (1975).
8) J. M. Martin, V. J. Corcoran and W. T. Smith: IEEE J. Quantum Electron. **QE-10** 191 (1974).

36th Annual Frequency Control Symposium - 1982

2-4 June 1982
Marriot Hotel
Philadelphia, Pensylvania
USA

FREQUENCY STABILIZATION OF AlGaAs LASERS

Motoichi Ohtsu*, Hidemi Tsuchida** and Toshiharu Tako**,

* International Cooperation Center for Science and Technology,
** Research Laboratory of Precision Machinery and Electronics,
Tokyo Institute of Technology,
2-12-1 O-okayama, Meguro-ku, Tokyo 152, Japan

SUMMARY

Spectral width measurements and frequency stabilizations of AlGaAs lasers were carried out, and their applications were demonstrated. It was shown that the spectral width can be reduced as narrow as 1MHz. A stabilized Fabry-Perot interferometer, absorption spectra in H_2O and ^{85}Rb were used as frequency references to improve the long-term($\tau \geq 1s$) frequency stability. The minimum of the square root of the Allan variance σ^2 in these experiments were 2.0×10^{-11}, 1.1×10^{-11}, and 1.4×10^{-12} (at τ = 100s), respectively. For the laser with an external grating, the minimum of σ obtained was 3.2×10^{-12} (at τ = 100s). Several experiments were carried out to improve the short-term ($\tau < 1s$) frequency stability, and power spectral density for frequency fluctuations was reduced to less than 10^{-2} of that of free running lasers for the Fourier frequency range lower than 200kHz.

An Allan variance real-time processing system (ARPS) was developed for frequency stability measurements, and optimal frequency control was carried out by using this apparatus.

As an application of frequency stabilized lasers, the precise wavelength measurements of the H_2O absorption spectra were demonstrated, in which the preliminary results of 8164.8737$\pm$ 0.0003A° for $R(4_2\text{-}3_3)$ line was obtained. Furthermore, a brief comment on the preparation of optical pumping experiments for Rb and Cs was given.

1. INTRODUCTION

Performances of semiconductor lasers have been remarkably improved by the demand of the optical communications industry. Recently, a single longitudinal mode, CW oscillation at room temperature has been realized. The price of each laser has been reduced as low as $250. These lasers are mostly oscillated in the near-infrared, and the coherent lights of 0.83μm and 1.3-1.6μm in wavelengths are obtained by AlGaAs lasers and InGaAsP lasers, respectively. Since few number of other kind of lasers oscillates in these wavelength regions, these semiconductor lasers could be conveniently used not only in optical communications but in many fields of application, e.g., laser spectroscopy, optical pumping, frequency and length standards, laser radar, air-borne gyroscope, etc.. For these applications, however, CW oscillation performances such as spectral width, mode structures, FM and AM noise, etc. have to be understood. If these performances are not sufficient enough for these applications, they must be improved by external optical components and electronic circuits, or by manufacturing thoroughly new type of semiconductor lasers. For example, long-term frequency stabilities of these lasers have to be improved for high resolution laser spectroscopy and short-term frequency stabilities have to be considerably improved for heterodyne-type optical communications. For these applications, the stabilities of semiconductor lasers are still considerably low.

In this paper, recent results on frequency stabilization of AlGaAs lasers, with the main purpose of looking for new possibilities for applications, will be discussed.

2. NOISE AND SPECTRAL WIDTH

In the present study, channeled- substrate-planar (CSP) type AlGaAs lasers were mostly used.[1] As an initial check for the present work, the intensity fluctuations, frequency fluctuations and spectral width were measured. The temperature at the heat sink for the laser was kept at the room temperature with the fluctuations of $\pm$0.1°C and the laser was driven by a current-regulator. The temperature coefficient of the current from the regulator was 30ppm. The power spectral density of the intensity fluctuations was lower than 10^{-12} (Hz^{-1}). The frequency fluctuations were measured by a stable Fabry-Perot intereferometer, and the results are shown in Fig. 1. In this figure, it is seen that power spectral density falls between 10^{-22} and 10^{-24} (Hz^{-1}) for the wide range of Fourier frequencies.

Figure 2 shows the spectral width of the laser measured by a long Fabry-Perot interferometer (≃ 10m).[2] The value of the spectral width $\delta\nu_L$ is decreased with increasing the injection current I and it can be seen that it gradually approaches the theoretically estimated value, which is expressed as[3]

$$\delta\nu_L = \frac{4\pi h\nu(\Delta\nu_c)^2}{P}, \qquad (1)$$

where $\Delta\nu_c$ is the spectral width of the cavity, $h\nu$ is the photon energy, and P is the laser power, respectively. In this figure, $\delta\nu_L$ is reduced as narrow as 1MHz, which means that this laser can be

used even for sub-Doppler spectroscopy.

3. METHODS FOR FREQUENCY TUNING AND STABILIZATION

The relative frequency shift $\Delta\nu/\nu$ can be expressed as

$$\Delta\nu/\nu = -A \frac{1}{n} \Delta N_c - (\alpha + \beta)(\Delta T_1 + \Delta T_2), \quad (2)$$

where $A = -4 \times 10^{-27}$ (m^3), n is the refractive index in the cavity, ΔN_c is the variation of the carrier density by the injection current, α and β are the temperature coefficients of the cavity length and refractive index, respectively. ΔT_1 and ΔT_2 are the temperature variations at p-n junction by the injection current and ambient temperature variation, respectively. Here, $\alpha + \beta$ = 25GHz/°C at 0.83μm, which corresponds to 0.06nm/°C. Both ΔN_c and ΔT_1 depend on the injection current, however, their response speeds are widely different, i.e., the response of ΔN_c to the injection current is fast and that of ΔT_1 is slow. On the other hand, the magnitude of the first term in eq. (2) is about ten times smaller than that of the second term. Therefore, when the laser is driven by a low frequency current, the frequency shift depends almost only on ΔT_1, and it induces the red shift. On the other hand, when the laser is driven by a high frequency current, the shift depends only on ΔN_c, which induces the blue shift. The cross-over frequency of the current between the red and blue shifts appears at around 10MHz.[5] When the laser was driven by a d.c. current, the following value of the frequency shift, i.e., the red shift through ΔT_1, was measured for the CSP laser used here.

$$\Delta\nu/\Delta I = -2.75\text{GHz/mA}. \quad (3)$$

Following the discussions described above, both of the injection current control (ΔT_1) and ambient temperature control (ΔT_2) can be employed to improve the long-term frequency stability. When the ambient temperature control (ΔT_2) method is employed, the temperature at the p-n junction has to be varied, for example, by using a Peltier electric cooler to compensate for the frequency fluctuations.[6] In this case, the accuracy of the temperature control should be better than 10^{-3}°C to get the frequency stability higher than 10^{-10}, which looks very difficult to realize and must need a sophisticated technique for temperature control. From this reason, in the present work, the authors employed the injection current control method. The ambient temperature was roughly fixed at around the room temperature with fluctiations of ± 0.1°C, and the injection current was accurately controlled by a wide band servo controller. By this method, the frequency stability higher than 10^{-10} can be expected.

The drift of the laser output power is one of the problem which is induced when the frequency is controlled by the current. The relation between the laser power P and the current can be expressed as

$$P = P_o (I - I_{th}), \quad (3)$$

where the threshold current I_{th} depends on the temperature which is given by[7]

$$I_{th} = I_{tho} \exp(T/T_o), \quad (4)$$

where I_{tho} = 4mA and T_o = 98.5K for the CSP laser used. Therefore, the power change ΔP due to the current and temperature changes is expressed as

$$\Delta P = P_o [\Delta I - (\Delta T_1 + \Delta T_2) I_{tho} \exp(T/T_o)]. \quad (5)$$

By controlling the current, ΔI is determined so that ΔT_2 is cancelled by ΔT_1 ($\Delta T_1 + \Delta T_2 = 0$), but as a result of this cancellation, the term of ΔI remains in eq.(5), i.e., the power drift of $P_o \cdot \Delta I$ is induced. Figure 3 shows this phenomenon. In this figure, the time dependences of the power are shown for the frequency stabilized laser and for the free running laser. In this figure, power drift can be clearly seen for the stabilized laser, as discussed above. Therefore, if one needs to stabilize the frequency and power simultaneously, one has to suppress the power drift by controlling the temperature while controlling the frequency by the current.

Mode hopping phenomenon also gives a trouble in the present study, which is due to the temperature dependence of the energy gap of the semiconductor. The red shift of about 90-130GHz (=0.2-0.3nm at 0.83μm) is induced by the mode hopping when the temperature is increased, which limits the continuous frequency tuning range of the laser. Furthermore, even if the lasers are made from the same material and using the same processes, the lasers have their own individual wavelength. To some extent, they can be compensated for by adjusting the temperature or current. However, a complete compensation can not be obtained because the working range of the temperature and current should be limited to 15°C $\leqq T \leqq$ 25°C and $I/I_{th} \leq 1.4$ to keep the life time of lasers long enough, which would also limits the continuous frequency tuning range.

To overcome these difficulties, it would be necessary to use other type of lasers with a high wavelength selectivity, e.g., DBR lasers developed by Suematsu's school.[8]

4. IMPROVEMENTS IN LONG-TERM FREQUENCY STABILITY

It would be necessary to improve the long-term frequency stability, especially for $\tau \geq 1$s, for such applications as spectroscopy, frequency standard, etc.. In this case, a stable Fabry-Perot interferometer and absorption spectra of several atoms or molecules can be used as frequency references. Figure 4 shows the apparatus for frequency stabilization by using a Fabry-Perot interferometer as a reference, which is also stabilized by a Lamb dip-stabilized He-Ne laser (SP119).[9] In this figure, the amplifier (I+P+D) for current control are composed of an integrator (I), a proportional amplifier (P), and a differentiator.[10] The frequency characteristics of their gains are shown in Fig. 5. Their gains and cut-off frequencies are manually adjusted to find the optimal control conditions in each experiment. These amplifiers were always used in the present work. Figure 6 shows the frequency stability obtained. The curve D represents the stability of the semiconductor laser, and the minimum of the square root of the Allan variance σ^2 on this curve is

$$\sigma = 2.0 \times 10^{-11} \text{ at } \tau = 100\text{s}. \quad (6)$$

The curve E is for the free running laser.

For this experiment, the apparatus is rather complicated because the Fabry-Perot interferometer has to be stabilized by the stable He-Ne laser to reduce the thermal drift. Furthermore, the stability higher than 10^{-11} cannot be expected

because the stability of the interferometer is limited by that of the Lamb dip of the Ne transition in the discharge tube of the He-Ne laser. If some absorption lines of stable atoms or molecules are used as references, the apparatus may become simpler and higher stability can be expected. The authors started this stabilization scheme by employing H_2O molecules as the reference. It has been well known that H_2O has a combination tone of the vibration spectra $(v_1, v_2, v_3) = (2, 1, 1)$ around 0.8μm.[11] Though the absorption by the combination tone is weak in general, that of this band is exceptionally strong because it is coupled with (0, 1, 3) band by Darling-Dennison resonance.[12] A great number of rotation structures can be found within this band, and they have been assigned by Baumann and Mecke.[13] Figure 7 shows some of these lines around the wavelength of AlGaAs lasers. It can be said from this figure that each laser can be tuned at least to one of those spectra even though the wavelenths of the lasers are individually distributed. It is expected that almost all of the lasers can be stabilized by using these spectra as references. Figure 8 shows the first and second derivatives of the linear absorption spectra observed. The H_2O absorption cell of 10cm in length was used at room temperature, which means the H_2O vapor pressure of about 20Torr. Figure 9(a) shows the simple exprimental apparatus for stabilization and, as an example, in Fig. 9(b), the third derivative of the spectra of $P(0\text{-}1_{-1})$ line used as a reference, is shown. Figure 10 showns the frequency stability obtained, in which the curve A represents the result of stabilization. The minimum of σ on this curve is

$$\sigma = 1.1 \times 10^{-11} \text{ at } \tau = 100\text{s}. \quad (7)$$

The curve B represents the result of the previous experiment (the curve D in Fig. 6). Comparison between these curves shows that higher stability was obtained in the present method by a simpler apparatus.

In the stabilization method employing atomic or molecular spectra as references, the stability would depend on the S/N value of the signals, i.e., higher stability is expected by using a stronger absorption line. For such a strong absorption line, ^{85}Rb-D_2 line at 780nm was employed to improve the stability. Though it is not so easy to tune the laser frequency to the D_2 line because of the mode hopping, it can be highly stabilized if such a wavelength coincidence can be obtained. Fortunately, the authors found such a laser among their several CSP lasers, and wavelength coincidence was attained with the temperature of 24.6°C at the heat sink. Figure 11 shows the linear absorption spectra and their first derivative line shapes. It can be seen that they have higher S/N values than those of H_2O spectra in Figs. 8 and 9. The quantum numbers F in this figure are for the lower level $(5S_{1/2})$. The lines for different velues of F in the upper level $(5P_{3/2})$ are not resolved in this figure. The ^{85}Rb absorption cell of 6cm was used at room temperature.*) The corresponding vapor pressure is about 10^{-5} Torr, and any buffer gas is not contained in it. Figure 12 shows the frequency stability obtained by locking the frequency at the center of the first derivative of the D_2 line. The minimum of σ in this figure is

$$\sigma = 1.4 \times 10^{-12} \text{ at } \tau = 100\text{s}. \quad (8)$$

By comparing it to that by H_2O spectra, it can be said that higher stability was obtained, as expected. The authors are now preparing to use the saturated absorption spectra in D_2 line as references to improve the stability. Figure 13 shows the saturated absorption spectra. The spectral width in this figure is 52.7MHz, which is consistent with the value estimated from the radiative life time of $5P_{3/2}$ level (27.0ns).[15] Six saturated absorption lines and six cross-resonance lines should be seen on the Doppler broadened profile in this figure because the upper and lower levels for D_2 line have four and two sublevels, respectively. However, only two lines can be seen in this figure. The cause of this discrepancy is still now under investigation. It is expected that the ^{85}Rb-stabilized lasers with such a high stability can be used as powerful tools for Rb atomic standards.[16]

The frequency tunable range of the laser used above was limited by the mode hopping phenomenon, as mentioned before. One way of overcoming this phenomenon is to use an external grating.[17] The authors just followed this method and have obtained preliminary experimental results. Figure 14 shows the experimental apparatus. All of the experiments described in this paper, the authors used CSP lasers, however, in this paticular experiment, a transverce junction stripe (TJS) laser was used.[18] One of the cleaved facet of this laser was AR coated and its reflectivity was reduced as low as 14%. A grating was placed at 6cm away from the facet to pick out one of the longitudinal modes. Seventeen longitudinal modes were separately picked out by rotating the grating. The frequency of each mode was tuned for 1-3GHz by translating the position of the grating, and was stabilized by using a stable Fabry-Perot interferometer as a frequency reference. Figure 15 shows the result. Comparison between the curves A and B tells us that the stability of the free running laser is improved by using the external grating, which is because the longitudinal mode competition is suppressed and the cavity -Q velue is increased. The curve C represents the result of stabilization, and the minimum of σ on this curve is

$$\sigma = 3.2 \times 10^{-12} \text{ at } \tau = 100\text{s}. \quad (9)$$

The stabilities of other longitudinal modes were almost the same as that shown by the curve C.

5. IMPROVEMENTS IN SHORT-TERM FREQUENCY STABILITY

In 4., several experiments were carried out to improve the long-term frequency stability, i.e., the stability for $\tau \geq 1\text{s}$. For applications in heterodyne-type communications, high speed optical measurements, etc., the short-term stabilities ($\tau < 1\text{s}$) of the lasers have also to be improved. In this case, even a simple Fabry-Perot interferometer made of a rigid fused quartz block can be satisfactorily used as a frequency reference. However, it is essentially necessary to expand the bandwidth of the servo controller as much as possible.

The stability for $1\text{ms} \leq \tau \leq 1\text{s}$ was easily improved by increasing the cutoff frequency f_c of the proportinal amplifier in Fig. 5. The dependence of the stability on f_c is shown in Fig. 16.[19]

*) This cell has been used for Rb atomic standard.

In this figure, the highest stability was obtained at f_c = 7.23kHz, and the minimum of σ was

$$\sigma = 2.1 \times 10^{-12} \text{ at } \tau = 100\text{ms}. \quad (10)$$

To improve short-term stability for τ < 1ms, one needs to use different type of servo-controller. Figure 17 shows the frequency characteristics of the gain of such a controller developed by the authors, The bandwidth was increased as high as 500kHz by connecting two differentiators (D_1 and D_2) in parallel with the proportional amplifier (P), which were constructed by using faster operational amplifiers than those in Fig. 5. Figure 18 shows the power spectral densities S of frequency fluctuations of the stabilized laser obtained by this circuit. It can be seen that the value of S for the stabilized laser is about 10^{-2} of that of free running laser for Fourier frequency up to 200kHz, and that this circuit is effective to improve the short-term frequency stability. This work is now in progress and faster servo controller is being designed by using faster video amplifiers.

As described in this and previous chapters, improvements of long and short term stabilities have been carried out separately until now. As the next step, several experiments are now in progress to improve the stability for a wide range of τ by combining both of these techniques.

6. APPLICATION OF MICRO COMPUTERS

It is quite favorable if the real-time measurement of frequency stability can be done when the laser is stabilized. Such a real-time measurement system can be inexpensively made by using microprocessors. Figure 19 shows the block diagram of an Allan variance real-time processing system (ARPS) which have been developed by the authors for this purpose.[20]

It is then possible to find the condition of optimal control for frequency stabilization by using the ARPS: The appropriate gains and cutoff frequencies of the amplifiers in Fig. 5 are found by a micro computer so that the value of σ, measured by the ARPS, will ensure the minimum value. Figure 20 and 21 show the experimental apparatus for optimal control and the result obtained by this apparatus, respectively. It can be seen that the stability obtained by this method is higher than the method in which the gains and cutoff frequencies of the controller are manually adjusted. By using this method, the conditions for optimal control can be kept so that the highest frequency stability is maintained even if the working conditions of the laser may change in time.

This system can be widely used not only for the present study, but for other frequency standards.

7. APPLICATIONS OF FREQUENCY STABILIZED SEMICONDUCTOR LASERS

Frequency stabilized semiconductor lasers can be used in many fields of applications. As an example, the authors are preparing the precise wavelength measurements of absorption spectra in H_2O to find more accurate values of the molecular constants of H_2O. These wavelengths can be measured by comparing the wavelength of H_2O-stabilized laser with that of a frequency stabilized He-Ne laser by using a pressure-scanned Fabry-Perot interferometer. As a preliminary result, the wavelength of $R(4_2\text{-}3_3)$ line has been measured to be 8164.8737 $\pm$ 0.0003Å.

As another example, the vibration-rotation spectra in several molecules can also be measured by InGaAsP lasers at 1.3 or 1.6μm, which may be used for pollutant gas monitoring system.

It has been proposed that AlGaAs lasers can be used for optical pumping of Rb and C_s beam atomic standards, and several experiments have already been carried out.[21] For this partucular study, it is very difficult to use commercially available lasers due to the mode hopping phenomenon. A specially designed semiconductor laser has to be made for this purpose. The authors are now preparing facilities for crystal growing to make DBR lasers[8] with good wavelength selectivity for the optical pumping study. It is expected that these new lasers can be used also for the spectroscopy of the Rydberg states in alkali atoms.

8. CONCLUSIONS

Recent results on spectral width measurements and frequency stabilization of AlGaAs lasers were described. It was demonstrated that the spectral width can be decreased as narrow as 1MHz. A stabilized Fabry-Perot interferometer, absorption spectra in H_2O and ^{85}Rb were used as frequency references to improve the long-term frequency stability. The minimum of the square root of the Allan variance in these experiments were 2.0×10^{-11}, 1.1×10^{-11}, and 1.4×10^{-12} (at τ= 100s), respectively. For the laser with an external grating, the stability obtained was 3.2×10^{-12} at τ= 100s. Several experiments were carried out to improve the short-term stability, and the power spectral density of frequency fluctuations was reduced to less than 10^{-2} of that of free running lasers for the Fourier frequency range lower than 200kHz.

An Allan variance real-time processing system (ARPS) was developed for frequency stability measurements, and optimal frequency control was carried out by using this apparatus.

As an application of the frequency stabilized lasers, the precise wavelength measurements of the absorption spectra in H_2O are prepared, and preliminary result of 8164.8737 $\pm$ 0.0003Å for $R(4_2\text{-}3_3)$ line was obtained. Finally, a brief comment on the preparation of optical pumping experiments for Rb and C_s was given.

ACKNOWLEDGEMENTS

The authors would like to express their thanks to Dr. M. Nakamura of Hitachi, Ltd. and Dr. W. Susaki of Mitsubishi, Ltd. for their support to the experiments. They also wish to thank Profs. Y. Suematsu and K. Iga of their institute for their valuable discussions, and to Prof. N. Oura and Dr. N. Kuramochi for offering a ^{85}Rb cell.

This work was partially supported by a Grant-in-Aid for Scientific Research from the Ministry of Education, Science and Culture.

REFERENCES

1. A. Aiki, M. Nakamura, T. Kuroda, and J. Umeda, Appl. Phys. Lett., 30, 649(1977).

2. T. Takakura, K. Iga and T. Tako, Japan. J. Appl. Phys., 19, L725(1980).

3. A. L. Schawlow and C. H. Townes, Phys. Rev., 112, 1940(1958).

4. M. Ito and T. Kimura, IEEE J. Quantum Electron., QE-16, 910(1980).

5. S. Kobayashi et. al., IEEE J. Quqntum Electron., QE-18, (1982).

6. H. Tsuchida, S. Sampei, M. Ohtsu and T. Tako, Japan. J. Appl. Phys., 19 L721(1980).

7. C. L. Tang, "Method of Experimental Physics, vol 15, Quantum Electronics", Part A, p224, Academic Press, New York, (1979).

8. K. Utaka, K. Kobayashi, K. Kishino and Y. Suematsu, Electron. Lett., 16, 455(1980).

9. H. Tsuchida, M. Ohtsu and T. Tako, Japan. J. Appl. Phys., 20, L403(1981).

10. M. Ohtsu, S. Katsuragi and T. Tako, IEEE J. Quantum Electron., QE-17, 1100(1981).

11. G. Herzberg, "Infrared and Raman Spectra", p473, Van Nostrand, Princeton, (1945).

12. B. T. Darling and D. M. Dennison, Phys. Rev., 57, 128(1940).

13. W.Baumann and R. Mecke, Zeits. Physik, 81, 445(1933).

14. H. Tsuchida, M. Ohtsu and T. Tako, Japan. J. Appl. Phys., 21, L1(1982).

15. J. K. Link, J. Opt. Soc. America, 56, 1195 (1966).

16. L. L. Lewis and M. Feldman, Proc. 35th Ann. Freq. Symposium, p612(1981).

17. M. W. Freming and A. Mooradian, IEEE J. Quantum Electron., QE-17, 44(1981).

18. H. Namizaki, IEEE J. Quantum Electron., QE-11, 427(1975).

19. H. Tsuchida, M. Ohtsu and T. Tako, Trans. IECE Japan, E-65, 65(1982).

20. I. Siio, M. Ohtsu and T. Tako, Bull. P. M. E. (T. I. T.), 48, 47(1981).

21. M. Arditi and J.-L. Picque, J. Phys. B. Atom. Mol. Phys., 8, L331(1975).

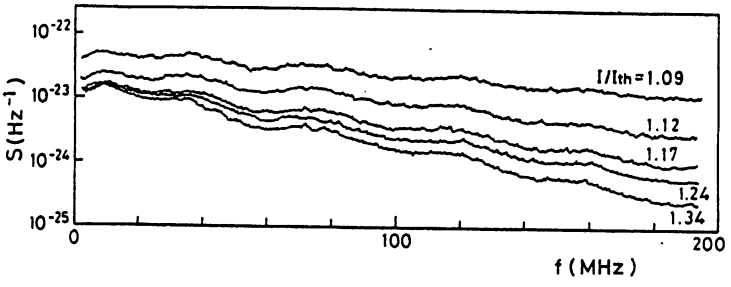

Fig.1. Power spectral density of the frequency fluctuations. I/Ith represents the injection current normalized to its threshold value.

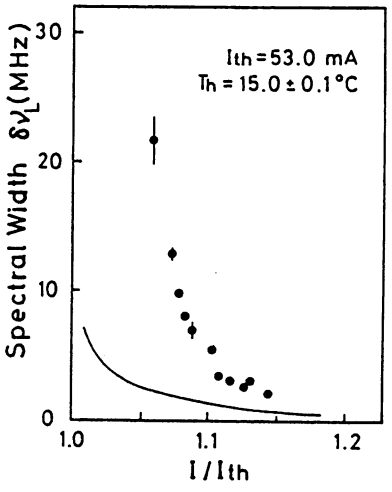

Fig.2. Relation between spectral linewidth $\delta\nu_L$(FWFM) and injection current. The solid curve represents the theoretical value.

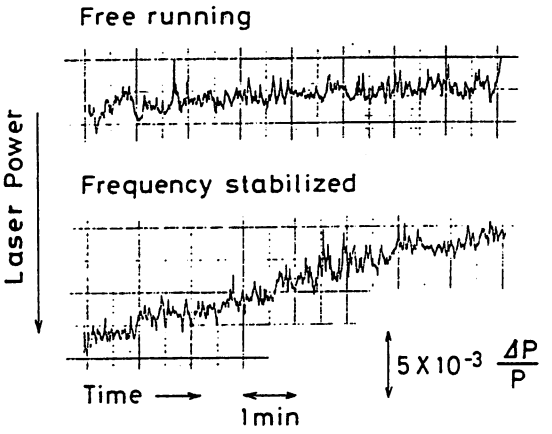

Fig.3. Time dependence of the laser power.

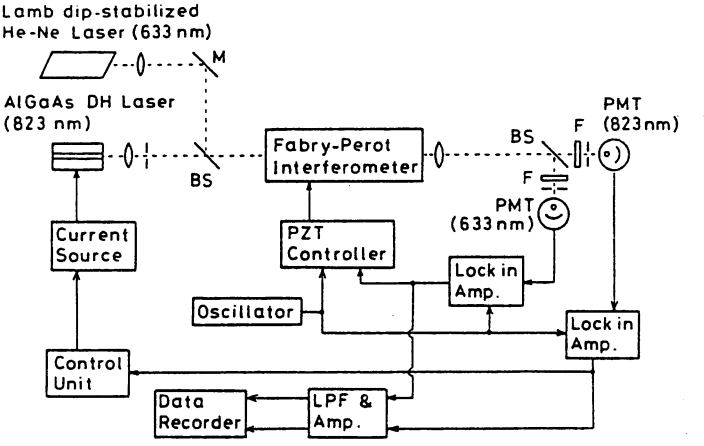

Fig.4. The experimental apparatus for frequency stabilization using the stabilized Fabry-Perot interferometer as a reference.

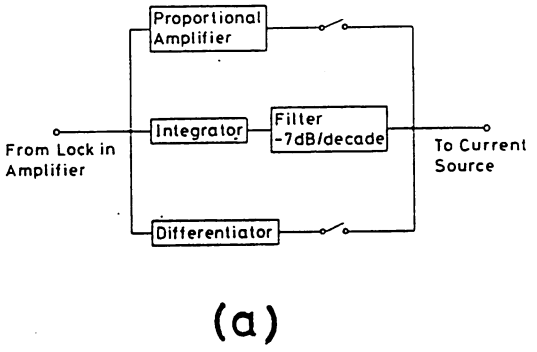

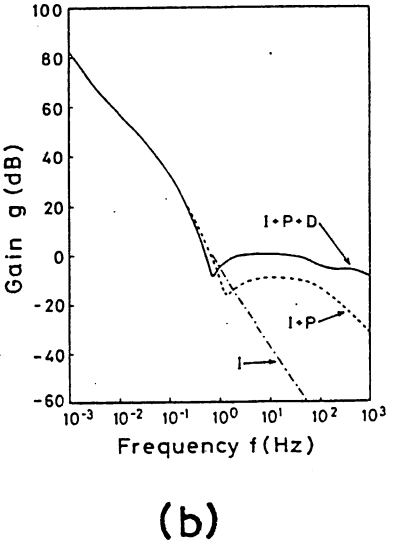

Fig.5. (a) The block diagram of the amplifiers used for the servo-controller.
(b) Frequency characteristics of the gains of the amplifiers in (a).

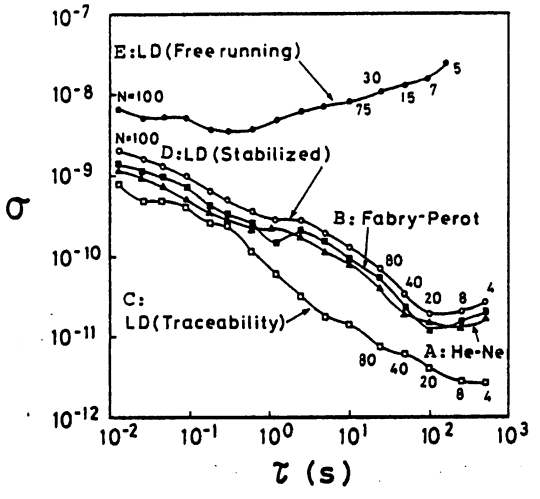

Fig.6. Experimental results. A: The frequency stability of the Lamb dip-stabilized He-Ne laser. B: The frequency traceability of the Fabry-Perot interfermoter to the He-Ne laser. C: The frequency traceability of the semiconductor laser to the interferometer. D: The frequency stability of the stabilized semiconductor lasers estimated by the curves A, B, and C. E: The frequency stability of the free running semiconductor laser

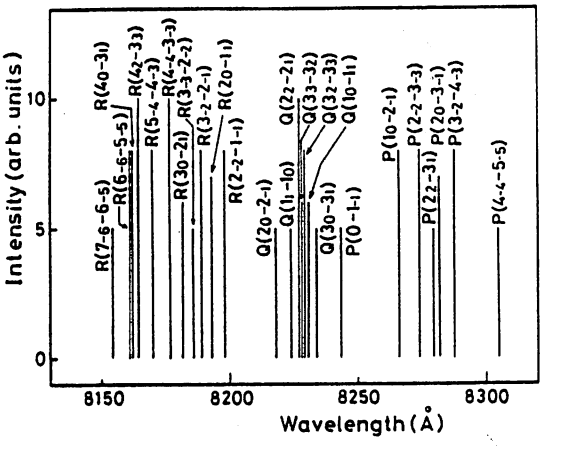

Fig.7. The assignment and relative intensities of the principal lines in the (2, 1, 1) band of H_2O spectra.

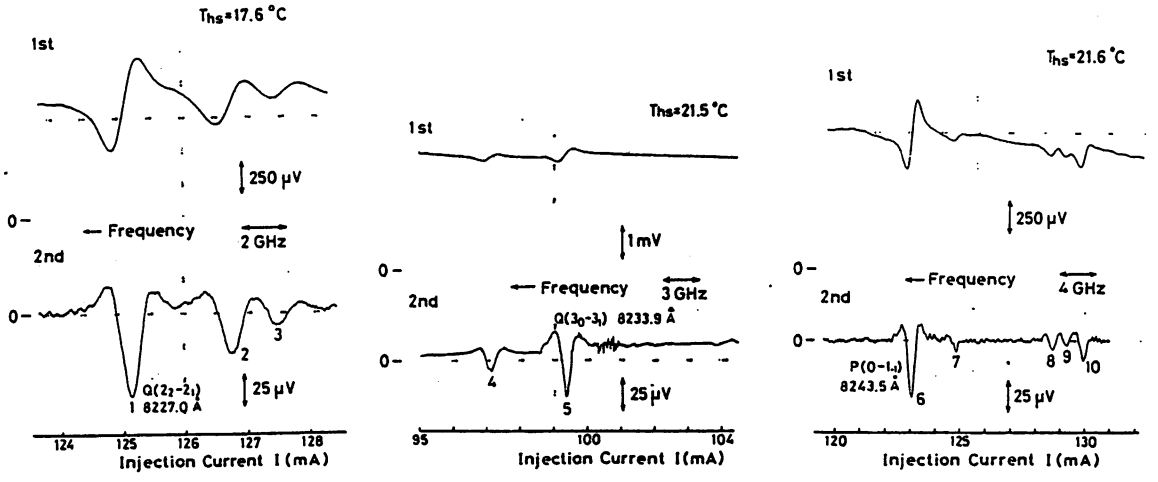

Fig.8. The first and second derivative signals of the absorplion spectra in H_2O.

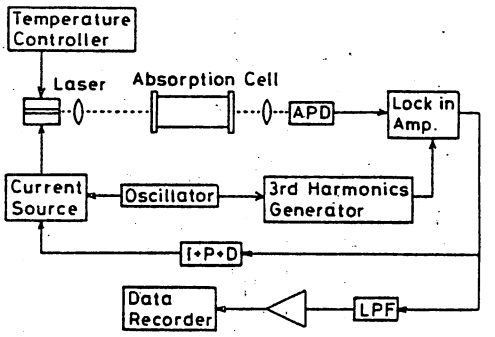

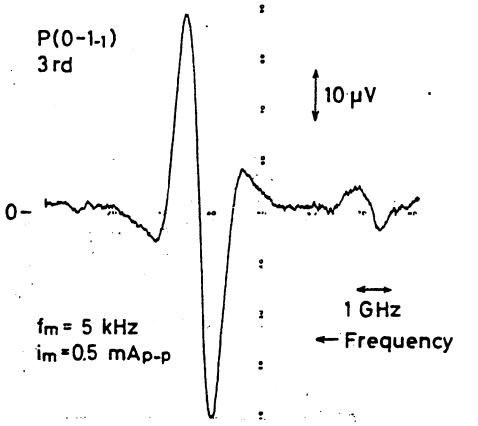

Fig.9. (a) Experimental apparatus for frequency stabilization by using H_2O spectra as a frequency reference. (b) The third derivative of the absorption spectrum in H_2O used as a frequency reference.

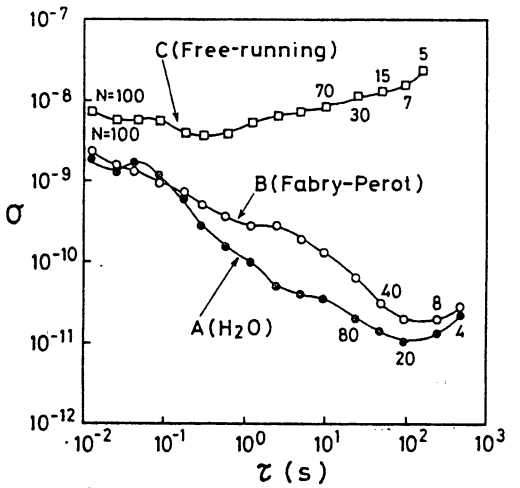

Fig.10. Frequency stability. The curves A and C represent the stability for H_2O-stabilized and free-running lasers, respectively. The curve B is for the result of the previous work (The curve D in Fig.6.)

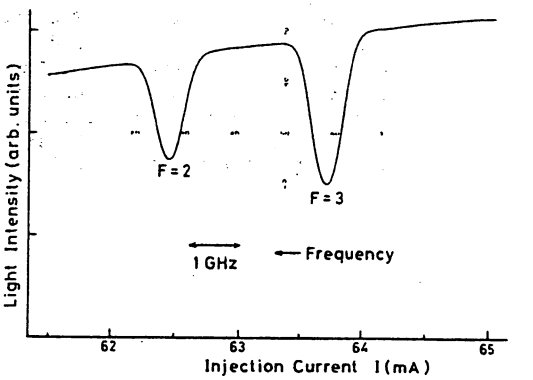

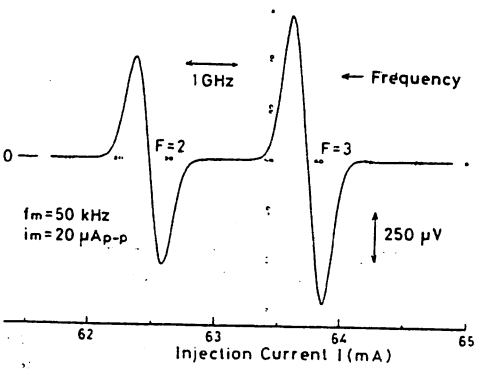

Fig.11. The linear absorption spectra of ^{85}Rb-D_2 line, and their first derivatives.

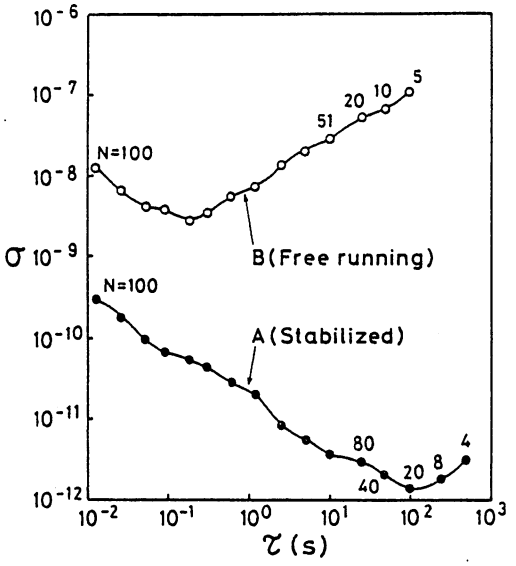

Fig.12. Frequency stabilities of the ^{85}Rb-stabilized (A) and free running (B) lasers, respectively.

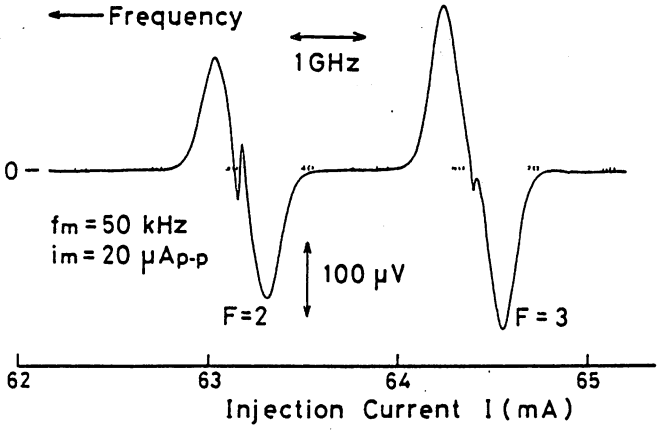

Fig.13. The first derivative signals of the saturated absorption spectra of ^{85}Rb-D_2 line.

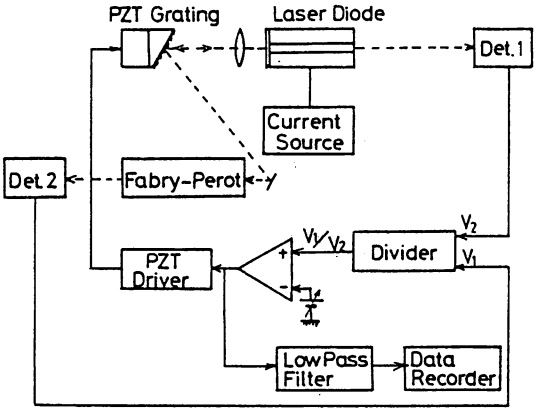

Fig.14. Experimental apparatus for frequency stabilization of a TJS laser with an exteranl grating.

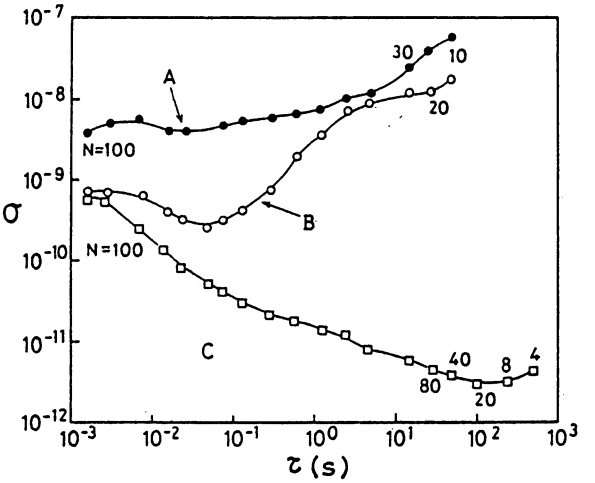

Fig.15. Frequency stability of the free running laser without an external grating (A), with an external grating (B), and of the stabilized laser with an external grating, respectively.

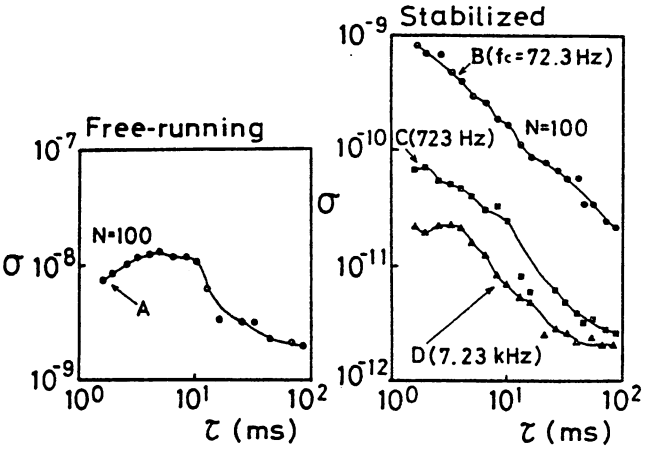

Fig.16. The dependence of the short-term frequency stability ($1ms \leq \tau < 1s$) on the cutoff frequency f_c of the proportional amplifier in Fig.5.

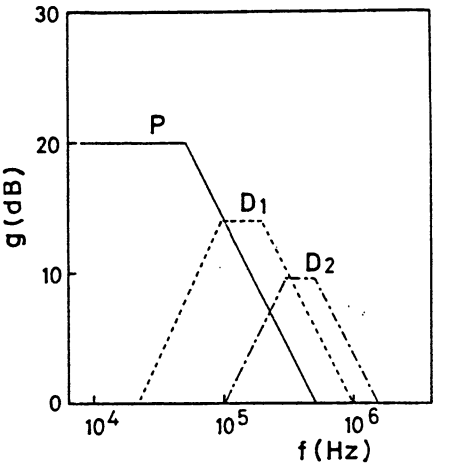

Fig.17. Frequency characteristics of the gain of the amplifiers used to improve the short-term frequency stability ($\tau < 1ms$).

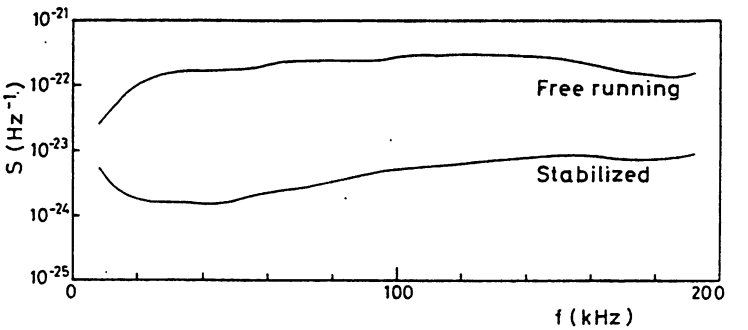

Fig.18. Power spectral density of the frequency fluctuations. The amplifiers in Fig.17 were used for stabilization.

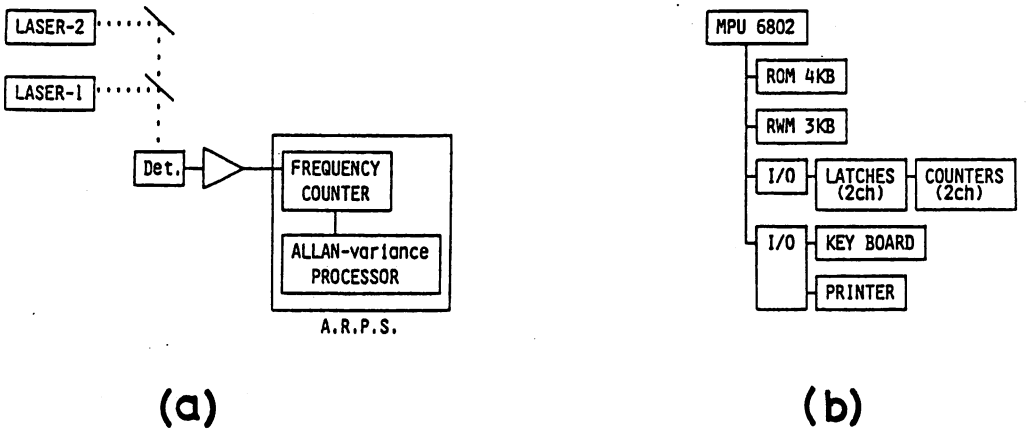

Fig.19. (a) The measurement system of the laser frequency stability. (b) The block diagram of the Allan variance real-time processing system.

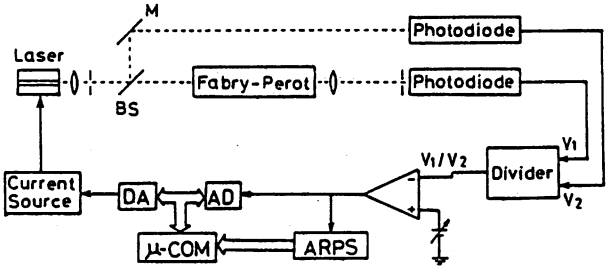

Fig.20. Experimental apparatus for optimal control for frequency stabilization by micro-computers.

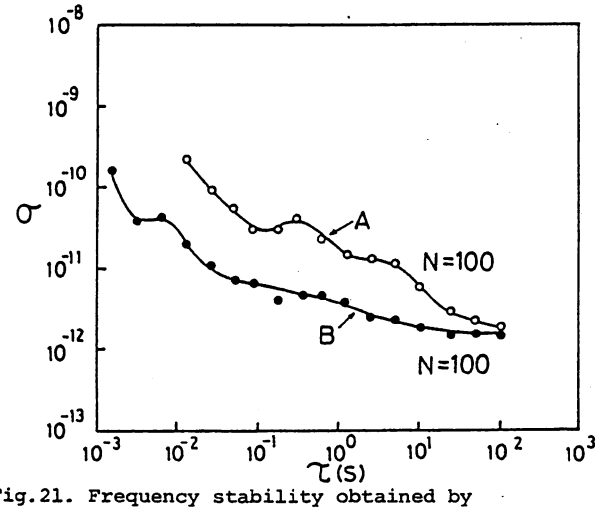

Fig.21. Frequency stability obtained by manual control (A) and by optimal control (B).

REPRINTED FROM PROCEEDINGS OF THE INTERNATIONAL CONFERENCE ON LASERS '83, DECEMBER 12-16, 1983
PRINTED IN USA

(Invited) Frequency Control of Semiconductor Lasers and Its Application to Metrology

Motoichi Ohtsu

International Cooperation Center for Science and Technology,
Tokyo Institute of Technology, 2-12-1 O-okayama, Meguro-ku,
Tokyo 152, Japan

[Abstract]
The spectral width of 0.8μm AlGaAs laser, derived from the experimental results of FM noise measurements, was less than 10MHz. The power-independent width was also estimated from 1/f noises, which was 2.0MHz. Several frequency controlling techniques of 0.8μm AlGaAs and 1.5μm InGaAsP lasers were demonstrated to improve their long-term frequency stabilities. The stabilities were about 1000 times improved than that of the free-running lasers. It was confirmed that the long-term stability of AlGaAs laser was almost equal to the theoretical limit. Several examples of application of these highly stabilized lasers were demonstrated in the field of coherent optical measurements, i.e., Rb and Cs atomic clocks, pollutant gas monitoring, and fiber-gyroscope.

§1. Introduction

Due to the increasing demand in optical communication industries for better characteristics of semiconductor lasers, several remarkable improvements in performances of 0.8 μm AlGaAs and 1.5μm InGaAsP lasers have been successfully carried out recently. If these lasers are used for coherent optical measurements, their spectral purities and long-term frequency stabilities (for integration time longer than 1μs), have to be further improved. From these points of view, the author has tried to measure the spectral widths and to improve the long-term frequency stabilities of these lasers. In this paper, these results and several examples of applications to coherent optical measurements are shown.

There are several lateral mode stabilized AlGaAs lasers at 0.8μm. Among them, Channeled-Substrate-Planar (CSP) type lasers[1] are used in the present study because they have larger stripe widths, that is, the cavity Q is larger, which means they show narrower spectral widths and lower quantum noises.

As for 1.5μm InGaAsP lasers, Plano-Convex -Waveguide (PCW) type lasers[2] were employed here, which are similar to CSP lasers.

§2. Spectral Width Measurements of 0.8μm AlGaAs Lasers

The spectral width $\Delta\nu$ (FWHM) has been conveniently expressed by the following modified Schawlow- Townes formula[3].

$$\Delta\nu = 2\frac{h\nu_0}{16\pi P_0}\left(\frac{c}{nL}\right)^2 (\ln R - \alpha_1 L)(\ln R) n_{sp}(1+\alpha^2). \quad (1)$$

Here, α represents the broadening by the extra FM noises induced by the carrier density fluctuations, which also corresponds to the ratio of the real and imaginary parts of the change of the complex refractive indices by the carrier density fluctuations[4]. The spectral width of CSP lasers with 300μm long has been measured in Japan as being less than 10MHz[5,6]. On the other hand, the values reported in other countries are sometimes as large as 100MHz, which is about ten times larger than Japanese results (see, for example [3]). As the other outstanding results, the power-independent spectral width has been observed for TJS lasers, which is 1.9MHz at room temperature[3], while this value for the CSP lasers has been reported as being 0.6 - 0.9 MHz[7]. Following these results, there are two problems to be solved, namely ; the real value of the spectral width and the origin of the power-independent spectral width. In this section, the experimental results are shown about these problems.

There are several techniques of measuring the spectral width. That is, measuring the beat spectrum between the two lasers, using a high resolution Fabry-Perot interferometer[5], and using an optical fiber which is called as the delayed self heterodyne technique[8]. However, these techniques have several difficulties in them, i.e., the extra FM noises are induced by the light reflected back from the mirror surface of the interferometer or the end of the optical fibers. These FM noises also induces extra spectral broadening, or sometimes, narrowing. To avoid this effect, an indirect method was employed in the present experiment, i.e., the spectral width was estimated from the measured value of the FM noises. The experimental setup is shown in Fig. 1. As a tilted Fabry-Perot interferometer can be used as a frequency discriminator for FM noise measurements because the finesse does not have to be high enough in this case, the reflected light does not come back into the laser cavity. Therfore , no extra noises are induced, and this method can be safe enough to estimate the intrinsic spectral width.

The spectral profile $I(\nu)$ can be given by the Fourier transformation of the auto-correlation function $R(\tau)$ of the amplitude $E(t)$ of the electric field of the laser light.

As given by eq.(2), the amplitude E(t) contains the fluctuating phase $\phi(t)$ in it.

$$E(t) = E_0 \exp[-i(2\pi\nu_0 t + \phi(t))]. \quad (2)$$

The time derivative of this fluctuating phase gives the frequency fluctuations (FM noises) y(t) ($= d\phi/dt/2\pi\nu_0$). The autocorrelation function $R(\tau)$ is, then, expressed by the second-order moment of the phase fluctuations $<\delta\phi^2(\tau)>$, which is expressed by eq.(3).

$$\begin{aligned} R(\tau) &= <E(t)\cdot E(t+\tau)^*>/ E_0^2 \\ &= \exp[i(2\pi\nu_0\tau + \phi(t+\tau) - \phi(t))] \\ &= \exp[i(2\pi\nu_0\tau + \delta\phi(\tau))] \\ &= \exp[i2\pi\nu_0\tau - <\delta\phi^2(\tau)>/2], \end{aligned} \quad (3)$$

where τ represents the integration time for the fluctuation measurements. The second-order moment of the phase fluctuations $<\delta\phi^2(\tau)>$ is proportional to that of the frequency fluctuations $<\delta\nu^2(\tau)>$, as is expressed in eq.(4). Here, $<\delta\nu^2(\tau)>$ can be also expressed by a measure known as the Allan variance $\sigma_y^2(\tau)$ [9], which is given also in eq.(4).

$$\begin{aligned} <\delta\phi^2(\tau)> &= (2\pi\tau)^2 <\delta\nu^2(\tau)> \\ &= (2\pi\tau)^2 \cdot \nu_0^2 \cdot \sigma_y^2(\tau). \end{aligned} \quad (4)$$

Therefore, $R(\tau)$, $I(\tau)$, and the spectral width $\Delta\nu$ can be given by the Allan variance (eqs.(5) and (6)) :

$$R(\tau) = \exp[i2\pi\nu_0\tau - 2(\pi\nu_0\tau)^2 \cdot \sigma_y^2(\tau)]. \quad (5)$$

$$I(\nu) = \int_0^\infty \exp[i2\pi(\nu_0-\nu)\tau - 2(\pi\nu_0\tau)^2 \cdot \sigma_y^2(\tau)]d\tau + c.c. . \quad (6)$$

The Allan variance is a convenient measure, which has been proposed by D. Allan, and is defined by eq.(7) [9].

$$\sigma_y^2(\tau) = \lim_{N-\infty} \frac{1}{N-1} \sum_{k=1}^{N-1} (y_{k+1} - y_k)^2/2. \quad (7)$$

Here, y_k represents the frequency fluctuations which is averaged over the integration time τ. The Allan variance can be also derived from the power spectral density of the frequency fluctuations $S_y(f)$ by eq.(8).

$$\sigma_y^2(\tau) = 2\int_0^\infty S_y(f) \frac{\sin^4(\pi f\tau)}{(\pi f\tau)^2} df. \quad (8)$$

By these procedures, the spectral width can be derived by measuring the Allan variance or the power spectral density of the frequency fluctuations, i.e., FM noises.

Figure 2 shows the experimental results of the power spectral density of FM noises at T = 293K. In the Fourier frequency range higher than 5MHz, the noise is governed by the quantum noises, i.e., the spontaneous emission and carrier density fluctuations. These quantum noises are the white noises, and in the case of the single longitudinal mode oscillation, this magnitude is inversely proportional to the injection current I, which is expressed as

$$S_y(f) = A_0 (I/I_{th} - 1)^{-1} \quad (Hz^{-1})$$
$$A_0 = 2.8 \times 10^{-24} \quad (Hz^{-1}) , \quad (9)$$

where I_{th} represents the threshold value of the current. When the value of the proportional constant A_0 is derived, one should be careful not to use the values of the FM noises in the multimode oscillation region. If these data are used, the proportional constant is overestimated. In the case of the present experiment, the intensity of the satellite longitudinal modes were only less than 1% of that of the main mode in this region. Even by such weak satellite modes, the extra FM noises can be induced and the deviation from this linear relation can be seen, which is illustrated by Fig. 3. This can be also said for direct measurement of the spectral width. If the spectral width is measured in this region, which is slightly multimode, its value can be overestimated because of the mode competition. This may be one of the reason why sometimes the value of the spectral width is measured as large as 100MHz. By using this proportional constant, the spectral width can be estimated by the procedure shown above. The broken line in Fig. 4 shows the result, which corresponds to the modified Schawlow-Townes formula. The conclusion obtained from this line is that the spectral width is less than about 10MHz in the single mode region, which is consistent with the results previously reported in Japan[5,6].

On the other hand, Kikuchi and Okoshi [10] pointed out that a power-independent 1/f noise appears in the power spectral density of FM noises, which can be formulated as :

$$S_y(f) = A_1 f^{-1} \quad (Hz^{-1})$$
$$A_1 = 3.4 \times 10^{-18} \quad (10)$$

It can be said that one of the origin of the power-independent spectral width is this noise. To estimate the effect of this noise, calculations were done by adding this value to eq.(9). The solid curve in Fig. 4 shows the result[11]. It is deviated from the modified Schawlow-Townes formula(the broken line), and has the power-independent spectral width of 2.0MHz at room temperature. This value is almost equal to the result for TJS laser[3], while it is about two times larger than those reported for CSP lasers[7]. Though there are several differences between each value,the power-independent 1/f noise

can be one of the origin of the power-independent spectral width because the existence of this noise is quite possible, as has been popularly observed in the current fluctuations and mobility fluctuations in conventional semiconductor devices[12].

§3. Frequency Control and Stabilization of 0.8μm AlGaAs Lasers

To improve the long-term frequency stability of the 0.8μm AlGaAs lasers, it has to be known how the frequency shift is induced. The frequency shift is due to the carrier density change and the temperature change by the injection current, and is also due to the change of the ambient temperature. The frequency shifts by the unit change in the injection current and temperature have been measured as being -2.5GHz/mA and -25GHz/K, respectively. for the CSP lasers. As the laser frequency is controlled by the injection current in the present experiments, its response characteristics to the injection current should be checked first. It has been known that the phase characteristics of the response can be expressed as

$$\arg\left(\frac{\delta\nu}{\delta I(f)}\right) = -0.32 \log_{10} f + 1.03 \quad \text{(rad)}$$

$$\text{for} \quad f < 10\text{MHz}, \qquad (11)$$

which shows the phase lag for the current frequency f up to 10MHz[13]. Therefore, to improve the long-term frequency stability within this range of the current frequency (i.e., $\tau \geqq 1\mu s$), the phase-lead compensation is required. That is, a differentiator has to be used to control the current. Furthermore, a proportional amplifier and integrator have to be also added to reduce a very slow frequency drift. Therefore, PID control is required for long-term frequency stabilization for $\tau \geqq 1\mu s$. Figure 5 shows the frequency characteristics of the gains of the PID controller employed.

A very stable frequency standard has to be prepared for the stabilization. Then, the laser frequency is locked to this standard frequency by controlling the injection current. At the same time, the Allan variance or the power spectral density of the residual frequency fluctuations (FM noises) are measured. To suppress the frequency fluctuations for $\tau \geqq 1\mu s$, a stable Fabry-Perot interferometer, spectra in stable atoms or molecules can be used as a frequency standard.

3.1. Improvements of the Stability for $\tau \geqq 1ms$

To suppress the slow fluctuations for $\tau \geqq 1ms$, several frequency standards can be used. The first example is the Fabry-Perot interferometer which is stabilized by a He-Ne laser with a higher frequency stability. The experimental setup is shown in Fig. 6[14]. The second example is the absorption spectra in H_2O vapor, which has a great number of spectral lines due to the rotational structure of the combination tones of the vibration transition around 0.8μm wavelength region. If these spectra are used, the experimental setup becomes simpler than that of Fig. 6, which is illustrated in Fig. 7 [15]. The third example is the Rb-D_2 line which shows stronger absorption than that by the H_2O vapor. The absorption spectra observed is shown in Fig. 8 [16]. Figure 9 shows the result of the frequency stabilizations using these three standard, where $\sigma_y(\tau)$, is the square root of the Allan variance of the residual frequency fluctuations. The frequency stability was about 1000 times improved than that of the free-running lasers. Especially, by using the Rb-D_2 line, the minimum of $\sigma_y(\tau)$ obtained was

$$\sigma_y(\tau) = 1.4 \times 10^{-12} \quad \text{at } \tau = 100 \text{ s}. \qquad (12)$$

3.2. Improvements of the Stability for $\tau < 1ms$

As the next step, to improve the stability for $\tau < 1ms$, a Fabry-Perot interferometer made of a rigid quartz block can be used as a frequency standard. In this case, several differentiators have to be connected to expand the bandwidth of the phase-lead compensation. Figure 10 shows the frequency characteristics of the gains of these differentiators designed by the author's colleague[17]. As shown by the curve C_2 of Fig. 11, the frequency stability was improved also for $5\mu s \leqq \tau \leqq 1ms$ by this stabilization. This figure also shows the summary of the experimental results obtained above. The frequency stability for $\tau \geqq 5\mu s$ was about 1000 times improved by the stabilization, which is almost equal to the theoretical limits. Here, the theoretical limit was estimated by using the semiclassical Langevin's equation including spontaneous emission, carrier density fluctuations, current fluctuations, etc.[18]. On the other hand, for $\tau < 1\mu s$, it can be seen from this figure that the frequency stability of the free-running lasers (the curve D) is already almost equal to the theoretical limit. This result means that frequency stability within this range of τ cannot be improved any more even if the stabilization is employed. However, if one wish to improve the stability for $\tau < 1\mu s$ (i.e., the short-term stability), the laser structure itself has to be changed. One of the effective way for this purpose is to increase the cavity Q by adding an external mirror or grating, which has been tried also by many peoples. By adding an external grating as shown by Fig. 12, the stability of the free-running laser was actually improved, and further improvements were obtained by the stabilization. The results are given by Fig. 13 [19]. Though they are still preliminary results, it can be expected that this technique is really effective to improve the short-term stability.

§4. Frequency Control and Stabilization of 1.5μm InGaAsP Lasers

As 1.5μm InGaAsP lasers are rather new type laser, some of their oscillating characteristics are still unknown. However, by several experiments, it has been known that the frequency shifts by the unit change in the injection current and temperature are -1.0GHz/mA and -11GHz/K, respectively[20]. Furthermore, it was found that absorption spectra in NH_3 and H_2O vapor can be used as the frequency standards for the long-term frequency stabilization[21]. Figure 14 shows the results of the stabilization[21]. The stability was improved about 1000 times than that of the free-running lasers. The minimum of $\sigma_y(\tau)$ was

$$\sigma_y(\tau) = 2.1 \times 10^{-11} \quad \text{at } \tau = 200 \text{ s}. \qquad (13)$$

§5. Applications to Metrology

One of the most important application of 0.8μm AlGaAs lasers is the optically pumped Rb atomic clock, which will be used for communication, navigation, astronomy, etc.[22]. That is, these lasers are used for optical pumping of Rb vapor to get a stable microwave signal of 6.8GHz. As a preliminary experiment, the Doppler-free saturated absorption spectra in Rb-D_2 line has been measured by the author, which is shown by Fig. 15 [16].

The second example is the optically pumped Cs atomic clock which shows a higher frequency stability than that of Rb atomic clock, and can be used as a primary standard of time[23]. The author's coleagues have already succeeded in fabricating a stable single mode CW laser (S-MIS type AlGaAs laser) used for this experiment [24]. Several laser fabrications are now in progress by the author's group to get a better wavelength coincidence with the Cs or Rb resonant lines for optical pumping.

The third example is the pollutant gas monitoring by 1.5μm InGaAsP lasers and optical fibers. The remote sensing of the local concentration of pollutant gases can be done by using the optical fiber as a transmission line. The experimental apparatus is shown by Fig. 16 [21]. Figure 17 shows the relation between the signal-to-noise ratio of the observed NH_3 spectral shape and the NH_3 vapor pressure. The minimum detectable concentration was estimated as being 3ppm from this result.

The last example is the fiber gyroscope composed of a 1.5μm InGaAsP laser and optical fibers. Figure 18 is the schematic diagram of the gyroscope proposed by the author, which is composed of a ring Fabry-Perot interferometer[25]. It was estimated that the sensitivity, shown by Fig. 19, of this gyro is as high as the one limited by the detector-shot noises, which is more sensitive than a conventional Mach-Zender interferometer-type fiber-gyro. The experiments are now in progress by following this design.

§6. Summaries

The results of the spectral width measurements and long-term frequency stabilizations of 0.8μm AlGaAs and 1.5μm InGaAsP lasers were presented. These highly stabilized lasers may be used as reliable light sources for coherent optical measurements in the future. As examples of such application, several results for Rb and Cs atomic clocks, pollutant gas monitoring, and fiber-gyro were also described.

Acknowledgements

The author would like to express his thanks to Profs. T. Tako and Y. Suematsu of his institute for their encouragements during this study.

References

[1] K. Aiki, M. Nakamura, T. Kuroda, J. Umeda, R. Ito, N. Chinone and M. Maeda : IEEE J. Quantum Electron., QE-14 (1978) 89

[2] Y. Noda, K. Sakai and Y. Matsuyama : Electron. Lett., 17 (1981) 226

[3] D. Welford and A. Mooradian : Appl. Phys. Lett., 40 (1982) 865

[4] C. Henry : IEEE J. Quantum Electron., QE-18 (1982) 259

[5] T. Takakura, K. Iga and T. Tako : Jpn. J. Appl. Phys., 19 (1980) L725

[6] Y. Yamamoto, S. Saito and T. Mukai : IEEE J. Quantum Electron., QE-19 (1983) 47

[7] W. Elsasser, E. O. Gobel and J. Kuhl : IEEE J. Quantum Electron., QE-19 (1983) 981

[8] T. Okoshi, K. Kikuchi and A. Nakayama : Electron. Lett., 16 (1980) 630

[9] D. Allan : Proc. IEEE, 54 (1966) 221

[10] K. Kikuchi and T. Okoshi : Electron. Lett., 19 (1983) 812

[11] S. Kotajima and M. Ohtsu : Proc. Meeting on Opto-Quamtum Electronics, IECE Japan, OQE83-67, October 1983 (in Japanese)

[12] T. J. Boem, H. R. Bilger and J. L. Tandon : Proc. Symposium on 1/f fluctuations, p.62, Tokyo, July 1977

[13] M. Ito : Ph.D. Thesis, Tokyo Institute of Technology, February 1982 (in Japanese)

[14] H. Tsuchida, M. Ohtsu and T. Tako : Jpn. J. Appl. Phys., 20 (1981) L403

[15] H. Tsuchida, M. Ohtsu and T. Tako : Jpn. J. Appl. Phys., 21 (1982) L1

[16] H. Tsuchida, M. Ohtsu, T. Tako, N. Kuramochi and N. Oura : Jpn. J. Appl. Phys., 21 (1982) L561

[17] H. Tsuchida and T. Tako : Jpn. J. Appl. Phys., 22 (1983) 1543

[18] M. Ohtsu, H. Fukada, T. Tako and H. Tsuchida : : Jpn. J. Appl. Phys., 22 (1983) 1157

[19] S. Sampei, H. Tsuchida, M. Ohtsu and T. Tako : Jpn. J. Appl. Phys., 22 (1983) L258

[20] M. Ohtsu, H. Tagawa and H. Kotani : Jpn. J. Appl. Phys., 22 (1983) 1876

[21] M. Ohtsu, H. Kotani and H. Tagawa : Jpn. J. Appl. Phys., 22 (1983) 1553

[22] L. L. Lewis and M. Feldman : Proc. 35th Annual Symposium on Frequency Control, p.612, Ft. Monmouth, May 1981

[23] M. Arditi and J. L. Picque : J. Phys. Lett., (Paris), 41 (1980) L379

[24] K. Kishino, S. Kinoshita, S. Konno and T. Tako : Jpn. J. Appl. Phys., 22 (1983) L473
[25] M. Ohtsu and Y. Otsuka : Proc. Meeting on Opto-Quantum Electronics, IECE Japan, OQE83-61, September 1983 (in Japanese)

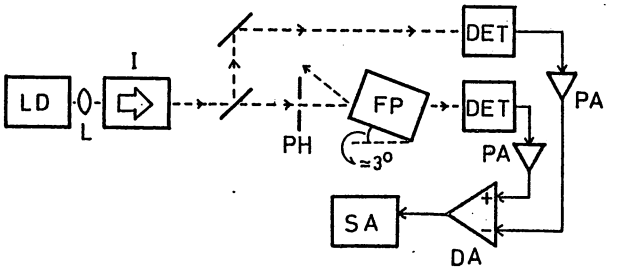

Fig. 1. Experimental setup for FM noise measurements [11].

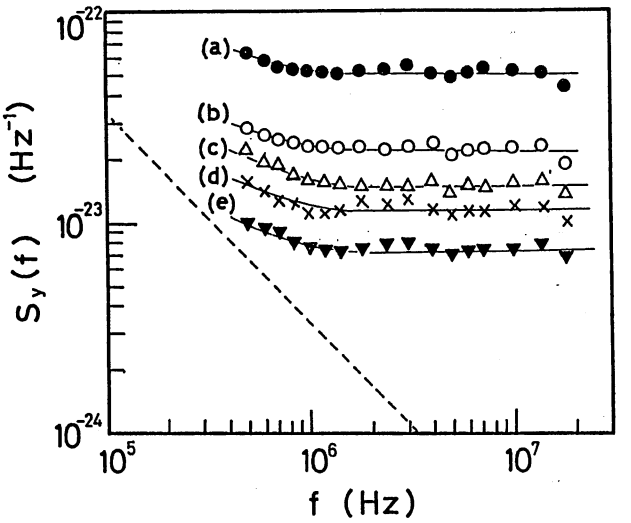

Fig. 2. Experimental results of the power spectral density of the FM noises at T = 293K [11].
$(I/I_{th} - 1)^{-1}$ = 11.1 (a), 8.3 (b), 5.9 (c), 4.2 (d), 2.9 (e).
---------: Power-independent 1/f noise by Kikuchi and Okoshi [10].

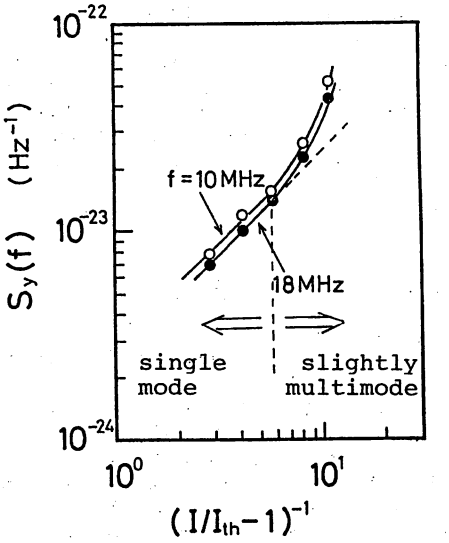

Fig. 3. The relation between the power spectral density and the injection current [11].

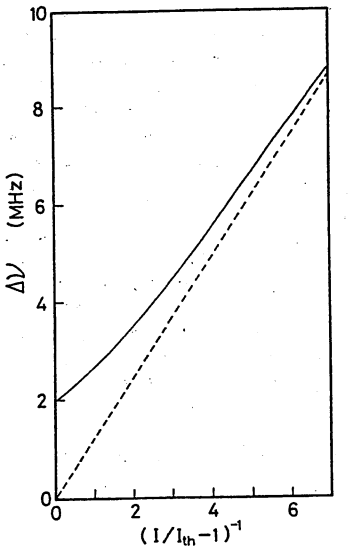

Fig. 4. The relation between the estimated spectral width and the injection current [11].
——— : The results obtained by considering also the 1/f noises.
------ : The result obtained by neglecting the 1/f noises.

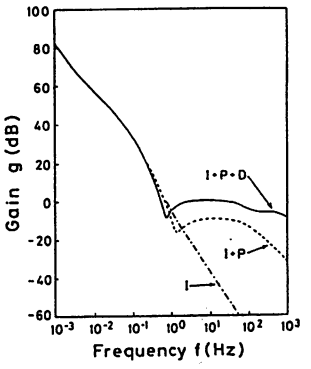

Fig. 5. The frequency characteristics of the gains of the PID controller

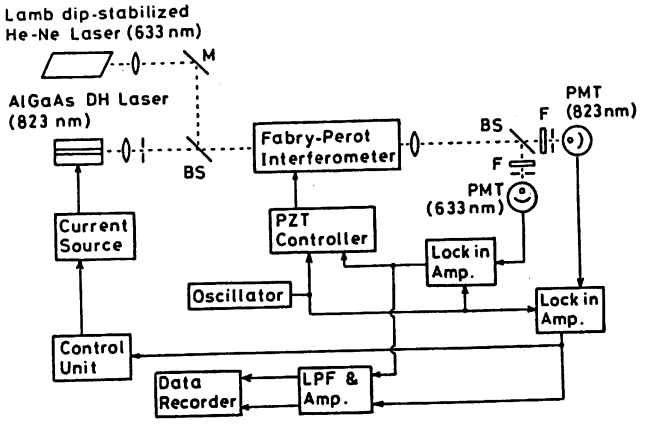

Fig. 6. Experimental setup of the frequency stabilization using a Fabry-Perot interferometer as a frequency standard, which is also stabilized by a He-Ne laser [14].

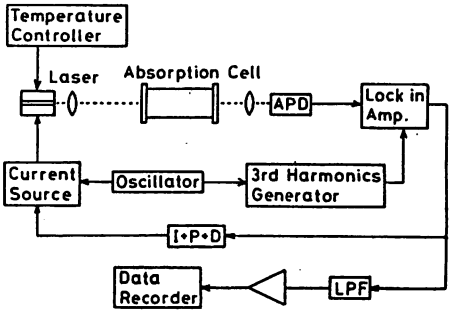

Fig. 7. Experimental setup of the frequency stabilization using an absorption line in H_2O vapor as a frequency standard [15].

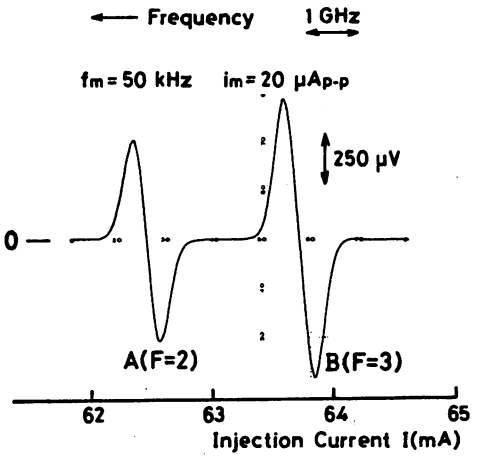

Fig. 8. Absorption spectra of ^{85}Rb-D_2 line used as the frequency standard [16].

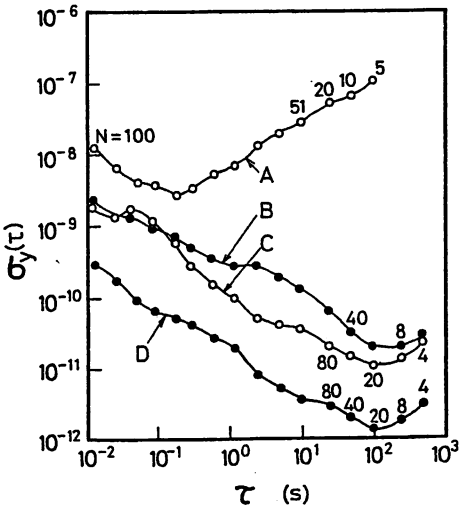

Fig. 9. The results of the frequency stabilization.
A : Free-running laser.
B : Stabilized laser by the stabilized Fabry-Perot interferometer.
C : Stabilized laser by H_2O
D : Stabilized laser by ^{85}Rb-D_2 line.

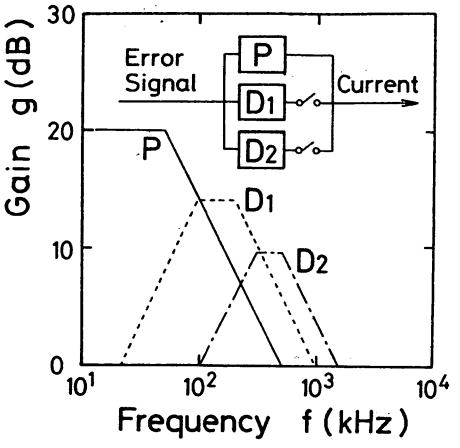

Fig. 10. Frequency characteristics of the gains of the differentiators used to expand the bandwidth of the phase-lead compensation [17].

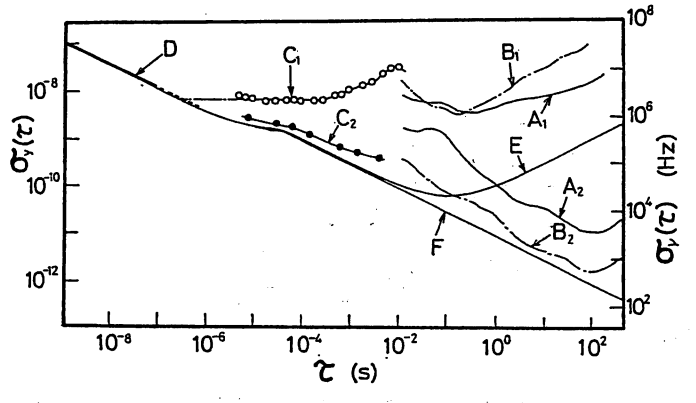

Fig. 11. Comparison between the experimental results of frequency stabilization and the theoretical limits.
A_1, B_1, C_1, D : Free-running.
A_2 : Stabilized by H_2O [15].
B_2 : Stabilized by ^{85}Rb-D_2 [16].
C_2 : Stabilized by a rigid Fabry-Perot interferometer [17].
E : Theoretical limit for the free-running laser [18].
F : Theoretical limit for the stabilized laser [18].

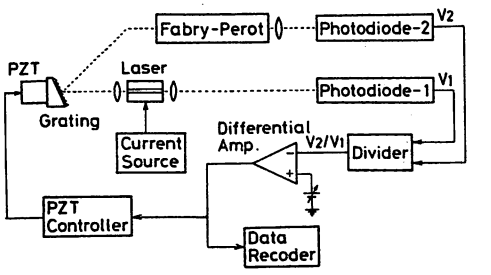

Fig. 12. Experimental setup of the frequency stabilization of the laser with an external grating [19].

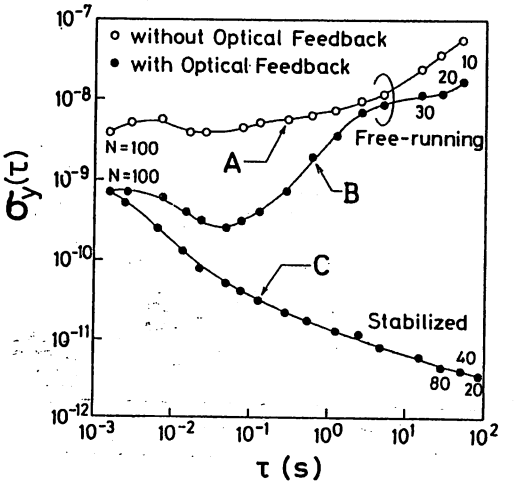

Fig. 13. Experimental results of the stabilization of the laser with an external grating [19].

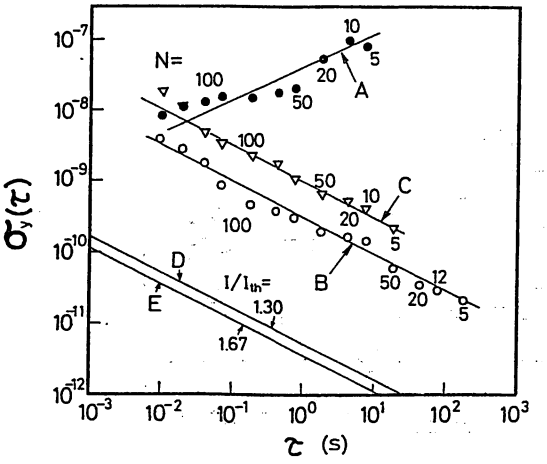

Fig. 14. Experimental results of the frequency stabilization of 1.5μm InGaAsP lasers [21].
A : Free-running.
B : Stabilized by NH_3 spectra.
C : Stabilized by H_2O spectra.
D, E : Theoretical limits.

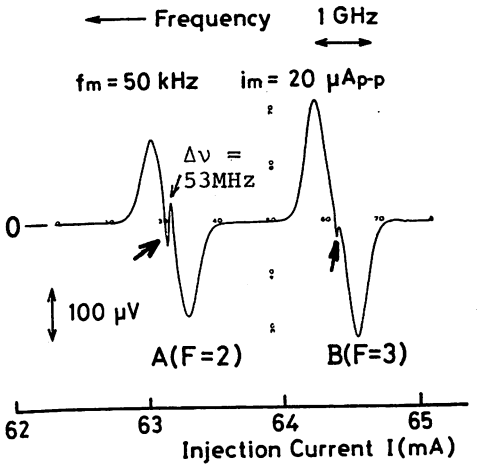

Fig. 15. Saturated absorption spectra in ^{85}Rb-D_2 lines, which are indicated by arrows in the figure [16].

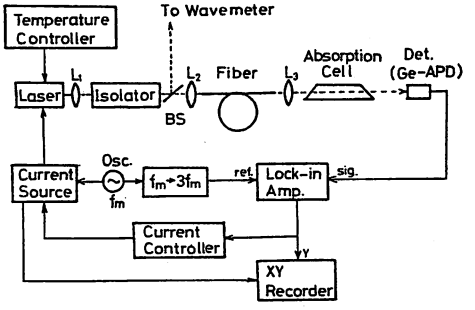

Fig. 16. Experimental setup of the pollutant gas monitoring using a 1.5μm InGaAsP laser [21]. The fiber length was 50 m .

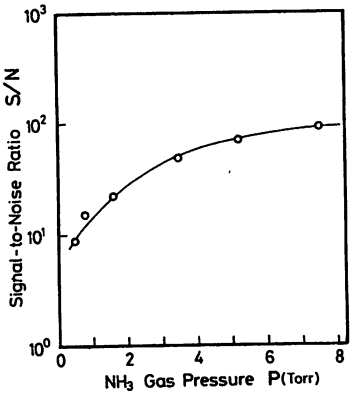

Fig. 17. The experimental results of the relation between the S/N value of the NH_3 spectral shape and its vapor pressure [21].

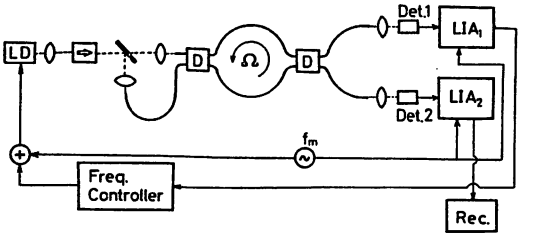

Fig. 18. Fiber-gyroscope which is composed of a ring Fabry-Perot interferometer [25].

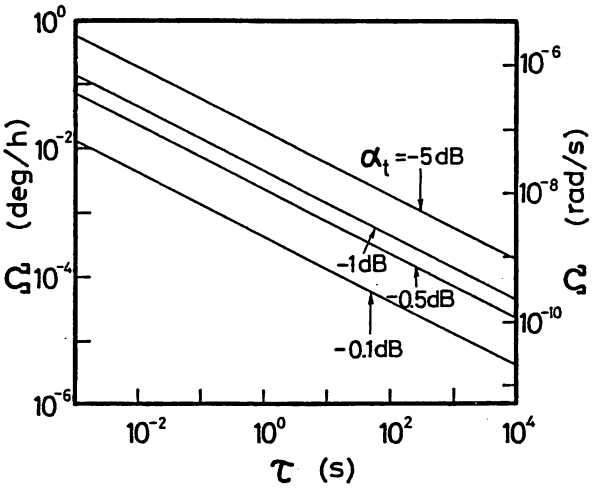

Fig. 19. Estimated sensitivity of the fiber-gyro of Fig. 18 [25].
α_t represents the total loss of the fiber and directional coupler D.

Postdeadline Paper
Conference on Lasers and
Electro-Optics
21-24 May 1985
Baltimore, Maryland
USA

ThZ5-1

Linewidth Reduction of a Semiconductor Laser by Electrical Feedback

Motoichi Ohtsu

International Cooperation Center for Science and Technology, Tokyo Institute of Technology, 2-12-1 O-okayama, Meguro-ku, Tokyo 152, Japan

Spectral linewidth of a semiconductor laser should be reduced for coherent optical communication, coherent optical measurement, and so on. One of the popular technique for linewidth reduction is to use an external mirror or an optical fiber, which has been called an optical feedback technique. The linewidth, as narrow as 1 kHz, has been realized by this technique[1]. However, it presents several problems, e.g., oscillation instabilities can be induced by the phase fluctuations of the reflected light. To overcome these difficulties, a novel and simple technique of electrical feedback is proposed here, in which the quantum FM noise can be directly controlled by the injection current. The linewidth can be stably reduced by this technique without changing the cavity structure. It has been pointed out that the electrical feedback can reduce the linewidth to a value limited by the noise of the feedback loop[2], which is far narrower than the one given by the modified Schawlow-Townes formula. This is a consequence of the analysis by using a quantum mechanical Langevin equation. From these reasons, the electrical feedback can be a more promising technique to realize an ultranarrow linewidth.

Figure 1 shows the estimated minimum attainable linewidth limited by the noise of the detector in the feedback loop. R_{FP} represents the reflectance of a Fabry-Perot interferometer used as a frequency discriminator. It is concluded from this estimation that the linewidth narrower than 1 kHz can be realized if $R_{FP} > 0.9$. It was also estimated that the required bandwidth f_c for the feedback does not have to be larger than 100 MHz, which means that any special wideband amplifiers are not required for the feedback.

Figure 2 shows the simple experimental apparatus used. A 1.5 μm InGaAsP laser (DFB type) was employed for the experiment. A compact Fabry-Perot interferometer of 10 mm long was used as a frequency discriminator, and f_c was fixed at 100 MHz. A delayed self-heterodyne technique was used for the linewidth measurement[3]. Figure 3 shows the

experimental result. Effect of the feedback is notable, and the minimum linewidth of 330 kHz was easily obtained. The spectral line shape showed none of the temporal fluctuations which have sometimes been observed in the optical feedback technique. Further reduction and approach to the minimum attainable linewidth of Fig. 1 can be expected by improving the sensitivity of the FM noise reduction, e.g., by stabilizing the laser power.

References

[1] R. Wyatt : Proc. Conf. Opt. Fiber Comm., TUP2, Feb., 1985, San Diego
[2] S. Saito, O. Nilsson, and Y. Yamamoto : Appl. Phys. Lett., 46 (1985) 3
[3] T. Okoshi, K. Kikuchi, and A. Nakayama : Electron. Lett., 16 (1980) 630

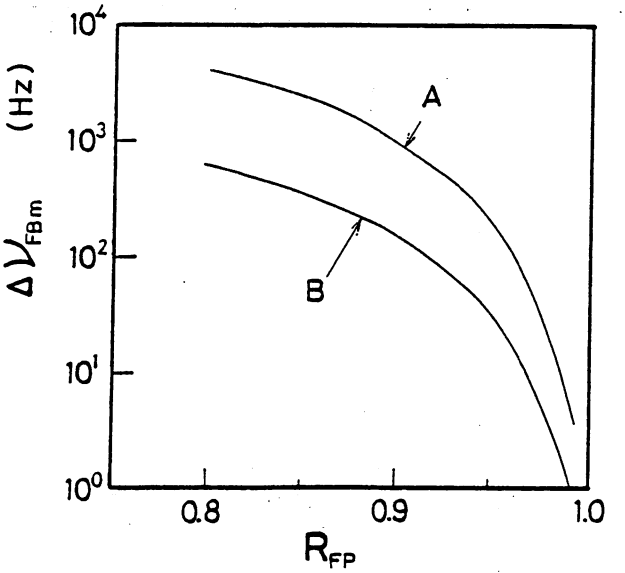

Fig. 1

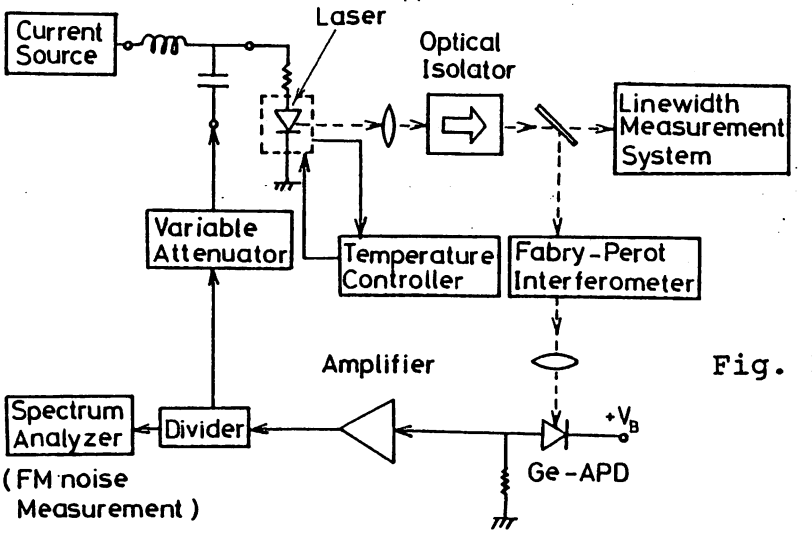

Fig. 2

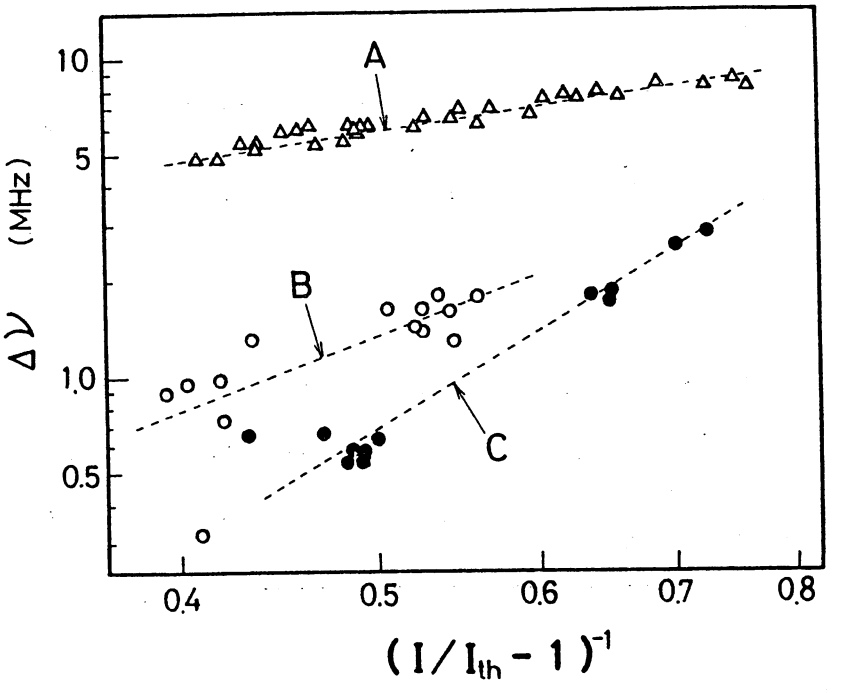

Fig. 3

Figure 1 Estimated minimum attainable linewidth. The curves A and B represent the results when a Ge-APD and PIN photodiode were used for the FM noise detection, respectively.

Figure 2 Experimental apparatus.

Figure 3 Relation between the linewidth and the inverse of the injection current normalized to its threshold value. A : Free-running laser. B : Under the feedback, R_{FP} = 0.9. C : Under the feedback, R_{FP} = 0.95.

JAPANESE JOURNAL OF APPLIED PHYSICS
VOL. 22, NO. 1, JANUARY, 1983 pp. L19–21

A Novel Technique for Measuring the Frequency Deviation of Semiconductor Lasers Under Direct Modulation

Hidemi TSUCHIDA, Toshiharu TAKO and Motoichi OHTSU†

Research Laboratory of Precision Machinery and Electronics
†International Cooperation Center for Science and Technology, Tokyo Institute of Technology, 4259 Nagatsuta-cho, Midori-ku, Yokohama, Kanagawa 227

(Received October 13, 1982; accepted for publication December 18, 1982)

A novel technique is proposed for measuring the frequency deviation of semiconductor lasers under direct modulation using a Michelson interferometer. This technique is applicable to a wide range of modulation frequency and does not require high-speed photo-detectors. The accuracy of the measurement is not reduced by the spectral linewidth of lasers, the misalignment of the optical axes, or the depth of intensity modulation.

Direct modulation of semiconductor injection lasers induces frequency modulation as well as intensity modulation because the refractive index in the active region depends on the temperature and the carrier density. Direct modulation of laser frequency is very attractive for such applications as coherent optical transmission systems,[1] precise metrology, and so on. Since the frequency deviation of semiconductor lasers under direct modulation depends on the laser structure and modulation frequency,[2] it is necessary for these applications to measure the frequency deviation characteristics precisely.

Several methods have been employed to measure these characteristics.[2-5] However, these methods were applicable to a narrow range of modulation frequency and, in some methods,[2,5] the accuracy of the measurements was reduced with the increase in the depth of intensity modulation.

In this paper, a novel technique is proposed for measuring these characteristics precisely using a Michelson interferometer. In this technique the above difficulties are drastically reduced because the dependence of the visibility of the interference fringes on the frequency deviation is used in the measurement.

Figure 1 shows the arrangement for the measurement which consists of a Michelson interferometer with an optical path difference of ΔL. The intensity of the interference fringes, which are produced by the frequency modulated optical wave, is detected with a Si APD. The dc component of the output signals from the APD is recorded by sweeping the optical path difference with a PZT. The visibility of the interference fringes is then estimated from this trace.

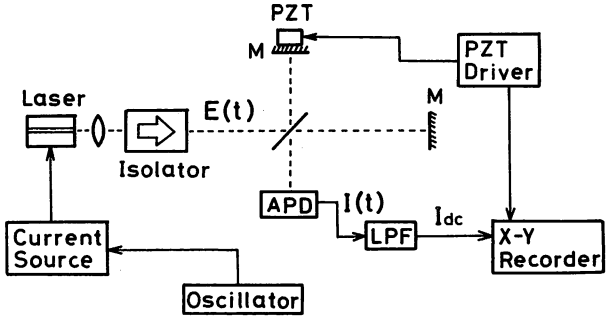

Fig. 1. The experimental arrangement for the measurement.

The electric field $E(t)$ of the frequency modulated optical wave is expressed as

$$E(t)=E_0 \exp\left[i\left(2\pi\nu_0 t+\frac{\Delta\nu}{f_m}\sin 2\pi f_m t\right)\right]. \tag{1}$$

where E_0 is the amplitude of the electric field, ν_0 is the center frequency, $\Delta\nu$ is the frequency deviation, and f_m is the modulation frequency. The intensity $I(t)$ of the interference fringes is expressed as

$$\begin{aligned} I(t) &= |E(t)+E(t+\tau)|^2 \\ &= I_0\left\{1+\cos\left[2\pi\nu_0\tau+\frac{\Delta\nu}{f_m}(\sin 2\pi f_m(t+\tau)-\sin 2\pi f_m t)\right]\right\}, \end{aligned} \tag{2}$$

where $\tau=\Delta L/c$ is the delay time and I_0 is the constant. Equation (2) can be expanded in terms of Bessel function of the first kind $J_n(x)$. The dc component I_{dc} of eq. (2) is expressed as follows:

$$I_{dc}=I_0\left\{1+\cos(2\pi\nu_0\tau)\left[J_0(A_c)J_0(A_s)+2\sum_{k=1}^{\infty}(-1)^k J_{2k}(A_c)J_{2k}(A_s)\right]\right\}, \tag{3}$$

$$A_c=\frac{\Delta\nu}{f_m}(1-\cos 2\pi f_m\tau), \tag{4}$$

$$A_s=\frac{\Delta\nu}{f_m}\sin 2\pi f_m\tau. \tag{5}$$

If $f_m\tau\ll 1$, A_c and A_s are approximated by

$$A_c\cong 0,\ A_s\cong 2\pi\Delta\nu\tau. \tag{6}$$

Substituting eq. (6) into eq. (3), the following equation is obtained.

$$I_{dc}\cong I_0[1+J_0(2\pi\Delta\nu\tau)\cos(2\pi\nu_0\tau)]. \tag{7}$$

Then, the visibility V of the interference fringes is derived from eq. (7) and is given by

$$V\cong|J_0(2\pi\Delta\nu\tau)|. \tag{8}$$

This equation represents the dependence of the visibility on the frequency deviation $\Delta\nu$ and the delay time τ.

In this measurement, the optical path difference is fixed and the visibility is measured as a function of the modulation current of the laser. It can be seen from

eq. (8) that the visibility becomes zero when the frequency deviation $\Delta\nu$ satisfies the condition $2\pi\Delta\nu\tau = j_{0,n}$, where $j_{0,n}$ represents the n-th zero of the Bessel function $J_0(x)$. Although visibility is sensitive to the spectral linewidth of lasers and the misalignment of the optical axes, the position where the visibility becomes zero is determined only by the zero points of the Bessel function $J_0(x)$, that is, by the frequency deviation and the delay time. Hence, the frequency deviation can be accurately estimated from the zero points of the visibility. But it is necessary that the laser oscillates in a single longitudinal mode because, for multimode lasers, the visibility becomes zero under a certain condition, even if the laser frequency is not modulated.[6]

It should be noticed that the visibility is not affected by the depth of the intensity modulation, because the component of the intensity modulation is eliminated by the low pass filter, as shown in Fig. 1. This technique can thus be applied to a case where the modulation index is high.

In the methods of Saito *et al.*[3] and Dandridge and Goldberg,[5] the maximum modulation frequency was limited by the response time of the photo-detectors. Another advantage of this technique is that high-speed photo-detectors are not necessary, because only the dc component of the light intensity is used in the measurement.

In this technique, the condition $f_m\tau \ll 1$ limits the maximum modulation frequency, that is, an error appears if the above condition is not satisfied. A numerical analysis shows that the error due to this is less than 1.7% for $f_m\tau \leqq 0.1$. Therefore, this technique is applicable to the modulation frequency up to several GHz, if the optical path difference is less than 1 cm. Another cause for the error is the measurement of the optical path difference. One of the methods to reduce this error is to measure it using the dc frequency deviation characteristics of the laser. Details of the error analysis will be reported later. The minimum modulation frequency lies around 1 Hz, which is limited mainly by the cut-off frequency of the low pass filter and by the intensity fluctuation of the laser.

As a demonstration, the frequency deviation characteristics are measured using an AlGaAs semiconductor laser with a channeled-substrate-planar (CSP) structure.[7] The laser chip is mounted with the p-side down. The laser is biased at $I/I_{th}=1.26$. The value of $f_m\tau$ is kept less than 6.0×10^{-3} throughout the measurement.

Figure 2 shows the visibility measured as a function of the amplitude of the modulation current i_m. The optical path difference and the modulation frequency are $\Delta L=0.36$ m and $f_m=100$ kHz, respectively. The solid line represents the Bessel function $J_0(x)$. Close agreement is obtained between the solid line and the experimental results.

Figure 3 shows the modulation efficiency $\Delta\nu/i_m$, that is, the frequency deviation per unit modulation current, measured as a function of the modulation frequency f_m. It can be seen from this figure that the modulation efficiency decreases with increasing modulation frequency, which is attributed to the thermal effect.[2] The results

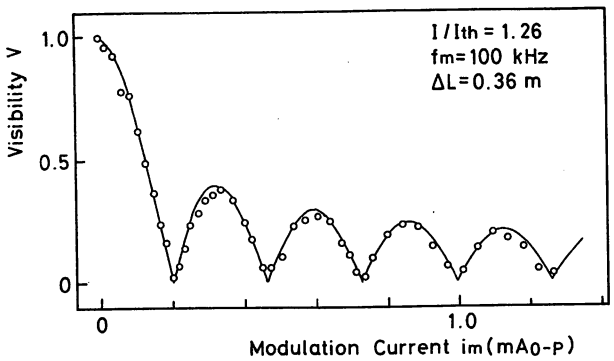

Fig. 2. Visibility of the interference fringes measured as a function of the modulation current. Solid line represents the Bessel function $J_0(x)$.

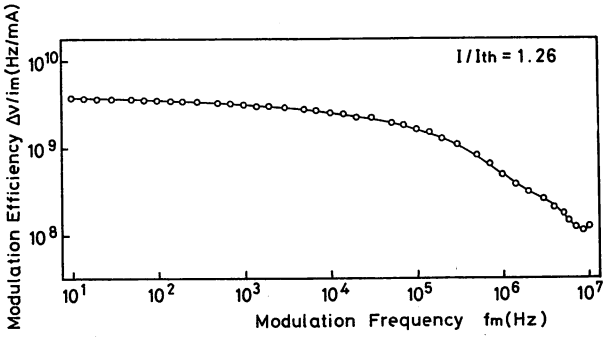

Fig. 3. Dependence of the modulation efficiency of the AlGaAs semiconductor laser on the modulation frequency in the 10 Hz–10 MHz frequency range.

in Fig. 3 agree well with the theoretical and experimental results of Kobayashi *et al.*[2]. Further experiments are now in progress to measure the modulation efficiency at higher frequency, which will be reported later.

In summary, a novel technique is proposed for measuring the frequency deviation of semiconductor lasers under direct modulation using a Michelson interferometer. This technique has the following advantages:

(1) The accuracy of the measurement is not reduced by the spectral linewidth of lasers, the misalignment of the optical axes, or the depth of the intensity modulation.

(2) High-speed photo-detectors are not necessary.

(3) It is applicable to a wide range of modulation frequency (1 Hz-several GHz).

Acknowledgement

The authors would like to express their thanks to Drs. M. Nakamura and K. Aiki of Hitachi, Ltd. for support in the experiment, and to Dr. K. Kishino of their laboratory for discussions.

This work was partially supported by a Grant-in-Aid for Scientific Research from the Ministry of Education, Science and Culture of Japan.

References

1) Y. Yamamoto and T. Kimura: IEEE J. Quantum Electron. **QE-17** (1981) 919.
2) S. Kobayashi, Y. Yamamoto, M. Ito and T. Kimura: IEEE J. Quantum Electron. **QE-18** (1982) 582.
3) S. Saito, Y. Yamamoto and T. Kimura: IEEE J. Quantum Electron. **QE-17** (1981) 935.

4) K. Kishino, S. Aoki and Y. Suematsu: IEEE J. Quantum Electron. **QE-18** (1982) 343.
5) A. Dandridge and L. Goldberg: Electron. Lett. **18** (1982) 302.
6) M. Born and E. Wolf: *Principles of Optics* (The Macmillan Company, New York, 1964) 2nd ed., p. 316.
7) K. Aiki, M. Nakamura, T. Kuroda, J. Umeda, R. Ito, N. Chinone and M. Maeda: IEEE J. Quantum Electron. **QE-14** (1978) 89.

JAPANESE JOURNAL OF APPLIED PHYSICS
VOL. 22, No. 5, MAY, 1983 pp. 815–820

The Alternating Quarter-Wavelength Layers Coating on 1.55 μm GaInAsP/InP Laser Facets

Motoichi OHTSU, Hiroki KOTANI and Haruo TAGAWA

International Cooperation Center for Science and Technology, Tokyo Institute of Technology, 2–12–1 O-okayama, Meguro-ku, Tokyo 152

(Received December 13, 1982; accepted for publication February 19, 1983)

The alternating quarter-wavelength layers of MgF_2 and ZnS were coated on the facets of 1.55 μm GaInAsP/InP BH lasers to decrease the threshold current by increasing the reflectivities of their facets. A precise optical thickness monitor was constructed, and its measurement error was about 3%. By coating five and six alternating layers, beginning with MgF_2 as the first layer, the threshold currents were decreased to 83% and 79% of the uncoated lasers, respectively. Calculations of the reflectivities, by considering also the coupling loss at the end of the waveguide due to diffraction, give estimations of 68% and 84% for five and six layers, respectively.

§1. Introduction

Performance of semiconductor lasers has been remarkably improved by the demands of the optical communication industry. When these lasers are used not only for the optical communication but also for other applications such as optical signal processing and spectroscopy, low threshold current and large external differential quantum efficiency are required. One way of satisfying these requirements would be to increase the reflectivity of laser cavity mirrors by coating thin films on cleaved facets. Application of this technique will suppress the AM noise caused by the reflected laser beam and reduce the spectral line broadening caused by the increase in the reflectivity. Therefore, it is expected that this technique wil have potential application in improving the performances of laser diodes. Alternating quarter-wavelength layers of Al_2O_3 and Si have already been used for 0.8 μm GaAs/AlGaAs lasers for these purposes.[1] Kokubun and Iga[2] have made some designs on the layers of SiO_2 and TiO_2 for short cavity or surface emitting GaInAsP/InP lasers at 1.3 μm by using a plane wave approximation method.

In the present study, the coatings of alternating quarter-wavelength layers were carried out for 1.55 μm GaInAsP/InP lasers, which can be widely used for several applications together with low-loss optical fibers in the near future. The authors employed popular and chemically stable dielectrics as coating materials for this purpose. A precise optical thickness monitor was also developed. Furthermore, the reflectivities of the layers were calculated to discuss the experimental results by including the effect of diffraction.

§2. Method for Measuring the Layer Thickness

ZnS and MgF_2 were employed as dielectric materials for alternating quarter-wavelength layers. These chemically stable materials have been commonly used to make high reflectivity mirrors for gas lasers, and are transparent at the wavelength region from visible to infrared. The refractive indices of ZnS and MgF_2 at 1.55 μm are 2.27[3] and 1.37,[4] respectively.

There are several ways of measuring layer thickness, such as using quartz oscillators,[5] however, an optical method was employed here for real-time and precise measurements. For these purposes, a precise optical thickness monitor was developed, whose optical part can be installed in the vacuum chamber for evaporation.

In this method, a stable and inexpensive infrared light source at the laser wavelength $\lambda = 1.55$ μm is required, however, such a source, *e.g.*, GaInAsP/InP laser itself, have not yet been so popular now. Therefore, instead of using such a light source, the one with the wavelength $\lambda/3 = 0.52$ μm was employed here for the measurements. This is a possible substitution because the reflectivity of the alternating quarter-wavelength layers has the same value for the odd-order harmonics of the light.[6] The visible light source at $\lambda/3 = 0.52$ μm can be easily prepared by using an inexpensive miniature bulb and a color glass filter. Figure 1 shows the principle of measuring layer thickness, where the difference in the reflectivities $R(\lambda_+)$ and $R(\lambda_-)$ at the wavelengths λ_+ and λ_- is measured while coating the layers. When this differences $\Delta R (= R(\lambda_+) - R(\lambda_-))$ becomes zero, it means that the layer has the optical thickness nD of a quarter-wavelength for the light of the wavelength $\lambda_0 = (\lambda_+ + \lambda_-)/2$ where n, D, and λ_0 are the refractive index, thickness of the layer, and $\lambda/3$, respectively. By this zero-method, one can precisely measure the thickness of quarter-wavelength layers.

Figure 2 shows the experimental setup of this equipment.

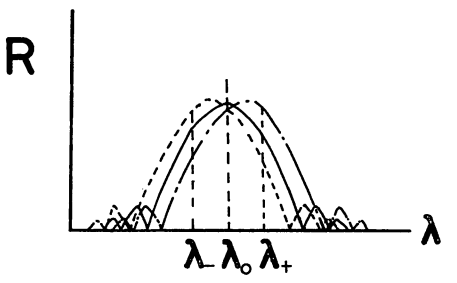

Fig. 1. The schematic explanation of the principle of the thickness measurements: ------; the reflectivity for $nD < \lambda_0/4$, where nD represents the optical thickness of the layer. ——; $nD = \lambda_0/4$, —·—·—; $nD > \lambda_0/4$. By measuring the difference ΔR between the reflectivity at λ_+ and that at λ_-, one can know that $nD = \lambda_0/4$ if $\Delta R = 0$, where $(\lambda_+ - \lambda_0)/\lambda_0 = (\lambda_0 - \lambda_-)/\lambda_0$, and $\lambda_0 = \lambda/3$, for the present experiment.

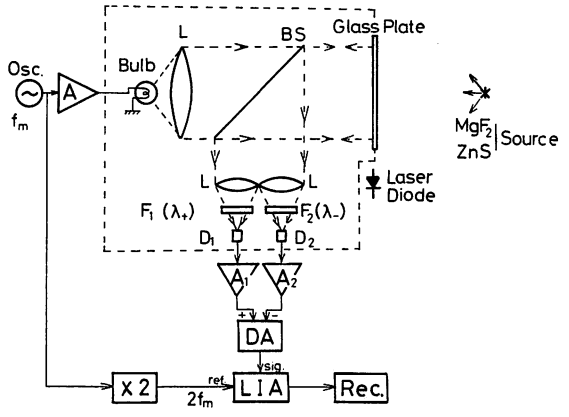

Fig. 2. An optical thickness monitor for the coated layers. The lights with the wavelengths λ_+ and λ_- were passed through the color glass filters F_1 and F_2, respectively, D_1, D_2; photodiodes. A_1, A_2; variable gain preamplifiers for the photodiodes. DA; a differential amplifier used to measure the difference between the reflectivity at λ_+ and that at λ_-. LIA; a lock-in amplifier. The block bounded by the broken lines corresponds to the optical part which was installed in the vacuum chamber used for evaporation.

The layer thickness on the laser facet was estimated by measureing the reflectivity of the glass plate, on which the dielectric materials are coated simultaneously with the laser. Here, λ_+ and λ_- were empirically selected so that $(\lambda_+-\lambda_0)/\lambda_0=(\lambda_0-\lambda_-)/\lambda_0=0.1$ to get the highest sensitivity of the measurements. The coarse adjustments were done by selecting the appropriate color glass filters F_1 and F_2 for the wavelength of each laser. Four filters with the bandwidth of 10 nm were prepared for this purpose, whose center wavelengths were 478.0 nm, 484.5 nm, 577.5 nm, and 593.5 nm, respectively. Fine adjustments were carried out by varying the gains of the preamplifiers A_1 and A_2 for the photodiodes D_1 and D_2. In this figure, the block bounded by the broken lines corresponds to the optical part, which was installed in an aluminium box and was fixed in the vacuum chamber for evaporation. The semiconductor laser mounted on a brass heat sink was fixed on the top of this aluminium box. The glass plate used for monitoring the layer thickness was fixed on the hole bored on the box. The noises from the detectors D_1 and D_2 by the intensive stray lights from the W filaments for evaporation were removed by selectively amplifying the signal by using a lock-in amplifier connected after the differential amplifier.

Figure 3 shows an output signal from the lock-in amplifier traced on a chart recorder. For this demonstration, ZnS was coated on the glass plate as the first layer, then MgF_2 as the second layer, and so on. Starting the evaporation, the output signal varies with time, and one can know the quarter-wavelength layer obtained for the laser when the curve crossed the abscissa for the third time. By repeating these procedures for ZnS and MgF_2, the layer thickness can be precisely controlled to the quarter-wavelength of each laser. In this method, the measurement error due to the residual noise on the curve in Fig. 3 was about 1%, which is caused by the stray lights from the W filaments. The error due to the misalignments of the optical axes of the optical part was about 2%. One may expect the errors due to the dispersions of ZnS and MgF_2, however, it

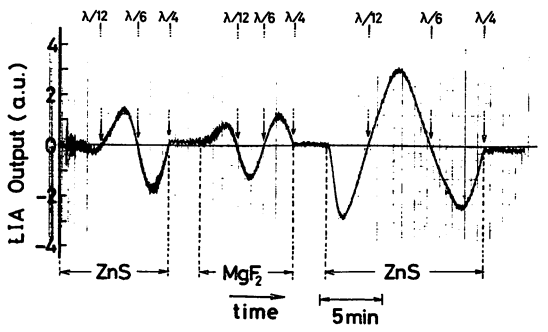

Fig. 3. The time dependence of the output signal from the lock-in amplifier in Fig. 2 recorded on a chart recorder. This curve is composed of three parts. The first and third parts are by the coating of ZnS, and the second part is by that of MgF_2, respectively. In each part, the first and third crossing points with the abscissa correspond to $nD=\lambda/12$ and $\lambda/4$, where nD and λ are the optical thickness of the layer and the laser wavelength, respectively.

will be shown in §4 that this phenomenon gives no errors in this experiment. Therefore, the total error in this method was estimated to be about 3%.

§3. Experimental Results

Semiconductor lasers used were GaInAsP/InP BH lasers provided by Prof. Suematsu of the authors' institute.[7] The length, thickness, and width of their active layers were 150 μm, 0.2 μm, and 3.5 μm, respectively. Their wavelengths fell between 1.55 μm and 1.56 μm for pulsed oscillation at room temperature. MgF_2 was coated as the first layer and ZnS was coated as the next, and both materials were alternatively coated on one of the laser facets in this order. Figure 4 shows the relations between the injected current and light intensity of one of the lasers. The curve A represents the result measured before the coating. For this laser, after five alternating layers were coated, the threshold current was measured again by detecting the light from the coated facet, which is shown by the curve B. As the transmissivity of the facet was decreased by the coating, the light intensity on the curve B is lower than that on the curve A. The threshold currents on the curves A and B are 43.2 mA and 36.4 mA, respectively, *i.e.*,

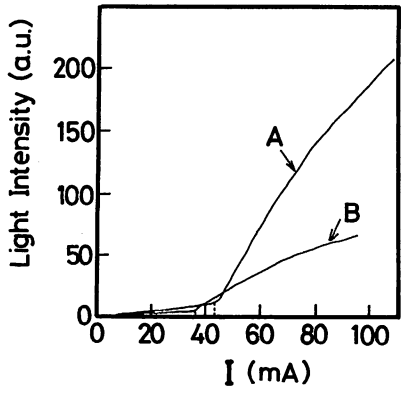

Fig. 4. The relation between the light intensity and the injected current. The laser diode used here corresponds to the laser c in Fig. 5. The curves A and B are the results measured before and after the coating, respectively. For the curve B, the five alternating layers were coated, beginning with MgF_2 as the first layer, and the light was detected through the coated facet. The threshold currents on the curves A and B are 43.2 mA and 36.4 mA, respectively.

the decrease of 6.8 mA was attained by the coating. Figure 5 shows the relation between the reflectivity of the coated facet and the ratio of threshold currents measured before (I_{th}) and after (I'_{th}) the coating. The black circles represent the experimental results. The alphabets attached to them represent the laser diode used. For the laser a, b, and c, five layers were coated, and for those d, e, and f, six layers were coated, respectively. The results shown in Fig. 4 are by the laser c. The solid curve in Fig. 5 was drawn by using the following equation for the threshold current.[8]

$$I_{th}=\frac{edwLB_{eff}}{(A_0-K_0)^2}\left[\alpha_{in}+\alpha_2+\frac{1-\xi}{\xi}\alpha_{ex}+\frac{1}{2\xi L}\ln(1/R_1R_2)\right]^2, \tag{1}$$

where e is the electron charge, d, w, and L are the thickness, width and length of the active layer, respectively, α_2 is the loss coefficient due to the transition between the split-off band and the acceptor level, α_{ex} is the loss coefficient in the cladding region, ξ is the confinement factor, R_1 and R_2 are the reflectivities of the uncoated and coated facets, respectively. Further details of this equation and the meanings of A_0, B_{eff}, K_0, and α_{in} are described in ref. 8. The following values were used for this equation[8]; $A_0-K_0=1.2\times10^{-16}$ cm^2, $B_{eff}=2\times10^{-10}$ cm^3/s, $\alpha_{in}=200$ cm^{-1}, $\alpha_2=20$ cm^{-1}, $\alpha_{ex}=5$ cm^{-1}, and $e=1.6\times10^{-19}$ C. Furthermore, in the present case, $d=0.2$ μm, $w=3.5$ μm, $L=150$ μm, and $\xi=0.47$, respectively. The reflectivity R_1 of the uncoated facet is 31% according to the results of §4 (see Fig. 10). The white circles on the solid curves in Fig. 5 represent the calculated results for each number of the layers N, where the relation between N and the reflectivity R_2 used here will be described in §4.

In Fig. 5, the average values of I'_{th}/I_{th} of the experimental results are 83% for $N=5$, and 79% for $N=6$, respectively.

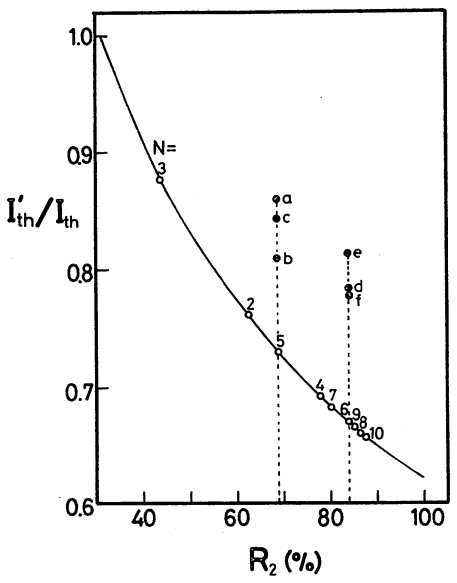

Fig. 5. The relation between the reflectivity of the coated facet and the ratio of the threshold currents measured before (I_{th}) and after (I'_{th}) the coating. The black circles represent the experimental results. The alphabets attached to them represent the laser diodes used. The solid curve represents the calculated result drawn by eq. (1). The white circles on this curve represent the calculated reflectivities for the number of layers N obtained by Fig. 10.

They are larger than the calculated values, i.e., 73% for $N=5$, and 67% for $N=6$, respectively. The differences between the experimental and calculated values may be due to the increase of the threshold current by the temperature increase of the laser when they were excited by the pulsed current, numerical errors of the parameters in eq. (1), and so on. However, it can be said that considerable decrease in the threshold current was experimentally obtained by this coating.

§4. Estimation of the Reflectivity of the Layers

Plane wave approximation has been conventionally used to estimate the reflectivity of the alternatng quarter-wavelength layers coated on the laser facet.[1,2] Actually, however, the light beam propagated through the layers will be divergent because of diffraction. Therefore, the coupling efficiency has to be included in the reflectivity estimation because the light beam re-entering to the end of the waveguide has a larger beam diameter than that of initially emitted one. To discuss the experimental results of §3, the calculation more accurate than the conventional one has to be carried out by including this diffraction phenomenon. Following this idea, several calculations are carried out in this chapter.

Figure 6 shows a schematic model used for the calculations. The reflectivity for the TE wave in the slab waveguide with the thickness d is calculated.* The x and z axes are fixed parallel to the directions of the polarization of the electric field and of the propagation, respectively. The refractive indices of the cladding and active layers are represented by n_1 and n_2, respectively. The electric field of the light at the end of the waveguide is now expressed as[9]

$$E(x,0)=\begin{cases}A\cos(\kappa x)\cdot\exp(i\omega t) & \text{for } |x|<d/2\\ A\cos(\kappa d/2)\cdot\exp(-\gamma|x-d/2|+i\omega t) & \text{for } |x|\geqq d/2,\end{cases} \tag{2}$$

where A and ω are the amplitude and angular frequency of the electric field, respectively. The values of κ and γ are given by

$$\begin{aligned}&(\kappa d/2)\tan(\kappa d/2)=(\gamma d/2)\\ &(n_2^2-n_1^2)(kd/2)^2=(\kappa d/2)^2+(\gamma d/2)^2,\end{aligned} \tag{3}$$

where $k=2\pi/\lambda$. Calculated values of κ and γ by eq. (3) are 5.24 μm^{-1} and 3.03 μm^{-1}, respectively, for $n_1=3.16$, $n_2=3.52$, $d=0.2$ μm, and $\lambda=1.55$ μm in the present case. The

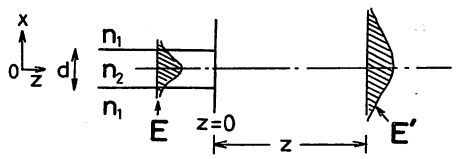

Fig. 6. The schematic model for calculations. The active layer of the laser is assumed to be the slab waveguide with the thickness d. The refractive indices n_1 and n_2 are for the cladding and active layers, respectively. The electric fields E and E' are for inside and outside the laser cavity.

*In this chapter, the TE wave in the waveguide will be dealt with because the TE wave is easier to oscillate than the TM wave in the actual semiconductor laser.[9] The discussion for the TM wave can be easily carried out by a minor modification of the formula in this chapter.

value of the electric field $E'(x',z)$ at the distance z away from the end of the waveguide can be calculated by eq. (2) and the following Kirchhoff-Huygens diffraction integral[10]

$$E'(x',z)=\frac{i}{4}k\int_{-\infty}^{\infty}E(x,0)\left\{\frac{z}{\sqrt{(x-x')^2+z^2}}H_0^{(2)'}(k\sqrt{(x-x')^2+z^2})-iH_0^{(2)}(k\sqrt{(x-x')^2+z^2})\right\}dx, \quad (4)$$

where $H_0^{(2)}$ and $H_0^{(2)'}$ represent the Hankel function and its derivative, respectively. This equation is valid even for the near field region ($z<\lambda$). Figure 7 shows the profiles of $E'(x,z)$ for several values of z calculated by eqs. (2), (3) and (4). These values of the electric field can be also used to represent the re-entering light to the waveguide, which is reflected back at the boundary between the adjacent layers located at $z/2$. The coupling efficiency $c^2(z)$ at the end of the waveguide, used to estimate the reflectivity in the following discussions, can be defined by

$$c^2(z)=\left|\int_{-\infty}^{\infty}E(x,0)E'(x,z)dx\right|^2\Big/\left|\int_{-\infty}^{\infty}E(x,0)dx\right|^2, \quad (5)$$

which was employed in discussing the coupling efficiency for the waveguide-type CO_2 lasers,[11] where $E'(x,z)$ represents the re-entering electric field calculated by eq. (4). Figure 8 shows the value of $c^2(z)$ calculated by eqs. (2), (4), and (5). The reflectivity can be calculated by considering this coupling efficiency due to the diffraction.

The amplitude reflectivity r_N of the alternating quarter-wavelength layers for the plane wave is calculated by the characteristic matrix $\bar{M}_N$ of the layers, and is expressed as [12]

$$r_N=\frac{(m_{11}+m_{12}\sqrt{\varepsilon_0/\mu_0})(n_2\sqrt{\varepsilon_0/\mu_0})-(m_{21}+m_{22}\sqrt{\varepsilon_0/\mu_0})}{(m_{11}+m_{12}\sqrt{\varepsilon_0/\mu_0})(n_2\sqrt{\varepsilon_0/\mu_0})+(m_{21}+m_{22}\sqrt{\varepsilon_0/\mu_0})}, \quad (6)$$

where N is the number of layers, $m_{i,j}(i,j=1,2)$ is the matrix element of $\bar{M}_N$, ε_0 and μ_0 are the dielectric constant and magnetic permeability in vacuum, respectively. The characteristic matrix $\bar{M}_N$ is derived by the characteristic matrix M_q of the qth layer, and is expressed as,

$$\bar{M}_N=M_1\cdot M_2\cdots\cdots M_q\cdots\cdots M_N=\begin{pmatrix}m_{11} & m_{12}\\ m_{21} & m_{22}\end{pmatrix}. \quad (7)$$

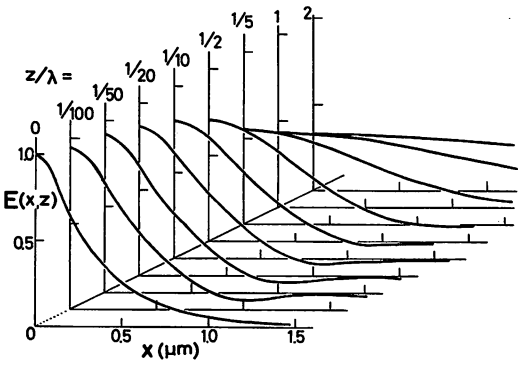

Fig. 7. The spatial profiles of the electric fields E' at several positions z from the end of the waveguide.

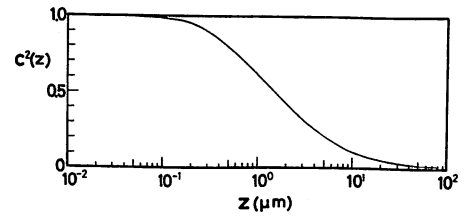

Fig. 8. The coupling efficiency $c^2(z)$ at the position z which is defined by the overlapping integral between $E(x,0)$ and $E'(x,z)$ (see eq. (5) in the text).[11]

The matrix M_q is given by [13]

$$M_q=\begin{pmatrix}\sqrt{\varepsilon_q/\varepsilon_{q-1}}\cos\theta_q, & i\sqrt{\mu_0/\varepsilon_0\varepsilon_q\varepsilon_{q-1}}\sin\theta_q\\ i\sqrt{\varepsilon_0\varepsilon_q\varepsilon_{q-1}/\mu_0}\sin\theta_q, & \sqrt{\varepsilon_{q-1}/\varepsilon_q}\cos\theta_q\end{pmatrix}. \quad (8)$$

In this matrix, θ_q is expressed as

$$\theta_q=\int_{z_{q-1}}^{z_q}\sqrt{\varepsilon(z)}\,dz,$$
$$\varepsilon_q=\varepsilon(z_q)\quad(q=1,2,\cdots\cdots,N), \quad (9)$$

where z_q is the position of the boundary between the q th and $q+1$ th layers, as shown by Fig. 9. This is given by

$$z_q=\frac{\lambda}{4n_H}\left[\frac{q}{2}\right]+\frac{\lambda}{4n_L}\left[\frac{q+1}{2}\right]$$
$$z_0=0, \quad (10)$$

where $[x]$ represents the largest integer which does not exceed x. The quantity $\varepsilon(z)$ represents the relative dielectric constant at the position z. The refractive index of the q th layer is expressed as

$$n_q=\begin{cases}n_L=1.37 & (MgF_2)\quad(q:\text{odd})\\ n_H=2.27 & (ZnS)\quad(q:\text{even}).\end{cases} \quad (11)$$

The matrix M_q of eq. (8) is for the plane wave propagating through the medium whose relative dielectric constant varies along the z axis. In the present case, however, as the electric field is not the plane wave but the one as given by eq. (40), it is the most exact procedure for the reflectivity estimation to start from eq. (4), whereas such a procedure must be quite complicated and take a long time for calculation. Hence, in the present case, as the first approximation, eq. (8) is employed and the effect of the coupling loss by the diffraction is simultaneously included by assigning the relative dielectric constant $\varepsilon(z)$ a complex value. For this purpose, the effective attenuating constant $\gamma_0(z)$ for the amplitude of the electric field is defined by

$$\exp[-2\gamma_0(z)\cdot z]=c^2(z). \quad (12)$$

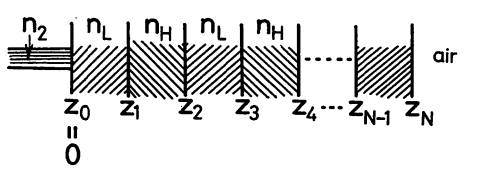

Fig. 9. The schematic explanation of the notations. The refractive indices n_2, n_L, and n_H are for the active layer of the laser, MgF_2, and ZnS, respectively. The coordinate z_q represents the position of the boundary between the q th and $q+1$ th layers, where $z_0=0$.

If this attenuation is considered to be due to the absorption by the medium, the relative dielectric constant $\varepsilon(z)$ of such a lossy medium is expressed as

$$\varepsilon(z)=n_q^2[1-2i\gamma_0(z)/n_q k] \quad (z_{q-1}\leqq z<z_q), \tag{13}$$

or, by substituting eq. (12) into eq. (13),

$$\varepsilon(z)=n_q^2\left[1+i\frac{1}{n_q kz}\ln\{c^2(z)\}\right] \quad (z_{q-1}\leqq z<z_q). \tag{14}$$

After calculating the amplitude reflectivity r_N by eqs. (5)–(14), the power reflectivity R_2 of the alternating quarter-wavelength layers is given by

$$R_2=|r_N|^2. \tag{15}$$

Figure 10 shows the calculated results of the relation between R_2 and N. Black circles represent the results calculated by the conventional plane wave approximation which are expressed as

$$R_2=\begin{cases}\left[\dfrac{n_2-(n_L/n_H)^N}{n_2+(n_L/n_H)^N}\right]^2 & (N;\text{even})\\[2ex] \left[\dfrac{n_2-n_H n_L(n_L/n_H)^N}{n_2+n_H n_L(n_L/n_H)^N}\right]^2 & (N;\text{odd}).\end{cases} \tag{16}$$

By the present calculation, represented by the white circles in this figure, $R_2=68\%$ and 84% for $N=5$ and 6, respectively, which are smaller than those by the conventional plane wave approximation i.e., 72% and 94%. Even for $N\to\infty$, the value of R_2 does not reach 100% but is limited to 88%. It can be said these smaller values of R_2 are due to the coupling loss owing to diffraction. The values of R_2 on the abscissa in Fig. 5 were plotted using the results shown in Fig. 10.

As the last part of this section, some comments are given with respect to the influence of the dispersion of ZnS and MgF_2 on the measurement error of the layer thickness. The ratio of the refractive indices of ZnS at $\lambda=1.55$ μm and at $\lambda/3=0.52$ μm is $n_H(\lambda)/n_H(\lambda/3)=0.95$.[2] Since that of MgF_2 is almost unity,[3] one has to consider the dispersion of ZnS only. By this dispersion of ZnS, the thickness of the coated ZnS layer is fixed to only 95% of the quarter-wavelength of the laser when it is monitored by the light with the wavelength of $\lambda/3$. The influence of this error on R_2 can be easily estimated by changing eq. (10) as follows;

$$z_q=\frac{\lambda}{4n_H}\left[\frac{q}{2}\right]\zeta+\frac{\lambda}{4n_L}\left[\frac{q+1}{2}\right], \tag{17}$$

where $\zeta=0.95$ represents this error in the thickness of ZnS layer. White triangles in Fig. 10 represent the results by using eq. (17) and the conventional plane wave approximation. These values are smaller than those of the black circles, which means that the reflectivity R_2 is estimated to be decreased as long as the conventional plane wave approximation is employed. On the other hand, the cross marks represent the results obtained by using eq. (17) and the present method for calculation. The values of these cross marks are almost the same as those of the white circles. This is due to the fact that the decrease in the value of R_2 by this error is prevented by the simultaneous decrease in the coupling loss of eq. (5) because the values of z_q are decreased by this error. Therefore, it can be concluded using the present calculations that the error in the thickness measurements due to the dispersion of ZnS has no effect on the value of R_2, i.e., the optical thickness monitor in §2 can be safely used for the present experiments.

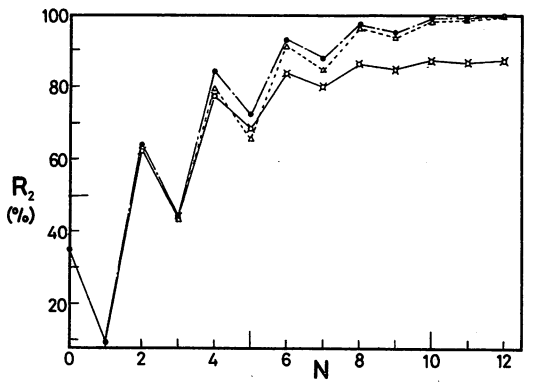

Fig. 10. Calculated results of the relation between the reflectivity R_2 and the number of layers N. White and black circles represent the results of the present calculation and by the conventional plane wave approximation, respectiviely. Cross marks and white triangles are also from these two calculations. In these cases, however, the thickness of ZnS layer is 95% of the quarter-wavelength of the laser.

Though the present method for calculation is more accurate than that by the plane wave approximation, it is still semiquantitative one as long as the matrices of eqs. (7) and (8) for the plane wave are employed. However, several physical insights, *e.g.*, the effect of the diffraction, that of dispersion of ZnS, were obtained with this calculation. Further quantitative discussions can be expected by improving the accuracies of the experiments and calculations.

§5. Summaries

The alternating quarter-wavelength layers of ZnS and MgF_2 were coated on the facets of GaInAsP/InP BH lasers at 1.55 μm to decrease the threshold current by increasing the reflectivities of the facets. Several experiments and calculations were carried out and the following results were obtained:

(1) A precise optical thickness monitor was developed for the coating. The measurement errors were estimated to be smaller than 3%.

(2) By coating five and six alternating layers, the threshold currents were decreased to 83% and 79% of the uncoated laser, respectively.

(3) Calculations of the reflectivities, by considering the coupling loss at the end of the waveguide due to diffraction, gave estimated results of 68% and 84% for five and six layers, respectively. It was also shown that the reflectivity is limited to 88% even if the number of the layers is increased.

Acknowledgements

The authors would like to express their thanks to Prof. Suematsu and the members of his laboratory for offering the laser diodes, for providing technical support, and for discussions. They also wish to thank Prof. Tako and Assoc. Prof. Furuya of their institute for valuable discussions.

References

1) M. Ettenberg: Appl. Phys. Lett. **32** (1978) 724.
2) Y. Kokubun and K. Iga: Bull. Precis. Mach. & Electron., Tokyo Inst. Technol. **50** (1982) 33.
3) S. J. Czyzak, W. M. Baker, R. C. Crane and J. B. Howe: J. Opt. Soc. Am. **47** (1957) 240.
4) A. Duncanson and D. W. H. Stevenson: Proc. Phys. Soc. **72** (1958) 1001.
5) R. Glang: *Handbook of Thin Film Technology*, eds. L. I. Maissel and R. Glang, Macgraw-Hill, New York, 1970 Part 1, Chapter 1.
6) M. Born and E. Wolf: *Principles of Optics* (Pergamon Press, Oxford 1970) 4th ed., Chapter 1.
7) S. Arai, M. Asada, T. Tanbun-ek, Y. Suematsu, Y. Itaya and K. Kishino: IEEE J. Quantum Electron. **QE-17** (1981) 640.
8) M. Asada, A. Adams, K. E. Stubkjaer, Y. Suematsu, Y. Itaya and S. Arai: IEEE J. Quantum Electron. **QE-17** (1981) 611.
9) H. C. Casey and M. B. Panish: *Heterostructure Lasers* (Academic Press, New York, 1978) Part A, Chapter 2.
10) D. Marcuse: *Light Transmission Optics* (Van Nostrand Reinhold, New York, 1972) Chapter 2.
11) R. L. Abram: IEEE J. Quantum Electron. **QE-8** (1972) 838.
12) R. Jacobsson: *Progress in Optics*, ed. E. Wolf (North-Holland, Amsterdam, 1966) Part V, Chapter 3.

JAPANESE JOURNAL OF APPLIED PHYSICS
VOL. 22, NO. 12, DECEMBER, 1983 pp. 1876–1882

Accurate Measurements of the Wavelengths and Material Constants of 1.5 μm InGaAsP/InP Lasers

Motoichi OHTSU, Haruo TAGAWA and Hiroki KOTANI

International Cooperation Center for Science and Technology, Tokyo Institute of Technology, 2-12-1, O-Okayama, Meguro-ku, Tokyo 152

(Received May 16, 1983; accepted for publication August 20, 1983)

The wavelengths of single longitudinal-mode 1.5 μm InGaAsP/InP lasers were measured at room temperature to an accuracy of 0.9 pm. An accurate wavementer was constructed for this purpose, and it exhibited an accuracy as high as 0.35 pm. The wavelength shifts of the lasers under unit changes in the injection current I and temperature T were derived from the results. By using the values of these wavelength shifts, the value of the temperature coefficient β of the refractive index in the cavity, and that of the thermal resistance R_T were accurately estimated. The results of these non-destructive measurements are as follows:

(Laser No. 1) $1.03\times10^{-4}\,\mathrm{K}^{-1}\leqq\beta\leqq1.07\times10^{-4}\,\mathrm{K}^{-1}$ and $79.8\,\mathrm{K/W}\leqq R_T\leqq98.1\,\mathrm{K/W}$ (for $290\,\mathrm{K}\leqq T\leqq295\,\mathrm{K}$ and $86\,\mathrm{mA}\leqq I\leqq96\,\mathrm{mA}$).

(Laser No. 2) $0.81\times10^{-4}\,\mathrm{K}^{-1}\leqq\beta\leqq0.83\times10^{-4}\,\mathrm{K}^{-1}$ and $133\,\mathrm{K/W}\leqq R_T\leqq136\,\mathrm{K/W}$ (for $291\,\mathrm{K}\leqq T\leqq295\,\mathrm{K}$ and $70\,\mathrm{mA}\leqq I\leqq80\,\mathrm{mA}$).

§1. Introduction

The performances of near-infrared semiconductor lasers have been greatly improved as a result of demand in the optical communication industries, and these laser have shown possibilities for use in new applications such as precise optical measurement, high-resolution spectroscopy, and so on. With these applications in mind, several experimental and theoretical studies have been carried out with the aim of improving the wavelength stabilities of GaAlAs/GaAs lasers[1,2] and InGaAsP/InP lasers.[3] However, further improvements in the wavelength stabilities necessitate a precise analysis of the dependence of the wavelengths on the laser material or the structural constants. For this purpose, the wavelength and material constants of individual lasers should be accurately measured by non-destructive methods, because the values differ considerably from laser to laser, probably because of variations introduced during fabrication. The accuracies of the wavelength values measured by conventional experimental techniques have not up to now been high enough for these studies, and precise values of laser materials or structural constants have not been fully reported, either.

In the present study, precise measurements of the wavelength of InGaAsP/InP lasers at 1.5 μm (BL-PCW type[4]), as well as their dependence on injection current and temperature, were carried out in order to analyse their oscillating mechanisms. An accurate and compact wavemeter was constructed for these measurements. Using the experimental results, several material constants for each laser were estimated.

§2. Accurate Wavemeter

The wavelength shifts produced by the injection current or temperature can be measured even with a conventional low-finesse Fabry-Perot interferometer. For example, those of the InGaAsP/InP lasers employed here were roughly measured by such an interferometer, and the values were about 8 pm/mA and 80 pm/K, respectively. Though the accuracy of a Fabry-Perot interferometer is generally high, direct measurements of the absolute values of wavelengths would be difficult as long as only a single interferometer is used. On the other hand, even though the absolute values of wavelengths can be measured with a high-performance grating monochromator, it is difficult in practice to obtain an accuracy as high as 10 pm. In the present study, an accurate and compact wavemeter was constructed to measure the absolute values of laser wavelengths, as with the grating monochromator, and simultaneously to obtain a high accuracy, as with the Fabry-Perot interferometer. The wavemeter was designed to achieve an accuracy higher than 1 pm. From the several types of wavemeter previously reported, such as those employing the Michelson interferometer, the Fizeau interferometer, multiple Fabry-Perot interferometers, and so on,[5] a Michelson interferometer-type wavemeter was chosen here because it is the simplest, and no computer-aided signal processing is required.[6] This type of wavemeter has been successfully used with high-power visible dye lasers, but its application to low-power, near-infrared semiconductor lasers has not previously been reported. Figure 1(a) shows the optical part of the wavemeter, which is composed of a Michelson interferometer with moving arms. The wavelengths of semiconductor lasers are obtained by comparing them with that of a 633 nm He–Ne laser, used as a wavelength standard. The beams of the semiconductor and He–Ne lasers are split into two arms by the beam splitter BS_2 after they are colinearly incident on the wavemeter. The laser beams are superimposed at BS_2 again after the beams have been reflected by the corner cubes (C_1, C_2) and folding mirrors (M_1, M_3). The two superimposed beams are split by a Si plate (BS_2), and then the interference fringes of the semiconductor and He–Ne lasers are detected by a Ge-avalanche photodiode and a Si-PIN photodiode, respectively.

The moving arms were prepared by smoothly driving the two corner cubes on steel rods. A low-noise synchronous motor was used as the driver. The speed v and excursion

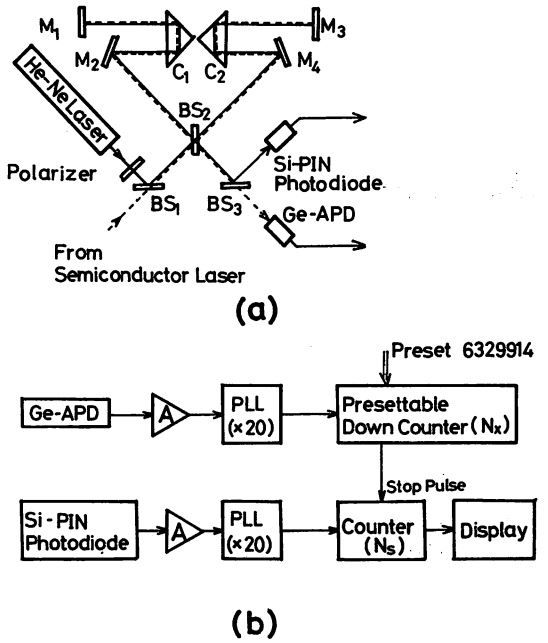

Fig. 1. Accurate wavemeter employing a moving-arm Michelson interferometer. (a) Optical components: M_1–M_4; Mirrors. C_1, C_2; Translating corner cubes. BS_1–BS_3; Beam splitters. (b) Electronic components: PLL; phase-locked loop circuits used to multiply the input frequency.

length Δl of the arms were 1.7 cm/s and 6 cm, respectively, i.e., the time required for this excursion was 3.5 s. The difference in the optical path length between the two arms was changed with time by the translating corner cubes. By using two corner cubes and two folding mirrors, the total change in the optical path length difference corresponded to $8 \cdot \Delta l$.

A small internal-mirror He–Ne laser (Spectra-Physics Model 136) was used as a wavelength standard. This was satisfactory for this purpose because its wavelength fluctuations were less than 0.1 pm. As two longitudinal modes were simultaneously oscillated in this laser, one of the modes was selectively extracted by using an external linear polarized as a mode filter. All the optical components including the He–Ne laser in Fig. 1(a) were fixed on rigid aluminium plate measuring 60 cm × 60 cm × 1 cm so that the wavemeter was compact and easy to carry.

As the intensities of the interference fringes are sinusoidally changed with time by translating the corner cubes, the number of changes, i.e., the changes in the orders of interference, were counted by the fringe counters in Fig. 1(b). To improve the counting accuracties, the frequencies of the TTL signals from the photodiodes were multiplied twenty times by phase-locked loop circuits. By these multiplications, the numbers of changes in the order of interference for the semiconductor and He–Ne lasers were $n_x = 2 \times 8 \cdot \Delta l/\lambda_x$ and $n_s = 20 \times 8 \cdot \Delta l/\lambda_s$, respectively. Here, λ_x and λ_s represent the wavelengths of the two lasers. The approximate values of n_x and n_s were calculated as 6.4×10^6 and 1.5×10^7 for $\lambda_x = 1.5$ μm and $\lambda_s = 633$ nm, respectively. Since the numbers n_x and n_s are not generally integers, they should be expressed as $n_x = N_x + \varepsilon_x$ and $n_s = N_s + \varepsilon_s$, respectively, where N_x and N_s represent the corresponding integers, and ε_x and ε_s are the decimal fractions. As only the integer-parts of n_x and n_s can be detected by the digital fringe counters, the observed value of the wavelength λ_x is expressed as

$$\lambda_x = (N_s/N_x)\lambda_s. \tag{1}$$

This value includes counting errors because the decimal fractions ε_x and ε_s were neglected. The error is, therefore, expressed as

$$\Delta\lambda_x = \left(\frac{\varepsilon_x}{n_x} + \frac{\varepsilon_s}{n_s}\right)\lambda_s \leqq \left(\frac{1}{N_x} + \frac{1}{N_s}\right)\lambda_s, \tag{2}$$

and is estimated to be $\Delta\lambda_x \leqq 0.34$ pm by substituting the above values into this equation, which satisfies the condition $\Delta\lambda_x \leqq 1$ pm required above. By following eq. (1), the integer $N_x = 6329914$ expressing the wavelength of the He–Ne laser in vacuum ($\lambda_s = 632991.4$ pm[7]) was loaded as an initial value of the presettable down-counter for the semiconductor lasers. Then, the wavelength value λ_x can be obtained by displaying the integer N_s counted by the counter for the He–Ne laser when the presettable counter for the semiconductor laser has finished counting down to zero beginning from the present value of N_x.

Seventy successive measurements of the laser wavelength were carried out to test the practical performance of the wavemeter. Figure 2a shows the distribution of the data. Laser No. 1 described in §3 was used for this measurement. The laser was fixed on a heat sink consisting of a copper plate, and its temperature fluctuations were roughly reduced to as low as ±0.05 K by using a Peltier element and a thermocouple. The heat sink temperature and the injection current were kept at around 292 K and 90 mA, respectively, so that the laser showed single longitudinal mode oscillation, as in Fig. 3 in §3. Furthermore, the laser wavelength was locked to a stable external Fabry-Perot interferometer to reduce the wavelength fluctuations by controlling the injection current. Figure 2b shows the residual wavelength fluctuations, which were lower than 0.1 pm. It can be seen in Fig. 2a that the standard deviation of the measured wavelength distribution was 0.35 pm, which is almost equal to the value of eq. (2). From this result, it can be confirmed that the wavemeter has the required accuracy. The accuracy of 0.35 pm is so high that it can also be used to measure the center wavelengths of the Doppler-broadened spectra of gaseous molecules. The results of the application of this wavemeter to such a spectroscopic measurement will be published elsewhere.[3]

§3. Measurements of Wavelength

As a preliminary experiment for the wavelength measurements, the oscillation spectra of the two lasers used were measured by a grating monochromator with a resolution of 0.3 nm. Figures 3a and 3b show the results. The shaded portions in these figures show the range of the heat sink temperature T and the injection current I, in which each laser exhibits the single longitudinal mode oscillation. Here, the single longitudinal mode oscillation was conveniently defined to be the state in which the intensities of the satellite longitudinal modes were less than 5% of the main longitudinal mode. For laser No. 1, the wavelengths in regions (I) and (II) were 1.503 μm and

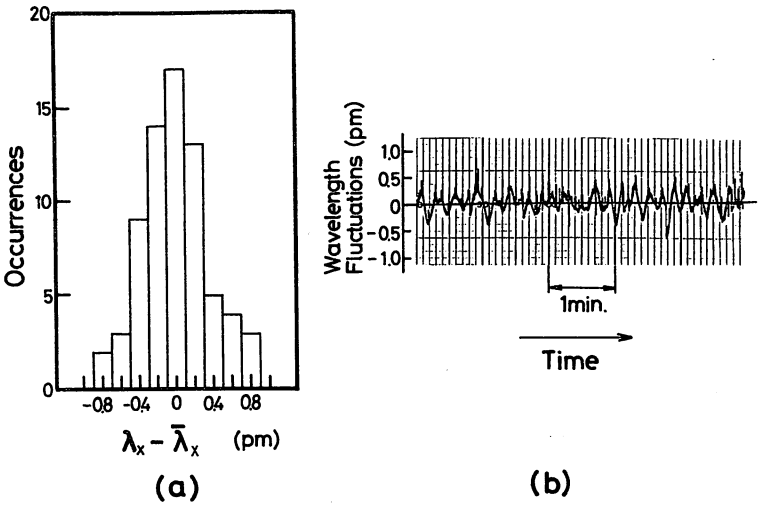

Fig 2. (a) Distribution of 70 successive measured values of the wavelength. The average value of the wavelength $\bar{\lambda}_x$ and the standard deviation σ_{N-1} are 1503235.0 pm and 0.35 pm, respectively. (b) residual wavelength fluctuations of laser No. 1 used for the measurements in (a). Here, the laser wavelength was stabilized to a stable external Fabry-Perot interferometer.

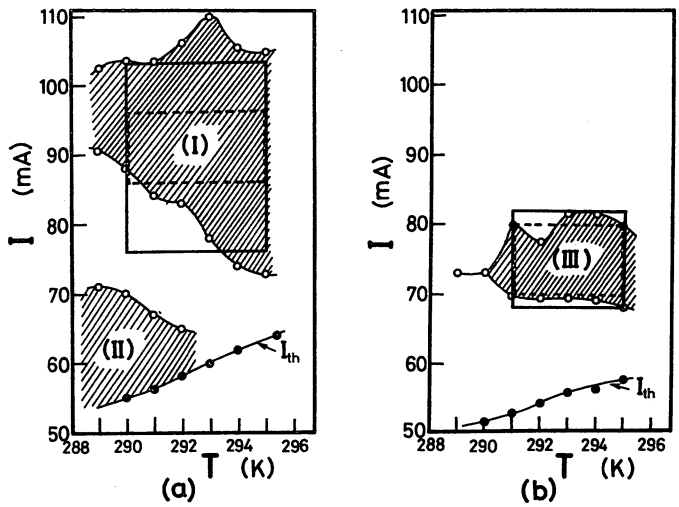

Fig. 3. Ranges of temperature T and injection current I of lasers with single longitudinal mode oscillations. (a) laser No. 1. (b) laser No. 2. The shadowed portions show the ranges. The wavelengths and their shifts were measured in the regions bounded by solid lines and broken lines, respectively. The temperature dependences of the threshold currents I_{th} are also shown here.

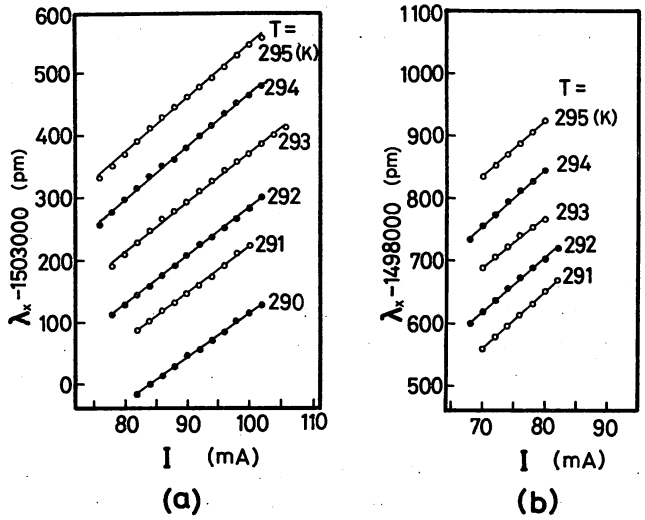

Fig. 4. Relations between wavelengths in vacuum, temperature T, and injection current I. (a) laser No. 1, (b) laser No. 2. These measurements were carried out in the regions bounded by solid lines in Fig. 3. The solid lines were drawn by least-squares fitting to the measured values.

1.496 μm, respectively. The wavelength of laser No. 2 in region (III) was 1.498 μm. The wavelengths and their shifts were measured in the regions bounded by solid lines and broken lines in these figures, respectively. These figures also show the relations between the threshold current I_{th} and the temperature. Typical output powers of lasers No. 1 and No. 2 were about 3.7 mW and 4.4 mW, respectively, when $T=293$ K and $I=80$ mA.

Figure 4 shows the experimental results of the relation between wavelength λ_x, temperature T, and injection current I. Some of the wavelength values of each laser were measured outside the single longitudinal mode oscillation region in Fig. 3, but they did not show distinct deviations from the linear relations between λ_x and I in Fig. 4. For laser No. 1, measurements were done in region (I) in Fig. 3(a). Systematic measurements were rather difficult in region (II) because the laser power in this region was not high enough for the measurements. However, as a reference, one example measured in region (II) is given in Table I. Several wavelength values measured in regions (I) and (II) are also shown in this table. The wavelengths in Fig. 4 and Table I are the values in vacuum, converted from the wavelength values measured in air by using the refractive index of air. This refractive index was derived by substituting the measured values of the pressure, temperature, and humidity of the air into the well-known Edlen formula.[8] The accuracy of this conversion was so high that no extra errors were introduced into the measured values of Fig. 4 and Table I by this procedure. The results in Fig. 4 and Table I represent the average values of five successive measurements. As shown in Table I, the maximum of the standard deviation of the measured values was as large as 0.9 pm, larger than the value of eq. (2). The main cause of this decrease in accuracy was confirmed to be the temperature fluctuations, because the temperature

Table I. Examples of the measured values of wavelengths in vacuum.

Laser	Region of the single longitudinal mode oscillation(*)	Temperature T	Injection current I	Average of the wavelength λ_x	Standard deviation σ_{N-1}	Number of data N
No. 1	(I)	292 (K)	86 (mA)	1503175.2 (pm)	0.8 (pm)	5
			88	1503191.9	0.9	
			90	1503206.8	0.5	
			92	1503223.9	0.6	
			94	1503236.8	0.7	
			96	1503251.8	0.4	
No. 1	(II)	290	60	1496311.1	0.8	5
No. 2	(III)	292	70	1498617.8	0.5	5
			72	1498637.5	0.3	
			74	1498655.2	0.2	
			76	1498672.9	0.4	
			78	1498689.2	0.4	
			80	1498703.8	0.7	

(*)see Fig. 3.

fluctuations of ± 0.05 K mentioned in §2 correspond to wavelength fluctuations of about ± 0.4 pm. Even with this decrease due to temperature fluctuations, the wavelengths were measured within the required accuracy of 1 pm, which is more than ten times better than that of conventional high-performance grating monochromators. Figure 5 shows the relations between the heat sink temperature T and the wavelength shift under unit change in the injection current $\Delta\lambda_x/\Delta I$, derived from the results in Fig. 4. Figure 6 shows the relations between the injection current I and the wavelength shift under unit change in the heat sink temperature $\Delta\lambda_x/\Delta T$, also derived from Fig. 4. Of the wavelength values in Fig. 4, those measured inside the regions bounded by the broken lines in Fig. 3 were used to derive the wavelength shifts in Figs. 5 and 6. In these regions, more reliable single longitudinal mode oscillations were obtained than in the regions bounded by the solid lines used for the measurements of Fig. 4; i.e., the intensities of the satellite longitudinal modes were less than 2% of that of the main mode. It can be seen from these figures that the quantities $\Delta\lambda_x/\Delta I$ and $\Delta\lambda_x/\Delta T$ do not have constant values but depend on I and T, respectively. By applying the least-squares fitting technique to the measured values, these dependence can be expressed as:

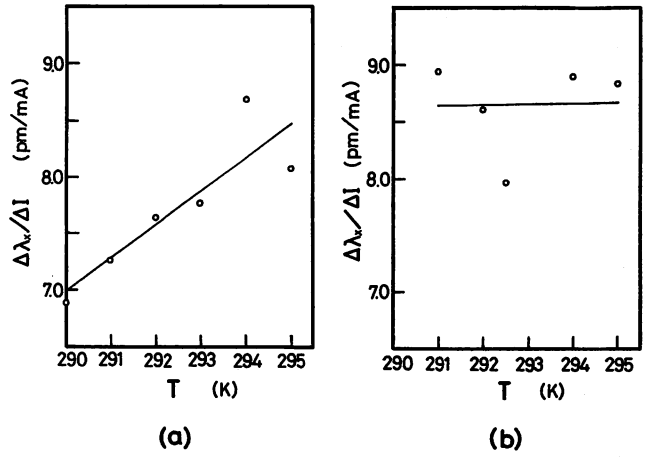

Fig. 5. Relations between temperature T and wavelength shift under unit change in injection current $\Delta\lambda_x/\Delta I$. (a) laser No. 1. (b) laser No. 2. These measurements were carried out in the regions bounded by broken lines in Fig. 3. The solid lines were drawn by least-squares fitting to the measured values, as expressed by eqs. (3) and (5) in the text.

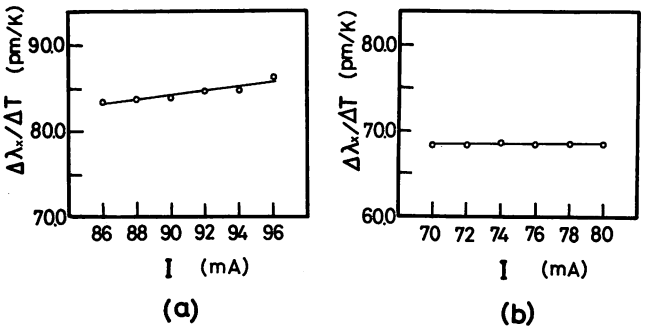

Fig. 6. Relation between injection current I and wavelength shift under unit change in temperature $\Delta\lambda_x/\Delta T$ (a) laser No. 1. (b) laser No. 2. These measurements were carried out in the regions bounded by broken lines in Fig. 3. The solid lines were drawn by least-squares fitting to the measured values, as expressed by eqs. (4) and (6) in the text.

(Laser No. 1)

$$\Delta\lambda_x/\Delta I = 2.96\times10^{-1}\cdot T - 78.9 \quad \text{(pm/mA)}$$
$$\text{for } 290\ \text{K} \leqq T \leqq 295\ \text{K}, \tag{3}$$

$$\Delta\lambda_x/\Delta T = 1.84\times10^{-1}\cdot I + 67.4 \quad \text{(pm/K)}$$
$$\text{for } 86\ \text{mA} \leqq I \leqq 96\ \text{mA}. \tag{4}$$

(Laser No. 2)

$$\Delta\lambda_x/\Delta I = 9.00\times10^{-3}\cdot T + 6.02 \quad \text{(pm/mA)}$$
$$\text{for } 291\ \text{K} \leqq T \leqq 295\ \text{K}, \tag{5}$$

$$\Delta\lambda_x/\Delta T = 9.57\times10^{-3}\cdot I + 66.7 \quad \text{(pm/K)}$$
$$\text{for } 70\ \text{mA} \leqq I \leqq 80\ \text{mA}. \tag{6}$$

§4. Estimation of Material Constants

Some of the material constants of the semiconductor lasers can be estimated by using the results of the wavelength shifts in §2. No accurate expressions for the wavelength shifts have yet been fully reported, and only a linear approximation of the relation between the

wavelength shift $\Delta\lambda_x$ and the temperature change ΔT has been given until now.[9] This is expressed as

$$\Delta\lambda_x=\lambda_x\left[\mathrm{A}\frac{1}{n}\Delta N_c+(\alpha+\beta)\Delta T\right], \tag{7}$$

In this equation, λ_x is the laser wavelength, n is the refractive index in the cavity, ΔN_c is the change in the carrier density produced by ΔT, α is the linear expansion coefficient of the cavity length, β is the temperature coefficient of n, and $A=\partial n/\partial N_c$, respectively. Here, the carrier density N_c is given by[10]

$$N_c=N_0\cdot\exp\{(T-T_1)/2T_0\}, \tag{8}$$

where N_0 is the density at temperature T_1. The quantity T_0 in this equation represents the characteristic temperature of the temperature dependence of the threshold current I_{th}, which is given by

$$I_{th}=I_{th0}\cdot\exp(T/T_0), \tag{9}$$

where I_{th0} is a constant value. By using eqs. (7) and (8), an expression for $\Delta\lambda_x/\Delta T$ can be derived and is expressed as:

$$\Delta\lambda_x/\Delta T=\lambda_x\left[\frac{AN_c}{2nT_0}+(\alpha+\beta)\right]. \tag{10}$$

The left-hand side of this equation has been experimentally obtained in §2, and is given by eqs. (4) and (6) for the two lasers. For the right-hand side of eq. (10), the following values have been reported, except for β:

$$\left.\begin{aligned}&A=-7.0\times10^{-21}\ \mathrm{cm}^3\ ^{10)}\\&n=3.54^{11)}\\&N_0=2.0\times10^{18}\ \mathrm{cm}^{-3}\ \text{at}\ T_1=297\ \mathrm{K}^{10)}\\&\alpha=5.42\times10^{-6}\ \mathrm{K}^{-1}\ \text{for}\ \mathrm{In_{0.47}Ga_{0.26}As_{0.6}P_{0.4}}.^{12)}\end{aligned}\right\} \tag{11}$$

The values of λ_x for lasers No. 1 and No. 2 were 1.503 μm and 1.498 μm, respectively. The values of T_0 were derived by substituting the measured values of I_{th} in Figs. 3(a) and 3(b) into eq. (9), and were found to be 33.7 K and 44.5 K for lasers No. 1 and No. 2, respectively. Accurate values of β for 1.5 μm InGaAsP/InP lasers have not yet been fully reported. However, in this work, they can be derived by substituting numerical values of eq. (11) into eq. (10) and by using eqs. (4) and (6). Since the values of $\Delta\lambda_x/\Delta T$ in eqs. (4) and (6) depend on the injection current I, the estimated values of β also depend on I as long as the other quantities in eq. (10) have the constant values shown by eq. (11). Figure 7(a) shows estimated values of β of laser No. 1 for the range of T and I in which eqs. (3) and (4) can be applied. That is, the value of β in this figure is expressed as

$$1.03\times10^{-4}\ \mathrm{K}^{-1}\leqq\beta\leqq1.07\times10^{-4}\ \mathrm{K}^{-1}$$
$$\text{for}\ 290\leqq T\leqq295\ \mathrm{K}\ \text{and}\ 86\ \mathrm{mA}\leqq I\leqq96\ \mathrm{mA}. \tag{12}$$

The estimated value of β of laser No. 2 is shown in Fig. 7(b) for the range of T and I in which eqs. (5) and (6) can be applied. The value of β in this range is given by

$$0.81\times10^{-4}\ K^{-1}\leqq\beta\leqq0.83\times10^{-4}\ \mathrm{K}^{-1}$$
$$\text{for}\ 291\leqq T\leqq295\ \mathrm{K}\ \text{and}\ 70\ \mathrm{mA}\leqq I\leqq80\ \mathrm{mA}. \tag{13}$$

As demonstrated by eqs. (12) and (13), the value of β for each laser was accurately estimated here by non-destructive measurements while these lasers were continuously oscillated at room temperature. Also, as mentioned in §2, it was shown that the values for each laser were different from each other, probably owing to inaccuracies in fabrication. Furthermore, it was shown that β did not have a constant value but depended on the temperature as long as the simple linear approximation of eq. (7) was employed, and that this dependence also differed from laser to laser. This means that a more accurate expression of the wavelength shift is required for further discussions of wavelength stabilities and FM noise characteristics. Such an expression is now being derived by the authors, but the simple expression of eq. (7) was conveniently employed in the present work.

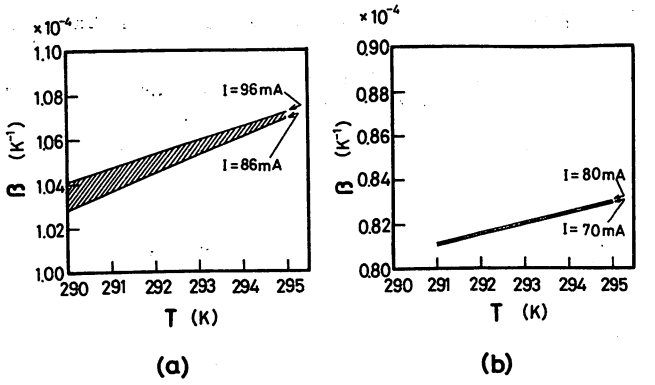

Fig. 7. Estimated values of temperature coefficient β of the refractive index. The value of β changed monotonically with the temperature T and the injection current I, and these values fall between the shadowed region for (a) laser No. 1 (290 K$\leqq T\leqq$295 K and 86 mA$\leqq I\leqq$96 mA) and (b) laser No. 2 (291 K$\leqq T\leqq$295 K and 70 mA$\leqq I\leqq$80 mA). The values are given by eqs. (12) and (13) in the text.

The other quantity which can also be estimated is the thermal resistance R_T. Even if the heat sink temperature T is kept constant, the temperature of the laser itself is changed by a change in the injection current ΔI. This temperature change ΔT can be expressed as

$$\Delta T=R_T[V_g(1-\eta)+2R_b\cdot I]\cdot\Delta I, \tag{14}$$

where V_g is the voltage corresponding to the band-gap energy of the semiconductor material, η is the external quantum efficiency, and R_b is the ohmic resistance, respectively. By using eq. (14), $\Delta\lambda_x/\Delta T$, and $\Delta\lambda_x/\Delta I$, the thermal resistance R_T can be expressed as follows:

$$R_T=\frac{(\Delta\lambda_x/\Delta I)}{(\Delta\lambda_x/\Delta T)[V_g(1-\eta)+2R_b\cdot I]}. \tag{15}$$

Therefore, the values of R_T can be estimated by substituting measured values of $\Delta\lambda_x/\Delta I$ and $\Delta\lambda_x/\Delta T$ (eqs. (3)–(6)) into eq. (15). Here, the values of V_g for lasers No. 1 and No. 2 are 0.872 V and 0.830 V, respectively, using the values of λ_x shown above. The value of η is expressed as

$$\eta=2P_0/V_g\cdot I, \tag{16}$$

where P_0 represents the single-ended output power of the laser. Figure 8 shows the experimental result of η obtained by measuring P_0 for several values of T and I. Furthermore, the value of R_b can be derived from the

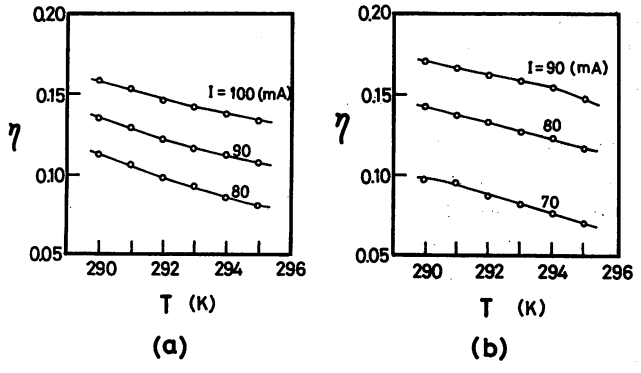

Fig. 8. Measured values of the external quantum efficiency η for several values of temperature T and injection current I. (a) laser No. 1. (b) laser No. 2.

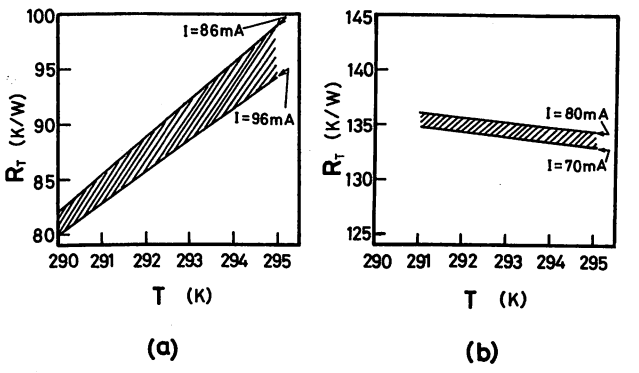

Fig. 10 Estimated values of the thermal resistance R_T. The value of R_T changed monotonically with the temperature T and injection current I, and values fall between the shaded regions for (a) laser No. 1 (290 K$\leqq T\leqq$295 K, 86 mA$\leqq I\leqq$96 mA) and (b) laser No. 2 (291 K$\leqq T\leqq$295 K, 70 mA$\leqq I\leqq$80 mA). The values are given by eqs. (17) and (18) in the text.

relation between the voltage V_{LD} across the laser diode and the injection current I above its threshold value I_{th}. Figure 9 shows the measured results of this relation. The values of R_b are given by the slope of the curve for $I>I_{th}$ in this figure, which are 1.71 Ω and 1.40 Ω for lasers No. 1 and No. 2, respectively. It was confirmed that these values of R_b were independent of T for 290 K$\leqq T\leqq$295 K. The value of R_T estimated from eq. (15) also depends on T and I, because $\Delta\lambda_x/\Delta I$ and $\Delta\lambda_x/\Delta T$ depend on T and I, respectively. Figure 10 shows the relation between R_T, T, and I obtained for the two lasers, Here, R_T was estimated in the range of T and I in which eqs. (3)–(6) can be applied. For laser No. 1, the value of R_T in Fig. 10a is expressed as

$$79.8\ \text{K/W}\leqq R_T\leqq 98.1\ \text{K/W}$$
$$\text{for } 290\ \text{K}\leqq T\leqq 295\ \text{K and } 86\ \text{mA}\leqq I\leqq 96\ \text{mA}. \tag{17}$$

And for laser No. 2, it is given by

$$133\ \text{K/W}\leqq R_T\leqq 136\ \text{K/W}$$
$$\text{for } 291\ \text{K}\leqq T\leqq 295\ \text{K and } 70\ \text{mA}\leqq I\leqq 80\ \text{mA}. \tag{18}$$

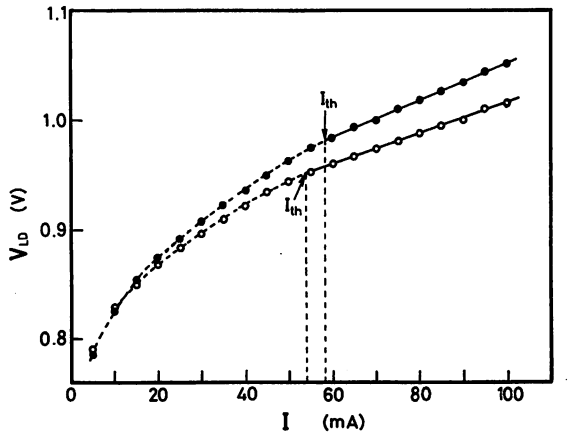

Fig. 9. Measured values of relation between voltage V_{LD} across the laser diode and injection current I. The black and white circles show the results for lasers No. 1 and No. 2, respectively. Here, the temperature T was fixed at 292 K. The solid lines were drawn by least-squares fitting to the measured values for $I>I_{th}$. The threshold currents of lasers No. 1 and No. 2 were 58 mA and 54 mA, respectively. The slopes of these lines represent the ohmic resistance R_b, which was 1.71 Ω and 1.40 Ω for lasers No. 1 and No. 2, respectively.

Equations (17) and (18) give accurate values of R_T for each laser, obtained by non-destructive measurement. As with β, it was also shown that the values of R_T differed for each laser. Furthermore, R_T depended on T and I as long as the simple expression of eq. (7) was employed. For reference, the value of R_T for a 1.3 μm InGaAsP/InP laser has been reported to be about 30 K/W,[13] with a laser fixed on a heat sink with a p-side down configuration. In the present study, however, it is quite reasonable for the estimated values of R_T to be larger than this previously-reported value because the lasers used here were fixed on the heat sink with the p-side up configuration, in which the efficiency of thermal dissipation is lower than that of the p-side down configuration.

The values of β and R_T were obtained by using accurately-measured values of $\Delta\lambda_x/\Delta I$ and $\Delta\lambda_x/\Delta T$. Since the accuracies of the measurements of $\Delta\lambda_x/\Delta I$ and $\Delta\lambda_x/\Delta T$ are high enough, the main cause of the errors in the estimated values of β and R_T are attributed to errors in the reported values of the material constants A, n, N_0, and α in eq. (11). Therefore, if these material constants are measured with higher accuracies by some new technique, further improvements in the accuracies of β and R_T can be expected. Furthermore, these accurately-measured values of the wavelength shifts and material constants may be used for the study of improving the wavelength stability as well as the FM noise characteristics, and also as the basic data to design higher-performance lasers in the future. These results may also be used to derive a more accurate expression than eq. (7). Such an expression is now being derived by the authors.

§5. Summary

The wavelengths of two 1.5 μm InGaAsP/InP lasers were measured to an accuracy of 0.9 pm. The lasers exhibited the single longitudinal mode oscillation at room temperature. For this purpose, an accurate wavemeter was constructed, which exhibited an accuracy of measurement as high as 0.35 pm. The wavelength shifts under unit change in the injection current I and temperature T were derived from the results of these measurements, and are expressed as:

(Laser No. 1)

$$\Delta\lambda_x/\Delta I = 2.96\times10^{-1}\cdot T - 78.9 \quad (\text{pm/mA})$$
$$\Delta\lambda_x/\Delta T = 1.84\times10^{-1}\cdot I + 67.4 \quad (\text{pm/K}) \qquad (19)$$

for $290\ \text{K} \leqq T \leqq 295\ \text{K}$ and $86\ \text{mA} \leqq I \leqq 96\ \text{mA}$.

(Laser No. 2)

$$\Delta\lambda_x/\Delta I = 9.00\times10^{-3}\cdot T + 6.02 \quad (\text{pm/mA})$$
$$\Delta\lambda_x/\Delta T = 9.57\times10^{-3}\cdot I + 66.7 \quad (\text{pm/K}) \qquad (20)$$

for $291\ \text{K} \leqq T \leqq 295\ \text{K}$ and $70\ \text{mA} \leqq I \leqq 80\ \text{mA}$.

By using the results of eqs. (19) and (20), the values of the temperature coefficient β of the refractive index in the cavity and the thermal resistance R_T for each laser were accurately estimated, and are given by:

(Laser No. 1)

$$1.03\times10^{-4}\ \text{K}^{-1} \leqq \beta \leqq 1.07\times10^{-4}\ \text{K}^{-1}$$
$$79.8\ \text{K/W} \leqq R_T \leqq 98.1\ \text{K/W} \qquad (21)$$

for $290\ \text{K} \leqq T \leqq 295\ \text{K}$ and $86\ \text{mA} \leqq I \leqq 96\ \text{mA}$.

(Laser No. 2)

$$0.81\times10^{-4}\ K^{-}1 \leqq \beta \leqq 0.83\times10^{-4}\ \text{K}^{-1}$$
$$133\ \text{K/W} \leqq R_T \leqq 136\ \text{K/W} \qquad (22)$$

for $291\ \text{K} \leqq T \leqq 295\ \text{K}$ and $70\ \text{mA} \leqq I \leqq 80\ \text{mA}$.

The results of eqs. (21) and (22) confirm that the material constants for each laser differ considerably from each other, and depend on T and I as long as a conventional linear approximation of the wavelength shifts is employed for the estimation. These accurately measured values of the wavelength shifts and material constants may be used as the basic data to improve the wavelength stability and to design a new type of laser in the future.

Acknowledgements

The authors would like to express their thanks to Drs. T. Yamamoto and S. Akiba of KDD Research and Development Laboralories for valuable discussions. They also wish to thank Profs. T. Tako and Y. Suematsu of their institute for their encouragement during this study.

References

1) M. Ohtsu, H. Tsuchida and T. Tako: *Proc. 36th Ann. Freq. Control Symposium, Philadelphia, June 1982* U.S. Army Electronics Research & Development Command, p. 327.
2) M. Ohtsu, H. Fukada, T. Tako and H. H. Tsuchida: Jpn. J. Appl. Phys. **22** (1983) 1157.
3) M. Ohtsu, H. Kotani and H. Tagawa: Jpn. J. Appl. Phys. **22** (1983) Phys. **22** (1983) 1553.
4) Y. Noda, K. Sakai and Y. Matsushima: Electron. Lett. **17** (1981) 226.
5) J. J. Snyder: Laser Focus, May (1982) 55.
6) J. L. Hall and S. A. Lee: Appl. Phys. Lett. **29** (1976) 367.
7) G. R. Hanes, K. M. Baird and J. DeRemigis: Appl. Opt. **12** (1973) 1600.
8) B. Edlen: Metrologia **2** (1966) 81.
9) M. Ito and T. Kimura: IEEE J. Quantum Electron., **QE-16** (1980) 910.
10) K. Stubkjaer, M. Asada, S. Arai and Y. Suematsu: Jpn. J. Appl. Phys. **20** (1980) 1499.
11) K. Sakai, F. Tanaka, Y. Noda, Y. Matsushima, S. Akiba and T. Yamamoto: IEEE J. Quantum Electron. **QE-17** (1981) 1245.
12) R. Bisaro, P. Merenda and T. P. Pearsal: Appl. Phys. Lett. **34** (1979) 100.
13) M. Yano, H. Imai, K. Hori and M. Takusagawa: IEEE J. Quantum Electron., **QE-17** (1981) 619.

レーザー技術ノート

マイクロコンピュータを用いたレーザー光軸調整

椎尾一郎*・アヌン-クスノボ**・大津元一***・田幸敏治*

(1983年1月31日　受理)

Laser Alignment Aided with a Microcomputer

Itiro SIIO*, Anung KUSNOWO**, Motoichi OHTSU***and Toshiharu TAKO*

(Received January 31, 1983)

1．はじめに

筆者らは 3.51μm の He-Xeレーザーを用いてH_2COの高分解能分光を行ない，He-Xeレーザーの周波数安定化[1]，H_2COのシュタルク効果の観測[2]などをすすめている。このレーザー分光システムの制御と分光データの処理のために，マイクロコンピュータを導入して周辺機器とソフトウェアの開発を行っているが，今回レーザー光軸の調整装置を試作した。

H_2COの高分解能分光のためのHe-Xeレーザー装置の配置をFig. 1に示す。この図はH_2COのシュタルク効果を測定する場合の実験系である。10mTorr圧のH_2COの吸収セルはレーザー共振器中に置かれ，この飽和吸収による反転ラムくぼみのシュタルク効果を測定する。分光対象としているH_2COの$5_{1,5}$ ($v=0$) → $6_{0,6}$ ($v_5=1$) の振動回転遷移はHe-Xeレーザーの発振線に比べて約180 MHz短波長側にあるため，ソレノイドによりレーザー管軸方向に124 Gの磁場を作り発振線の同調を行っている。光検出器の前に置かれたλ/4板と偏光板は磁場により分裂した2つのゼーマン成分のうち短波長

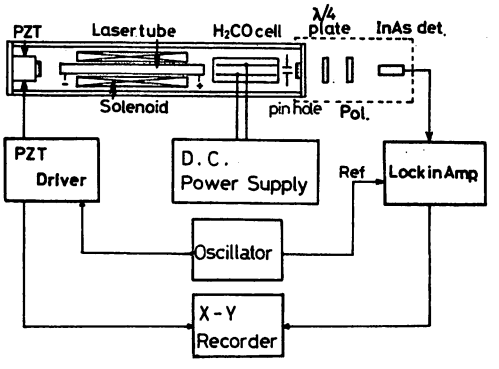

Fig. 1　3.51 μm He-Xe laser system for high resolution Stark spectroscopy of H_2CO.

* 東京工業大学精密工学研究所（〒227 横浜市緑区長津田4259）
** Graduate School for Opto-Electrotechniques and Laser Applications, University of Indonesia, (Jakarta, Indonesia.)
*** 東京工業大学理工学国際交流センター（〒152 東京都目黒区大岡山2—12—1）
* Research Laboratory of Precision Machinery and Electronics, Tokyo Institute of Technology, (Nagatsuta, Midori-ku, Yokohama 227)
** Graduate School for Opto-Electrotechniques and Laser Applications, University of Indonesia, (Jkarta, Indonesia)
*** International Cooperation Center for Science and Technology, Tokyo Institute of Technology, (O Okayama, Meguro-ku, Tokyo 152)

側の成分を分離するものである。レーザーミラーの片方は電歪素子(PZT)に取り付けられ，波長掃引と周波数変調を行う。

この装置で得られる反転ラムくぼみの半値全幅は約500 kHzである。シュタルク分裂の大きさは電場が4 KV／cmで1 MHz程度であるため，精密なシュタルク効果の測定のためにはH_2COのガス圧や変調を小さくして数10KHzの分解能を得る必要がある。この場合反転ラムくぼみの大きさも数10分の1程度になるため，最大の反転ラムくぼみが得られるようにレーザーの光軸を調整しておかねばならない。

このようなレーザーの調整は次の手順で行う。まず光軸合せ用の633 nm　He-Neレーザーを用いてレーザー管，ソレノイド，吸収セル，検出器，レーザーミラーを同一軸上に配置する。次に，レーザー管を放電させて発振強度が最大でかつ明瞭で滑らかな同調曲線が得られるように各光学素子の光軸に対する位置と傾きを調整する。同調曲線が不明瞭であったり，折れ曲りがある場合は反転ラムくぼみが観測されないからである。これは高次のモードが発生することにより効果的に飽和が起らないためと考えられる。

そこで同調曲線の大きさと形を評価するため従来は各光学素子の微動の度に，同調曲線をX－Yレコーダーに記録して，その強度と形の変化から微動の適否を判断して最適位置を探索していた。

一方，各光学素子の位置のパラメータは多い。Fig. 1の場合レーザー管，吸収セル，ソレノイドの各々に光軸に対する位置と傾きを決める4個，ピンホールの位置の2個，各レーザーミラーのそれぞれに傾き2個，及び検出器の位置と傾き各々2個のパラメータがあり，合計22個ものパラメータを最適化する必要がある。このためレーザーの調整は多くの時間と経験を要する厄介な仕事であった。特に筆者らの場合装置が大型であり，また複数のレーザーを用いたビートの測定を計画しているのでこの調整は更に困難なものになる。

そこでこの作業の合理化をはかり，調整時間を短縮する目的で，マイクロコンピュータを用いた光軸調整装置を試作した。

2．装置の構成と機能

本装置は，各光学素子の微動前後の同調曲線を比較して微動の適否の評価を行うものである。すなわち，微動前後の2つの同調曲線をCRT表示器に重ね合せて表示し，同時に同調曲線の強度と形を評価して数値で表示する。操作者は各光学素子を手動で微調して最適な調整を行うことが出来るように設計した。

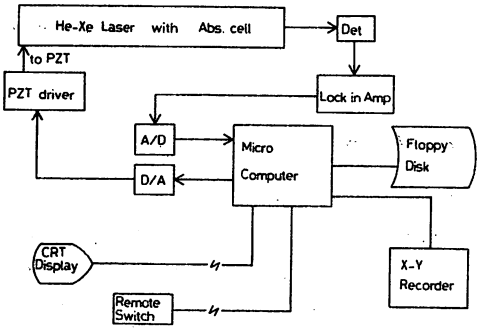

Fig. 2　Block diagram of the optical alignment equipment for laser systems.

装置の構成をFig. 2に示す。マイクロコンピュータはAPPLE Ⅱで，64K Byteのメモリーと280×192画素のグラフィック表示機能があり，オペレーティングシステムはUCSD-Pascalである。A/D及びD/Aコンバーターはそれぞれ12bit分解能である。D/Aコンバーターの出力はPZTドライバにより増幅され，レーザー周波数の掃引と制御を行う。リモートスイッチは，PZTの掃引の開始と，チェックのための停止を行うものである。操作者はCRT表示器とリモートスイッチを調整箇所に持って行くことが出来るため，大型のレーザー装置でも効率の良い調整が可能である。また，ディスク装置を使って同調曲線のデータを保存できるようにした。これにより種々のデータ処理や以前のデータとの比較が可能である。

本装置の基本的な動作はPZTの印加電圧を

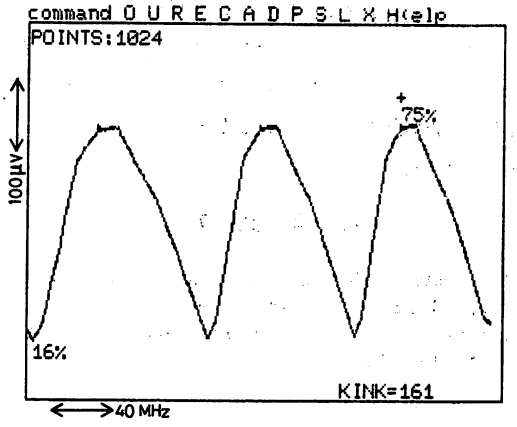

(a)

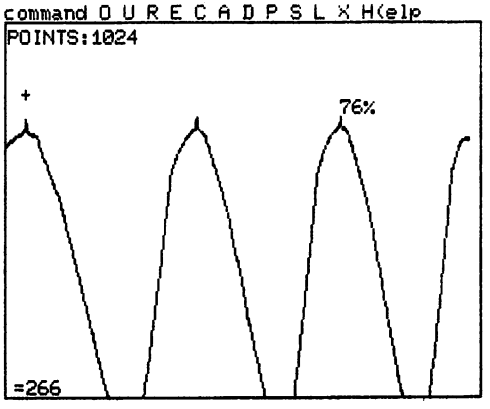

(b)

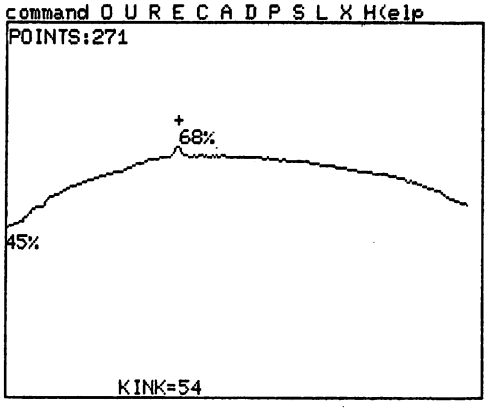

(c)

Fig. 3　Examples of display on CRT (a) before, (b) after alignment and (c) eight times expanded of (b), using the equipment. Alphabetic characters indicated upper are lists of commands for several data acquisition and processing.

くり返し掃引して同調曲線をCRTに表示することである。この例をFig. 3に示す。図中にある数値のうちパーセント記号の付されたものは同調曲線の最大値と最小値をロックインアンプのフルスケールに対する百分率で示したものである。KINK値として表示された数値は同調曲線の二次微分を差分で計算しその最大値を表している。図中で十記号は差分値が最大になった場所を示している。通常，この差分の最大値は同調曲線の滑らかさを表すが，反転ラムくぼみが現れている場合にはここで差分値が大きくなるためこの値は反転ラムくぼみの大きさを表すことになる。Fig. 3 (a)はレーザー調整が不完全な場合で，同調曲線が不明瞭でまた折れ曲りが大きく，その結果小さな反転ラムくぼみが現れている。本装置を用いて同調曲線の強度と滑らかさが最適になるように調整を行った結果がFig. 3 (b)である。表示される数値が同調曲線と反転ラムくぼみの明瞭さを正しく評価しているので，本装置により従来より的確な調整が可能である。

基本的なくり返し掃引の他に，同調曲線の拡大掃引の機能を持たせた。これは最初にPZTを大まかに掃引して同調曲線の概形を調べ，次にその最大値付近を拡大して掃引，表示するためである。Fig. 1の実験系では反転ラムくぼみが同調曲線の頂上付近に現れるようにレーザー周波数がゼーマン同調されているので，この拡大掃引機能により同調曲線の大きな変動に関係なく常に反転ラムくぼみ付近のくり返し掃引と観察が可能である。反転ラムくぼみの拡大掃引の結果をFig. 3 (c)に示す。これはFig. 3 (b)の横軸を8倍に拡大したものである。

3．まとめと使用結果

レーザー調整作業の能率向上のため，マイクロコンピュータを使用した調整装置を試作した。この装置の特徴を以下に示す。

1）同調曲線が自動掃引され，その最大値と最小値，滑らかさが数値で評価出来る。

2）同調曲線の頂上付近の自動拡大掃引機能

によりラムくぼみの変化が観測出来る。

3）同調曲線の観察と掃引の一時停止が操作者の手元で可能である。

レーザーシステムの光軸調整の作業に本装置を採用することにより，従来1日以上かかっていた調整作業を1時間程度に短縮することが出来た。これは各光学素子の微動の度にPZTドライバーとX－Yレコーダーを操作して同調曲線を記録して評価していた従来の作業が自動化されたためである。このような作業はレーザーの調整において一般的なものであるので，他のレーザーシステムに対しても本装置は極めて有用であると考えられる。特に調整箇所の多い複雑なシステムや大型のレーザー装置では同調曲線の評価機能やリモート操作の機能が有益になるであろう。

参考文献

1）M. Ohtsu, R. Koyama, A. Kusnowo and T. Tako: Jpn. J. Appl. Phys. **18** (1979) 1619.
2）I. Siio, M. Ohtsu and T. Tako: Jpn. J. Appl. Phys. **21** (1982) 813.

BULL. P.M.E. (T.I.T.), *No. 52, September 1983* 621.375.826

An Optical Alignment Equipment for Laser System

By

Itiro Siio*, Anung Kusnowo**, Motoichi Ohtsu***
and Toshiharu Tako****

(Received April 22, 1983)

Authors have developed an optical alignment equipment for laser systems for the purpose of speeding up of laser adjustment process. Optical alignment of a laser apparatus is generally troublesome especially for such a large-sized laser apparatus as optical elements are located separately. This equipment is designed to display tuning curves of laser power and evaluate the distinction and smoothness of the curves numerically. The optimum position of optical elements are found by monitoring changes of tuning curves before and after slight move of elements. The controller and the display of this equipment can be brought to the place of the optical element. After having applied this equipment for the optical alignment of the H_2CO stabilized He-Xe laser system, alignment time has been reduced to one hour from one day which was required in manual adjustment.

Key words: laser, optical alignment, micro computer.

1. Introduction

Authors have utilized a He-Xe laser at 3.51 μm for the high resolution Stark spectroscopy of H_2CO[1] and for the stabilization of the laser frequency using a component of the spectrum. An optical alignment process of a laser is generally troublesome because of many optical elements to be adjusted. For the purpose of speeding up of this process, the authors developed a micro computer aided alignment equipment.

Figure 1 shows a diagram of the experimental apparatus for high resolution Stark spectroscopy. Stark effect of saturated absorption signal (inverted Lamb dip) is observed, as H_2CO of 10 mTorr is contained in the intracavity Stark absorption cell. The laser cavity is 155 cm long, the overall length of the apparatus is 2 m of some size. One of the cavity mirrors is mounted on a piezoelectric transducer (PZT) for frequency tuning and modulation. Since the frequency of the transition $5_{1,5}$ ($v = 0$) – $6_{0,6}$ ($v_5 = 1$) of H_2CO is about 180 MHz higher than the center of the gain curve of the He-Xe laser, axial magnetic field of 124 G is applied to the laser tube to compensate for this frequency gap using a solenoid. A quarter-wave plate and a polarizer is necessary to separate higher-frequency circularly-polarized Zeeman component from lower-frequency oppositely circularly-polarized one.

The full width of half maximum (FWHM) of inverted Lamb dip is about 500 kHz when using present apparatus. Resolution of several tens kHz is necessary for precise measurement of Stark effect because Stark shifts are order of 1 MHz at electric field of 4 kV/cm. This improvement in resolution power will be achieved by reducing

* Graduate student, M. Eng., Department of Information Processing, Tokyo Institute of Technology, Nagatsuta.
** Graduate School for Opto-Electrotechniques and Laser Applications, University of Indonesia, Jakarta, Indonesia.
*** International Cooperation Center for Science and Technology, Tokyo Institute of Technology, Dr. Eng.
**** Professor, Dr. Sci.

Published by Research Laboratory of Precision Machinery and Electronics,
Tokyo Institute of Technology, Nagatsuta, Mirodi-ku, Yokohama 227, Japan

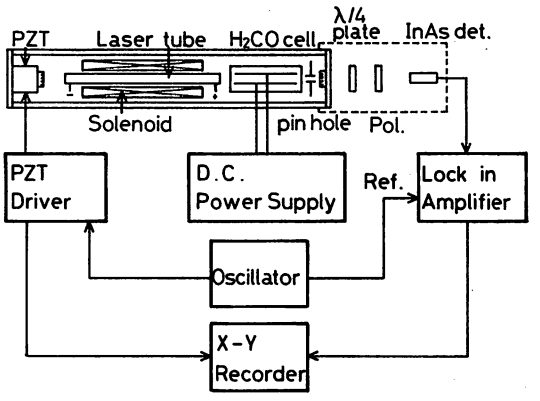

Fig. 1 A 3.51μm He-Xe laser apparatus for high resolution Stark spectroscopy of H_2CO.

the depth of the laser frequency modulation and reducing the H_2CO gas pressure. On the other hand this improvement results in several tens times smaller spectrum intensity than usual, the laser must be carefully aligned to get the maximum intensity of the dip.

The usual procedure for alignment is as follows; bring optical elements such as a laser tube, a solenoid, an absorption cell, a detector and mirrors into line using a 633 nm He-Ne laser. Subsequently discharge the laser tube and adjust position and angle against the optical axis of elements, in order to get high laser oscillation and to get a distinct and smooth tuning curve of laser power. In case the tuning curve is indistinct or kinky, the inverted Lamb dip is not observed. This can be interpreted that saturation occurs unsuccessfully because higher order modes arise.

Conventionally, the tuning curve is recorded in an X-Y recorder in every slight move of optical elements, and the changes of both intensity and shape of the curve are checked manually. The optimum position of optical elements are searched after a lot of such process because there are many parameters in the positions of components. For instance, as shown in Fig. 1, there are four parameters of the position and angle against optical axis in a laser tube, an absorption cell, a solenoid and a detector, two of position in a pin hole, two of angle in each cavity mirrors; in total there are as many as 22 parameters. The difficulty of optical alignment process increases remarkably in such a large-sized laser equipment as in our system, because every optical elements are located separately. Furthermore measurement of beat signal of two lasers are planned in order to measure precise Stark coefficient, speeding up of the optical alignment process has been desired.

2. The Constitution and Function of the Equipment

This equipment is designed to draw two tuning curves before and after slight manual move of every optical elements on CRT display, and to indicate the distinction and smoothness of the curves numerically. The optimum position of every optical element can be easily found by indicated evaluation of curves.

Figure 2 shows the block diagram of the equipment. A micro computer (Apple II) with memory of 64 kBytes and display function of 280 x 192 dots, works under UCSD Pascal operating system. An A/D (analog to digital) and a D/A (digital to analog) converters are 12 bits of resolution power. The laser frequency is controlled by the computer through the D/A converter. Sweep of the laser frequency is controlled remotely using extended switch box. This device is useful, especially for large-sized laser apparatus because the remote switch and the CRT display can be brought to the place of the optical

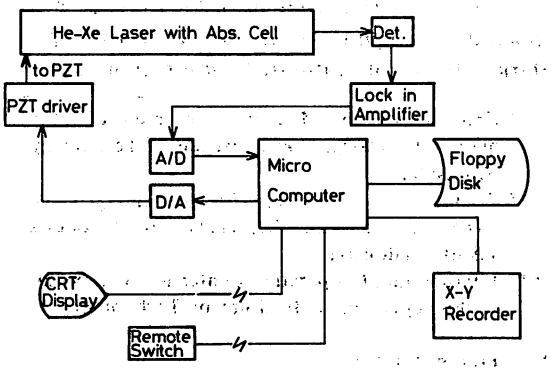

Fig. 2 The block diagram of the optical alignment equipment for laser system.

elements to be adjusted. A mini floppy disk driver is used to store data of tuning curves. The stored data is utilized for comparison to previous tuning curves and it can be applied for some kind of data processing.

Figure 3 shows typical examples of display on CRT. Indicated numbers are the maximum and minimum values of intensity and the maximum value of 2nd order finite differences of tuning curves, respectively. The latter can be considered to indicate a kinky point of the tuning curve usually. In the case inverted Lamb dips are observed, this value indicates the intensity of the dip. Figure 3 (a) shows a tuning curve when the optical alignment is not appropriate. An indistinct and kinky tuning curve results small intensity of inverted Lamb dips. Figure 3 (b) shows a tuning curve when optical elements have been adjusted to maximize inverted dips using this equipment. As distinction of a tuning curve and inverted Lamb dip is successfully evaluated on the display, an optimum optical alignment can be realized more easily than conventional process.

In addition to the function of repetitive laser frequency sweep, the function of automatically magnifying sweep around inverted Lamb dip is programmed in this equipment. Since the laser is Zeeman tuned to the inverted Lamb dip, dips appear at the top of tuning curves as shown in Fig. 3 (b). Using this function, the laser frequency is swept around the inverted Lamb dip after a gross sweep for detection of the top of the tuning curve. The inverted Lamb dip is automatically magnified on the display as in Fig. 3 (c), without influence of change in the tuning curve originated from temperature drift of the laser cavity length. The inverted Lamb dip shown in Fig. 3 (c) is 8 times magnification of Fig. 3 (b) in frequency axis. This function can be applied for investigating the change of a inverted Lamb dip against the change of some parameters.

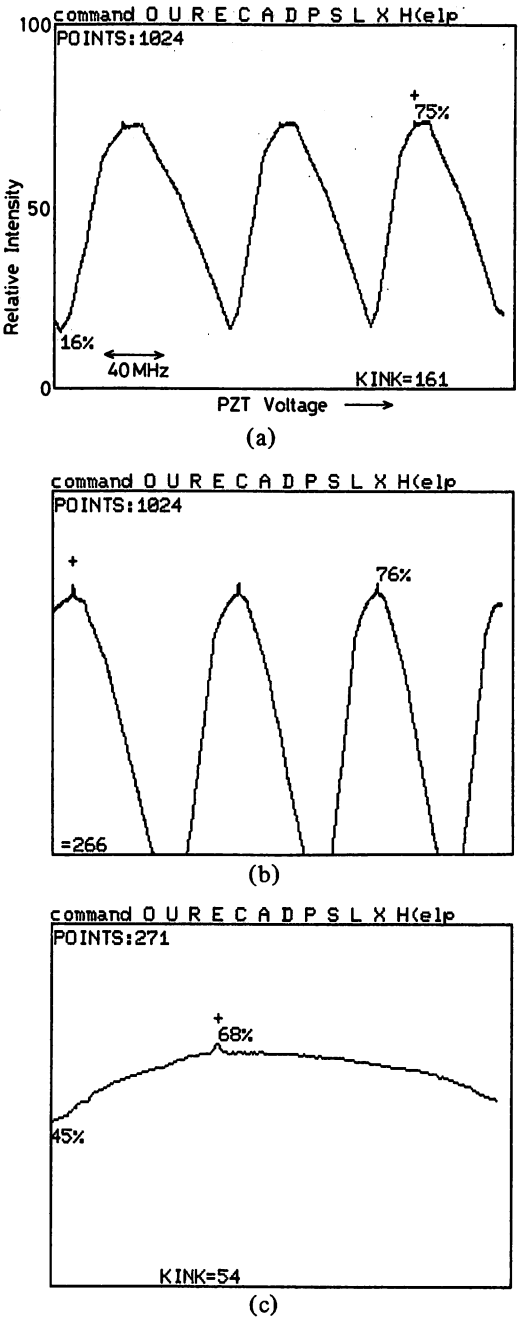

Fig. 3 Examples of display on CRT (a) before, (b) after alignment and (c) eight times expanded of (b), using the equipment. Alphabetic characters indicated upper are lists of commands for several data acquisition and processing.

3. Summary

The authors have developed a microcomputer aided alignment equipment for the prupose of

speeding up of optical alignment process of a laser apparatus. Performances of this equipment are as follows;

i) The tuning curve of a laser is swept and the distinction and smoothness of the curve are evaluated numerically.

ii) The detail of the inverted Lamb dip can be observed continuously by magnifying sweep function.

iii) Control of frequency sweep and observation of tuning curves are possible at the place of optical elements to be adjusted.

Applying this equipment to the optical alignment process of the laser, conventional required time of over one day is reduced to one hour because time for manual operation of X-Y recorder and for evaluation of tuning curves are eliminated. Since such procedure as mentioned above includes common optical alignment processes, this equipment may be applicable to various kinds of laser apparatus especially to complex structured and large-sized laser systems.

Reference

1) I. Siio, M. Ohtsu and T. Tako: Jpn. J. Appl. Phys., 21, 813 (1982).

Precise measurements and computer simulations of mode-hopping phenomena in semiconductor lasers

M. Ohtsu and Y. Otsuka
International Cooperation Center for Science and Technology, Tokyo Institute of Technology, 2-12-1 O-okayama, Meguro-ku, Tokyo 152, Japan

Y. Teramachi
Graduate School at Nagatsuta, Tokyo Institute of Technology, 4259 Nagatsuta, Midori-ku, Yokohama, Kanagawa 227, Japan

(Received 23 July 1984; accepted for publication 22 October 1984)

We precisely measured temporal intensity variations of each longitudinal mode of a two-mode 1.5-μm InGaAsP laser. The intensities of these modes showed clear hopping between each other. It became clear for the first time that their power spectral densities represented typical Lorentzian with a cut-off frequency between 0.7 and 1.9 MHz. This means that mode hopping follows the stochastics of a Poisson process, i.e., it occurs completely at random in time. The results of analog computer simulation, using a detailed theoretical model, supported the experimental results. It is concluded that spontaneous emission acts as a trigger to this hopping.

Performances of semiconductor lasers have been remarkably improved so that they can be used for a variety of optical applications. For example, in the case when they are used for video disc system, their intensity fluctuations should be reduced to a low level. However, it has been empirically found that high level fluctuations are induced in the low Fourier frequency range when the laser is operated with multilongitudinal modes.[1,2] Systematic studies on quantitative measurements and precise analysis of these fluctuations have not yet been performed. In this letter, first successful results of quantitative and precise measurements of these fluctuations and results of theoretical analysis on the origin of the fluctuations are demonstrated.

An InGaAsP laser (plano-convex-waveguide type)[3] of 1.5-μm wavelength was employed for the experiments. The laser was installed in a small vacuum chamber and the temperature fluctuations of the heat sink for the laser were reduced as low as 1×10^{-5}–3×10^{-4} K. The laser was driven by a low noise dc current source with a current fluctuation of 0.6 nA/$\sqrt{\text{Hz}}$. By realizing such extremely stable conditions of temperature and injection current, reproducible experimental results could be obtained, i.e., the effects of temperature and current fluctuations on the laser intensity could be neglected in the present measurements.

Hatched areas in Fig. 1(a) give the regions of the injection current I and heat sink temperature T, where the laser showed a single longitudinal mode oscillation, which was measured by a conventional grating monochromator. Here, the single longitudinal mode oscillation was defined to be the situation in which the intensities of the satellite longitudinal modes were less than 5% of that of the main longitudinal mode. In the dotted area of this figure, the laser oscillated with two longitudinal modes, the intensities of which differed less than 10%. Out of these areas, the laser showed multilongitudinal mode oscillation. In the present experiments the intensity fluctuations under these two-mode oscillation, which is the simplest case of multimode oscillation, were precisely measured to investigate the characteristics of intensity fluctuations of each mode. Figure 1(b) gives the intensities of two longitudinal modes at the position (A) in the dotted area of Fig. 1(a), where $T = 291$ K and $I = 90$ mA. From this figure, it could be concluded that these two modes oscillate simultaneously with almost equal intensity. To investigate the temporal variations of these intensities, measurements were carried out. Laser beams of two modes were spatially separated by a grating and were simultaneously detected by two germanium avalanche photodiodes. The output signals from the photodiodes were recorded by a two-channel digital memory. The bandwidth of the detection system was 50 MHz. Figure 2(a) gives the temporal variations of the laser intensities of both modes. It can be observed clearly that the two modes do not oscillate simultaneously but show switching phenomena, which can be called as mode hopping. Furthermore, it is seen for both modes that the mean duration time of the hopping phenomenon is about 1 μs. Figure 2(b) gives the power spectral densities of the laser intensity fluctuations of both modes measured by a spectrum analyzer. These curves show typical Lorentzians with a cut-off frequency f_c of 1.4 MHz, which means that the mode hopping

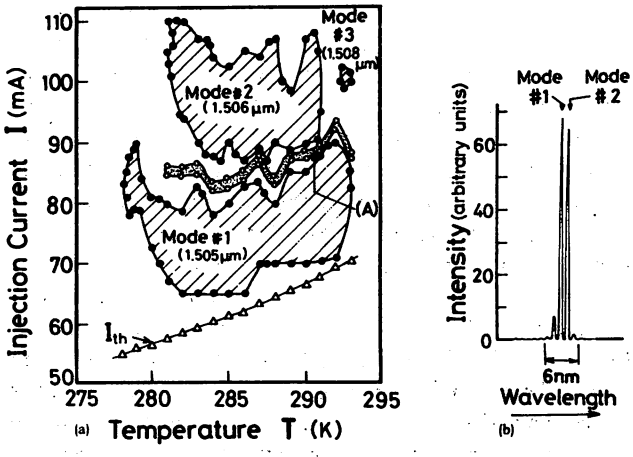

FIG. 1. (a) Regions of the injection current and temperature of the heat sink of the laser, where single longitudinal mode oscillation was observed (hatched areas). #1, #2, and #3 represent a series of longitudinal mode numbers. In the dotted area, the laser oscillates with two longitudinal modes #1 and #2, whose intensities are almost equal. I_{th} represents the threshold current. (b) Intensities of longitudinal modes #1 and #2 measured at the position (A) of (a). A conventional grating monochromator was used for the measurement.

 0003-6951/85/020108-03$01.00

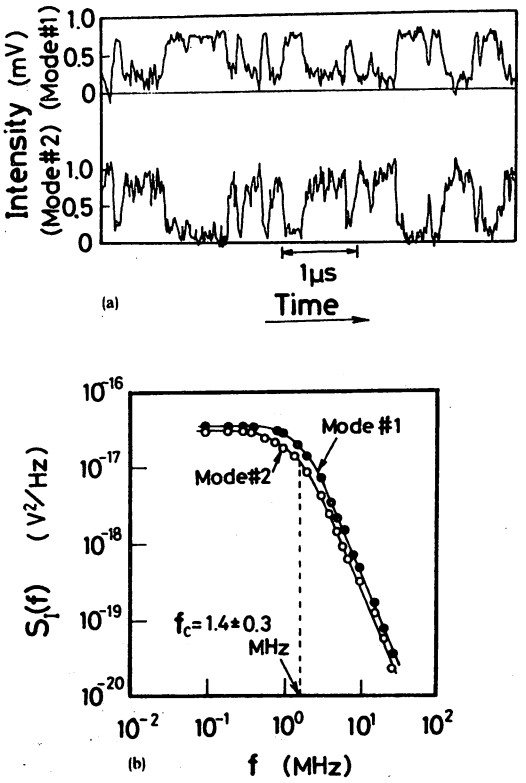

FIG. 2. (a) Temporal intensity variations of the two modes as mentioned in Fig. 1(a). (b) Power spectral densities $S_I(f)$ of intensity variations.

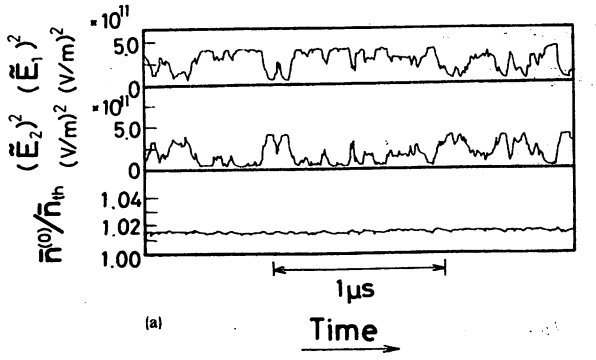

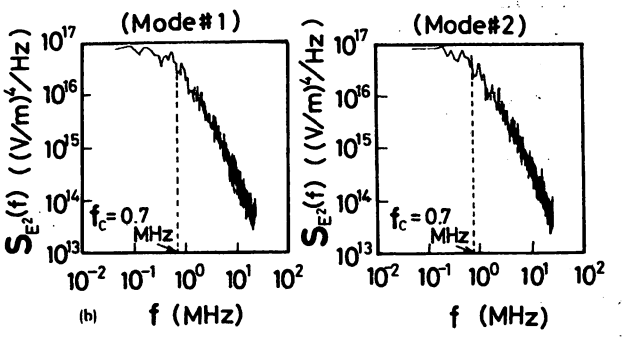

FIG. 3. (a) Output waveforms of $\tilde{E}_1^2$, $\tilde{E}_2^2$, and $\bar{n}^{(0)}$ as calculated by analog computer. (b) Power spectral density of $\tilde{E}_1^2$ and $\tilde{E}_2^2$.

follows the stochastics of a Poisson process,[4] i.e., mode hopping occurs completely at random in time. This also means that mode hopping is not determined by its past events. Furthermore, these curves also imply that the average duration time corresponds to $1/\pi f_c$.[5]

It has previously been reported that the relevant power spectral density $S(f)$ is proportional to f^{-m} $(1 \leqslant m \leqslant 2)$.[1,2] These results, different from the present one, can be due to insufficient temperature and current stabilities. In the present experiment, measurements were done at several points within the dotted area of Fig. 1(a), and reproducible Lorentzian line shapes of 0.7 MHz $\leqslant f_c \leqslant$ 1.9 MHz were obtained.

It is not probable that the origin of mode-hopping phenomenon we observed is the temperature or current fluctuations because the magnitudes of these fluctuations were so low that jumping between two hatched areas in Fig. 1(a) was not likely to occur. An analog computer simulation was carried out to investigate this origin. One of the most precise models of semiconductor laser oscillations, as it was proposed by Yamada and Suematsu,[6] was employed. This model is composed of two van der Pol equations for the amplitudes $E_i (i = 1,2)$ of the electric field of two modes derived from the density matrix formulation, and an equation for temporal variation of the active carrier density $\bar{n}^{(0)}$ in the laser diode. The equations can be expressed as follows:

$$\frac{d}{dt}\tilde{E}_i^2 = \frac{1}{n_I\sqrt{\epsilon_0\mu_0}} \times [\tilde{\alpha}_i^{(1)} - \alpha_{th} - \tilde{\alpha}_i^{(3)}\tilde{E}_i^2 - \tilde{\alpha}_{i(j)}^{(3)}\tilde{E}_j^2]\tilde{E}_i^2 \quad (i,j = 1,2;\ i \neq j) \tag{1}$$

$$\frac{d}{dt}\bar{n}^{(0)} = -n_I\left(\frac{\epsilon_0}{\mu_0}\right)^{1/2}\left(\frac{2}{\hbar\omega_1}\tilde{\alpha}_1^{(1)}\tilde{E}_1^2 + \frac{2}{\hbar\omega_2}\tilde{\alpha}_2^{(1)}\tilde{E}_2^2\right) - \frac{\bar{n}^{(0)}}{\tau_s} + \frac{I}{V_I e}, \tag{2}$$

where $\tilde{\alpha}_i^{(1)}$, $\tilde{\alpha}_i^{(3)}$, and $\tilde{\alpha}_{i(j)}^{(3)}$ represent a linear gain, self-saturation coefficient, and cross-saturation coefficient, respectively, and all of them are proportional to $\bar{n}^{(0)}$. For derivations of these equations and the meaning of other coefficients in these equations, we referred to Yamada and Suematsu.[6] A coupling constant C between the two modes can be given by[3,6]

$$C = \frac{\tilde{\alpha}_{1(2)}^{(3)}\tilde{\alpha}_{2(1)}^{(3)}}{\tilde{\alpha}_1^{(3)}\tilde{\alpha}_2^{(3)}} = \frac{16}{9}. \tag{3}$$

This result means that strong coupling exists between the two modes because $C > 1$. That is, only one of the two modes can oscillate at a given moment. However, if some triggering forces are applied to the laser, the oscillation of the other mode can be stimulated so as to suppress the initially oscillating mode.[7] This feature is qualitatively consistent with that of the experimental results of Fig. 2(a). Because we expected that spontaneous emission acts as triggering force, several analog computer simulations were carried out by adding the square of the amplitude $\tilde{E}_{Ni}$ $(i = 1,2)$ of the electric field of spontaneous emission to the right side of Eq. (1) and by using also Eq. (2). Two uncorrelated white noises, generated from two noise generators, were applied to the analog computer as the additional spontaneous emission terms $\tilde{E}_{Ni}$ of Eq. (1). The amplitudes of the output signals from the noise generators were adjusted so that the root mean square values of $\tilde{E}_{Ni}$ could be fixed at several percent of

those of $\tilde{E}_i$. These values are reported as appropriate for spontaneous emission.[8] Figure 3(a) gives the output waveforms of $\tilde{E}_1^2$, $\tilde{E}_2^2$, and $\bar{n}^{(0)}$ from the analog computer obtained when the noise terms were applied. In this figure, mode hopping is observed with a mean duration time of about 1 μs, as was experimentally found [see Fig. 2(a)]. Figure 3(b) shows the power spectral densities of the temporal variations of $\tilde{E}_i^2$ of Fig. 3(a). The curves also show typical Lorentzian with the cut-off frequency f_c of 0.7 MHz, which is consistent with the experimental results of Fig. 2(b). From these results, it was concluded for the first time that the temporal fluctuations of spontaneous emission acted as a triggering force for the mode hopping.

Since the temperature or current fluctuations induce fluctuations of the values of the third and fourth terms on the right side of Eq. (2), further analog computer simulations were carried out by adding a noise term to Eq. (2). In this case, the spontaneous emission term $\tilde{E}_{Ni}$ was removed. However, no mode hopping occurred. Through this simulation, it was also recognized that temperature or current fluctuations did not act as a triggering force for mode hopping.

In the present study, it has been clarified by precise experiments and detailed analog computer simulation that the main origin or mode hopping is spontaneous emission. It is also concluded that the mode-hopping phenomenon follows the stochastics of a Poisson process, i.e., that the shape of the power spectral density of intensity fluctuations was Lorentzian with a cut-off frequency of 0.7 MHz$\leqslant f_c \leqslant$1.9 MHz.

We wish to thank Professor Musha, Professor Suematsu, and Dr. Asada of our institute for their valuable discussions.

[1]A. Arimoto, M. Ojima, and K. Tatsuno, Kogaku **11**, 629 (1982) (in Japanese).
[2]Y. Yoshikuni, H. Kawaguchi, and T. Ikegami, Proceedings of Fourth International Conference on Integrated Optics and Optical Fiber communication, June 1983, Tokyo, 29D3-12.
[3]Y. Noda, K. Sakai, and Y. Matsushima, Electron. Lett. **17**, 226 (1981).
[4]A. Papoulis, *Probability, Random Variables, and Stochastic Process*, 2nd ed. (McGraw–Hill, NY, 1984), p. 211.
[5]A. Papoulis, *Probability, Random Variables, and Stochastic Process*, 2nd ed. (McGraw–Hill, 1984), p. 270.
[6]M. Yamada and Y. Suematsu, J. Appl. Phys. **52**, 2653 (1981).
[7]W. E. Lamb, Jr., Phys. Rev. A **134**, 1429 (1964).
[8]Y. Suematsu, S. Akiba, and T. Hong, IEEE J. Quantum Electron. **QE-13**, 596 (1977).

 0003-6951/85/020110-03$01.00

レーザーオリジナル

1.5μmInGaAsPレーザーのモードホッピング現象の解析

大津元一*・大塚祥広*・大崎昭雄**・寺町康昌***

(1985年2月27日 受理)

Analysis of Mode Hopping Phenomenon in a 1.5μm InGaAs Laser

Motoichi OHTSU*, Yoshihiro OTSUKA*, Akio OSAKI**
and Yasuaki TERAMACHI***

(Received February 27, 1985)

Experiments and analog computer simulations were carried out to analyze the characteristics of mode hopping phenomenon in a 1.5 μm InGaAsP laser when it oscillated with two longitudinal modes. It becomes clear for the first time that intensity fluctuation of the spontaneous emission acts as a trigger to the mode hopping, and that this hopping follows the stochastics of a Poisson process. Furthermore, it was found that highly biased operation is effective to reduce the frequency of the mode hopping.

1. まえがき

半導体レーザーは光通信のみでなくビデオディスクなど各種光応用機器にも多く用いられるようになってきている。このレーザーはたてモードに関して多モード発振時，低いフーリエ周波数領域で光強度の大きなゆらぎを示すことが知られており，応用上の問題となっている[1,2]。しかしこのゆらぎについての十分な定量的測定はない。いくつかの報告では戻り光の影響も同時に存在する場合[3]，レーザーが変調されている場合[4]など，現象が複合された状態で測定されているので特性把握が困難になっている。さらにこのゆらぎの発生機構についての高精度な理論もない。これに対し著者らはこのゆらぎの発生機構の解明と，その抑圧のために精密測定と計算とを行ない，その途中経過をすでに報告してきた[5,6]。本論文ではこれらの結果を含めてその後得られた結果についてまとめて述べる。

* 東京工業大学理工学国際交流センター（〒152 東京都目黒区大岡山2—12—1）
** 株式会社日立製作所生産技術研究所（〒244 横浜市吉田町292）
*** 東京工業大学総合理工学研究科（〒227 横浜市緑区長津田4259）
* International Cooperation Center for Science and Technology, Tokyo, Institute of Technology (2-12-1, O-okayama, Meguro, Tokyo, 152)
** Production Engineering Research Laboratory, Hitachi, Ltd., (292, Yoshida-cho, Totsuka, Yokohama 244)
*** Graduate School at Nagatsuta, Tokyo Institute of Technology (4259, Nagatsuta, Midori, Yokohama 227)

2．実験装置

実験には波長1.5μm の InGaAsP レーザーを使用した。導波路構造はBL-PCW型(Buffer Layer Loaded Plano-Convex Waveguide)である[7]。発振するたてモードの光強度はヒートシンク温度，流入電流のゆらぎにより著しく変動するので定量的測定のためにはこれを抑圧する必要がある。そこで二重構造のクライオスタットを製作し，内箱の中を温度ゆらぎ0.01K以内に安定化したメチルアルコールを流した。外箱中は真空（0.01 Torr）にし，内箱の外壁にペルチェ素子とヒートシンク用の銅板をとりつけた。サーミスタブリッジで銅板の温度ゆらぎを検出し，ペルチェ素子に流す電流を制御してその温度を安定化した。このような二段階温度制御により銅板の温度ゆらぎを1×10^{-5}～3×10^{-4}Kに抑圧できた。この銅板にレーザーを固定した。一方，レーザー駆動用の定電流源は出力電流ゆらぎ0.6nA/$\sqrt{\text{Hz}}$のものを開発して用いた[8]。これらの温度ゆらぎ，電流ゆらぎは今日の電子回路技術で達成できる限界値に近い値まで抑圧されており[8]，これによって以下に示す再現性のよい測定結果が得られた。

温度，電流の値を掃引して回折格子分光器で発振スペクトル特性を測定し，多モード動作の最も単純な場合，すなわち二つのたてモードで発振する状況を見い出した。そこに温度，電流値を固定して両モードの光強度のゆらぎを測定した。測定装置全体をFig.1 に示す。両モードの光は回折格子で空間的に分離し，それぞれGeのアバランシェフォトダイオード（APD）で受光してその出力信号をディジタルメモリーに記録した。測定の周波数帯域はディジタルメモリーによって制限され，50MHzであった。

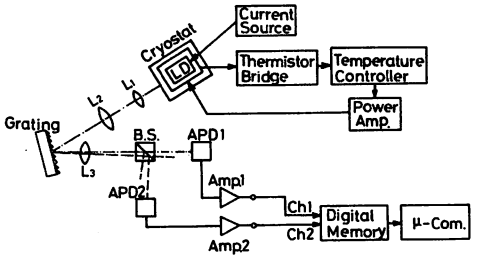

Fig.1 Experimental apparatus.

3．実験結果と考察

Fig.2 (a) には温度，電流の値を掃引しながら回折格子分光器で測定した発振スペクトル特性を示す。図中斜線で示した領域では単一たてモード発振を示した。ここでは単一たてモード発振の定義として，他のたてモードの発振光強

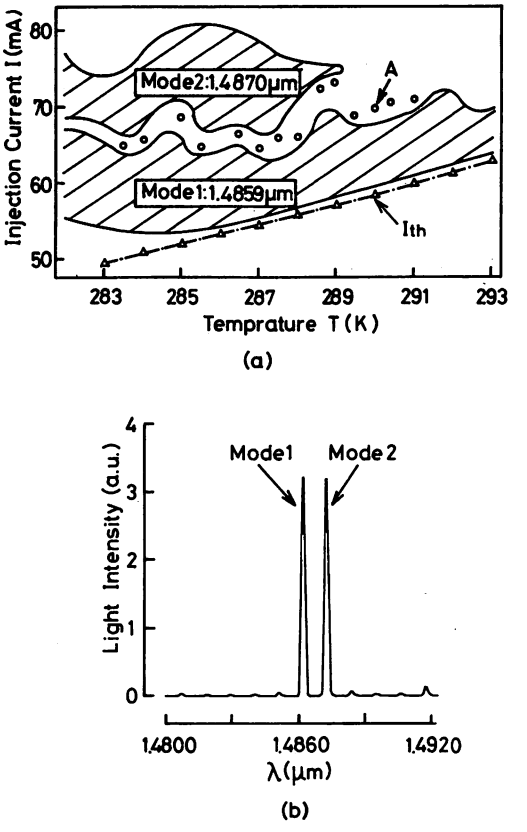

Fig.2 (a) Regions of the injection current and temperature of the heat sink of the laser, where single longitudinal mode oscillation was observed (hatched areas). At the positions given by the white circles, the laser ocsillated with two longitudinal modes whose intensities were almost equal. I_{th} represents the threshold current. b) Intensities of two longitudinal modes measured at the position A of (a).

度が注目しているたてモードのそれの5％以内の状態，とした。これら二つの領域の間では二つのたてモードで発振する状態が見出せた。そこで図中白丸で示す各動作点に温度と電流値とを固定し，両モードの光強度ゆらぎを測定した。これらの動作点ではFig.2（b）に示すように二つのモードの光強度の差が10％以内であるような状態，すなわち二つのモードが同等に発振している状態がほぼ実現できた。これらの動作点からはずれ，斜線の領域の境界線に近い点では

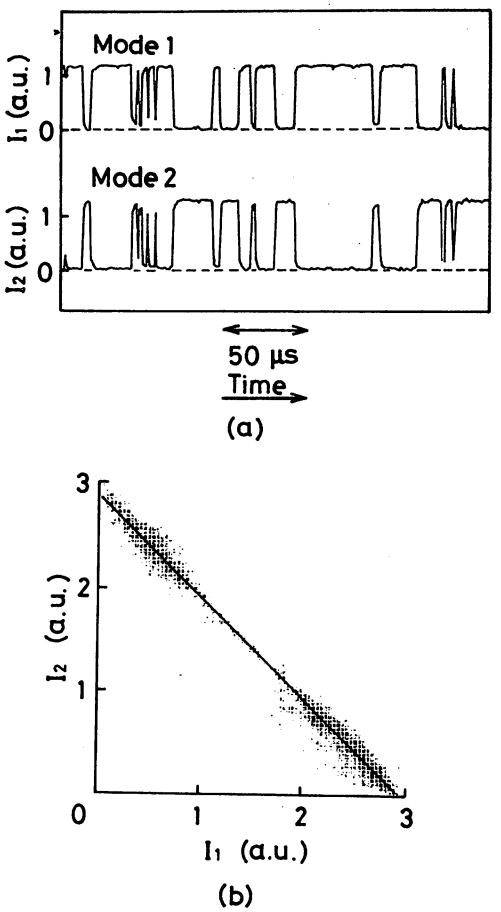

Fig.3 (a) Temporal intensity fluctuations of the two modes. (b) Distributions of the intensities of both modes at every moment of the sampling time. Solid line represents the one which was least-square fitted to the data.

両モードの光強度差は大きく，一方，二つの斜線領域からはなれた点では三モード以上で多モード発振が見られたので，それらの動作点での測定は避けた。なお，Fig.2（a）中の一点鎖線はしきい値電流を示す。

Fig.3（a）は二つのモードの光強度のゆらぎの測定結果を示す。各モードは互いに発振と非発振とをくりかえし，いわゆるスイッチングが見られる。これがモードホッピングと呼ばれる現象である。これらの光強度の時間積分値を測定したものがFig.2（b）であるといえる。一般にはFig.2（b）と異なり両モードの光強度には差がある場合が多い。すなわちFig.3（a）の矩形波状の信号の高さが異なり，デュティ比も50％でない場合が多い。このような状態で全モードの光強度を測定する時間的に大きくゆらいでいるのが観測される。これが1.で述べたように各種光応用機器の性能を制限する要因となり，モードホッピング雑音として知られているものである[1,2]，さて，Fig.3（b）は両モードの光強度の値の散布図である。すなわちこれらの光強度の値をたて軸，横軸にとり，Fig.3（a）において50nsごとにこれらの値をサンプリングして図示したものである。この図より両モードの光強度の間には強い負の相関があることが認められる。図示されたそれぞれの値をもとに定義式[9]

$$R=\sigma_{12}/\sqrt{\sigma_1\cdot\sigma_2} \qquad (1)$$

（σ_1，σ_2は各モードの光強度ゆらぎの自己分散の値，σ_{12}は両者の共分散の値）にしたがって相互相関係数Rを求めると−0.995であり，強い負の相関の存在，すなわち両モードの光強度の間でのスイッチングが確認された。

Fig.4（a）（b）には両モードの光強度ゆらぎのパワースペクトル密度$S(f)$を示す。両者とも遮断周波数f_cをもつ高域遮断特性を示している。ここではf_c=330kHzである。さらに，$f<f_c$では$S(f)\propto f^0$，$f\geqq f_c$では$S(f)\propto f^{-2}$であること，すなわち$S(f)$はローレンツ型の曲線であることが認められる。これはモードホッピングの事象が過去の経歴によらず，時間的にランダムに発

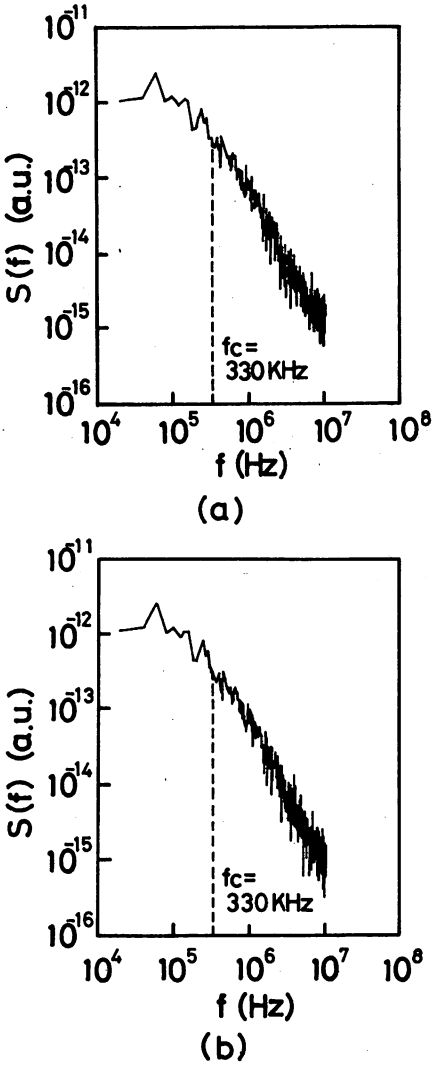

Fig. 4 Power spectral densities of intensity fluctuations of the mode 1(a) and 2(b).

生すること，すなわちポアッソン過程であることを意味している[10]。さらに，ホッピング発生の平均周期は$1/\pi f_c$に対応する[10]。従来，$S(f) \propto f^{-m}$ $(1 \leqq m \leqq 2)$ であるという報告例もあるが[2]，それらは測定の精度不足によるものと思われる。

さて，このようなモードホッピングの発生原因については温度，電流のゆらぎによるものであるとは考えにくい。これらのゆらぎの量は2.で示したように十分抑圧されており，Fig. 2 (a) 中の二つの単一たてモード発振領域の境界間隔にくらべずっと小さい値になっているからである。事象がポアッソン過程であることから，時間的にランダムなゆらぎが両モードに対して互いに無相関で混入することが原因であると考える方が，より妥当である。このようなゆらぎとして可能性の最も大きいものは自然放出光である。

このように，もし自然放出光強度のゆらぎが発生原因であるならばバイアスレベル（すなわち注入電流Iとそのしきい値I_{th}との比I/I_{th}）の増加とともにホッピングの頻度を表わすf_cは小さくなるはずである。つまり$I/I_{th} > 1$のとき，よく知られているように伝導帯中の電子数，すなわちキャリヤ数，はしきい値における値に固定され，自然放出光強度はI/I_{th}によらず一定となる。これに対しレーザーの光強度はI/I_{th} に比例して増加するのでレーザー発振特性に影響を与える自然放出光強度のゆらぎの寄与の割合はI/I_{th}の増加とともに小さくなっていくからである。このことを確認するためにFig. 2 (a) の白丸で示す各点に電流，温度を設定してI/I_{th}とf_cとの関係を測定した、その結果をFig. 5に示す。f_cはI/I_{th}の増加とともに減少しており，上記の考

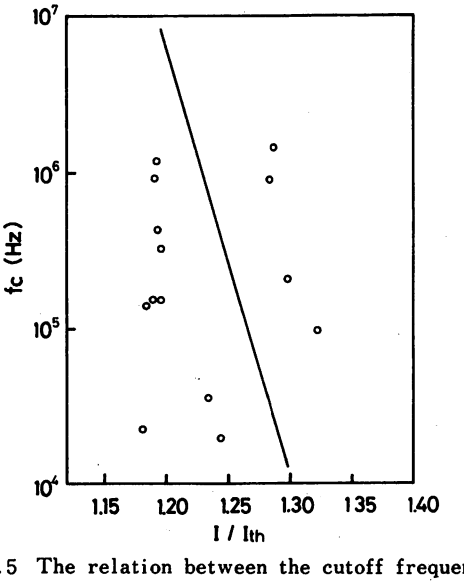

Fig. 5 The relation between the cutoff frequency of the power spectral density f_c and the injection current I normalized to its threshold value I_{th}.

察の結果と一致している。測定値がややばらついているのは，実際には今考えている二つのたてモード以外のたてモードもわずかに発振しており，その光強度がこれらのモードの10%程度になる場合もあったこと，Fig. 3 (a) に示す波形のデュティ比が50%からややずれた場所もあったこと，などによると考えられる。この図に見られるようにf_cはI/I_{th}の増加とともに指数関数的に減少しており，このことは従来報告されていたホッピングの頻度の測定値にばらつきが多かったことの理由の一つと考えることができる[1,2]。さらに，この測定結果より，ホッピング頻度を抑圧するには高バイアスレベルで動作させるのがよいことがわかる。先の報告では[5,6]今回使用したレーザー素子とは製品番号の異なるものを用いたが，その値f_c=1.4MHz (I/I_{th}=1.33において) もFig. 5の結果とほぼ合っている。

最後に自然放出光強度のゆらぎが時間的にランダムであり，かつレーザー発振している二つのたてモードに混入してくる自然放出光成分の強度ゆらぎは互いに無相関であることを確認するための実験を行なった。これについては著者らの知る限り従来報告されていないので，本節の考察の有効性を確認するためにはここで実測する必要がある。そのためには本研究に使用したレーザーをしきい値以下で動作させ，その自然放出光強度のゆらぎを測定すればよいが実際にはそのような動作状態では光強度不足のため測定不可能であった。そこでその代りに波長0.73μmの高輝度AlGaAs発光ダイオードを用いた。これは材質，活性層の構造，波長，光強度などに関し使用したレーザーとは異なるが自然放出光強度のゆらぎの統計的性質には著しい差は見られないと推測される。実験装置はFig. 1とほぼ同様である。ここではFig. 6 (a) に示すように自然放出光のスペクトル曲線の中で約0.3nmはなれた二つのたてモードに対応する波長値において幅0.1nmの中に入る自然放出光強度のゆらぎを同時測定し，これをレーザーの二つのたてモードに混入する自然放出強度のゆらぎと見なした。そのためにFig. 1の回折格子の代りに二台の同型の回折格子分光器を用い，Fig. 6 (a) にあるように波長値，波長幅を設定して光強度のゆらぎを同時測定した。光検出器としてはSiのAPDを用い，その出力はディジタルメモリに記録した。Fig. 6 (b) に二つのたてモードに混入する自然放出光成分の強度ゆらぎの実時間波形を示す。次にこれらの強度の分布をFig. 7に示す。両方の成分についてほぼ同じ分布が得られたので一方に対する結果のみを示した。これはFig. 6 (b) の波形を10nsごとにサンプリングした値の度数分布を図示したもので，ほぼガウス分布と考えられる。Fig. 8にはこれらのゆらぎのパワースペクトル密度を示す。ここでも両方の成分についての結果はほぼ同じなので一方に対する結果のみを示した。測定可能な周波数帯域50MHz以内で白色雑音になって

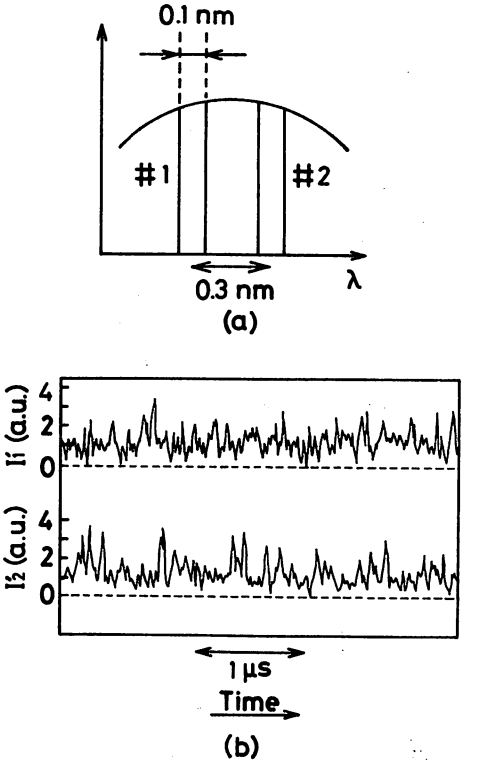

Fig. 6　(a) Schematic explanations of the two wavelength components of the spontaneous emission from 0.73 μm AlGaAs light emitting diode (LED).

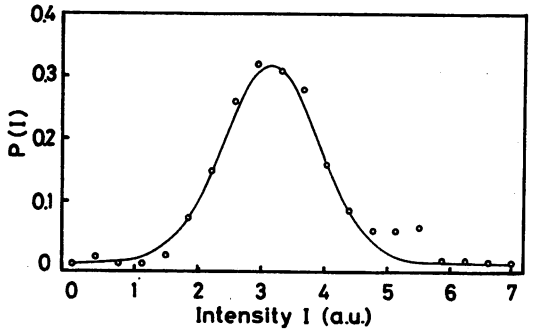

Fig.7 Distribution of the intensity fluctuations of the LED output shown in Fig.6 (b). The solid curve represents the least-square fitted Gaussian.

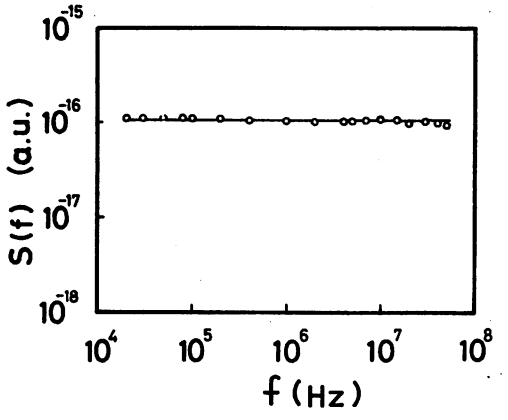

Fig.8 Power spectral density of the intensity fluctuations in Fig.6 (b).

いることがわかる。この50MHzという値はFig. 5からもわかるように測定されたf_cの値より十分大きいので，モードホッピングに寄与する自然放出光の強度ゆらぎは白色雑音であるとみなすことができる。次に，二つの自然放出光成分の強度ゆらぎの間の相関の度合いを見るためにFig.3 (b) と同様の散布図を求めたものをFig. 9に示す。この図中の各測定点はランダムに分布しており相関は認められない。(1)式に従って相互相関係数Rを求めると0.056であり非常に小さい値であった。これらより両者は互いに無相関であることがわかる。以上により自然放出光強度のゆらぎはガウス分布を有する白色雑音であり，レーザーの二つのたてモードに混入するそれぞれの自然放出光成分の強度ゆらぎの間

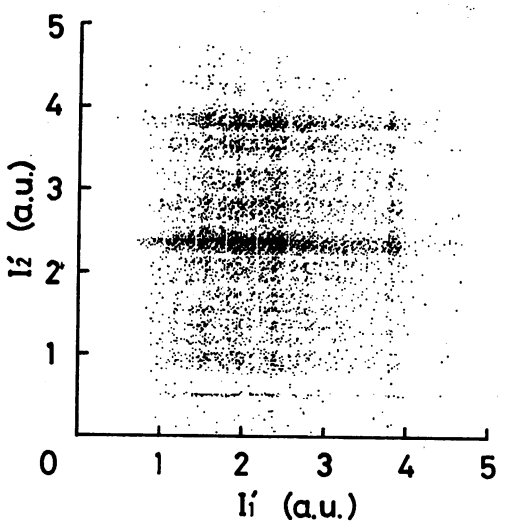

Fig.9 Distributions of the intensities of both components of Fig.6 (b) at every moment of the sampling time.

には相関がないことが確認された

4．アナログ計算機シミュレーション

モードホッピングが自然放出光強度のゆらぎに起因するポアッソン過程であることを確認するためにシミュレーションを行なった。基礎式として用いたものは下記のように二つのモードの光の電場振幅$\widetilde{E}_i$ ($i=1,2$) についてのvan der Pol方程式とキャリヤ密度$\overline{n}^{(0)}$の時間変化を表わす式である[11]。

$$\frac{d}{dt}\widetilde{E}_i^2=\frac{1}{n_i\sqrt{\varepsilon_0\mu_0}}\{\widetilde{\alpha}_i^{(1)}-\alpha_{th}-\widetilde{\alpha}_i^{(3)}\widetilde{E}_i^2 - \widetilde{\alpha}_{i(j)}^{(3)}\widetilde{E}_j^2\}\widetilde{E}_i^2 \quad (i,j=1,2,\ i\neq j) \tag{2}$$

$$\frac{d}{dt}\overline{n}^{(0)}=-n_i\sqrt{\frac{\varepsilon_0}{\mu_0}}\left(\frac{2}{h\nu_1}\widetilde{\alpha}_1^{(1)}\widetilde{E}_1^2+\frac{2}{h\nu_2}\widetilde{\alpha}_2^{(1)}\widetilde{E}_2^2\right) - \frac{\overline{n}^{(0)}}{\tau_s}+\frac{I}{V_i e} \tag{3}$$

両式に表われる記号の意味は次のとおりである。n_i：活性層の屈折率，ε_0：真空誘電率，μ_0：真空透磁率，$\widetilde{\alpha}^{(1)}$：線形利得，α_{th}：共振器損失，$\widetilde{\alpha}_i^{(3)}$：自己飽和係数，$\widetilde{\alpha}_{i(j)}^{(3)}$：相互飽和係数，$h$：プランク定数，$\nu_i$：$i$番目のたてモード周波数，$\tau_s$：自然放出寿命，$I$：注入電流，$V_i$：活

性層体積，e：電荷素量。

(2)式中の各係数$\widetilde{\alpha}_i^{(1)}$，$\widetilde{\alpha}_i^{(3)}$，$\widetilde{\alpha}_{i(j)}^{(3)}$は密度行列の手法を用いて求めたもので半導体レーザーの構造定数と直接対応がつき，定量的な議論には適している。各係数の詳細は原論文[11]にゆずるが，これらはキャリ密度$\bar{n}^{(0)}$に依存しており，$\bar{n}^{(0)}$は(2)式のように時間とともに変化するので(2)式中の各係数は定数でない。これが気体レーザーなどの場合と異なる点である。ここで，まず近似的にこれらを定数とみなして両モード間の結合のつよさを表わす結合定数Cを求めると[12]

$$C=\frac{\widetilde{\alpha}_{1(2)}^{(3)}\ \widetilde{\alpha}_{2(1)}^{(3)}}{\widetilde{\alpha}_1^{(3)}\ \widetilde{\alpha}_2^{(3)}}=\frac{16}{9} \tag{4}$$

となり，$C>1$であって両モードは互いに強結合の状態にあることがわかる。すなわち定常状態では一方のたてモードのみが発振し，何らかの駆動力により発振するたてモードが入れかわること，すなわちスイッチングが起こることを意味し，モードホッピングが生じることが定性的に裏づけられる。そこで，より定量的に議論するために以後はこれらの係数を定数とは見なさず，かつ駆動力として3で与えた自然放出光強度のゆらぎを想定し，(2)式右辺の最終項にそのゆらぎを表わす項$\widetilde{E}_{Ni}^2$ $(i=1,2)$を付加して計算する。3の結果によるとこのゆらぎはガウス分布を有する白色雑音であり，かつ$\widetilde{E}_{N1}^2$と$\widetilde{E}_{N2}^2$とは互いに無相関である。すなわちその相関関数は

$$<\widetilde{E}_{Ni}^2(t)\cdot\widetilde{E}_{Nj}^2(t+\tau)>\propto\delta_{ij}\cdot\delta(\tau) \tag{5}$$

と書ける。ここで$<>$は無限時間平均，δ_{ij}はクロネッカーのデルタ，$\delta(\tau)$はデルタ関数を表わす。

以上(2)，(3)，(5)式を用いてシミュレーションを行なうとき，スペクトル推定の精度を上げるためには非常に長い時間にわたって演算実行をくりかえさなくてはならない。このような長い時系列発生には，丸め誤差が蓄積されないアナログ計算機を用いる方法が優れている。また，自然放出光強度ゆらぎを表わす二つのランダム雑音を発生する方法としても，熱雑音を源にしたアナログ的な雑音の発生法が相互無相関，広い周波数範囲にわたって白色であるようなゆらぎを得るのには有利である。すなわち(2)，(3)式で規定される自励発振系をアナログ計算機中の電子回路により構成し，(5)式に対応する不規則信号として雑音発生器からの信号をこの系に付加する。この方針に従い，定常状態でのレーザー光電場の振幅の値の0.20%の平均振幅値をもちガウス分布を有する白色雑音を二台の独立な雑音発生器から発生させ，無相関で(2)式に加えた。この平均振幅値のみについては従来報告されている値をもとに設定した[13]。また$I/I_{th}=1.24$とした。得られた結果をFig. 10に示す。両モードの光強度は平均くりかえし周期約1μsでスイッチングを生じていること，すなわちモードホッピングが発生することが確認できた。さらに同図に示すようにキャリヤ密度の値$\bar{n}^{(0)}$は時間的にほとんど変化していないことがわかった。このことは二つのたてモードの光強度が定常状態においてほぼ等しいとき，各モードの光強度はモードホッピングによって変化していても全光強度はあまり変動しないので(3)式右辺の( )の中の値もほぼ一定となり，従って$\bar{n}^{(0)}$はほとんど変化しないと解釈できる。そうすると(2)式中の各係数$\widetilde{\alpha}_i^{(1)}$，$\widetilde{\alpha}_i^{(3)}$，$\widetilde{\alpha}_{i(j)}^{(3)}$はこの場合定数そみなせ，気体レーザーと同様の取り扱いができる。また(4)式で与えた結合定数Cも一定値と考えられ，そこで議論された内容も有効である

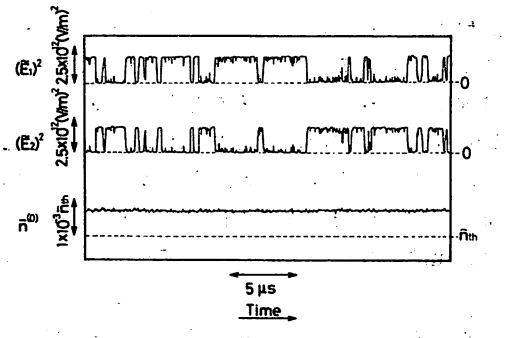

Fig. 10 Output waveforms of $\widetilde{E}_1^2$, $\widetilde{E}_2^2$, and $\bar{n}^{(0)}$, which were calculated by an analog computer. $\bar{n}_{th}$ represents the threshold carrier density.

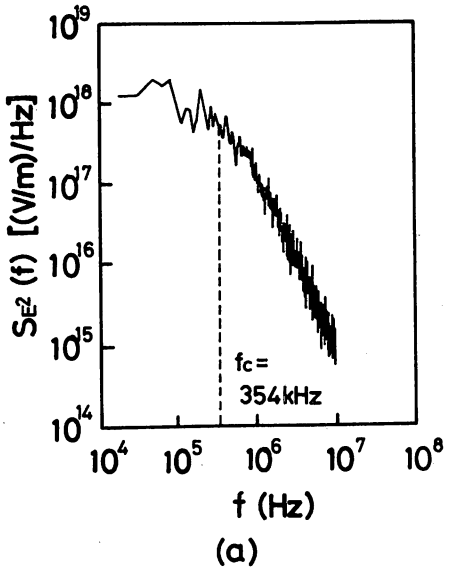

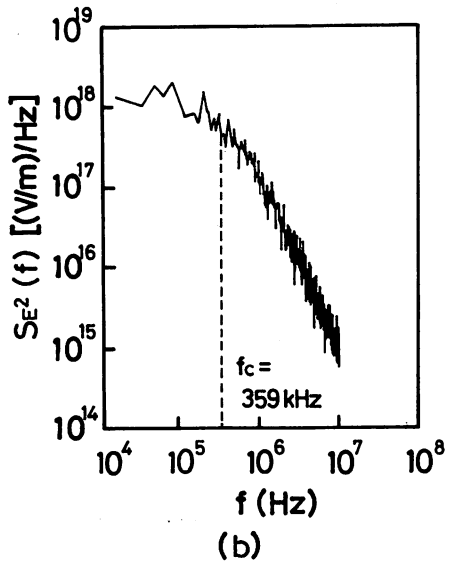

Fig.11 Power spectral densities of $\widetilde{E_1^2}$ (a) and $\widetilde{E_2^2}$ (b) of the results in Fig.10.

といえる。Fig.11には各モードの光強度のゆらぎに対応するパワースペクトル密度を示す。これは実験結果（Fig.4）と同様ローレンツ型となり，モードホッピングの事象がポアッソン過程であることが再確認された。その遮断周波数 f_c と I/I_{th} との関係をFig.12に示すが，これも実験結果（Fig.5）と同様 I/I_{th} の増加とともに f_c は減少することを示している。以上よりモードホッピングは自然放出光強度のゆらぎが発生

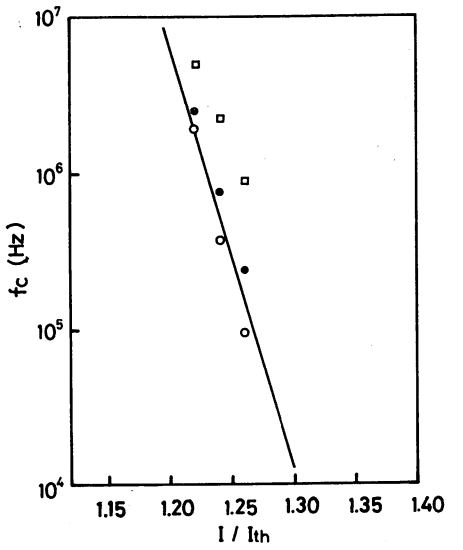

Fig.12 The relation between f_c and I/I_{th} estimated by analog computer simulation. The ratios of the amplitude between the fluctuation the spontaneous emission and the laser light were 0.46 % (□), 0.40 % (●), and 0.18 % (○), respectively. The solid line represents the one which was fitted to the exprimental results shown in Fig.5.

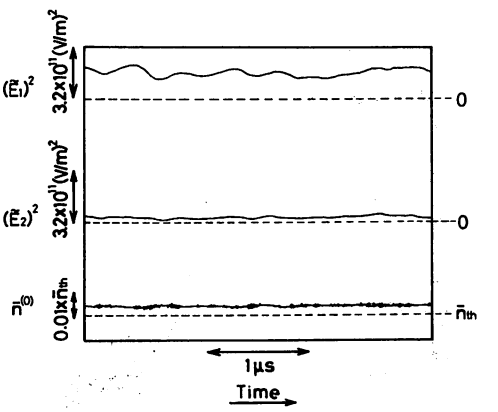

Fig.13 Output waveforms of $\widetilde{E_1^2}$, $\widetilde{E_2^2}$, and $\bar{n}^{(0)}$, which were calculated by an analog computer. Here, only the injection current fluctuations were added to the system.

原因となっていることが確認された。

以上の議論をさらに裏づけるために，自然放出光強度のゆらぎ $\widetilde{E_{N1}^2}$, $\widetilde{E_{N2}^2}$ は(2)式に付加せず，

(3)式右辺の電流のみにゆらぎ項δIを加えてシミュレーションを行なった。δIとして雑音発生器より白色雑音，平均振幅値$\delta I/I_{th}=0.030$に対応する雑音を発生させて用いた。ここでは$I/I_{th}=1.20$と設定した。その結果をFig. 13に示す。この図はモードホッピングが発生せず，二つのモードは互いに異なるパワーで同時発振していることを示している。これは(2)，(3)式からもわかるように電流のゆらぎが$\bar{n}^{(0)}$のゆらぎを通じて二つのモードの発振に使われる利得$\tilde{\alpha}_1^{(1)}$，$\tilde{\alpha}_2^{(1)}$を同時に変化させていることに起因する。利得の変化を通じてモードホッピングを生じるには両モードの利得の変化が少なくとも時間的に互いに逆相でなくてはならないが，電流のゆらぎはそのような逆相の変化を誘起しない。Fig. 14にこの場合の各モードの光強度のゆらぎを表わすパワースペクトル密度を示す。これはローレンツ型になっておらず，Figs. 13, 14より電流ゆらぎはモードホッピングの発生原因ではないことが確認できる。

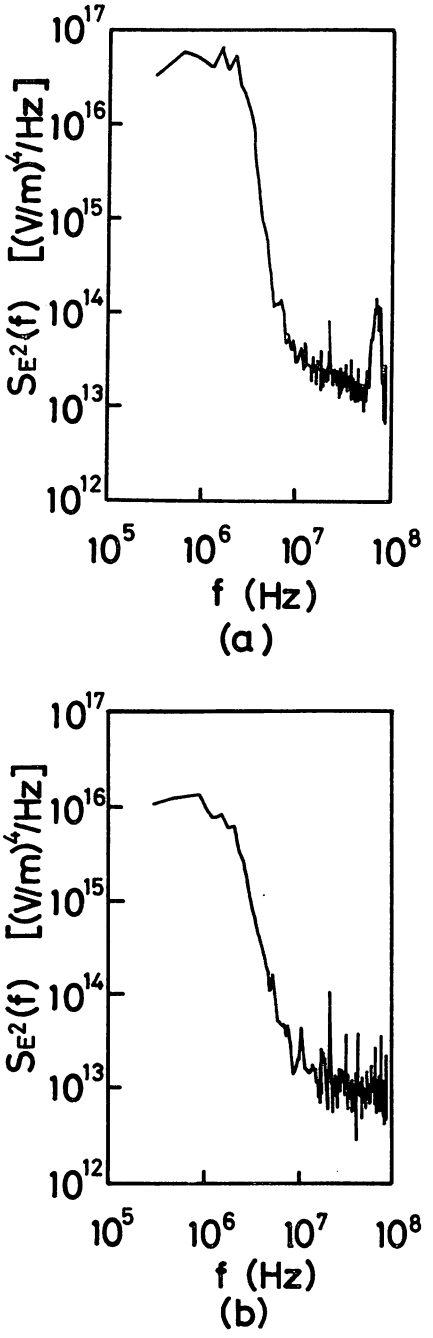

Fig. 14 Output waveforms of $\tilde{E}_1^2$ (a) and $\tilde{E}_2^2$ (b) of the results in Fig. 13.

以上のシミュレーションの結果により自然放出光強度のゆらぎがモードホッピングの発生原因であるということができる。そこで最後にこのような自然放出光強度ゆらぎの存在下での注入電流ゆらぎがモードホッピングの特性に与える影響を考察する。Fig. 10と同じ条件下で$\delta I/I_{th}=0.023$の電流ゆらぎを与えたときのシミュレーションの結果をFig. 15に示す。電流ゆらぎのためにFig. 10の場合にくらべ波形のゆらぎが大きくなっていることがわかる。この場合光強度ゆらぎのパワースペクトル密度の遮断周波数

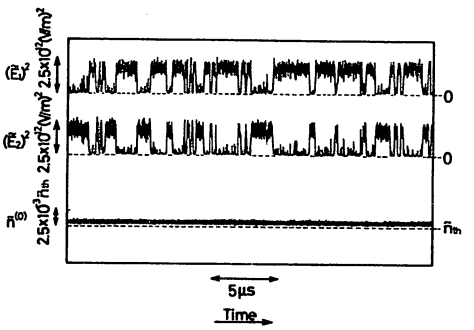

Fig. 15 Output waveforms of $\tilde{E}_1^2$, $\tilde{E}_2^2$, and $\bar{n}^{(0)}$, which were calculated by an analog computer. Here, the fluctuations of spontaneous emission and that of the injection current were simultaneously added to the system.

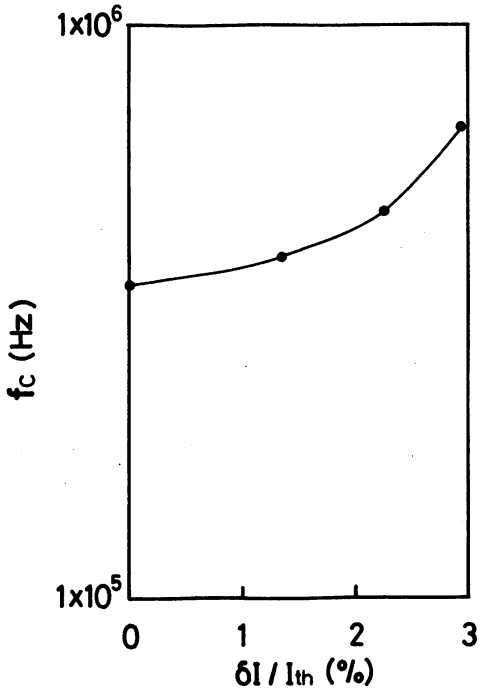

Fig. 16 The relation between the cutoff frequency f_c and the magnitude of the injection current fluctuations, which was calculated by an analog computer.

f_cと$\delta I/I_{th}$との関係をFig. 16に示す。電流ゆらぎによってモードホッピング頻度が助長されていることが確認される。

5. まとめ

波長1.5μm InGaAsPレーザーが二つのたてモードで発振している場合に生ずるモードホッピングについて解析するために実験とアナログ計算機シミュレーションを行なった。その結果，モードホッピングは自然放出光強度のゆらぎに起因するポアッソン過程であることが示された。また，ホッピング頻度はしきい値電流値で規格化された電流の値I/I_{th}の増加とともに減少することが明らかになった。このことからホッピングを抑圧するにはI/I_{th}の値を大きくすること，すなわち高バイアス動作が有効であることがわかった。

謝辞

御討論頂いたＫＤＤ研究所山本果也博士，秋葉重幸博士に感謝します。また御指導頂く本学武者利光教授，末松安晴教授，御討論頂いた本学浅田雅洋博士に感謝します。

参 考 文 献

1) A. Arimoto, M. Ojima and K. Tatsuno: Kogaku **11** (1982) 629 (in Japanese).
2) Y. Yoshikuni, H. Kawaguchi and T. Ikegami: Proceedings of Fourth International Conference on Integrated Optics and Optical Fiber Communication, June, 1983, Tokyo, 29D3-12.
3) J. W. M. Biesterbos, A. J. D. Boef, W. Linders and G. A. Acket: IEEE J. Quantum Electron. **QE-19** (1983) 986.
4) J. A. Copeland: J. Appl. Phys. **54** (1983) 2813.
5) Y. Teramachi, Y. Otsuka and M. Ohtsu: Proceedings of the 13th Congress of the International Commission for Optics, August, 1984, Sapporo, B4-2.
6) M. Ohtsu, Y. Otsuka and Y. Teramachi: Appl. Phys. Lett. **46** (1985) 108.
7) Y. Noda, K. Sakai and Y. Matsushima: Electron. Lett. **17** (1981) 226.
8) M. Ohtsu, H. Fukada, T. Tako and H. Tsuchida: Jpn. J. Appl. Phys. **22** (1983) 1157.
9) J. S. Bendat and A. G. Piersol: *RANDOM DATA: Analysis and Measurement Procedures* (John Wiley & Sons, New York, 1971) p. 124.
10) A. Papoulis: *Probability, Random Variables, and Stochastic Process, 2nd* ed. (McGraw-Hill, New York, 1984) p. 211.
11) M. Yamada and Y. Suematsu: J. Appl. Phys. **52** (1981) 2653.
12) M. Sargent III, M. O. Scully and W. E. Lamb, Jr.: *Laser Physics,* (Addison-Wesley, London, 1974) p. 123.
13) Y. Suematsu, S. Akiba and T. Hong: IEEE J. Quantum Electron. **QE-13** (1977) 596.

[B4-2]

PRECISE EXPERIMENTAL AND THEORETICAL APPROACH TO ANALYZE AND REDUCE MODE-HOPPING NOISE IN SEMICONDUCTOR LASERS FOR OPTICAL APPLICATIONS

Y. TERAMACHI, Y. OTSUKA* and M. OHTSU*

Graduate School at Nagatsuta, Tokyo Institute of Technology, 4259 Nagatsuta
**International Cooperation Center for Science and Technology, Tokyo Institute of Technology*
2-12-1, O-okayama, Meguro-ku, Tokyo 152, Japan

1. INTRODUCTION

It is essential to reduce mode-hopping in semiconductor lasers designed for applications in optical communication and video-disc systems. Several preliminary measurements have been performed[1]. However, precision measurements and theoretical works have not yet been carried out. In this presentation, the first successful results of a systematic study of this type of noise are demonstrated.

2. EXPERIMENTS

A 1.5 μm InGaAsP laser of Plano-Convex-Waveguide type was used for the experiments. To obtain quantitatively reproducible experimental results, the fluctuations in temperature and injection current were reduced to values as low as 1×10^{-4} K and 0.6 nA/$\sqrt{\text{Hz}}$, respectively. Figure 1 shows longitudinal mode spectra measured by a grating monochromator, from which one may believe the two modes oscillate simultaneously. However, by using the apparatus of Fig.2, the switching in oscillation between these modes was clearly observed, which means only one mode oscillates at every moment. This is the phenomenon of so-called the mode-hopping. The results are shown in Fig.3. It should be stressed here that this switching occurred even under such a very stable condition of temperature control and d.c. injection current, where no a.c. current modulations were applied. Power spectral densities S(f) of these waveforms are given in Fig.4. The shape of both curves in this figure clearly shows a Lorentzian with a cutoff frequency f_c of 1.4MHz, which means the mode-hopping occurs completely at random in time (Poisson process) with the average duration time of $1/f_c$. These clear Lorentzian shapes were quantitatively observed for the first time in the present measurements, while it has been reported previously as being proportional to f^{-m} $(1 \lesssim m \lesssim 2)$[1]

3. ANALOG-COMPUTER SIMULATIONS

Analog-computer simulations were carried out to investigate the origin of the mode-hopping. One of the most precise and practical models of semiconductor laser oscillations, as it was proposed by Yamada and Suematsu[2], was employed. This model is composed of two-mode van der Pol equations derived from the density matrix formulation, and an equation for temporal variation of the active carrier density. Figure 5 shows the simulated waveforms of the intensities of both modes, which clearly shows the mode-hopping as it was shown in Fig.3. Figure 6 gives their power spectral densities, which also show Lorentzian shapes as was observed in Fig.4. The curves of both figures are consistent with the experimental results mentioned in the previous section. These consistent simulated results were obtained only when white noises for both modes and of appropriate magnitude were added to the van der Pol equations[3]. These white noises correspond to the spontaneous emission. From these results, it can be concluded that the spontaneous emission plays a role as a trigger for the mode-hopping.

4. DISCUSSION

It can be said that the experimental and simulated results in the previous two sections agree well with each other, which means that the origin of the mode-hopping can be known in more details and practical design of hopping-free lasers can be done by using these results. For these purposes, the probability density functions, which are related to the potential curves of the stability of the modes, were derived from the simulated results, and presented in Fig.7. On the other hand, these potential curves can be also directly given by solving the Fokker-Planck equation which is derived from the van der Pol equations employed for the simulation. The comparison of the potential curves given by these two procedures can give further information about the origin of mode-hopping. Further details on this discussion will be presented at the session.

5. SUMMARY

The mode-hopping phenomenon was precisely measured and also simulated by an analog computer. The power spectral densities of the temporal intensity variation of both modes were found to be Lorentzians with a cutoff frequency of 1.4MHz. It was concluded that the spontaneous emission acts as a trigger to the hopping. The present results can be used for detailed investigation of the origin of mode-hopping and for the design of novel, hopping-free lasers.

ACKNOWLEDGEMENTS

The authors are much indebted to Profs. Suematsu. Musha. and Dr. Asada of their institute for valuable discussions.

REFERENCES

1) A. Arimoto, M. Ojima, and K. Tatsuno : Kogaku, 11 (1982) 629 (in Japanese)
2) M. Yamada and Y. Suematsu : J. Appl. Phys., 52 (1981) 2653
3) Y. Suematsu, S. Akiba and T. Hong : IEEE J. Quantum Electron., QE-13 (1977) 596

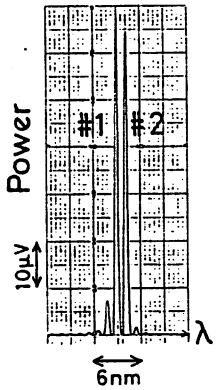

Fig. 1. Two longitudinal modes (18°C. 90mA).

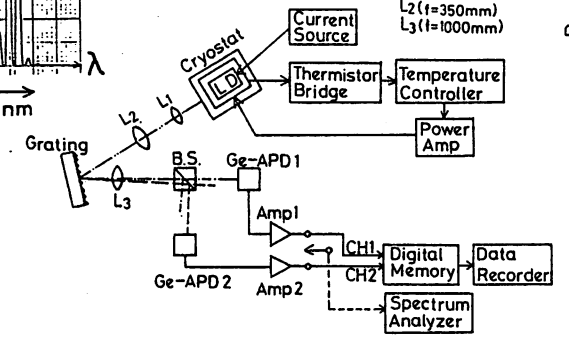

Fig. 2. Experimental apparatus.

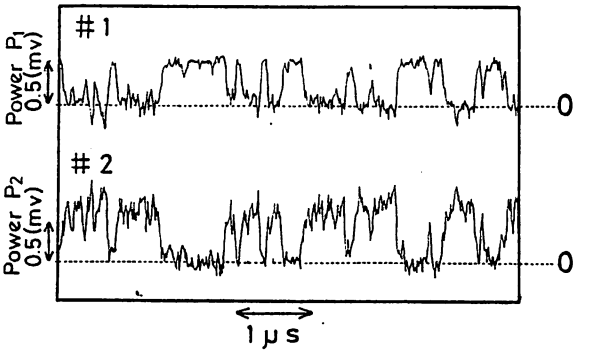

Fig. 3. Waveforms of the intensities of both modes.

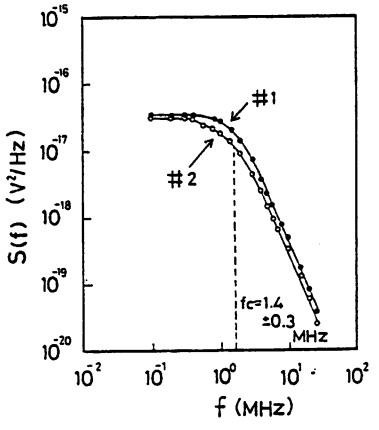

Fig. 4. Power spectral densities of intensity variations of both modes.

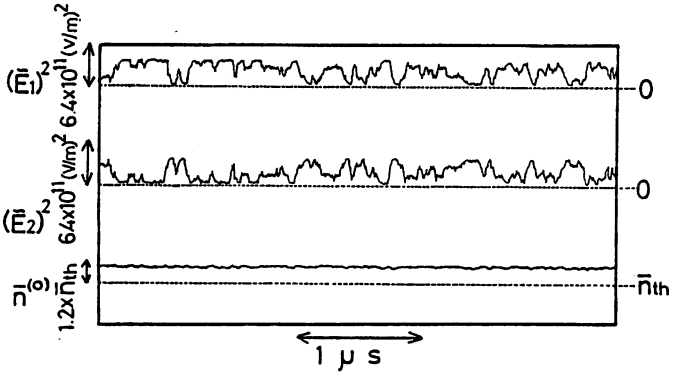

Fig. 5. Simulated waveforms of the intensities of both modes, and also the carrier density variations.

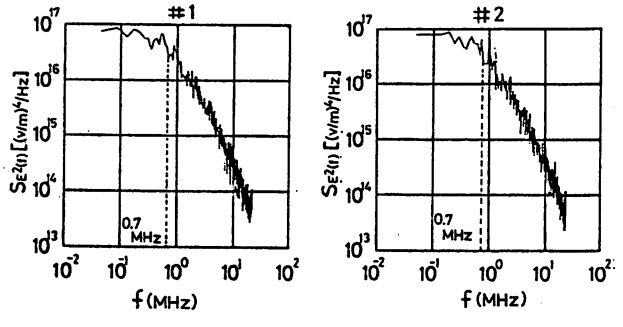

Fig. 6. Power spectral densities of simulated results of both modes.

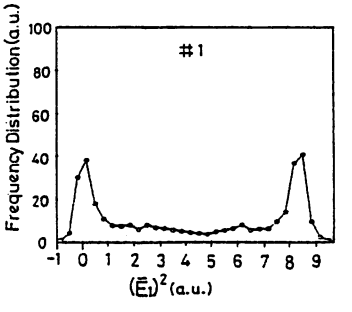

Fig. 7. Probability density functions of the mode 1, derived from the simulated result.

JAPANESE JOURNAL OF APPLIED PHYSICS
VOL. 22, NO. 10, OCTOBER, 1983 pp. 1553–1557

Spectral Measurements of NH_3 and H_2O for Pollutant Gas Monitoring by 1.5 μm InGaAsP/InP Lasers

Motoichi OHTSU, Hiroki KOTANI and Haruo TAGAWA

International Cooperation Center for Science and Technology, Tokyo Institute of Technology, 2-12-1, O-okayama, Meguro-ku, Tokyo 152

(Received April 25, 1983; accepted for publication July 23, 1983)

The absorption spectral lines of the combination tones of the vibration-rotation transitions in NH_3 and H_2O were measured with 1.5 μm InGaAsP/InP lasers for the purpose of pollutant gas monitoring. The numbers of observed NH_3 and H_2O lines were 21 and 1, respectively. The wavelengths of these lines were measured within the inaccuracy of 1.6 pm by a precise wavemeter. For these measurements, the laser wavelength was stabilized to NH_3 and H_2O lines. The resultant stabilities were $3.0 \times 10^{-10} \cdot \tau^{-1/2}$ and $1.1 \times 10^{-9} \cdot \tau^{-1/2}$, respectively, where τ represents the integration time. The sensitivity of NH_3 gas monitoring was measured as being 2.3×10^{-3} Torr · m. Furthermore, spectral measurements obtained by using an optical fiber are also presented.

§1. Introduction

Several practical systems for monitoring of pollutant gas have been realized by using YAG lasers, CO_2 lasers, and so on.[1] Furthermore, tunable lead-salt semiconductor lasers have been utilized to reduce the volume of the infrared light source in these systems.[2] However, the reliability of these expensive semiconductor lasers have not yet been high enough because of the low temperature operation and short lifetime. On the other hand, since the performance of the semiconductor lasers in the near infrared have been remarkably improved as a result of the demand in optical communications, they may now also be used as reliable and inexpensive light sources for the gas monitoring. Since it has been demonstrated that the optical fibers show ultra low losses (e.g., about 0.2 dB/km[3]) in the wavelength region of about 1.5 μm, they can be also used together with these semiconductor lasers as powerful tools for an improved gas monitoring system.

Since a great number of the molecular spectral lines are distributed around 1.5 μm region due to the combination tone of the vibration-rotation transitions,[4] the molecular gas can be monitored by measuring these lines. Though several results have been already published concerning use of near infrared LEDs for the light sources,[5] systems using semiconductor lasers and fibers have not yet been fully reported on. In this paper, the absorption spectral lines in NH_3 and H_2O are measured with 1.5 μm semiconductor lasers to demonstrate the applicability of these lasers towards gas monitoring. Moreover, the wavelength of these lines are precisely measured, and the applications of optical fibers to the gas monitoring are shown.

§2. Experimental Apparatus

Figure 1 shows the experimental apparatus used. The light sources are two InGaAsP/InP lasers at 1.5 μm.[6] Their threshold currents are about 60 mA at around 20°C, and the output powers were about 6 mW at 100 mA. Each laser was fixed on a heat sink made of a copper plate, and its temperature fluctuations were reduced to as low as ± 0.05 K with a Peltier element and a thermocouple. The coarse and fine adjustments of the laser wavelengths were

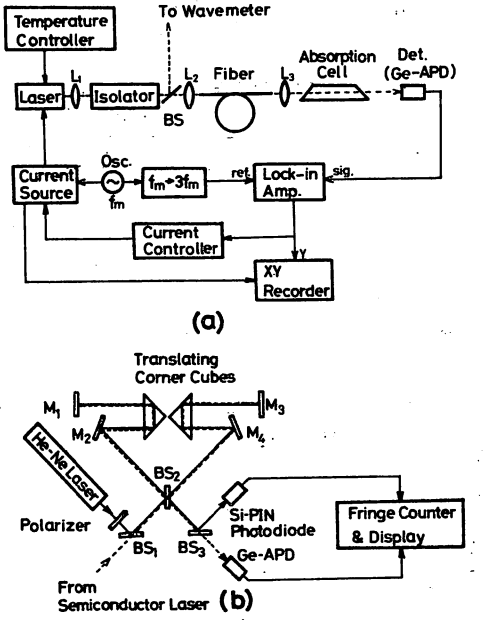

Fig. 1. Experimental apparatus. (a) An optical fiber and collimator lenses (L_2 and L_3) were used in the latter half of the present work. The absorption cell was 0.55 m in length. (b) A precise wavemeter.[8] The excursion lengths of the corner cubes were 6 cm within the time period of 3 s. The measurement error induced by this wavemeter itself was 0.35 pm.

carried out by varying the heat sink temperature and injection current, respectively. The wavelength shifts of the laser due to temperature and injection current were measured as being 75 pm/K and 7.5 pm/mA, respectively, by using the wavemeter shown in Fig. 1(b). The optical isolator in Fig. 1(a) was composed of a Glan-Thompson prism and a Fresnel prism. The optical fiber used in the latter half of this study was a multimode fiber with a core diameter of 30 μm. Low pressure NH_3 or H_2O gas was allowed to fill the absorption cell of 0.55 m in length after the cell was evacuated. The transmitted laser intensity was detected by a Ge avalanche photodiode (Ge-APD), and the output signal from the Ge-APD was amplified by a lock-in amplifier and recorded on a XY-recorder. Figure 1b shows the precise wavemeter[7] used to measure the wavelengths of the absorption spectra. This Michelson interferometer-

type wavemeter employs a short He–Ne laser with 633 nm as the wavelength standard. The time required for getting one wavelength value was about 3 s with this wavemeter, and the measurement error induced by this wavemeter upon itself was 0.35 pm. Further details of this wavemeter will be published elsewhere.[8] Figure 2 shows the range of the injection current and heat sink temperature, in which each laser shows the single longitudinal mode oscillation. A grating monochromator with a resolution of 0.3 nm was used to measure the longitudinal mode intensities. Here, the single longitudinal mode oscillation was defined to be the situation in which the intensities of the satellite longitudinal modes were less than 5% of that of the main longitudinal mode. The measurements of the absorption spectral lines in NH_3 and H_2O were carried out under these conditions of the single longitudinal mode oscillations in Fig. 2.

§3. Experimental Results and Discussions

In the first half of this section, several results of the spectral measurements are presented which were obtained without the use of optical fibers. Figure 3 shows 21 absorption spectral lines in NH_3 measured by two lasers. The gas pressure P was 4 Torr. Each curve in this figure represents the third derivative of the spectral line shape, which was obtained by modulating the laser wavelength by the a.c. current. The modulation frequency f_m and the maximum wavelength deviation $\Delta\lambda$ for this modulation were 1.1 kHz and 7.5 pm, respectively. These lines can be attributed to the rotation structure in the $2\nu_1$ or $2\nu_3$ vibration transitions,[4] however, complete assignment has not yet been given. Though the measurements of several lines have been demonstrated by using a grating monochromator,[9] their sensitivity and resolution have been far lower than those of the present results. Figure 4 shows an absorption spectral line in H_2O measured by the laser No 1, where the value of P, f_m, and $\Delta\lambda$ were 20 Torr, 1.1 kHz, and 9.0 pm, respectively. No lines in H_2O were measured by the laser No. 2. The spectral line in Fig. 4 can be attributd to the $2\nu_2+\nu_3$ vibration transition,[4] however, complete assignment has not yet been given.

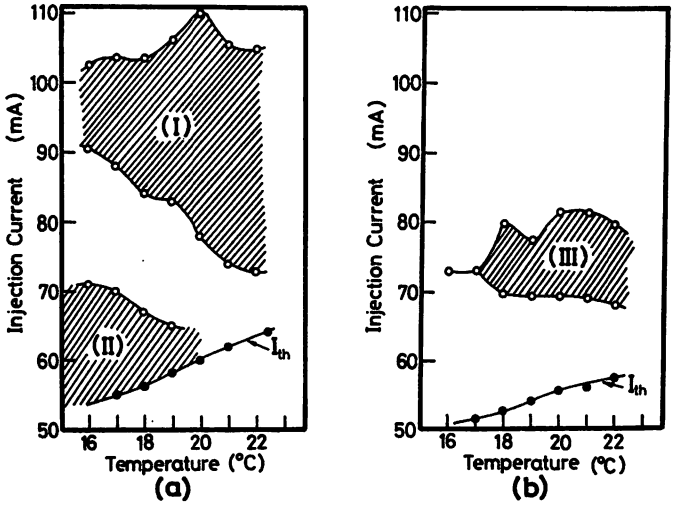

Fig. 2. The ranges of the injection current and the temperatures of the heat sinks of the two lasers when they show the single longitudinal mode oscillations. The shadowed portions show these ranges. The temperature dependences of the threshold currents (I_{th}) of these lasers are simultaneously shown in these figures. (a) Laser No. 1. In the areas (I) and (II), the laser oscillated with wavelengths of 1.503 μm and 1.496 μm, respectively. (b) Laser No. 2. The wavelength of this laser was 1.498 μm in the area (III).

In the present work, as will be shown in Table I, the experimental results for the center wavelengths of NH_3 and H_2O spectral lines are represented by the average value of five succesive measurements for each line done in order to reduce the accidental error. The time required for these five succesive measurements is therefore about 15 s. However, preliminary measurements have shown that the wavelength of the free running laser fluctuated due mainly to the residual fluctuations of the heat sink temperature. The amount of these fluctuations was as large as 0.2 pm ~ 0.4 pm for the integration time of 15 s. These results of the wavelength fluctuations for the free running laser will be shown later more quantitatively in Fig. 5. This value of the thermal drift of the wavelength can not be neglegibly smaller than the value of the measurement error of 0.35 pm induced by the wavemeter itself. Therefore, the inaccuracy of the wavelength measurements would be increased by this thermal drift as long as the free running laser is used. The inaccuracy due to this thermal drift will in general be increased by increasing number of successive measurements for each line, i.e., by increasing the total time required for the measurements. It is therefore necessary to stabilize the laser wavelength to the center of these spectral lines to suppress this drift and to reduce the total error of the measurements to as low as that induced by only the wavemeter itself. Figure 5 shows the results of the wavelength stabilization of laser No. 1 carried out for this purpose. The laser wavelength was stabilized to the center of the third derivative of the spectral lines by controlling the injection current. The PID servo-control technique was used for effecting stabilization.[10] The value of P, f_m, and $\Delta\lambda$ were the same as those in Figs. 3 and 4. The parameters σ, τ, and N in Fig. 5 represent the square root of the Allan variance of the wavelength stability,[11] the integration time, and the number of data, respectively. Since the output signals from the lock-in amplifier in Fig. 1(a) are proportional to the wavelength fluctuations, the value of σ was calculated by using these signals after analog-to-digital conversion. The curve A in Fig. 5 represents the wavelength stability of the free running laser, which can be expressed as

$$\sigma = 3.3 \times 10^{-8} \cdot \tau^{1/2}. \quad (10\ \text{ms} \leqq \tau \leqq 10\ \text{s}) \qquad (1)$$

The curve B represents the result obtained by stabilizing the wavelength to the NH_3 spectral line No. 20 in Fig. 3. The value of on the curve B can be expressed as

$$\sigma = 3.0 \times 10^{-10} \cdot \tau^{-1/2}. \quad (10\ \text{ms} \leqq \tau \leqq 20\ \text{s}) \qquad (2)$$

Nearly equal stability was obtained when the laser wavelength was stabilized to other NH_3 absorption lines except for the lines Nos. 7, 8, 10, and 13 in Fig. 3. When the laser wavelength was stabilized to these four weak lines, the resultant values of σ were about five times larger than that of eq. (2). The curve C represents the results obtained by stabilizing the laser wavelength in accordance to the H_2O absorption line in Fig. 4. The value of σ on this curve can be expressed as

$$\sigma = 1.1 \times 10^{-9} \cdot \tau^{-1/2}. \quad (10\ \text{ms} \leqq \tau \leqq 20\ \text{s}) \qquad (3)$$

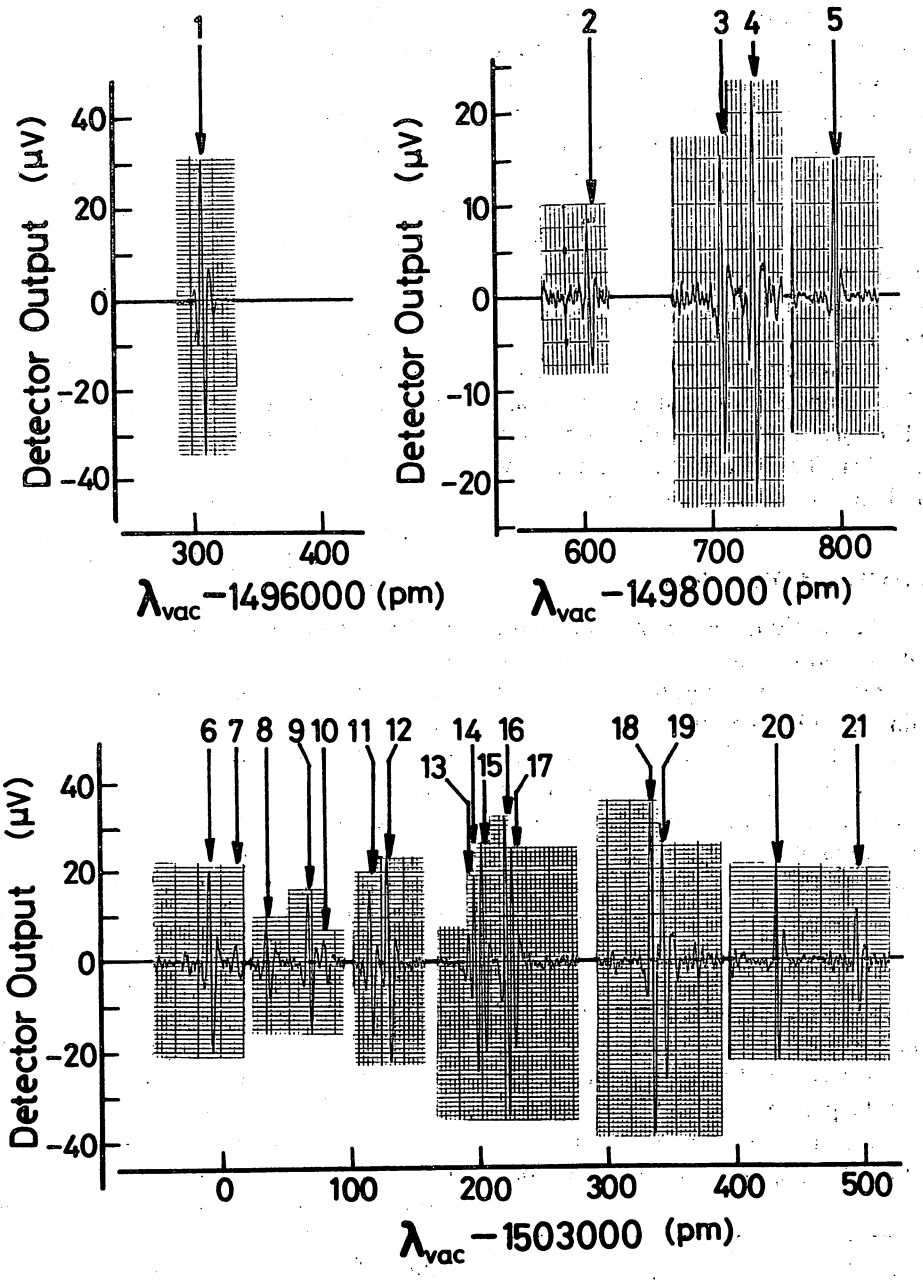

Fig. 3. The third derivatives of NH_3 spectral lines measured by the two lasers. λ_{vac} represents the wavelength in vacuum. The gas pressure P, modulation frequency f_m, and the maximum wavelength deviation $\Delta\lambda$ were 4 Torr, 1.1 kHz, and 7.5 pm, respectively.

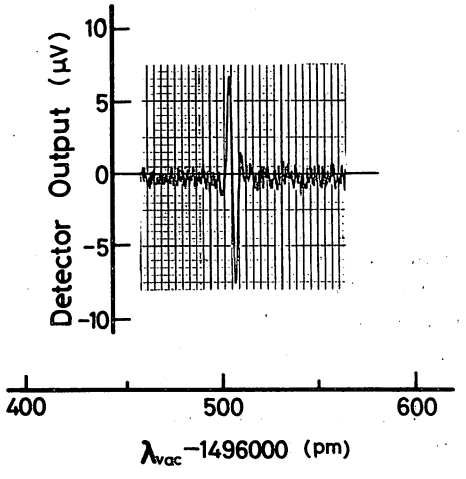

Fig. 4. The third derivatives of H_2O spectral line measured by the laser No. 1. λ_{vac} represents the wavelength in vacuum. The values of P, f_m, and $\Delta\lambda$ were 20 Torr, 1.1 kHz, and 9.0 pm, respectively.

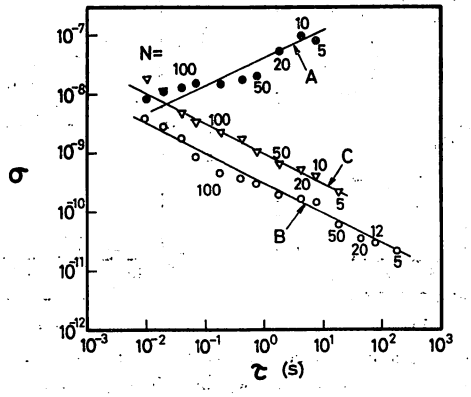

Fig. 5. The wavelength stabilities of the laser No. 1. The paremeters σ, τ, and N represent the square root of the Allan variance,[11] the integration time, and the number of data, respectively. A: The stability of the free running laser. B: The result obtained by stabilizing the laser wavelength to the NH_3 spectral line No. 20 in Fig. 3. C: The result obtained by stabilizing the laser wavelength to the H_2O spectral line in Fig. 4.

It was also confirmed that laser No. 2 showed nearly equal stabilities as those in Fig. 5. It was confirmed from the results of this wavelength stabilization that the thermal drift of the wavelength was suppressed so that it did not induce any extra errors in the wavelength measurements. The wavelengths of the absorption lines in NH_3 and H_2O were obtained with the wavemeter shown in Fig. 1(b) by measuring the wavelength of the laser which was stabilized to these relevant absorption lines. Table I shows the results of the wavelength measurements. Here, the wavelength of the He–Ne laser in the wavemeter was assumed to be 632991.4 pm.[12] Each value in this table represents the average value of the results of five successive measurements. The largest value of the standard deviations in this table is 1.6 pm. The main cause of this inaccuracy was shown to be due to the wavelength modulation used for measuring the third derivative signal of the spectral line shape. The left column of this table shows the wavelengths measured in the air. The wavelengths in vacuum were derived from these values and the refractive index of the air. This refractive index was estimated by substituting the measured values of the pressure, temperature, and humidity of the air into the well-known Edlen's formula.[13] The results are shown in the right column of the Table I. Figure 3 and Table I can be used as the basic data for the assignments of the spectral lines or the gas monitoring experiments in the future.

Figure 6 shows the relation between the NH_3 pressure P and the signal-to-noise ratio S/N of the NH_3 spectral line. Here, the signal-to-noise ratio was defined as the ratio between the peak-to-peak value of the third derivative curve recorded on the XY recorder and that of the randomly fluctuating waveforms on this curve. For this measurement, the spectral line No. 20 in Fig. 3 was used, where the value of f_m, $\Delta\lambda$, and the time constant of the lock-in amplifier were 1.1 kHz, 7.5 pm, and 10 ms, respectively.

Table I. Wavelength of the spectral lines in NH_3 and H_2O.

	No.	Wavelength in the air (pm)	Wavelength in vacuum (pm)
(NH_3)	1.	1496315.8±0.8	1496311.1±0.8
	2.	1498610.7±0.7	1498605.9±0.7
	3.	1498713.4±0.4	1498708.6±0.4
	4.	1498743.3±0.4	1498738.5±0.4
	5.	1498802.8±0.8	1498798.0±0.8
	6.	1503013.7±0.6	1503008.9±0.6
	7.	1503032.6±1.0	1503027.8±1.0
	8.	1503051.9±1.2	1503047.1±1.2
	9.	1503084.9±0.9	1503080.1±0.9
	10.	1503097.1±0.8	1503092.3±0.8
	11.	1503125.1±0.8	1503120.3±0.8
	12.	1503137.3±0.5	1503132.5±0.5
	13.	1503195.6±1.3	1503190.8±1.3
	14.	1503200.5±1.6	1503195.7±1.6
	15.	1503207.1±0.9	1503202.3±0.9
	16.	1503226.7±1.0	1503221.9±1.0
	17.	1503232.6±0.5	1503227.8±0.5
	18.	1503342.6±0.9	1503337.8±0.9
	19.	1503354.0±1.0	1503349.2±1.0
	20.	1503431.7±0.7	1503426.9±0.7
	21.	1503506.6±1.1	1503501.8±1.1
(H_2O)		1496508.9±0.9	1496504.2±0.9

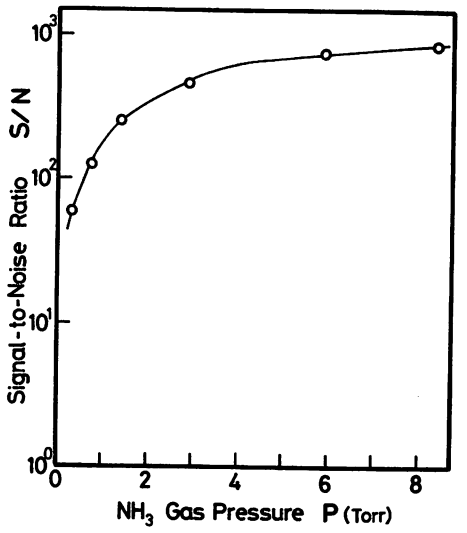

Fig. 6. The relation between the NH_3 gas pressure (P) and the signal-to-noise ratio (S/N) of the third derivative of the spectral line No. 20 in Fig. 3, where f_m, $\Delta\lambda$, and the time constant of the lock-in amplifier were 1.1 kHz, 7.5 pm, and 10 ms, respectively.

The following linear relation can be derived between P and S/N in Fig. 6 by applying least square fitting to the values measured for $P \leqq 2$ Torr:

$$S/N = 180P - 0.74. \quad (P \leqq 2 \text{ Torr}) \tag{4}$$

The minimum detectable pressure P_m can be obtained by fixing $S/N=1$ in eq. (4), i.e., $P_m = 4.1 \times 10^{-3}$ Torr. In the alternative expression, the sensitivity of the NH_3 gas monitoring by the present method can be defined by expressing the minimum detectable pressure for an absorption cell with a unit optical path length, which can be given by 2.3×10^{-3} Torr · m.

We now discuss the experimental results obtained by using the optical fibers. Figure 7 shows the third derivative signal of the spectral line No. 20 in Fig. 3 obtained by irradiating the laser light on the NH_3 gas after the light was

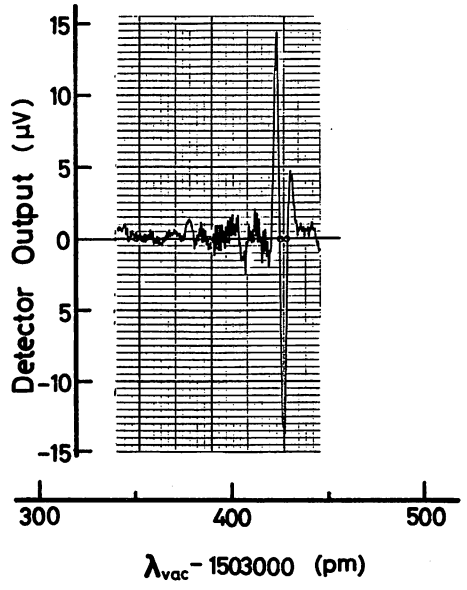

Fig. 7. The third derivative of the NH_3 spectral line No. 20 measured by a multimode fiber with the length of 50 m. λ_{vac} represents the wavelength in vacuum. The gas pressure was 5.2 Torr, while the other experimental conditions were the same as those in Fig. 3.

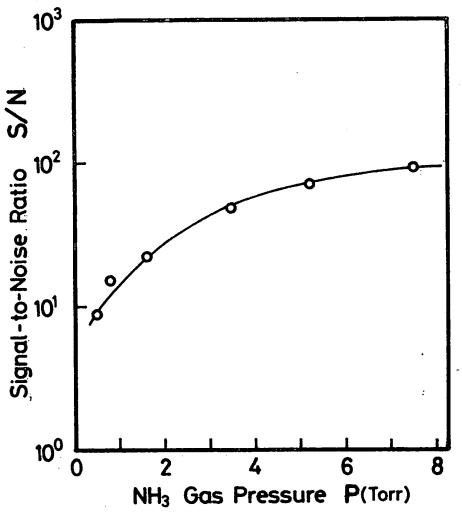

Fig. 8. The relation between the NH_3 gas pressure (P) and the signal-to-noise ratio (S/N) of the third derivative of the spectral line No. 20 in Fig. 3, where the multimode fiber with the length of 50 m was used. Other experimental conditions were the same as those of Fig. 6.

transmitted through an optical fiber of length 50 m. The gas pressure P was 5.2 Torr while the other experimental conditions were the same as those in Fig. 3. Figure 8 shows the relation between P and S/N of this line. Experimental conditions for this figure are the same as those of Fig. 6. By comparing Figs. 6 and 8, the decrease in the S/N value can be seen when the optical fiber was used, which was attributed to the speckle noise of the laser intensity transmitted through the multimode fiber, the instabilities of the laser oscillation by the reflected lights from the fiber ends, and the coupling loss of the laser light into the fiber. Figure 9 shows the relation between the fiber length L and S/N of this NH_3 line where the NH_3 pressure was fixed at 6 Torr. Other experimental conditions were the same as in Figs. 6 and 8. It can be seen again that the S/N value is decreased about ten times when the fiber is used. However, a distinct decrease in S/N value cannot be seen by increasing L, which would mean that the optical fiber worked as a reliable, low-loss transmission line for this type of the experiment, also.

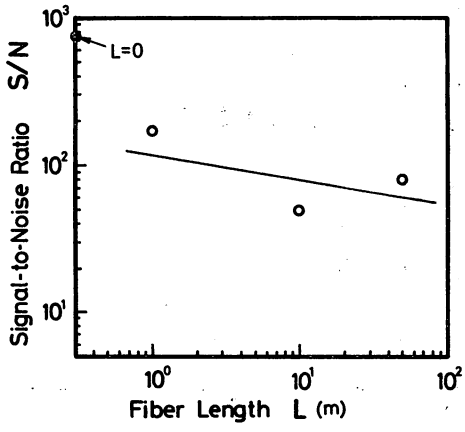

Fig. 9. The relation between the length of the multimode fiber (L) and the signal-to-noise ratio (S/N) of the third derivative of the NH_3 spectral line No. 20. The gas pressure was fixed at 6 Torr, while other experimental conditions are the same as in Figs. 6 and 8. The black circle on the ordinate represents the result obtained when the fiber was not used.

Though the maximum length of the optical fiber employed here was only 50 m, optical fibers much longer than 50 m would be required for practical gas monitoring systems. Improvements in S/N ratio and optical fiber length can be expected through the use of a single mode fiber, precise optical isolators, and so on. Further experiments are now in progress in order to develop more practical gas monitoring systems by using the 1.5 μm semiconductor lasers and single mode fibers.

§4. Summary

The absorption spectral lines of the combination tones of the vibration-rotation transition in NH_3 and H_2O were measured by using 1.5 μm InGaAs/InP lasers. The numbers of the NH_3 and H_2O lines measured were 21, and 1, respectively. The wavelengths of these lines were precisely measured within the inaccuracy of 1.6 pm. For these measurements, the laser wavelength was stabilized to NH_3 and H_2O lines. The resultant stabilities were $3.0\times10^{-10}\cdot\tau^{-1/2}$, and $1.1\times10^{-9}\cdot\tau^{-1/2}$, respectively, where τ represents the integration time. The sensitivity of NH_3 gas monitoring was measured as being 2.3×10^{-3} Torr · m. Spectral measurements using the multimode fiber were also demonstrated. The signal-to-noise ratio of the spectral measurement was reduced by about ten times when the fiber was used. The main reason for this reduction is attributed to the speckle noise, oscillation instabilities of the laser by the reflected light, and the coupling loss into the optical fiber. Higher sensitivity can be expected by using a single mode fiber and a precise optical isolator. The results of the present work have demonstrated several possibilities for use in a novel system for the monitoring of pollutant gas.

Acknowledgements

The authors would like to express their thanks to Drs. T. Yamamoto and S. Akiba of KDD Research and Development Laboratories for valuable discussions. They also wish to thank Profs. T. Tako and Y. Suematsu of their institute for their support in the present work.

References

1) E. D. Hinkley ed.: *Topics in Applied Physics*, vol. 14, *Laser Monitoring of the Atmosphere*, (Springer Verlag, Berlin, 1976).
2) R. T. Ku, E. D. Hinkley and J. O. Sample: Appl. Opt. **14** (1975) 854.
3) T. Miya, Y. Terumura, T. Hosaka and T. Miyashita: Electron. Lett. **15** (1979) 106.
4) G. Herzberg: *Molecular Spectra and Molecular Structure II, Infrared and Raman Spectra of Polyatomic Molecules*, (Van Nostrand Reinhold, New York, 1945).
5) H. Inaba, T. Kobayashi, M. Hirama and M. Hamza: Electron. Lett. **15** (1979) 749.
6) Y. Noda, K. Sakai and Y. Matsushima: Electron. Lett. **17** (1981) 226.
7) J. L. Hall and S. A. Lee: Appl. Phys. Lett. **29** (1976) 367.
8) M. Ohtsu, H. Tagawa and H. Kotani: to be published in Jpn. J. Appl. Phys. **22** (1983) No. 12.
9) H. J. Unger: Phys. Rev. **43** (1933) 123.
10) M. Ohtsu, S. Katsuragi and T. Tako: IEEE J. Quantum Electron. **QE-17** (1981) 1100.
11) D. W. Allan: Proc. IEEE **54** (1966) 221.
12) G. R. Hanes, K. M. Baird and J. DeRemigis: Appl. Opt. **12** (1973) 1600.
13) B. Edlen: Metrologia **2** (1966) 81.

JAPANESE JOURNAL OF APPLIED PHYSICS
VOL. 23, NO. 2, FEBRUARY, 1984 pp. L117–L120

Accurate Wavelength Measurements of the Absorption Lines in H_2O Vapor by a 0.8 μm AlGaAs Laser

Kazuo FUKUOKA,* Motoichi OHTSU and Toshiharu TAKO†

International Cooperation Center for Science and Technology, Tokyo Institute of Technology, 2-12-1 O-okayama, Meguro-ku, Tokyo 152
†*Research Laboratory of Precision Machinery and Electronics, Tokyo Institute of Technology, 4259 Nagatsuta, Midori-ku, Yokohama, Kanagawa 227*

(Received December 27, 1983; accepted for publication January 28, 1984)

The first results of accurate measurements of vacuum wavelengths of six spectral lines of a (2, 1, 1) vibration band in H_2O were presented using a 0.8 μm AlGaAs laser. For these measurements, the technique known as the coincidence method was employed using a stabilized He–Ne laser as a wavelength standard. Accidental error was kept between 1.7×10^{-7} and 5.5×10^{-8}. Systematic error was estimated as being 2.0×10^{-8}.

§1. Introduction

Performances of near-infrared semiconductor lasers have been remarkably improved by the demands of optical communication industries so that they can be used not only for communications but for a variety of precise optical measurements. One of the important applications can be the spectroscopy of atoms or molecules, utilizing the high temporal coherence of these lasers. One of the authors (M.O.) has already measured the spectra in combination tones of vibration-rotation spectra in NH_3 and H_2O by 1.5 μm InGaAsP lasers and has applied it to a pollutant gas monitoring system.[1] 0.8 μm AlGaAs laser have also been used for spectral measurements of Cs and Rb.[2,3] Two of the authors (M.O. and T.T.) have measured combination tones of the vibration-rotation spectra in H_2O vapor using this 0.8 μm AlGaAs laser, and have used these spectral lines to stabilize the laser frequency.[4] These combination tones have been assigned as $(v_1, v_2, v_3)=(2, 1, 1)$ vibration band, and this band is composed of a great number of lines because of its rotation structure.[5]

In this letter, the results of the first accurate wavelength measurements of these lines are presented to obtain basic data for spectroscopy in the near-infrared region. These results demonstrate that the reliability of these lasers is high enough for their use as novel sources for high resolution spectroscopy.

§2. Experimental Apparatus

Wavelengths of H_2O absorption spectral lines in (2, 1, 1) vibration band have already been measured with the accuracy of $1\times10^{-6}\sim1\times10^{-7}$ using a high resolution grating monochromator.[5] The experimental apparatus shown in Fig. 1 was employed here to get even higher accuracy than these conventional results. A Lamb-dip stabilized He–Ne laser (Spectra Physics, Model SP-119) was used as a standard, whose wavelength in vacuum λ_s has been measured as 632991.40 pm.[6] Its wavelength stability was measured as 1×10^{-9} for $1\ \mathrm{s}<\tau<10^2$ s by preliminary

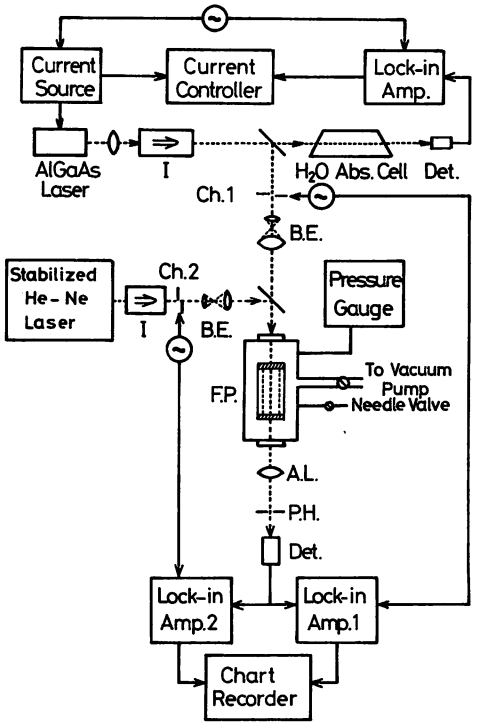

Fig. 1. Experimental apparatus. I: Isolator composed of a Fresnel prism and a Glan-Thompson prism. B.E: Beam expander. Ch.: Chopper. F.P.: Pressure-scanning Fabry-Perot interferometer. A.L.: Achromatic lens. P.H.: Pin hole.

experiments, where τ represents the integration time of the stability measurements. On the other hand, the wavelength of an AlGaAs laser (CSP-type) was stabilized at the center wavelength of the relevant absorption spectral line in H_2O. The technique for wavelength stabilization and its stability measurements employed in this study are the same as in ref. 4. The interference fringes of the stabilized He–Ne and AlGaAs laser were simultaneously measured by a pressure-scanning Fabry-Perot interferometer, and the vacuum wavelength of the stabilized AlGaAs laser, i.e., that of the H_2O spectral line, was then obtained from these results by the coincidence method. This method has been conventionally used for accurate wavelength measurements of He–Ne lasers,[6–8] He–Xe lasers[9] and others. Two Al-

*Present address: Toshiba Co. Ltd., 72 Horikawa-cho, Saiwai-ku, Kawasaki, Kanagawa 210.

coated flat mirrors were used for the Fabry-Perot interferometer, whose finesse was about 6. Two Invar cylinders of 22 mm and 82 mm lengths were used as interferometer spacers. These spacer lengths were preliminarily measured using a laser interferometer (Hewlett Packard, Model HP5526A), and the results were $L_1 = 22223.4 \pm 0.5\ \mu m$ and $L_2 = 82252.4 \pm 0.5\ \mu m$, respectively.

The vacuum chamber for the interferometer was evacuated as low as 50 mTorr before the measurements to reduce the systematic error associated with the results. The surfaces of two mirrors were fixed in parallel using precise screws within the errors of 2×10^{-5} rad. This was done by observing the interference fringes with a small telescope.[8] The beam radii of lasers were expanded to 5 mm by beam expanders to reduce the intensities of higher-order transverse modes in the interferometer, which can be generated by diffraction. By these procedures, the systematic errors associated with the measured value of the wavelengths due to residual gas pressure, nonparallelism between the two mirrors, and the higher-order transverse modes were estimated as lower than 2×10^{-9} using the estimation formula given by Ito and Tanaka.[10]

The laser beams transmitted through the interferometer were focused by an achromatic lens with a focal length of 510 mm. The central portion of the focused beams was picked up by a pinhole with an aperture radius of 0.15 mm and detected by a Si-photodiode. The inaccuracies of fixing the position of the pinhole can also induce systematic error. To reduce this error, the longitudinal and transversal positions of the pinhole were adjusted within the deviations of 0.13 mm and 0.01 mm from the focal point, respectively, using precise screws. By these precise adjustments, the induced systematic errors were estimated as being less than 2×10^{-9}.[10]

On the other hand, further systematic errors can be induced if the directions of the two laser beams are not in parallel. The angle between these two directions was reduced as low as 2.0×10^{-4} rad., which corresponded to the systematic error of 2.0×10^{-8}. This is the largest value amoung the induced systematic errors shown above, and it can be concluded that this nonparallelism gave a dominant contribution to the systematic error in the present wavelength measurements.

§3. Experimental Results and Discussions

Figure 2 shows the third derivative of 2_1-2_2 absorption spectral line in H_2O measured by the AlGaAs laser. The wavelength of this laser was then locked at the center wavelength of this third derivative shape. The square root of the Allan variance σ^2 of the wavelength fluctuations of this locked laser was measured as

$$\sigma = 6.2 \times 10^{-10} \tau^{-1/2} \text{ for } 1 \times 10^{-2}\ \text{s} < \tau < 5 \times 10^{2}\ \text{s}. \quad (1)$$

This quantity, σ^2, has been popularly used as a measure of the stability.[11] Here, τ represents the integration time. It can be confirmed from this equation that the wavelength fluctuations of this laser would not induce any extra errors in the measured value of the wavelength if the time required to scan the Fabry-Perot interferometer is longer than 1×10^{-2} s because σ is less than 1×10^{-8} for $\tau \geqq 1 \times 10^{-2}$ s.

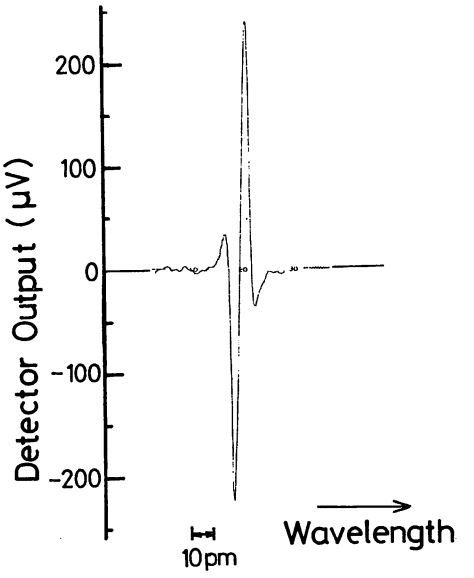

Fig. 2. The third derivative of 2_1-2_2 absorption line in H_2O.

This condition can be easily satisfied because this scanning time was kept longer than 20 minutes as shown in Figs. 3 and 4.

Figure 3(a) and (b) shows the interference fringes of the He–Ne laser and AlGaAs laser recorded by a chart recorder, respectively, when the 22 mm interferometer was used. The time required for the pressure scanning was 24 minutes. The orders of interferences of both lasers, $m_{s1}+\varepsilon_{s1}$ and $m_{x1}+\varepsilon_{x1}$, in vacuum ($P=0$), can be expressed as

$$L_1 = \frac{\lambda_s}{2} \cdot (m_{s1}+\varepsilon_{s1}) = \frac{\lambda_x}{2} \cdot (m_{x1}+\varepsilon_{x1}), \quad (2)$$

where λ_x represents the vacuum wavelength of the AlGaAs laser. The quantities m_{s1} and m_{x1} represent the integer of the orders of interference of the He–Ne and AlGaAs lasers, while ε_{s1} and ε_{x1} represent their fraction. The values of ε_{s1} and ε_{x1} are derived by measuring the separation between each peak of the curves in Fig. 3 and its extrapolation to $P=0$. On the other hand, m_{s1} and m_{x1} can be obtained from the value of λ_s, the preliminarily measured value of L_1 in §2, and the values of ε_{s1} and ε_{x1} obtained above. These are the procedures to determine the values of $m_{s1}+\varepsilon_{s1}$ and $m_{x1}+\varepsilon_{x1}$, which has been well known as the coincidence method for wavelength measurements. Figure 4(a) and (b)

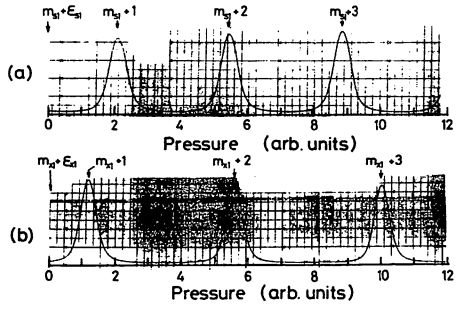

Fig. 3. Interference fringes of the He–Ne (a) and AlGaAs lasers (b) measured using a Fabry-Perot interferometer of 22 mm length. In this figure, $m_{s1}+\varepsilon_{s1}$ and $m_{x1}+\varepsilon_{x1}$ represent the orders of interference of both lasers in vacuum. The time required to record these fringes was 24 minutes.

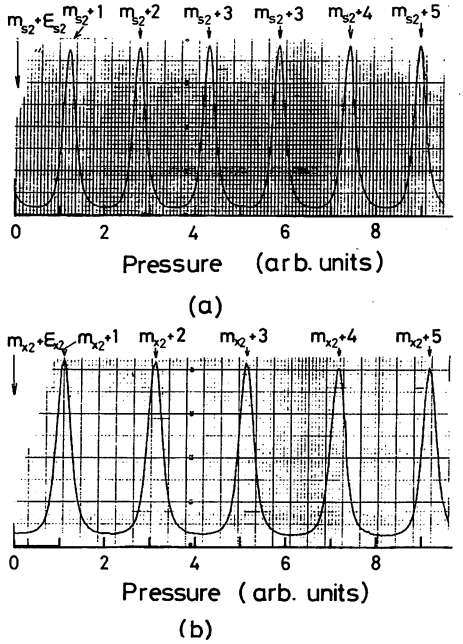

Fig. 4. Interence fringes of the He–Ne (a) and AlGaAs lasers (b) measured using an interferometer of 82 mm length. In this figure, $m_{s2}+\varepsilon_{s2}$ and $m_{x2}+\varepsilon_{x2}$ represent the orders of interference of both lasers in vacuum. The time required to record these fringes was 24 minutes.

shows the interference fringes of both lasers measured by the 82 mm long interferometer. As was true in eq. (2), the orders of interferences in vacuum, $m_{s2}+\varepsilon_{s2}$ and $m_{x2}+\varepsilon_{x2}$ of both lasers are also given by

$$L_2=\frac{\lambda_s}{2}\cdot(m_{s2}+\varepsilon_{s2})=\frac{\lambda_x}{2}\cdot(m_{x2}+\varepsilon_{x2}). \tag{3}$$

The application of the coincidence method to the results of Figs. 3 and 4 gave the following results:

$$\left.\begin{aligned} m_{s1}&=70218 \quad \varepsilon_{s1}=0.3410\\ m_{x1}&=54014 \quad \varepsilon^{x}1=0.7489\\ m_{s2}&=259882 \quad \varepsilon_{s2}=0.2729\\ m_{x2}&=199911 \quad \varepsilon_{x2}=0.4430 \end{aligned}\right\} \tag{4}$$

Here, the least-square fitting was employed to the curve of Figs. 3 and 4 to get the values of ε with five significant digits as shown in this equation. The wavelength value λ_x can be derived by eqs. (2)~(4). However, the orders of interference for each interferometer determined above may be biased from the real values because of the laser beam phase changes at the reflection on the mirrors of the interferometer. To eliminate this bias, the virtual spacer method is now employed.[8] That is, the order of interference for the virtual interferometer with the spacer length of L_2-L_1 is derived by subtracting eq. (2) from eq. (3). By this subtraction, the effect of the phase change, commonly included in the order of interferences for shorter and longer interferometers, can be eliminated. Then, the value of vacuum wavelength λ_x, free from the effects of the phase changes, is given by

$$\lambda_x=\lambda_s[(m_{s2}+\varepsilon_{s2})-(m_{s1}+\varepsilon_{s1})]/[(m_{x2}+\varepsilon_{x2})-(m_{x1}+\varepsilon_{x1})]. \tag{5}$$

The value of λ_x can be derived by substituting eq. (4) and the value of λ_s into this equation.

Measurements of λ_x described above were repeatedly done to reduce the accidental errors. Table I shows the average value $\bar{\lambda}_x$ of the results of these successive measurements, and its standard deviation σ_{n-1}, respectively, where n represents the number of data. The first line in this table gives the result for the 2_1-2_2 spectral line of Fig. 2. Including this spectral line, the wavelengths of six others were successfully measured and are also given in this table. The accidental errors, $\sigma_{n-1}/\bar{\lambda}_x$, were kept between 1.7×10^{-7} and 5.5×10^{-8}. Systematic errors, due to the inaccuracies of the experimental apparatus, were estimated as being 2.0×10^{-8}, as described in §2. Conventional results are also presented in this table, as obtained by a grating monochromator.[5] Comparison between these and the present results shows that more accurate values were obtained by the present method, which also proves the high reliability and high temporal coherence of the AlGaAs laser for these precise optical measurements.

Higher accuracies can be expected by improving the mechanics of optical alignments and low-noise electronic circuits for the measurements. A larger number of H_2O absorption lines can be observed by preparing more AlGaAs lasers because the wavelengths of these lasers are individually distributed at around the 0.8 μm region. several molecular constants of H_2O, a basic molecule in nature, may be determined more accurately from these wavelength values in the future. Furthermore, the present results may be used as basic data for the spectroscopy of organic molecules in the near-infrared region, and for the pollutant gas monitoring system.

§4. Summaries

Vacuum wavelengths of six absorption lines of the (2, 1, 1) vibration band in H_2O vapor were accurately measured by a 0.8 μm AlGaAs laser. The accidental errors were kept between 1.7×10^{-7} and 5.5×10^{-8}. The systematic error was estimated as being 2.0×10^{-8}. These errors were less than those of conventionally reported values, which proves that this near-infrared laser possesses high reliability for application to high resolution spectroscopy.

Acknowledgements

The authors would like to express their thanks to Dr. M. Nakamura of Hitachi Ltd. for his support in the experiments. They are also much indebted to Prof. Emertus. A.

Table I. Vacuum wavelengths of H_2O absorption lines in (2, 1, 1) vibration band.

Assignments (J_i-J_k)	λ (pm)	$\bar{\lambda}_x$ (pm)	σ_{n-1} (pm)	n	σ_{n-1}/λ_x
2_1-2_2	822876.0	822875.517	0.087	15	1.1×10^{-7}
4_2-4_1	822975.3	822974.79	0.14	10	1.7×10^{-7}
3_0-3_1	823390.7	823393.47	0.10	7	1.2×10^{-7}
1_1-2_0	826344.5	826346.408	0.057	12	6.9×10^{-8}
$3_{-3}-3_0$	827870.8	827870.814	0.046	6	5.5×10^{-8}
2_0-3_{-1}	828202.7	828202.70	0.10	3	1.2×10^{-7}

J_i, J_k: Rotational quantum number of upper and lower levels of the transition, respectively.
λ: Wavelength values reported by Baumann and Mecke.[5]
$\bar{\lambda}_x$: Average of the wavelength of the present measurements.
σ_{n-1}: Standard deviation.
n: Number of data.

Toyama and Assoc. Prof. A. Shimokobe of their institute for their help with the preliminary measurements of the spacer lengths of the interferometers.

References

1) M. Ohtsu, H. Kotani and H. Tagawa: Jpn. J. Appl. Phys. **22** (1983) 1553.
2) T. Yabuzaki, T. Ibaragi, H. Hori, M. Kitano and T. Ogawa: Jpn. J. Appl. Phys. **20** (1981) L451.
3) H. Tsuchida, M. Ohstu and T. Tako: Jpn. J. Appl. Phys. **21** (1982) L561.
4) H. Tsuchida, M. Ohstu and T. Tako: Jpn. J. Appl. Phys. **21** (1982) L1.
5) W. Baumann and R. Mecke: Z. Phys. **81** (1933) 445.
6) G. R. Hanes and K. M. Baird: Metrologia, **5** (1969) 31.
7) R. L. Barger and J. L. Hall: Appl. Phys. Lett. **22** (1973) 196.
8) N. Ito and K. Tanaka: Metrologia, **14** (1978) 47.
9) T. Tako, M. Ohstu, S. Katsuragi, M. Ohi and Y. Akimoto: Jpn. J. Appl. Phys. **19** (1980) 1683.
10) N. Ito and K. Tanaka: Rep. NRLM, **28** (1979) 63.
11) D. Allan: Proc. IEEE **54** (1966) 221.

[Proceedings of the 39th Annual Symposium of Frequency Control,
May 29 - 31, 1985, Philadelphia, Pennsylvania]

A Highly Stabilized Semiconductor Laser and Its Application to Optically Pumped Rb Atomic Clock

Motoichi Ohtsu, Minoru Hashimoto, and Hidetaka Ozawa

International Cooperation Center for Science and Technology,
Tokyo Institute of Technology,
2 - 12 - 1, O-okayama, Meguro-ku, Tokyo 152, Japan

Abstract

Frequency stability of 1×10^{-12} at $\tau = 100$ s was obtained for 0.8 μm AlGaAs laser by using spectral lines of Rb vapor as frequency references. It was confirmed that this value of the stability was as high as the value limited by spontaneous emission noise. Through an analysis based on a semiclassical Langevin's equation, it was estimated that the stability can be improved to as high as $1.7 \times 10^{-14}\ \tau^{-1/2}$. Spectral linewidth reduction was also tried to improve the coherence of the semiconductor laser. A novel technique, i.e., electrical feedback, was proposed for this reduction instead of using a conventional technique of optical feedback. The linewidth was stably reduced by this technique. The minimum value obtained was 330 kHz for an InGaAsP laser at 1.5 μm, which was fifteen times narrower than that of a free-running laser. It was estimated that the linewidth can be ultimately reduced to a value less than 1 kHz by this technique. Experiments on optical pumping for Rb atomic clock were carried out by using the highly stabilized semiconductor laser mentioned above. As the first step, experiments on saturated absorption spectroscopy of ^{87}Rb - D_2 lines were carried out. Eleven lines, including cross-resonance lines, were clearly observed. As the next step, double resonance signal was obtained by laser optical pumping. The microwave frequency shift by the laser frequency and power were measured. The microwave frequency stability was also evaluated. Furthermore, a comment on the spectral lifetime of semiconductor laser for Rb atomic clock was given.

I. Introduction

The spectral properties of semiconductor lasers have been recently improved as a result of the demands of the optical communication industry. These lasers can be used as reliable light sources for coherent optical communication and coherent optical measurements. For these purposes, we have improved their frequency stabilities, and carried out their spectral linewidth measurements. A part of these works has been reported in this symposium[1]. In the present paper, recent progresses on this study and its application to Rb atomic clock are reported.

II. Frequency Stabilization of Semiconductor Lasers

Frequency stabilization of a 0.8 μm AlGaAs laser was carried out by using a stable Fabry-Perot interferometer, absorption spectral lines of H_2O and ^{85}Rb as frequency references[2] - [4]. The injection current of the laser was controlled for stabilization by employing a PID servo-control circuit. Figure 1 summarizes the experimental results[5]. When the ^{85}Rb - D_2 line was used as a frequency reference, the highest frequency stability of $\sigma_y(\tau) = 1.4 \times 10^{-12}$ was obtained at $\tau = 100$ s. Figure 2 shows the limit of the frequency stability estimated through an analysis based on a semiclassical Langevin's equation[5]. Comparison between Figs. 1 and 2 shows that experimental results have already approached to the value limited by spontaneous emission. Quite recently, Saito, et. al., pointed out that the electrical feedback may control the quantum FM noise of 0.8 μm AlGaAs lasers, and reduce the FM noise to a value less than that limited by spontaneous emission[6]. If this result is applied to the present case, the frequency stability can be improved to the value limited by noise of the detector in the feedback loop. This value is given by the curve G of Fig. 2,

i.e., the stability can be improved as high as $\sigma_y(\tau) = 1.7 \times 10^{-14}\ \tau^{-1/2}$.
Figure 3 shows the result of frequency stabilization by using a ^{87}Rb - D_2 line as a frequency reference, which was recently obtained for developing a ^{87}Rb atomic clock. The laser was installed in a small vacuum chamber, and the fluctuations of the temperature and injection current were reduced as low as 1×10^{-4} K and 0.6 nA/$\sqrt{Hz}$, respectively. Two kinds of ^{87}Rb absorption cells were used, i.e., with buffer gases and without buffer gases. For the ^{87}Rb absorption cell without buffer gases, saturated absorption spectral lines as well as linear absorption spectral lines were measured, and were used as frequency references for stabilization. For the ^{87}Rb absorption cell with buffer gases (Ar/N_2 = 1.65, total pressure ; 43 Torr), linear absorption spectral lines were used as a frequency reference. In all of these cases, frequency stability as high as $\sigma_y(\tau) = 1 \times 10^{-12}$ at τ = 100 s was obtained. Higher frequency stability can be expected by improving the servo-controlling circuits. For 1×10^{-2} s < τ < 1×10^{1} s, the stability of the curve D is slightly higher than others because of higher frequency discrimination of the frequency reference by saturated absorption line.
Figure 4 shows the deterioration in the power stability observed when the laser frequency was stabilized by controlling the injection current. This is due to that the power was disturbed by the change in the injection current for frequency stabilization. Since the deterioration in power stability will reduce the detection sensitivity of double resonance signal in ^{87}Rb atomic clock, simultaneous stabilization of the power should be required by controlling, e.g., temperature. Simultaneous power stabilization is now in progress.

III. Linewidth Reduction of Semiconductor Lasers by Electrical Feedback

It has been reported that the linewidth of a free-running semiconductor laser was larger than several mega herz[7]. However, if this laser is used for coherent optical communication or coherent optical measurements, the linewidth should be narrower than 1 MHz. Several techniques have been proposed to reduce the linewidth for these applications. One of them is to increase the cavity Q factor by using an external mirror. This has been called an optical feedback technique, and it makes use of the injection of reflected light into the laser from an external mirror. The linewidth has been reduced to a value as narrow as 1 kHz by this technique[8]. However, this technique presents several problems. One of them is that the linewidth can be temporally affected by phase fluctuations of the reflected light induced by the mechanical vibration of the external mirror. Furthermore, it is essentially required to considerably increase the size of the laser cavity in this technique, which sacrifices such an advantageous property of the semiconductor laser as its small size.
To overcome these difficulties, we have proposed a simpler and more stable technique, i.e., an electrical feedback to reduce the linewidth by controlling the injection current[9]. Saito, et. al.[6] have also pointed out that the electrical feedback can reduce its linewidth to a value smaller than the one given by the modified Schawlow - Townes formula[10]. This makes the electrical feedback a more promising technique to realize a stable and ultranarrow linewidth laser. Figure 5 shows the experimental apparatus. In this experiment, a distributed feedback (DFB) - type InGaAsP laser at 1.5 μm was used to get a single longitudinal mode oscillation for a wide range of the injection current. However, this technique can be applied also for 0.8 μm AlGaAs lasers. FM noise of the laser was detected by using a compact Fabry - Perot interferometer of 10 mm length as a frequency discriminator. The output signal from a Ge - APD, which is proportional to FM noise, was fed back to the injection current after amplified by a video amplifier with 100 MHz bandwidth. A delayed self - heterodyne technique was employed for linewidth measurements[11]. Figure 6 shows the experimental results. The minimum value obtained was 330 kHz, which is 15 times narrower than that of a free - running laser. The spectral line shape showed none of the temporal fluctuations which have sometimes been observed in the optical feedback technique[8]. Figure 7 shows the minimum attainable linewidth, where R_{FP} represents the reflectance of the mirrors of the Fabry - Perot interferometer. For this estimation, it was assumed that the linewidth can be reduced to a value limited by the noise of the detector which is installed in the initial stage in the feedback loop, as was pointed out by Saito, et. al.[6]. From Fig. 7, it can be concluded that the linewidth can be ultimately reduced to a value less than 1 kHz when $R_{FP} > 0.9$.

IV. High Resolution Spectroscopy of ^{87}Rb

Highly stabilized semiconductor laser described in II and III can be used for high resolution spectroscopy and optical pumping of atomic clocks. In this section, experimental results of high resolution spectroscopy of ^{87}Rb - D_2 lines are presented. Figure 8 shows a popular energy levels of ^{87}Rb atoms, in which each optical transition is assigned (o ~ t). Two kinds of ^{87}Rb absorption cells, employed in II, were also used here at room temperature. Figure 9 shows the linear absorption spectral shapes observed by both of the absorption cells. By comparing these figures, it was found that the frequency of F = 1 line for

the cell with buffer gases was located 260 MHz lower than that of the cell without buffer gases, i.e., this transition suffered the pressure shift.
Figure 10 shows saturated absorption spectral shapes observed by the cell without buffer gases. Five lines for F = 1 and six lines for F = 2 were clearly resolved, which were assigned to be the saturated absorption and cross - resonance lines. Least-square fitted curves are also shown in Fig. 10, which was derived by using a model given by Nakayama[12]. These curves fit well with those of the experimental results, and the linewidth of these spectral lines were estimated as 40 MHz through this fitting. Further calculations are now in progress by employing a more detailed model which includes also the dependence of the line shapes on the polarization of the laser light[13].
Figures 11 and 12 shows the dependences of the signal strength and linewidth of two cross - resonance lines (s - t, p - q) on the laser power density, where the cross - sectional area of the laser beam was about 0.1 cm^2. A saturation due to the laser power can be clearly seen in these figures.

V. Application to ^{87}Rb Atomic Clock

The laser frequency was locked at the center of a linear absorption spectral line of F = 1 of the ^{87}Rb absorption cell with buffer gases. The frequency stability and power stability of the laser have been given in Figs. 3 and 4. Fig. 13 shows the derivative of a double resonance signal of ^{87}Rb obtained by using this stabilized laser as a pumping source. Figure 14 shows the dependences of the linewidth and S/N value of this signal on the laser power density. In Fig. 14, the linewidth decreases for the power density range of larger than about 100 $\mu W/cm^2$.One of the possible reasons may be due to anomalous line narrowing, which has been recently predicted[14].
Figures 15 and 16 show the shifts of the stabilized microwave frequency due to the laser frequency and power density. Center of the dispersive curve of Fig. 15 was selected as zero point of the axes of this figure, i.e., frequency shifts of the microwave $\Delta\nu_M$ and laser $\Delta\nu_L$ represent the shifts from this point. Figure 17 shows the slopes of the curves of Figure 15 at $\Delta\nu_L = \Delta\nu_M = 0$.
Figure 18 shows the frequency stability of the microwave of the ^{87}Rb atomic clock. In this measurement, the laser power density incident into the atomic clock and $\Delta\nu_L$ were fixed at 88.5 $\mu W/cm^2$ and 0, respectively. The curve A represents the contribution of the FM noise of the frequency stabilized laser estimated by using the results of Figs. 3 and 17. The curve B also represents this contribution obtained by assuming that the laser frequency stability is improved as high as the ultimate value given by the curve G in Fig. 2. AM noise does not give direct contributions to this stability as long as the laser frequency is fixed at $\Delta\nu_L = 0$ because the power shift of Fig. 16 is zero at $\Delta\nu_L = 0$. However, since the AM noise could reduce the S/N value of the double resonance signal detection, this will limit the frequency stability of the atomic clock. Quantitative estimation of this effect is now in progress. Experimental results in this figure show that the stability of the laser-pumped ^{87}Rb atomic clock obtained in this preliminary exkperiment was already as high as that of a conventional atomic clock, and is almost equal to the value reported by L. Lewis[15] Further improvements of this stability can be expected by reducing the noise from the photodetector and servo - control circuit.

VI. Spectral Lifetime of Semiconductor Lasers

When a semiconductor laser is used for ^{87}Rb atomic clock , its spectral lifetime should be long enough. That is, the wavelength of a free-running should stay at the resonance wavelength of ^{87}Rb - D_2 line at 780.0 nm for at least more than several years. However, since the wavelengths of commercially available AlGaAs lasers distribute in a wide range of between 760 - 800 nm, it is not easy to find a laser with the wavelength accurately coincident with that of ^{87}Rb - D_2 line even though the wavelength tuning can be performed by widely varying the temperature. If the lasers are operated at the room temperature for practical use, the probability of finding appropriate lasers at 780.0 nm among commercially available lasers are only between 10 - 40 %. Even though an appropriate laser can be found, it often shows the long - term variation of the wavelength. By these reasons, the spectral lifetime, i.e., the time period in which the laser wavelength stays at that of ^{87}Rb - D_2 line, is rather limited. This spectral lifetime is a limiting factor to the performances of a laser - pumped ^{87}Rb atomic clock. However, the detailed investigation has not yet been carried out. The discussion in this section gives a comment on this point.
Figure 19 shows a experimental results of the variation of the range of injection current for stable oscillation of each longitudinal mode, which represents the lifetime of the modes. It is seen that the lifetime of the mode A, oscillated with a lower injection current just above the threshold current, is rather long. On the other hand, those of the modes with higher injection current (modes B $\sim$ E)are quite short. From this result, it may be concluded that it is safer to use the laser with a lower injection current to maintain the spectral lifetime long enough. Furthermore, the variation of the range of these injection currents is not gradual but stepwise, which may induce such a catastrophic phenomenon that a laser-pumped ^{87}Rb atomic clock

suddenly dies. The phenomenon in Fig. 19 is completely different from a popularly observed mode hopping[16]. This could be explained by a temporal decrease of the thermal resistance due to an oxidation of the In bonding layer or by thermal effects due to nonradiative recombinations of carriers near the facets, which has been pointed out also by Fabre and Guen[16]. By this decrease in self-heating, the wavelength change of each mode shows blue shift, which is shown by Fig. 20. Figure 20 shows the variation of the injection current required to tune wavelength of a longitudinal mode to that of the optical transition from F = 1 of ^{87}Rb - D_2 lines. Increase in this injection current means that the laser actually suffers a blue shift. It should be pointed out that this shift is also stepwise. Average of the shift given by this figure was about + 40 MHz/hour. From the discussion presented so far, it may be concluded that the thermal effect is a dominant factor to limit the spectral lifetime of semiconductor lasers.

Further reduction of the thermal resistance can be expected by improving the design of laser structures. We are now trying to fabricate an improved laser for this purpose in cooperation with laser fabricating group, and a prototype of these lasers have been already fabricated[18].

VII. Summary

Recent progress in frequency stabilization and linewidth reduction in semiconductor lasers were presented. From these results, it may be concluded that the semiconductor lasers have a possibility of becoming an ultrahigh coherent light sources by applying electrical feedback technique. These lasers were used for high resolution spectroscopy of ^{87}Rb, and eleven saturated absorption lines were well resolved. The laser-pumped ^{87}Rb atomic clock was constructed, and its stable operation was confirmed. Furthermore, several comments on spectral lifetimes of the laser were given to develop a reliable light source for the atomic clock.

Acknowledgements

We would like to express our gratitudes to Messrs. Kasai, Hashi, Chiba (Fujitsu Co. Ltd.), Prof. Kano (Univ. of Elefctro-Comm.), Dr. Nakayama (Kyoto Inst. Tech.), Prof. Oura, Drs. Kuramochi, and Teramachi (Tokyo Inst. Tech.), for their valuable discussions.

References

[1] M. Ohtsu, H. Tsuchida, and T. Tako, "Frequency Stabilization of AlGaAs Lasers", 36th Annual Frequency Control Symposium, pp. 327 - 337, 1982, Philadelphia

[2] H. Tsuchida, M. Ohtsu, and T. Tako, "Improvements in the Short-Term Frequency Stability of AlGaAs DH Laser", Trans. IECE Japan, vol. E65, pp.65 - 66, 1982

[3] H. Tsuchida, M. Ohtsu, and T. Tako, "Frequency Stabilization of AlGaAs Semiconductor Laser to the Absorption Line of Water Vapor", Jpn. J. Appl. Phys., vol. 21, pp. L1 - L3, 1982

[4] H. Tsuchida, M. Ohtsu, T. Tako, N. Kuramochi, and N. Oura, "Frequency Stabilization of AlGaAs Semiconductor Laser Based on the ^{85}Rb - D_2 Line", Jpn. J. Appl. Phys., vol. 21, pp. L561 - L563, 1982

[5] M. Ohtsu, H. Fukada, T. Tako, and H. Tsuchida, "Estimation of the Ultimate Frequency Stability of Semiconductor Lasers", Jpn. J. Appl. Phys., vol. 22, pp. 1157 - 1166, 1983

[6] S. Saito, O. Nilsson, and Y. Yamamoto, "Frequency modulation noise and linewidth reduction in a semiconductor laser by means of negative frequency feedback technique", Appl. Phys. Lett., vol. 46, pp. 3 - 5, 1985

[7] Y. Yamamoto, S. Saito, and T. Mukai, "AM and FM Quantum Noise in Semiconductor Lasers. Part II : Comparison of Theoretical and Experimental Results for AlGaAs Lasers", IEEE J. Quantum Electron., vol. QE - 19, pp. 47 - 57, 1983

[8] R. Wyatt, "Line-narrowed lasers for coherent optical fiber systems", Proceedings of Conference on Optical Fiber Communication, TUP2, February 11 - 13, 1985, San Diego, California, USA

[9] M. Ohtsu and S. Kotajima, "Linewidth Reduction of a 1.5 μm InGaAsP Laser by Electrical Feedback", Jpn. J. Appl. Phys., vol. 24, pp. L256 - L258, 1985

[10] C. H. Henry, "Theory of the Linewidth of Semiconductor Lasers", IEEE J. Quantum Electron., vol. QE - 18, pp.259 - 264, 1982

[11] T. Okoshi, K. Kikuchi, and A. Nakayama, "Novel method for high resolution measurement of laser output spectrum", Electron. Lett., vol. 16, pp. 630 - 631, 1980

[12] S. Nakayama, "Theoretical Analysis of Rb and Cs D_2 Lines in Saturation Spectroscopy with Optical Pumping", Jpn. J. Appl. Phys., vol. 23, pp. 879 - 883, 1984

[13] S. Nakayama, "theoretical Analysis of Rb and Cs D_2 Lines in Doppler- Free Spectroscopic Techniques with Optical Pumping", Jpn. J. Appl. Phys., vol. 24, pp. 1 - 7, 1985

[14] J. Camparo and R. P. Frueholz, "Linewidths of the 0 - 0 hyperfine transition in optically pumped alkali - metal vapors", Phys. Rev. A, vol. 31, pp.1440 - 1448, 1985

[15] L. L. Lewis and M. Feldman, "Optical Pumping by Lasers in Atomic Frequency Standards", 35th Annual Frequency Control Symmposium, pp. 612 - 624, 1981

[16] M. Ohtsu, Y. Otsuka, and Y. Teramachi,

"Precise measurements and computer simulation of mode-hopping phenomena in semiconductor lasers", Appl. Phys. Lett., vol. 46, pp. 108 - 110, 1985

[17] F. Favre and D. Le Guen, "Emission frequency stability in single - mode - fibre optical feedback controlled semiconductor lasers", Electron. Lett., vol. 19, pp. 663 - 665, 1983

[18] K. Kishino, S. Kinoshita, S. Konno, and T. Tako, "Selective Meltbacked Substrate Inner - Stripe AlGaAs/GaAs Lasers Operated under Room Temperature CW Condition", Jpn. J. Appl. Phys., vol. 22, pp. L473 - L475, 1983

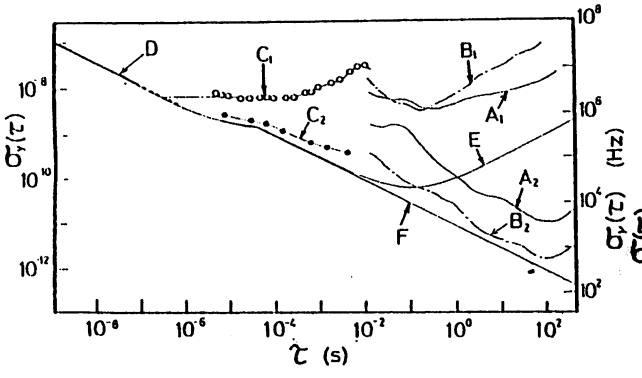

Fig. 1 Summary of the experimental results of frequency stabilization[5].
A_1, B_1, C_1, D : Free-running.
A_2 : Stabilized by H_2O.
B_2 : Stabilized by ^{85}Rb - D_2.
C_2: Stabilized by a rigid Fabry - Perot interferometer.
E : Theoretical limit for the free - running laser (curve F of Fig. 2).
F : Theoretical limit given by spontaneous emission (curve H of Fig. 2)

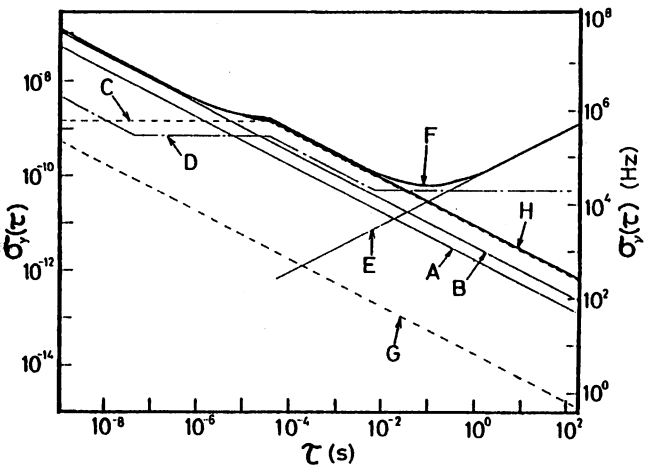

Fig. 2 Calculated results of the frequency stability of a 0.8 μm AlGaAs laser[5].
A : Spontaneous emission noise.
B : Carrier noise.
C : Current noise.
D : Current source noise.
E : Temperature noise.
F : Free-running laser.
G: Detector noise limited value for the stabilized laser.
H : Spontaneous emission noise limited value for the stabilized laser.

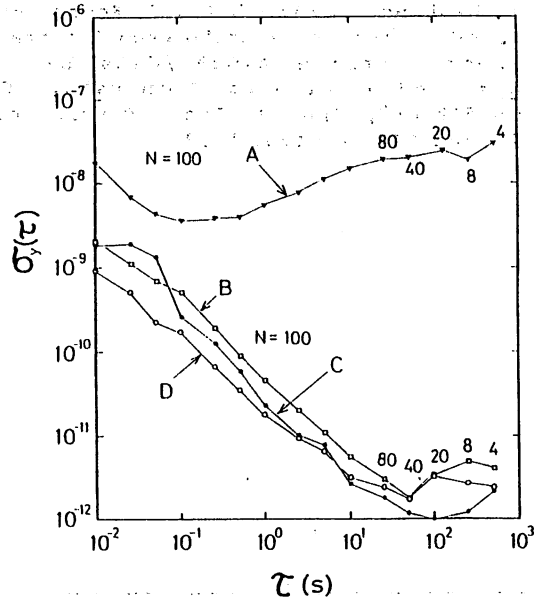

Fig. 3 Results of the frequency stabilization of an AlGaAs laser by using the ^{87}Rb - D_2 line as a frequency reference.
A : Free-running.
B : ^{87}Rb with buffer gases, linear absorption.
C : ^{87}Rb without buffer gases, linear absorption.
D : ^{87}Rb without buffer gases, saturated absorption.

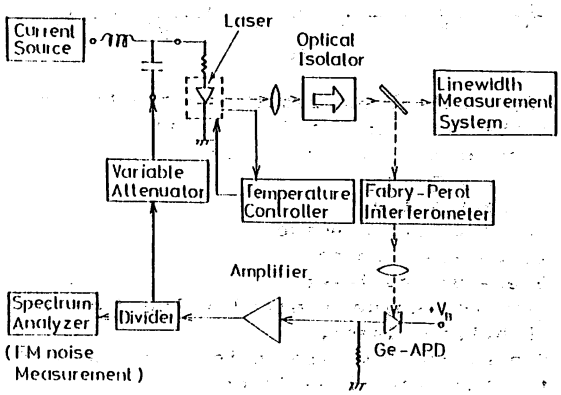

Fig. 5 Experimental apparatus for linewidth reduction of the laser

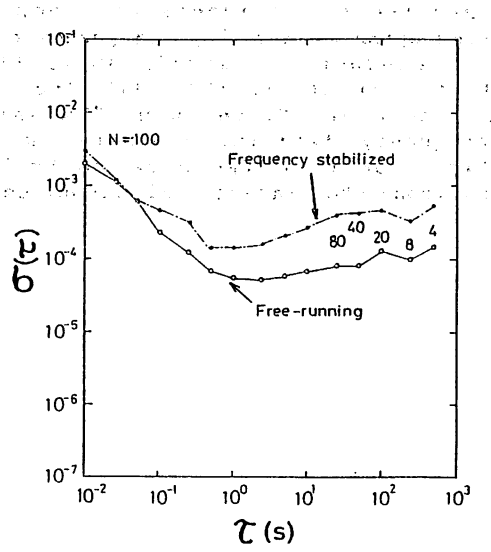

Fig. 4 Stabilities of the laser power when the laser frequency is in free-running and stabilized conditions.

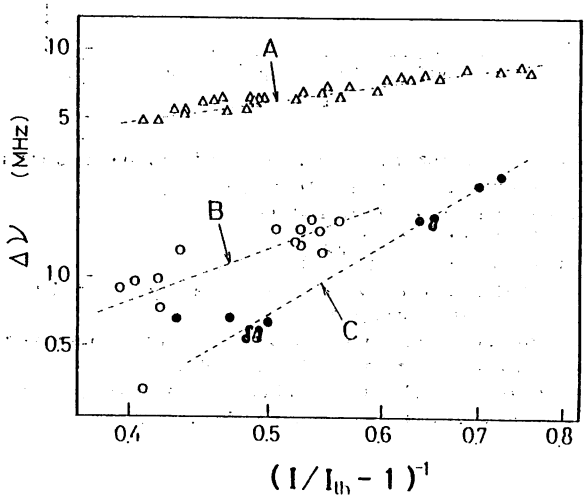

Fig. 6 Experimental results of the linewidth reduction of the laser. I/I_{th} represents the injection current normalized to its threshold value. A : Free-running laser. B, C : Under feedback condition with R_{FP} = 0.9 and 0.95, respectively. R_{FP} represents the reflectance of the Fabry - Perot interferometer in Fig. 5.

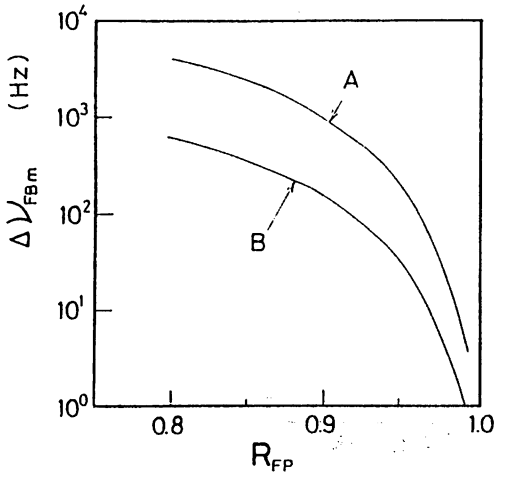

Fig. 7 Estimated minimum attainable linewidth limited by the detector noise in the feedback loop. The curves A and B represent the results when a Ge - APD and Ge - PIN photodiode were used as detectors in the feedback loop, respectively.

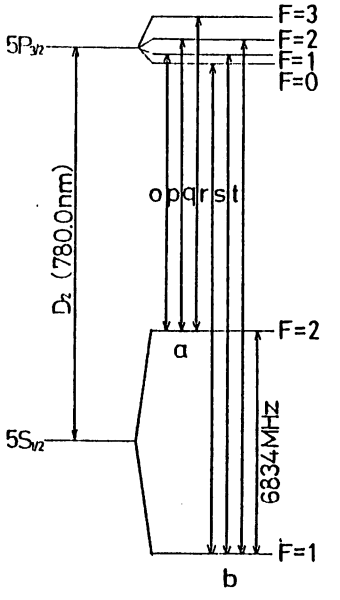

Fig. 8 Energy level diagram of ^{87}Rb atoms.

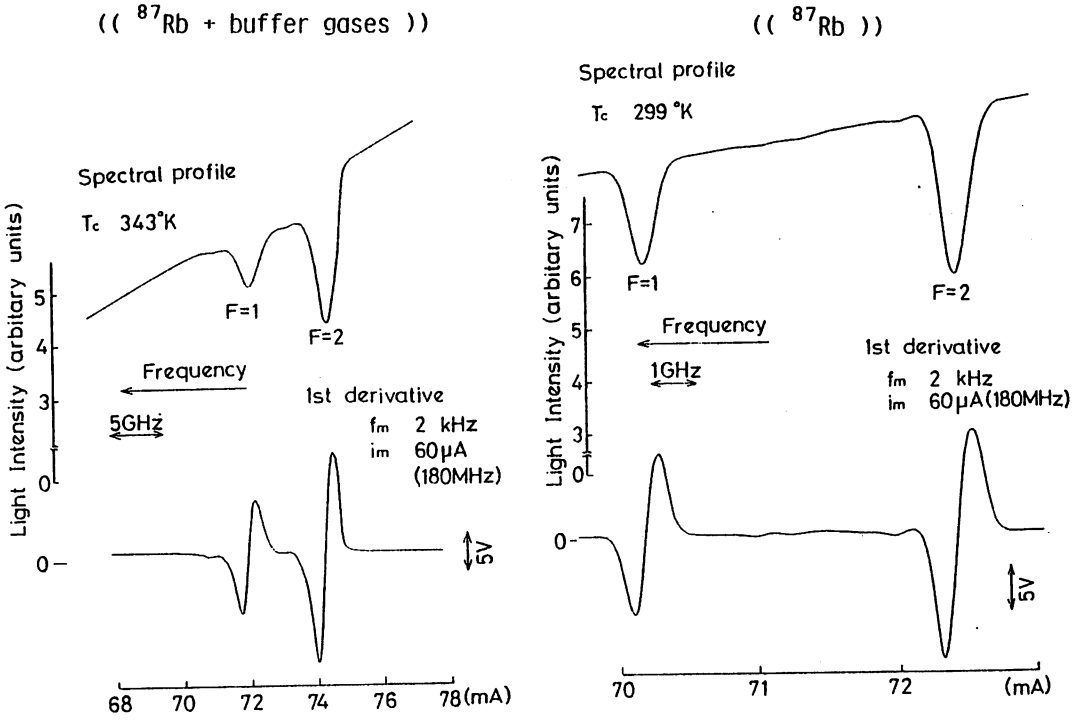

Fig. 9 Linear absorption spectral shapes observed by using ^{87}Rb cells with and without buffer gases.

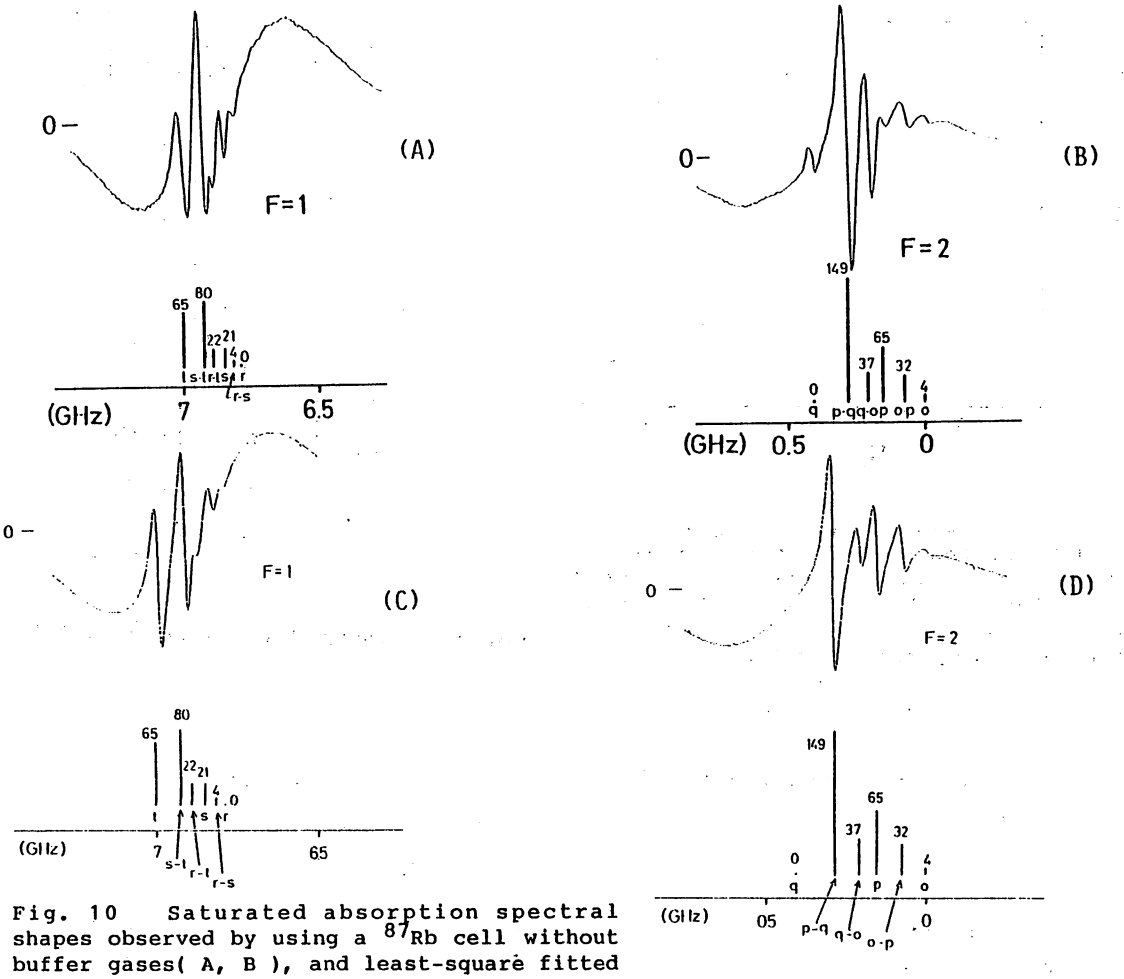

Fig. 10 Saturated absorption spectral shapes observed by using a ^{87}Rb cell without buffer gases(A, B), and least-square fitted curves (C, D).

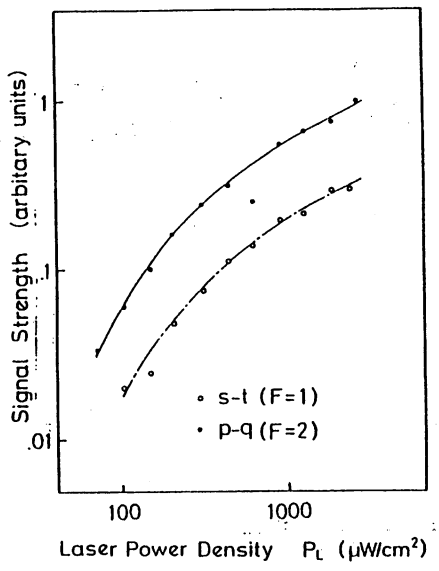

Fig. 11 Dependence of the signal strengths of two cross-resonance lines (s - t, p - q) on the laser power density.

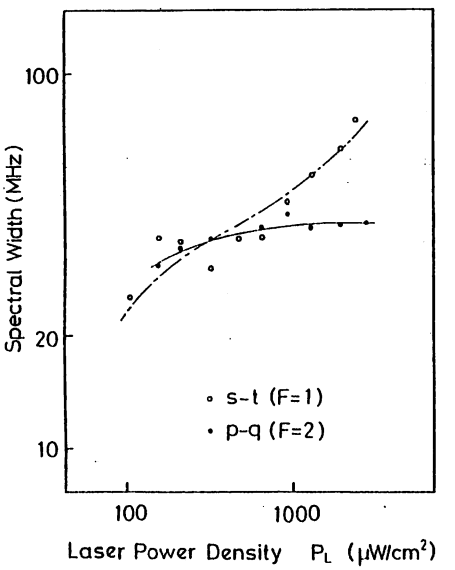

Fig. 12 Dependence of the linewidths of two cross-resonance lines (s - t, p - q) on the laser power density.

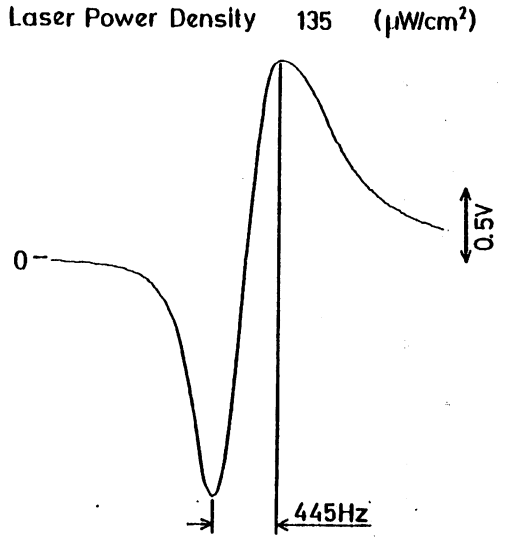

Fig. 13 Derivative of the double resonance signal of ^{87}Rb obtained by using the stabilized laser as a pumping source.

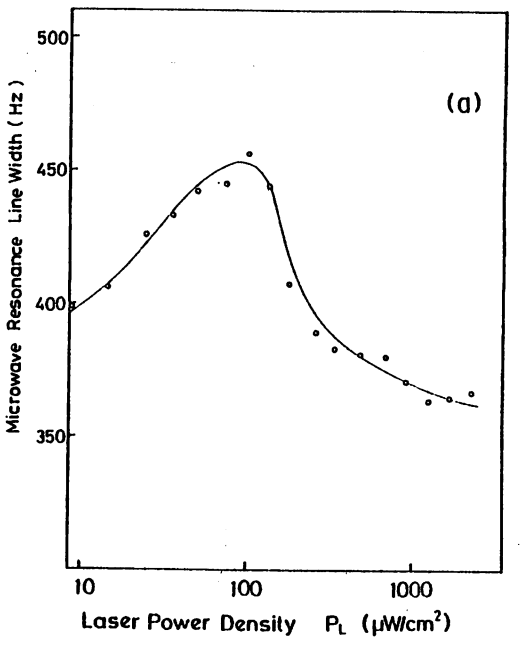

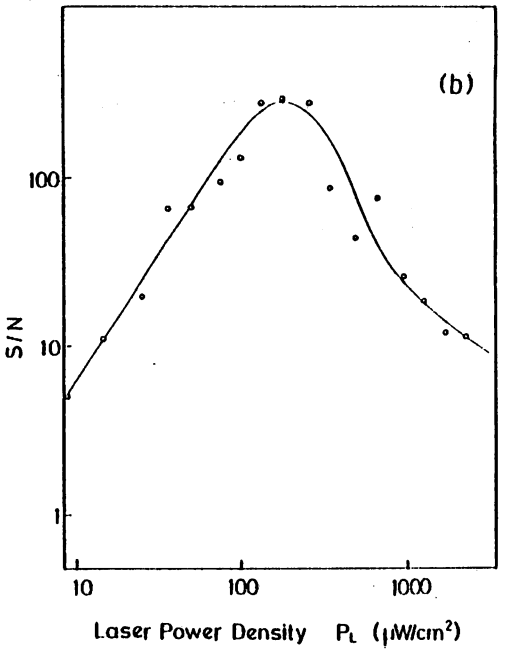

Fig. 14 Dependences of the linewidth (a) and S/N value (b) of the double resonance signal on the laser power density.

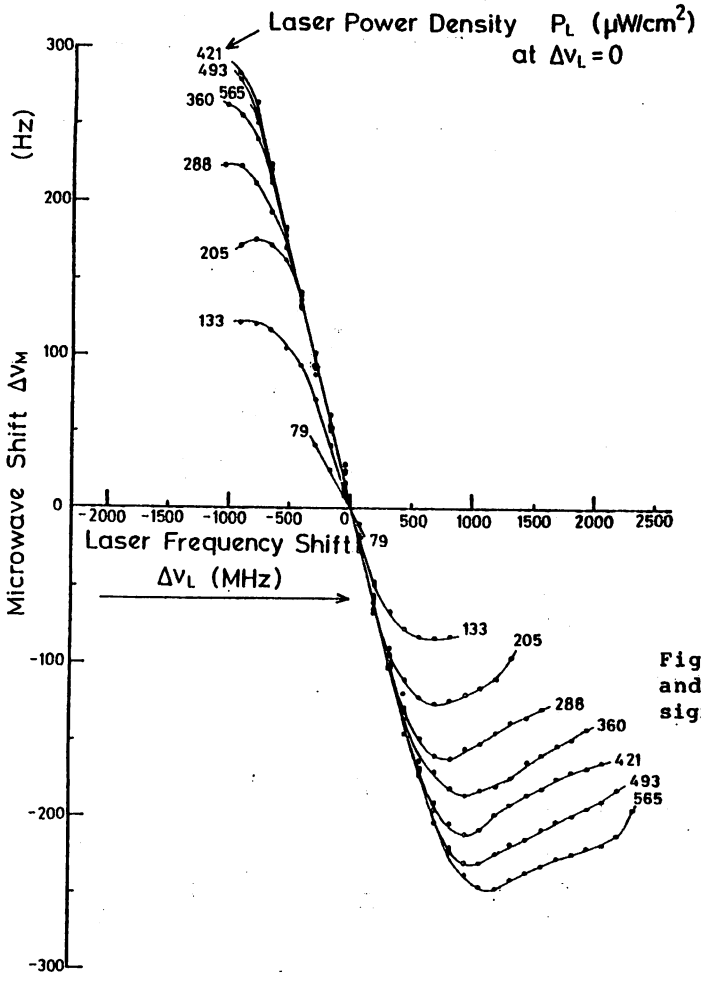

Fig. 15 Shift of the stabilized microwave frequency due to the shift of the laser frequency.

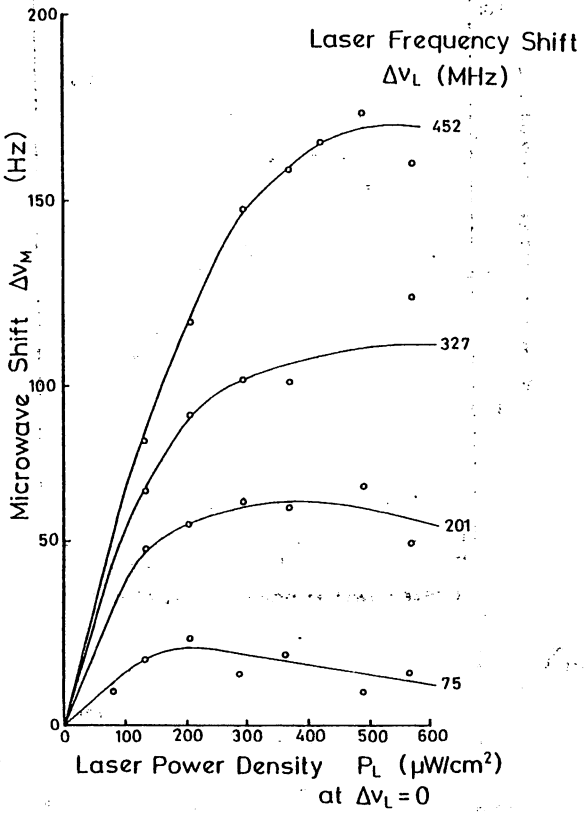

Fig. 16 Shift of the stabilized microwave frequency due to the laser power density.

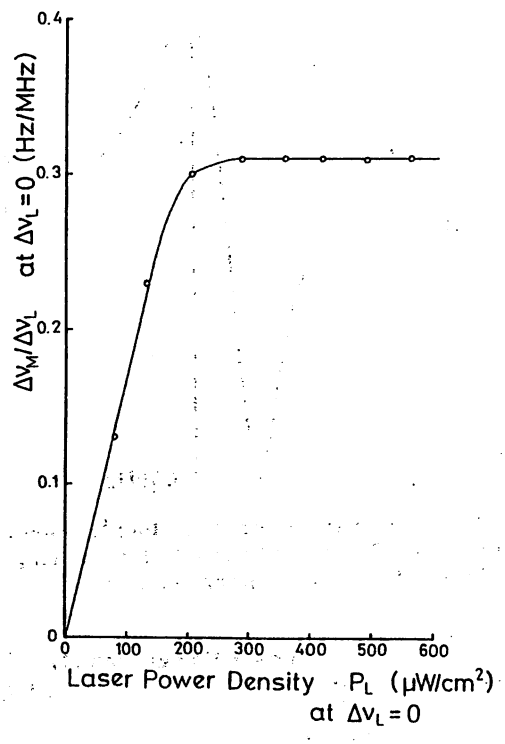

Fig. 17 Slope of the curves of Fig. 15 at $\Delta\nu_L = 0$.

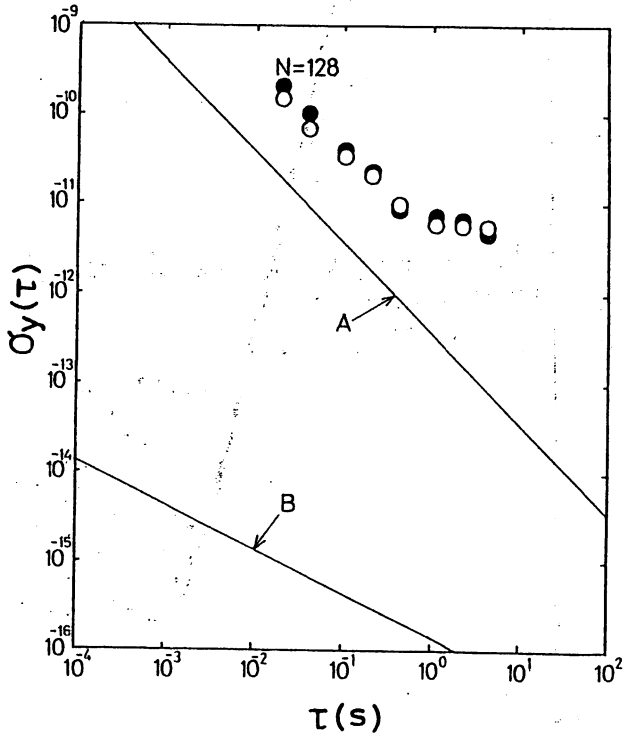

Fig. 18 Frequency stability of the microwave.
A : Contribution of the FM noise of the frequency stabilized laser estimated by using the curve B of Fig. 3 and Fig. 17.
B : Contribution of the FM noise of the laser obtained by using the curve G of Fig. 2 and Fig. 17.
O : Experimental results of the laser-excited ^{87}Rb atomic clock.
● : Experimental results of the conventional ^{87}Rb atomic clock.

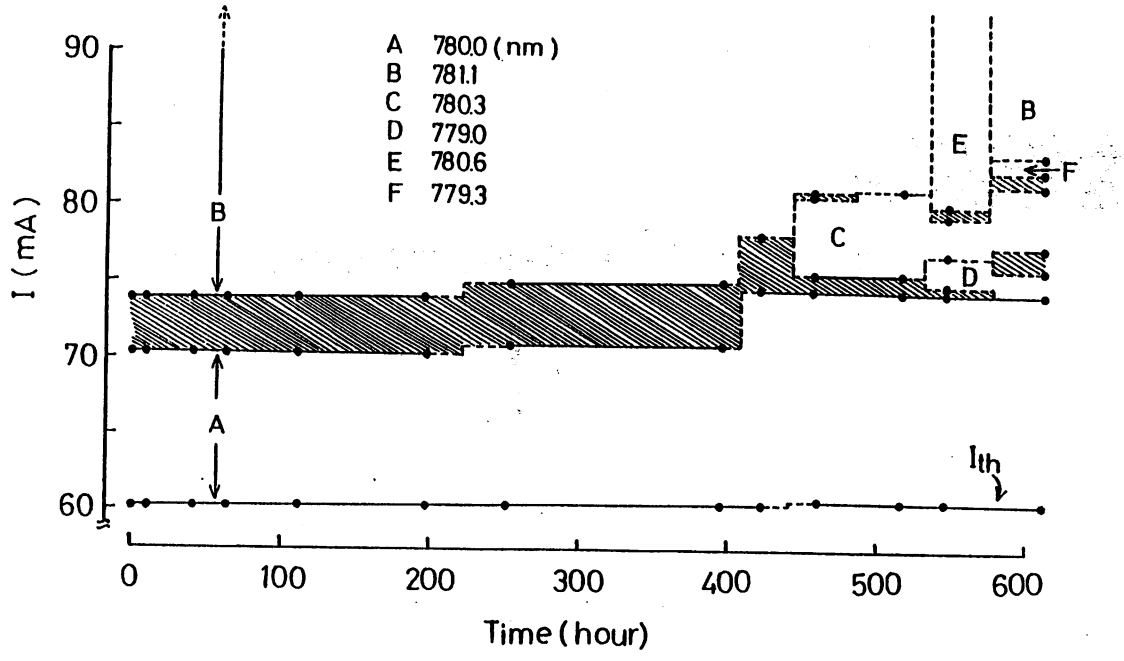

Fig. 19 Spectral lifetimes of longitudinal modes (A - F) of the laser. Hatched area represents the area of multi-longitudinal mode oscillation.

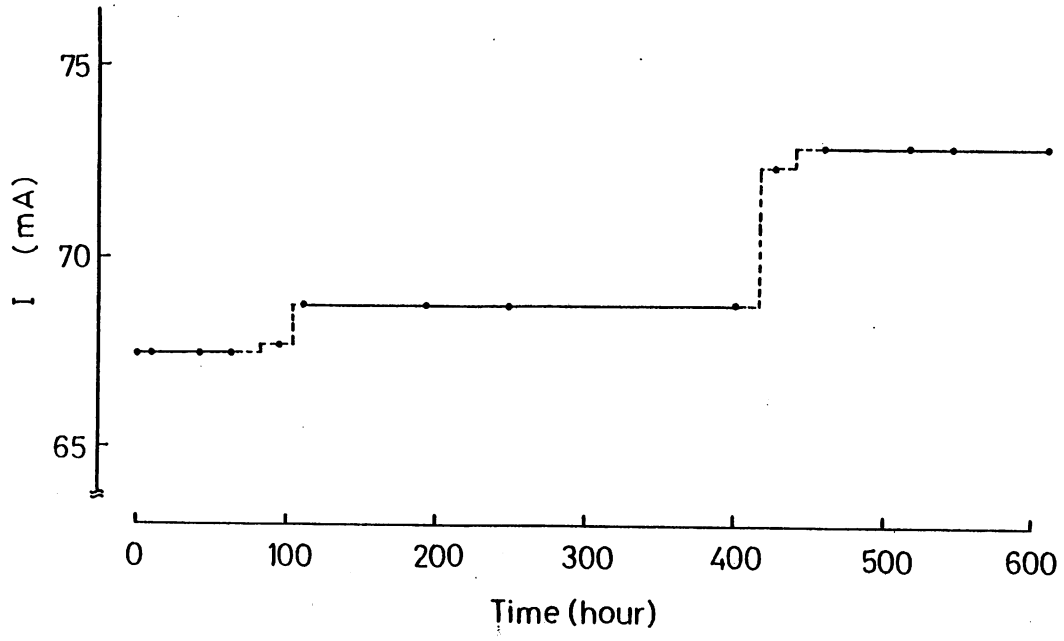

Fig. 20 Variation of the injection current required to tune the wavelength of a longitudinal mode to that of the optical transition from F = 1 of ^{87}Rb - D_2 lines.

総説と解説

レーザー周波数安定度，再現性向上のための分光的手法

大津元一*・田幸敏治**

* 東京工業大学理工学国際交流センター　東京都目黒区大岡山 2-12-1（〒152）
** 東京工業大学精密工学研究所　神奈川県横浜市緑区長津田町 4259（〒227）

（1983年8月8日受理）

Spectroscopic Technique to Improve the Stability and Reproducibility of Laser Frequencies

Motoichi OHTSU* and Toshiharu TAKO**

* International Cooperation Center for Science and Technology, Tokyo Institute of Technology, 2-12-1, Ō-okayama, Meguro-ku, Tokyo 152
** Research Laboratory of Precision Machinery and Electronics, Tokyo Institute of Technology, 4259 Nagatsuta-cho, Midori-ku, Yokohama-shi, Kanagawa 227

(Received August 8, 1983)

1. まえがき

レーザーの出現以後すでに20年以上を数えるが，この光源をその時間的コヒーレンスの良さを利用した研究，たとえば高分解能分光，精密光学計測などに用いるとき，必ずしも周波数の安定度が十分高いとはいえない場合に出会うことが多く，周波数の安定化を施して用いる必要が生じる．さらにレーザーを光領域の周波数標準として用いるような場合には必然的に周波数安定度の向上をめざすことが要求される．このように周波数安定化はレーザーの時間的コヒーレンスの良さを引き出し，向上させ，コヒーレント光源の特長を生かした応用には不可欠な技術としてレーザーの出現当初から研究が開始され，安定度は着実に向上している[1]．現在までに気体レーザー，半導体レーザーといった連続発振レーザーに対し周波数安定化が試みられ，その安定度は 1×10^{-14} に達している[1]．今後，周波数安定化に要求される事項としては安定度の向上，すなわち周波数変動の抑圧のみならず，安定化されたレーザー周波数の値の再現性の向上，位相安定度の向上などが挙げられる．また，近年，連続発振色素レーザーの性能が著しく向上し，すでに数多くの高分解能レーザー分光に用いられているが，その際可視域の任意の波長値において周波数を安定化する必要があることなどから波長可変レーザー，さらにまた短波長レーザーの周波数安定化が必要となる．

これらの周波数安定化に使用しうる周波数基準としてはファブリ・ペロー干渉計，原子・分子スペクトルなどがあるが，上記のように安定度，再現性の向上のためにはこれらのスペクトルの中心周波数値を精度よく見出すことが必要である．さらに波長可変レーザーの周波数安定化に必要な数多くの原子・分子スペクトルの強度は必ずしも大きくないことがあり，微弱な信号を高感度かつ高分解能で測定し，周波数基準として用いる必要がある．このように考えると周波数安定化は高分解能レーザー分光の進歩と密接な関係があり，高分解能レーザー分光における新しい手法のうちのいくつかは周波数安定化に応用しうる．また，こうしてレーザーの周波数安定度が向上すると，これを光源として用いた高分解能レーザー分光の分解能，感度の向上が期待される．周波数安定化に応用しうる高分解能レーザー分光の手法としては補助的なレーザーを必要としないこと，実時間でスペクトル測定可能なこと，さらにサブ・ドプラー分光と同等かそれ

以上の分解能を有し高感度であることなどを満たすことが必要である．そこで本稿では今後の周波数安定化のために応用可能な分光的手法について概説することを目的とする．従来の飽和吸収分光法を応用した安定化法に加え，近年，光の偏光特性を利用したり，マイクロ波技術との類推による分光技術が開発されつつあり，これらは周波数安定化や精密光学計測にも応用しうる分光法であるという意味合いから Precision Spectroscopy と呼ばれ，急速な進歩を示している[2]．本稿は将来の周波数安定化の展望としてこれらの各手法のもつ独創性を重視して述べる．

レーザーの周波数を安定化するには Fig. 1 (a) のような周波数基準となるスペクトルの中心周波数 ν_0 をまず正確に見出さなければならない．そのためには方法 (I) として同図 (b) のように (a) の微分に相当する曲線を求めてその横軸との交点を精度よく見つけるのが一つの方法である．(a) のスペクトルとして周波数安定化に用いられているのは一般に原子・分子の飽和吸収スペクトルであり簡便な安定化の場合には原子分子の線形吸収スペクトル，ファブリ・ペロー干渉計の共振スペクトルが用いられる．他方，分光研究の手法の主流ともいうべき方法 (II) としてまず同図 (c) のようにスペクトル測定の分解能を向上させて (a) よりも幅のせまいスペク

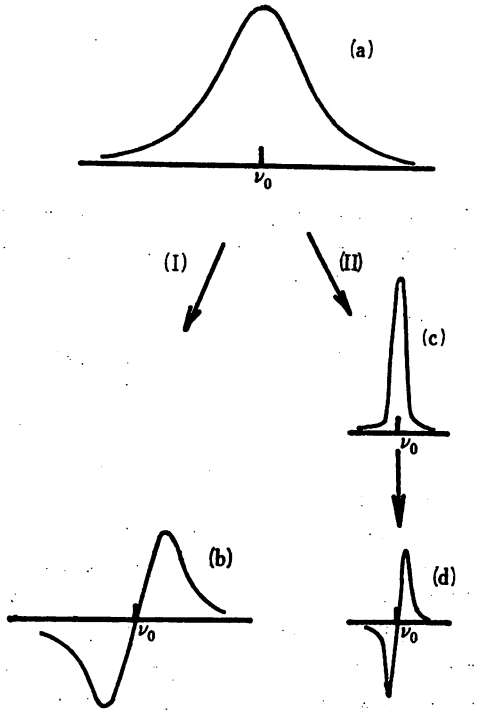

Fig. 1. 周波数基準となるスペクトルの共鳴周波数を見出す二つの方法
(I) (a) のスペクトルから (b) のように周波数弁別特性を有する分散形の信号を得る．
(II) (a) のスペクトルよりも幅のせまいスペクトル (c) を得る．その後必要に応じて (I) と同様に (c) から分散形の信号 (d) を得る．

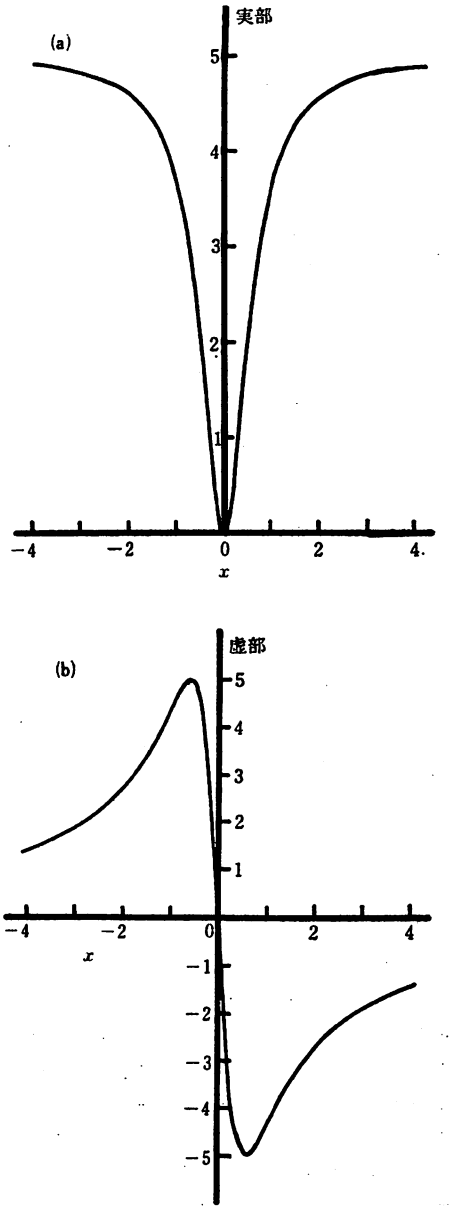

Fig. 2. ファブリ・ペロー干渉計からの反射光の電場の実部 (a) と虚部 (b) の周波数依存性．ここで横軸の x はレーザー周波数のファブリ・ペロー干渉計の共振周波数からの離調度を表わす．

トルを得る工夫をし，その後 (d) のように (c) の微分を求めて ν_0 を見出す方法がある．現在までのところ原子・分子の飽和吸収スペクトルのような線幅のせまい周波数基準を用いる場合には方法（I）が多く行なわれ周波数安定化への応用可能性も高まりつつあるのでこれについて 2，および 3 で述べる．方法（II），すなわち飽和吸収スペクトルよりさらに幅のせまいスペクトルを得ようとする試みについてはまだ信号の S/N 値が小さく実時間測定が困難な段階であるが周波数安定度向上のための有望な技術であるので 4 で略記する．

Fig. 1 (a) に相当する周波数基準としてのファブリ・ペロー干渉計も原子・分子内のエネルギー準位間の遷移もいずれも光と共鳴相互作用するものであるから，これらと相互作用後の光の電場は，これら周波数基準に関する情報を担っている．一例としてまずファブリ・ペロー干渉計からの反射光の電場振幅のうち入射光と同位相成分，$\pi/2$ 位相差の生じた成分，すなわち複素表示の場合の実部，虚部の周波数依存性を Fig. 2 (a) (b) に示す．ここで虚部の値はファブリ・ペロー干渉計の共振周波数値において 0 とおり，電子回路における FM 復調器出力の周波数特性と同様に鋭い周波数弁別特性を有することがわかり，これをレーザー周波数安定化の際の弁別器として使うことができる．ファブリ・ペロー干渉計からの透過光の電場振幅はこのような分散形の周波数弁別特性は示さない．一方，原子・分子と相互作用後の光の電場の特性から原子・分子についての情報を得るには相互作用後の光電場の位相おくれ，減衰量を測定すればよく，これはこの光に対する原子・分子の屈折率，吸収率を測定することに相当する．両者は光により原子・分子中に誘起される分極の大きさを表わす複素感受率 $\chi(\nu)$ の実部 $\chi'(\nu)$，虚部 $\chi''(\nu)$ に比例する．ローレンツ形のスペクトルの場合を例にとると

$$\chi(\nu)\propto\frac{1}{(\nu-\nu_0)+i\gamma} \qquad (1)$$

と表わせる．ここで ν はレーザー周波数，ν_0 は原子・分子の遷移周波数，γ は横緩和定数である．(1) 式より

$$\chi'(\nu)\propto\frac{(\nu-\nu_0)}{(\nu-\nu_0)^2+\gamma^2} \qquad (2)$$

となり $\chi'(\nu)$ は Fig. 2 の場合と同様，周波数弁別特性を有することがわかる．本稿の 2，3 ではこのような周波数弁別特性を有する信号を光学技術，マイクロ波技術を活用して精度よく測定する方法を記すものである．Table I に本稿で記す各方法を分類して示す．

Table I　本論文の構成

手法 ＼ 周波数基準	（I） スペクトル共鳴周波数の探索		（II） スペクトルの狭帯域化
	光学技術（偏光，干渉）	マイクロ波技術(周波数変，復調)	
ファブリ・ペロー干渉計	**2.1.** 偏光，干渉を利用した反射光の位相おくれ測定[8,5]	**3.1.** 周波数変，復調による反射光の位相おくれ測定[2]	
原子，分子	**2.2.** 偏光分光法[13,15-18]	**3.2.** 周波数変調分光法[2,29,30]	**4.** 超自然幅分光[33,34,40,41]
	とじこめられたイオンをレーザーで冷却[42-44]		

2. 光学技術を利用する方法

2.1. 周波数基準がファブリ・ペロー干渉計の場合

本章ではレーザー光のもつ偏光，干渉などの光学的特性を利用して周波数安定化のための周波数弁別特性を有する信号を得る方法について記すが，まず本節ではそのうちとくに周波数基準としてファブリ・ペロー干渉計を用いる場合について示す．この周波数基準は原子・分子のスペクトルを用いる場合より安定度は劣るが装置が簡単なこと，波長可変レーザーにも使用可能なことから従来比較的よく用いられている．従来の方法ではファブリ・ペロー干渉計の透過スペクトルを測定し，レーザー周波数を変調して透過スペクトルの微分曲線を求め，その周波数弁別特性を利用して共振周波数値にレーザー周波数を安定化するか，または無変調のまま透過スペクトル曲線の肩の位置に安定化することが一般的であった．前者の方法では信号検出に同期検波方式を使うため制御帯域がせまいこと，また，スペクトルの微分曲線のすそ引きが少ないため，色素レーザーに見られるように何らかの外乱によりレーザー周波数が跳び，一度制御がはずれると，そのはずれが生じたことを認識することが困難であることが欠点である．一方，後者の方法では干渉計の

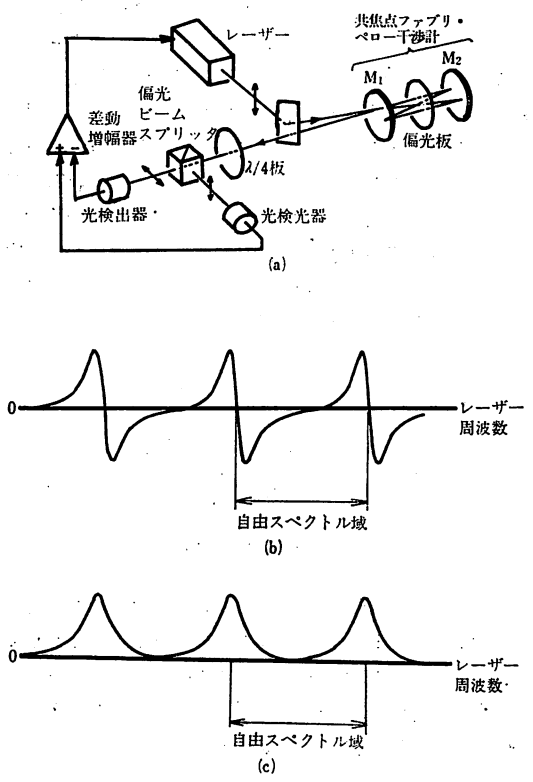

Fig. 3. 偏光板を光路内に含むファブリ・ペロー干渉計を周波数基準とする周波数安定化の方法[3]
(a) 実験装置 (b) 本方法により得られたファブリ・ペロー干渉計からの反射光の共振スペクトル．自由スペクトル域は 2 GHz．(c) 透過光の共振スペクトル．

フィネスが低いとき制御利得が小さいことや，干渉計の光軸のずれ，および光強度変動により周波数安定度がわるくなることなどが欠点である．

これらを克服するために提案されている一つの方法を Fig. 3 に示す[3]．この方法ではファブリ・ペロー干渉計からの透過光ではなく反射光を用い，かつその偏光特性を利用している．すなわち，ファブリ・ペロー干渉計の中に偏光板を置けば，偏光板の主軸の方向と平行な偏光成分に対し，これはフィネスの高い干渉計として動作するのでこの偏光成分の光は干渉計内で多重反射して，一部は干渉計を通過し，一部は反射される．一方これと垂直方向の偏光成分に対してはこの干渉計は高い損失を示す．この成分は鏡 M_1 で単に反射されるのみであるので，この反射光と上記の平行方向偏光成分の反射光との合成光の偏光状態は，光の周波数が干渉計の共振周波数に一致しているときは直線偏光，高周波または低周波側にあるときは左まわりまたは右まわりの楕円偏光になる．この楕円偏光の向きを図中の λ/4 板，偏光ビームスプリッタ，二つの光検出器と差動増幅器によって符号を含めて検出すると，レーザー周波数に対して Fig. 3 (b) のように周波数弁別特性を有する信号が得られる．これを用いればレーザー周波数を変調することなく干渉計の共振周波数の値にレーザー周波数を安定化することが可能である．この方法は簡単な装置で無変調安定化ができること，得られるスペクトル曲線のすそ引きがなだらかであるため，制御がはずれた場合にもそれを認識でき，回復のための操作を施すことが可能であることなどの利点を有する．一方，欠点としては使用する二つの光検出器の感度差によりスペクトル波形がひずみ，真の共振周波数に安定化できない場合があること，干渉計の中の偏光板により干渉計のフィネスが減少し，制御利得が小さくなること，偏光板の熱膨張，機械的振動により共振周波数が変動することなどが挙げられる．この方法は色素レーザーに適用され，レーザー発振スペクトル線幅が数 MHz 以下まで減少している[3]．

このように，ファブリ・ペロー干渉計からの反射光を周波数安定化に用いることはすでにマイクロ波発振器の周波数安定化で行なわれている方法の類推になっている．すなわち Pound は周波数基準用共振器からの反射電場の振幅の虚部は周波数弁別用の信号として理想的であると指摘し，マイクロ波発振器の周波数安定化に応用している[4]．本章での議論はこの方法の光領域への拡張と考えることができる．

Fig. 3 の方法に対しレーザーの周波数をやはり変調することなくファブリ・ペロー干渉計の真の共振周波数に安定化する試みを Fig. 4 に示す[5]．Fig. 3 の場合と同様，ファブリ・ペロー干渉計からの反射光を利用するものである．Fig 4 においてファブリ・ペロー干渉計と図の上方の鏡 1，ビームスプリッタ 1 によりマイケルソン干渉計が構成されている．光検出器 1 によりマイケルソン干渉計による干渉じまが測定できる．その光強度 I_1 は

$$I_1=I_0+I_{RC}+2\sqrt{I_0}[\cos\theta\cdot\mathrm{Re}(E_{RC})+\sin\theta\cdot\mathrm{Im}(E_{RC})] \quad (3)$$

である．ここで I_0 はマイケルソン干渉計の二つの光路のうち鏡 1 で反射される方の光の強度である．I_{RC}, E_{RC} はファブリ・ペロー干渉計からの反射光の強度と，その光電場の振幅を表わす．また，$\theta=2\pi z/\lambda$ であり，z はマイケルソン干渉計の二つの光路の光路長差，λ は光の波長である．Re, Im は複素数の実部，虚部を表わす．ここで光検出器 2 によって (3) 式中の I_0+I_{RC} に相当する光強度を差し引き，かつ，光軸にそった鏡 1 の位置，

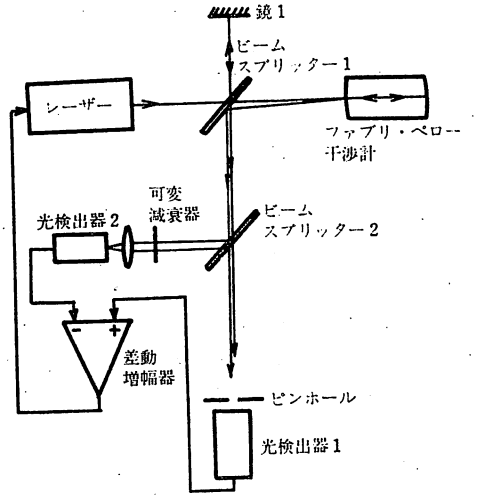

Fig. 4. 周波数基準用ファブリ・ペロー干渉計からの反射光を用いた周波数安定化の方法[5]．マイケルソン干渉計を構成する方法ではこの図の装置を使う．モード不整合のファブリ・ペロー干渉計を使う場合には図中の鏡 1 は不要である．

すなわち光路長差 z を調整して $\theta=90°$ とすれば (3) 式中の $\mathrm{Im}(E_{RC})$ に比例した信号が得られる．この信号は Fig. 2 (b) に示したものにほかならず，この周波数弁別特性を用いれば，ただちにファブリ・ペロー干渉計の共振周波数の値にレーザー周波数を安定化できる．この方法の原理は以上のとうりであるが実際にはいくつかの困難が付随する．すなわち，例えば θ の値が 90° からずれた場合 (3) 式からもわかるように $\mathrm{Im}(E_{RC})$ に $\mathrm{Re}(E_{RC})$ が加算され周波数弁別特性を有する信号波形は歪み，共振周波数値に安定化することが不可能になり再現性および安定度の劣化を生ずる．θ の値の調節のためには z の値を波長の値以内の精度で調整する必要があり，これは実際には容易ではない．

そこで，より実際的な方法がさらに提案されている[5]．すなわち Fig. 4 の方法で得られたような干渉じまをモード不整合のファブリ・ペロー干渉計を用いて得ようというものである．Fig. 4 中のファブリ・ペロー干渉計として，入射光に対しモード不整合のものを用意する．この場合には同図中の鏡 1 は不要であり，マイケルソン干渉計を構成する必要はない．このファブリ・ペロー干渉計にレーザー光を入射すると TEM_{00} モードと共に高次の横モードが発生する．簡単のためにそれを TEM_{01} モードとする．両モードの光によって光検出器 1 の受光面上で干渉じまが観測されるが，レーザー周波数が TEM_{00} モードに対するファブリ・ペロー干渉計の共振周波数付近にあり TEM_{01} モードのそれから遠くはなれているとき TEM_{01} モードの振幅，位相はほとんど周波数依存性をもたない．従って (3) 式において I_0 がこの TEM_{01} モードの光強度に相当する．一方，TEM_{00} モードは (3) 式中の I_{RC}, E_{RC} に相当するもので，先にマイケルソン干渉計を用いた場合と同様，光検出器 1 で干渉じまが観測できる．しかし，今の場合 θ の値が先の場合と大きく異なる．すなわち，TEM_{00} モードと TEM_{01} モードの光の位相差はファブリ・ペロー干渉計の TEM_{00} モードのビームウェストと光検出器 1 との距離を z' として

$$\theta=\arctan(\lambda z'/\pi w_0^2) \qquad (4)$$

と表わされる．ここで w_0 はビームウェストにおける TEM_{00} モードのスポットサイズである．(4) 式中 $\pi w_0^2/\lambda$ はファブリ・ペロー干渉計の長さと同程度の値をとる．すなわちたとえば共焦点形の干渉計の場合，これは干渉計の長さ 1/2 の値になる．これによると θ の値を 90° に設定するためには z' の値に要求される精度は先のマイケルソン干渉計を構成する場合の z の設定精度にくらべはるかにゆるやかになるので $\mathrm{Im}(E_{RC})$ に比例する信号のみを精度よく測定することが可能になり，真の共振周波数値に安定化することができる．実験では色素レーザーの安定化に応用し，フリーランニング時の周波数変動値 50 MHz（積分時間 10 秒において）をこの方法により 0.5 MHz まで減少させている．この方法の利点は θ の値を 90° に設定し，周波数弁別特性を有する信号を純粋に光学的手法のみを用いて得ているため，装置が簡単なことである．欠点としては (3) 式中の I_0+I_{RC} の値を I_1 の値から正確に差し引く際の光検出器 2 の感度調整の誤差により信号に一定のオフセットが加わって真の共振周波数値に安定化されない可能性が残ることである．

2.2. 周波数基準が原子・分子の場合

周波数基準として安定な原子・分子スペクトルを用いればファブリ・ペロー干渉計の場合よりさらに高い周波数安定度を実現しうる．安定度を向上させるのみでなく周波数基準となる原子・分子スペクトルの真の共鳴周波数値にオフセットのないよう安定化し，安定化されたレーザー周波数値の再現性をも向上させようとする試みはまず 3.39 μm He-Ne レーザーに対してなされた[6]．従来の一般的な方法ではレーザー共振器内に置かれた吸収セル内の CH_4 気体の飽和吸収スペクトルを周波数基準として用いて安定化を行なっていた[7]．この場合，飽和吸収スペクトルはレーザー出力同調曲線の頂上付近に現われるが，周波数弁別特性をもつ信号を得るためにこのスペクトルの一次微分信号を測定すると，その信号には

レーザー出力同調曲線の傾斜の大きさに比例したオフセット量が加わり，レーザー周波数は真の共鳴周波数とは異なった値に安定化される．このオフセット量はスペクトルの三次微分を周波数弁別に用いればほぼ完全に消去しうるはずである．しかし実際には飽和吸収が生じるときに同時に現われる飽和分散，すなわち CH_4 の屈折率の周波数依存特性のためにこのオフセット量は依然として残る[6]．さらにこのオフセット量はレーザー光強度のドリフト，レーザー共振器外の各光学素子からの反射光による微弱なファブリペロー共振現象などにより時間とともに変化するため，再現性のみでなく，長期の安定度も低下する．これらについての理論的研究が Titov により行なわれている[8]．

従来の方法ではこのように飽和分散の影響で形の歪んだ飽和吸収スペクトルを測定していたことが再現性，さらに長期安定度の低下をひきおこしていたので，これらを向上させるために Fig. 5 に示す方法が提案された[6]．

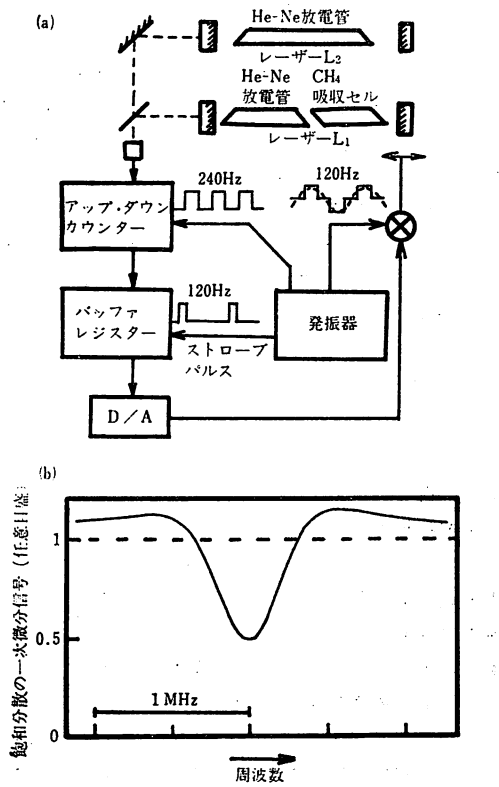

Fig. 5. CH_4 の飽和分散のスペクトルを周波数基準として用いた 3.39 μm He-Ne レーザーの周波数安定化の方法[6]．
(a) 実験装置．L_1；安定化対象のレーザー L_2；ビート測定用の局部発振器としてのレーザー (b) CH_4 の飽和分散の一次微分信号．

この方法では飽和吸収ではなく飽和分散を測定しその信号曲線の傾きの最も急峻な位置にレーザー周波数を安定化する．飽和分散は CH_4 の飽和吸収スペクトルの位置における周波数と波長との関係に他ならないのでそれを測定するには局部発振器としてのレーザー L_2 と安定化を施そうとする対象のレーザー L_1 との間のビート周波数の値を，レーザー L_1 の共振器長の値に対して測定すればよい．実際の測定では共振器長を変調しながら同図 (b) に示すように飽和分散の一次微分を測定し，その中心周波数にレーザー周波数を安定化している．この方法では飽和分散の信号は飽和吸収の影響をうけることなく独立に分離測定可能であり，その中心周波数は真の共鳴周波数に等しい．この方法で安定化した結果，積分時間10秒以上の長期の安定度が従来の飽和吸収による結果よりもよくなっている．すなわちたとえば積分時間 100 秒において安定度は 2×10^{-13} であり，これはレーザー L_1 に対し飽和吸収による方法で安定化した場合の安定度よりも約10倍よい．さらに，この方法により安定化されたレーザーの再現性は 1 kHz 以内であり従来方法よりも 10 倍以上よい値になっている．この方法の利点は真の共鳴周波数を求められることである．そのために飽和吸収ではなく飽和分散を用いているが，これは **2.1.** のファブリ・ペロー干渉計の場合において，透過光ではなく反射光を測定し，その信号のもつ周波数弁別特性を利用して真の共鳴周波数を見出すことに対応している．欠点としては飽和分散の測定のために補助的なレーザー (Fig. 5 のレーザー L_2) を必要とするので装置が複雑になることが挙げられる．

Fig. 5 の例のように原子・分子の分散特性はその屈折率の周波数依存性に他ならないから，**1** でも述べたように，その情報は原子・分子と相互作用したレーザー光の位相にたくわえられるはずである．従ってそれを測定するには原子・分子と相互作用後の光の偏光状態の変化を調べるのが一つの方法である．この目的に使うことができ，かつ周波数安定化にも十分使用可能な分光法としては Wieman と Hänsch によって提案されている偏光分光法がある[9]．この分光法についてはすでに和文の解説がなされているが[10] 原理は Fig. 6 に示すように円偏

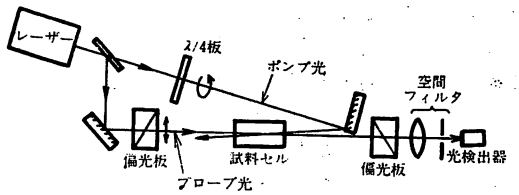

Fig. 6. 偏光分光法の実験装置[9]．

光の強いポンプ光によって試料気体中に生じた飽和分散を反対方向から入射する直線偏光のプローブ光によって検出するものである．すなわち，ポンプ光によって生じた光誘起円複屈折性によってプローブ光である直線偏光を構成する左右円偏光間に位相差が発生するので，その位相差に対応するプローブ光の偏光状態の変化量を測定する．これは従来の飽和吸収測定時に同時に生ずる飽和分散を零位法で測定するものであり，レーザーの AM 雑音による S/N 値の低下を防ぎ高感度で信号検出が可能である．同様な方法として干渉分光法[11]，さらに，一方の光の偏光状態を変調して高感度に飽和吸収を検出する偏光相互変調励起分光 (POLINEX 分光) が提案されており[12]，いずれも高感度でドプラーフリースペクトルを測定できる方法として周波数安定化への応用可能性を有するものである．偏光分光法は Ar^+ レーザーの周波数安定化に応用された例があり，I_2 の飽和分散信号の中心周波数に安定化した結果，積分時間 10 秒で約 2×10^{-13} の安定度が得られている[13]．この方法は高感度にドプラーフリースペクトルが測定可能で，周波数弁別特性を有する飽和分散が得られるため，レーザー周波数を変調することなく安定化できるところに利点を有する．しかし一方 Fig. 9 の二枚の偏光板主軸方向間の角度が 90° からずれると，得られる飽和分散の信号波形に飽和吸収の信号波形が重畳されるために波形歪みが生じ，真の共鳴周波数の値に安定化できない欠点を有する．さらにまた，Fig. 6 の方法では，ポンプ光がレーザー共振器に戻りレーザー発振状態を乱して AM, FM 雑音を増大させるのを防ぐために，ポンプ光とプローブ光とは互いに平行状態から若干ずらす必要がある．すると，得られるスペクトルの幅は，このずれの角度に比例した残留ドプラー幅だけさらに広くなり，周波数安定化時の安定度，再現性の低下をひきおこす．

この残留ドプラー幅を消去するために吸収セルをレーザー共振器内に設置する，いわゆる内部共振器形偏光分光法が提案され[14]，また，さらに簡単な装置による内部共振器形偏光分光法の提案と周波数安定化への応用に関する実験，および理論的研究が筆者らによってなされた[15-17]．この方法の原理を Fig. 7 に示す．これは Fig. 5 の場合と同じく CH_4 のスペクトルを周波数基準として用いて 3.39 μm He-Ne レーザー周波数を安定化するための実験である．Fig. 7 (a) に示すようにレーザー共振器内の位相板により楕円偏光の定在波が CH_4 と相互作用する．レーザー共振器内の定在波を構成する右向きの進行波がポンプ光として働き CH_4 の円複屈折性を誘起する．これを左向きの進行波をプローブ光として測

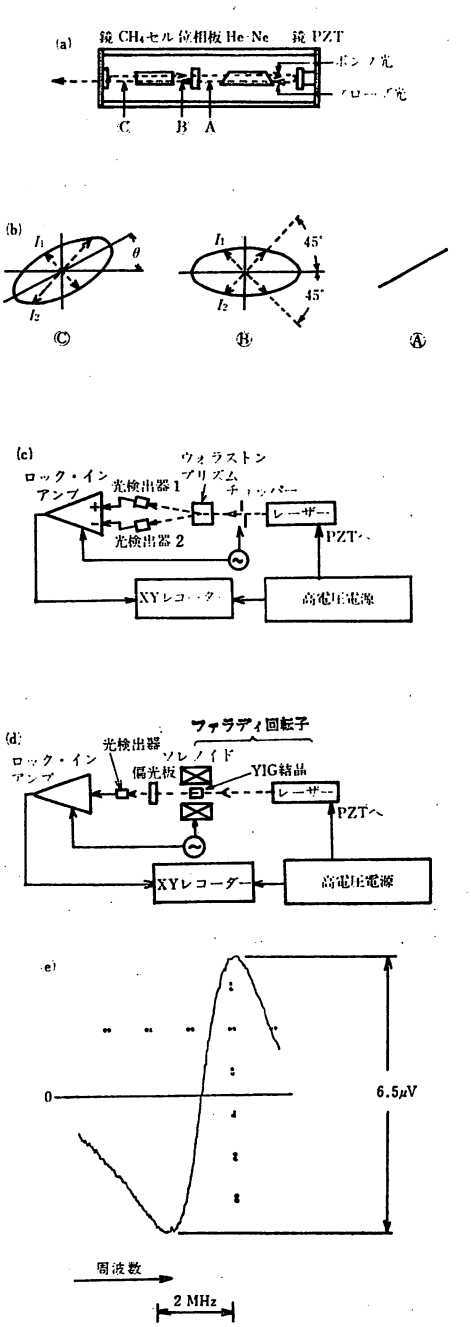

Fig. 7. 内部共振器形偏光分光法による 3.39 μm He-Ne レーザーの周波数安定化の方法[15-17]
(a) レーザー共振器の構成．(b) レーザー共振器内の各位置における レーザー光の 偏光状態．(c) (b) 中の光強度成分 I_1 と I_2 との差を測定する第一の方法．(d) I_1 と I_2 との差を測定する第二の方法．(e) (c) の方法により得られた CH_4 の飽和分散の信号．

定する．それにはこの光誘起円複屈折性によるプローブ光の楕円偏光主軸の方向変化を同図 (c) のようにウォラストンプリズムと二つの光検出器により測定すればよく，これにより同図 (e) のような飽和分散を検出することができる．この飽和分散の信号を周波数基準としてレーザー周波数を安定化した結果，積分時間200秒で 1.1×10^{-12} の安定度が得られた[15]．この方法ではポンプ光とプローブ光の非平行による残留ドプラー幅が完全に消去できること，この飽和分散の信号の周波数弁別特性を用いればレーザー周波数を変調することなく安定化できること，さにレーザー共振器の構成は従来の飽和吸収による安定化の場合に対し，位相板を付加するのみでよく簡単であること，レーザー共振器用の右側の鏡からの出力を測定すると従来の飽和吸収の信号が得られ，従来方法でも安定化ができ，新しい方法によって得られた周波数安定度の評価ができることなどの利点を有する．

一方，欠点としてはウォラストンプリズムの光軸のずれや二つの光検出器の感度差が生じたとき，飽和分散の信号に飽和吸収の信号が重畳されて信号波形が歪み，真の共鳴周波数に安定化できない点がある．これを改良するために，同図 (d) のように信号検出系としてファラディ回転角が時間的に正弦振動するフデァラィ回転子と光検出器一つを用い，さらにレーザー光強度も同時に安定化することが試みられ積分時間200秒で 3.3×10^{-13} の安定度が得られた[17]．この方法では Fig. 5 の場合と同様飽和分散が測定できるので，飽和吸収の場合の場合よりも真の共鳴周波数を見出すことは容易であり，これに伴なって長期の周波数安定度を飽和吸収による安定化の結果よりも向上させることが可能である．そこで飽和分散によって真の共鳴周波数をさらに精度よく見出し長期安定度を向上させるために信号検出系を改良し，かつ飽和分散の二次微分信号を測定してその中心周波数に安定化することを試みた結果，積分時間70秒以上では飽和吸収を用いた安定化の結果よりも安定度が約3倍向上していることが確認された[18]．以上の例により **2.1.** のファブリ・ペロー干渉計の反射光を利用する場合と同様，原子・分子のスペクトルからの分散信号を周波数安定化に利用することは安定度，再現性の向上の点で有利であることがわかる．しかし分散信号を原子・分子と相互作用後の光の位相の変化量を通して検出する場合，信号検出用の光学素子の光軸のずれなどにより真の共鳴周波数を精度よく見出すことがやや困難になる可能性がある．これは **2.1.** の最後に記した問題と同一である．

3. マイクロ波技術を利用する方法

3.1. 周波数基準がファブリ・ペロー干渉計の場合

2.1. の例のように光学的方法により周波数弁別特性を有する分散形の信号を得る方法に対しマイクロ波技術を用いて電気的方法により得るものが提案された[2]．その原理を Fig. 8 に示す．これは **3.2.** で述べる周波数変調分光法と同じ手法によるものであり，**2.1.** の例より実験装置は複雑になるが，より精度よく真の共鳴周波数の値を見出し，それに安定化しうるものである．レーザー周波数を変調器により数 MHz の変調周波数で変調し，周波数基準用ファブリ・ペロー干渉計に入射させる．その反射光を偏光プリズムと $\lambda/4$ 板によって光検出器1の方向へ送り，この検出器により周波数変調をうけた光の搬送波成分と高周波側第一側波帯との間のビート，および搬送波と低周波側第一側波帯との間のビートを同時測定する．もし搬送波の周波数がファブリ・ペロー干渉計の共振周波数と一致しているとき，上記の両ビート信号の位相差は π であり，互いに打ち消し合い光検出器出力は生じない．しかし，もし搬送波周波数がファブリ・ペロー干渉計の共振周波数と一致していない場合には両ビート間の位相差は π からずれるので，光検出器1からは符号も含めて，この差異に比例した強度のビート信号出力が得られる*．すなわちレーザー周波数とファブリ・ペロー干渉計の共振周波数の差に対して Fig. 2 (b) と同じく分散形の周波数弁別特性を有する信号が得られるのでこれを安定化に用いることができる．これは **2.1.** に示した Pound によるマイクロ波発振器の安定化方法の類推から得られた方法で，Drever が重力波検出用レーザーの周波数安定化に用いていることから Pound/Drever 安定化法とも呼ばれている[2]．この方法の利点はもちろんファブリ・ペロー干渉計の共振周波数が高精度で測定できることであるが，さらにレーザー光強度変動による信号測定の際の S/N 値の低下を抑えられるという利点も有する．すなわち一般にレーザー光強度変動量，AM雑音のパワースペクトル密度の値はフーリエ周波数の増加とともに減少するため，変調周波数の値を大きく設定すればAM雑音の影響を抑圧することができる．この方法で 633 nm He-Ne レーザーと 633 nm 色素レーザーとを同一のファブリ・ペロー干渉計を周波数基準として同時に周波数安定化し，これら異種レーザー間のビート信号を測定して，その周波数雑音 100 Hz

* これらの議論をより定量的に行なったものが **3.2.** の式 (5)～(8) である．ここでの議論もこれらの式を流用して行なえるがここでは略す．

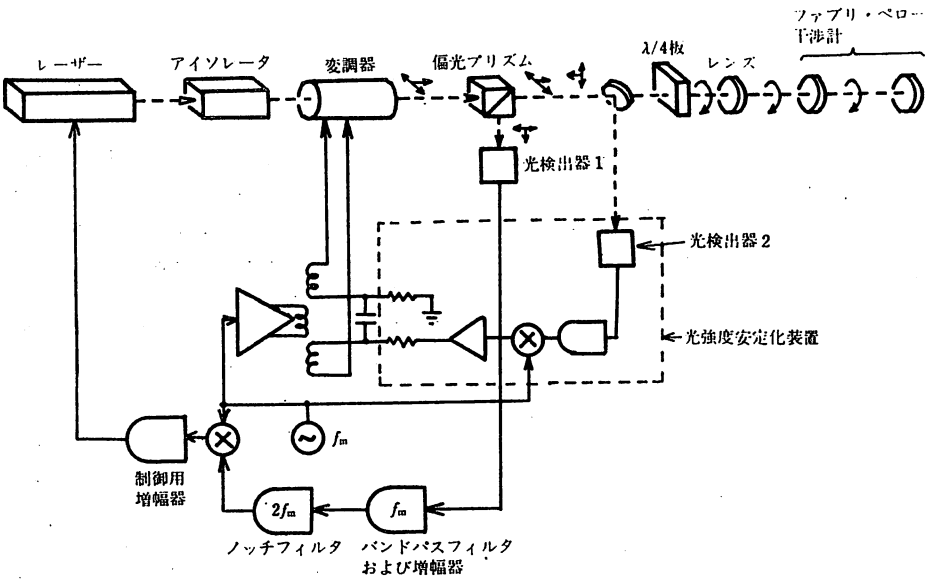

Fig. 8. レーザーの周波数変調により生じた側波帯を利用し，周波数基準となるファブリ・ペロー干渉計からの反射光を検出する方法による周波数安定化の装置[2].

以下，スペクトル幅 60 Hz といった非常に高い安定度が達成されたことを確認した．この実験で用いた色素レーザーのAM雑音はフーリエ周波数 2 MHz 以上でショット雑音によって決まる最小値に達するため，変調周波数は 2 MHz 以上の値に設定されている．Fig. 8 ではさらに同時に破線で囲まれた装置によってレーザー光強度も安定化している．これを併用することにより安定化されたレーザー周波数の，ファブリ・ペロー干渉計の共振周波数からのずれはファブリ・ペロー干渉計の共振スペクトル幅の値の 1/100 以内に留まり，非常によい精度で真の共振周波数に安定化されていることがわかる[2]．この方法では実験装置が **2.1.** の例の場合にくらべて複雑であるが安定度，再現性の点では優れたものである．この方法は受動リングファブリ・ペロー干渉計を用いたレーザージャイロスコープにも応用されており[19]，また，測定される信号曲線の形についての理論的な研究も報告されている[20]．

3.2. 周波数基準が原子・分子の場合

3.1. でファブリ・ペロー干渉計に対して用いたマイクロ波技術を原子・分子のスペクトル測定に適用し，その真の共鳴周波数を **2.2.** の場合よりもさらに高い精度で見出そうとする試みが報告されている．IBM のグループにより提案されたその周波数変調分光法の原理を Fig. 9 に示す[21]．変調器によりレーザー周波数を変調して原子・分子の試料気体に照射する．図のように変調前，変調後のレーザ光電場をそれぞれ $E_1(t)$, $E_2(t)$ とするとそれは次のように表わせる．

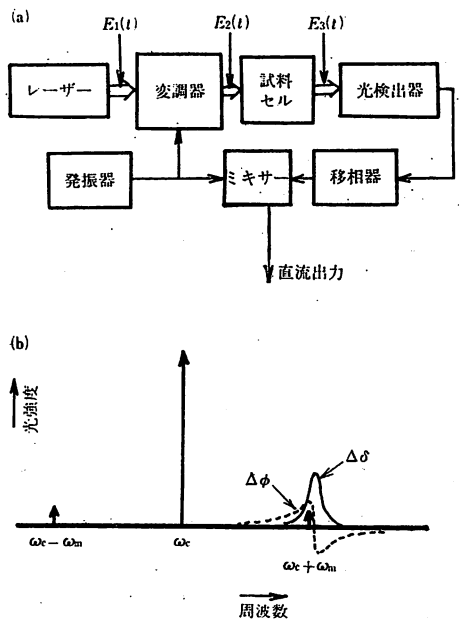

Fig. 9. 周波数変調分光法[21]
(a) 実験装置 (b) 周波数変調をうけたレーザーの周波数分布および (8) 式中の $\Delta\delta$, $\Delta\phi$ のスペクトル波形．

$$\left.\begin{aligned} E_1(t)&=\frac{1}{2}E_0\exp(i\omega_c t)+\text{c.c.}\\ E_2(t)&=\frac{1}{2}E_0\sum_{n=-\infty}^{\infty}J_n(M)\cdot\exp[i(\omega_c+n\omega_m)t]+\text{c.c.}\end{aligned}\right\}\quad(5)$$

ここで E_0 は振幅，ω_c, ω_m は搬送波角周波数，変調角周波数，J_n はベッセル関数，M は変調指数，c.c. は複素共役を表わす．ここで $M\ll1$ として変調による第一次の側波帯のみを考えると，原子・分子気体透過後の電場は

$$E_3(t)=\frac{1}{2}E_0\left[T_0e^{i\omega_c t}+T_1\frac{M}{2}e^{i(\omega_c+\omega_m)t}-T_{-1}\frac{M}{2}e^{i(\omega_c-\omega_m)t}\right]\quad(6)$$

と書ける．ここで $T_n=\exp(-\delta_n-i\phi_n)$ であり $n=\pm1$ をとる．$\delta_n(=\alpha_nL/2)$ は角周波数 $\omega_c+n\omega_m$ における原子・分子の吸収による光電場振幅の減衰率，$\phi_n(=\eta_nL\cdot(\omega_c+n\omega_m)/c)$ は位相おくれを表わす．また，α_n, η_n は原子・分子の吸収係数，屈折率，L, c は吸収セル長，光速度である．原子・分子気体を透過した後の光を二乗検波特性を有する光検出器によって受光し，搬送波成分と $n=\pm1$ に相当する側波帯の間のビート，すなわち ω_m の成分を検出するとその出力信号は

$$I_3(t)=A\cdot e^{-2\delta_0}[1+(\delta_{-1}-\delta_1)M\cos\omega_m t+(\phi_1+\phi_{-1}-2\phi_0)\cdot M\sin\omega_m t]\quad(7)$$

となる．ここで A はレーザー光強度に比例する定数である．もし ω_m の値が原子・分子のスペクトル幅より十分小さいときは (7) 式の余弦成分が吸収の一次微分，正弦成分が分散の二次微分の値を近似的に表わすことは (7) 式からただちにわかるが，これはすでに波長変調分光法として知られている方法の原理である[22]．ここでは逆に ω_m の値を原子・分子のスペクトル幅より大きくとり，高周波側側波帯 ($n=+1$) のみを原子・分子スペクトルに同調する．そのとき低周波側側波帯 ($n=-1$) および搬送波成分はこのスペクトルとは十分離調しており δ_{-1}, δ_0 および ϕ_{-1}, ϕ_0 は周波数に依存しない一定値とみなせるので，これらを $\bar{\delta}$, $\bar{\phi}$ と表わす．そして $\Delta\delta\equiv\delta_1-\bar{\delta}$, $\Delta\phi\equiv\phi_1-\bar{\phi}$ とすると (7) 式より

$$I_3(t)=Ae^{-2\bar{\delta}}[1-\Delta\delta M\cos\omega_m t+\Delta\phi M\sin\omega_m t]\quad(8)$$

を得る．すなわちこの式の余弦成分は高周波側側波帯に対する原子・分子の吸収を，正弦成分は分散を与える．従って位相敏感検波により正弦成分を測定すれば分散の信号を独立にとり出せ，その信号のもつ周波数弁別特性を用いてレーザー周波数を安定化することが可能である．(5) または (6) 式からもわかるように原子・分子がない場合には搬送波と高周波側側波帯との間のビートの位相は，搬送波と低周波側側波帯との間のビートのそれに対し π ずれているので互いに打ち消し合い光検出器の ω_m 成分出力は生じない．しかし原子・分子があるとそれによる吸収と分散のために高周波側側波帯の振幅に減衰，位相おくれが生じて両ビート間のつり合いがくずれ，光検出器出力に ω_m 成分の信号が現われる．それが (8) 式で与えられるものであり，このように本方法は零位法であるため高感度に信号検出ができる．また，(8) 式の余弦，正弦成分に位相同期をとるとき同時に用いられるマイクロ波用移相器は精度が高いので，吸収または分散の信号のみを高精度に分離してとり出すことができる．この精度は **2.2.** の偏光分光法における分散信号のとり出しのための偏光板の主軸方向調節精度よりも十分高く，真の共鳴周波数を見つけやすい．さらに **3.1.** にも述べたように変調周波数の値が大きいのでレーザーAM雑音の影響をうけにくいこと，高速測定が可能なことなどの利点を有する．色素レーザーを 440 MHz の変調周波数で変調し I_2 の線形吸収スペクトルを測定する実験では 0.005% の吸収量まで検出可能であるという高い感度を示している[21]．また，この方法は高感度，かつ高速であることから波長 607 nm の NaF の色中心のゼロフォノン線の光化学的ホールバーニングをパルス光により本方法を用いて測定することが試みられ[23]，5 ns 程度の時間内でスペクトル測定が可能になっている[24]．このホールバーニングは光メモリーとしての応用が検討されている[25]．また，本方法は二光子分光法[26]，励起分光法[27]へも適用されている．さらに半導体レーザーの周波数は注入電流により高速の直接変調が容易に行なえることからこの方法を半導体レーザーを光源として適用する試みも報告されている[28]．

Fig. 9 に示す装置では線形吸収および分散のみが測定されることになるが，同じ IBM のグループによってこの方法を飽和吸収，分散測定に用いる試みが色素レーザーを光源とし I_2 を試料分子気体として報告されている[29]．また，このグループとは独立に，かつ同時期に JILA* において同様の方法による飽和吸収，分散測定の試みが報告された．光領域でのヘテロダイン飽和分光法と名付けられているが原理は周波数変調分光法と同じである．しかし IBM のグループにくらべ，より周波数安定化への応用可能性を重視しており精密な実験を行なっ

* Joint Institute for Laboratory Astrophysics, National Bureau of Standards and University of Colorado, USA

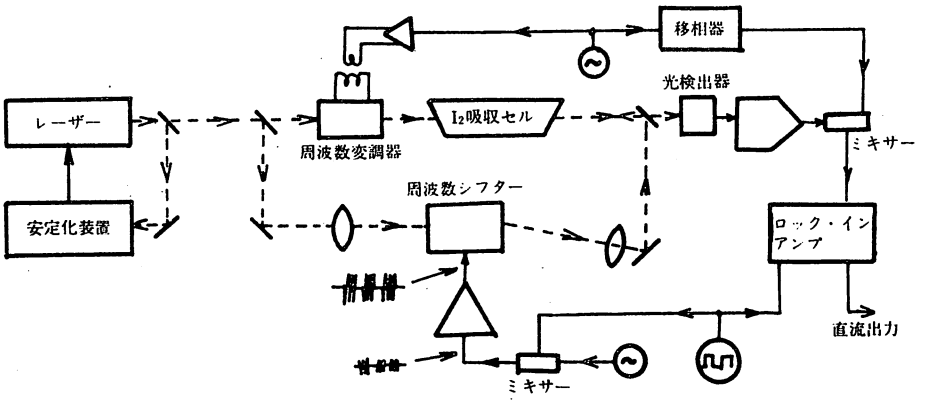

Fig. 10. ヘテロダイン飽和分光法による I_2 の飽和吸収，飽和分散測定の装置[2,30]

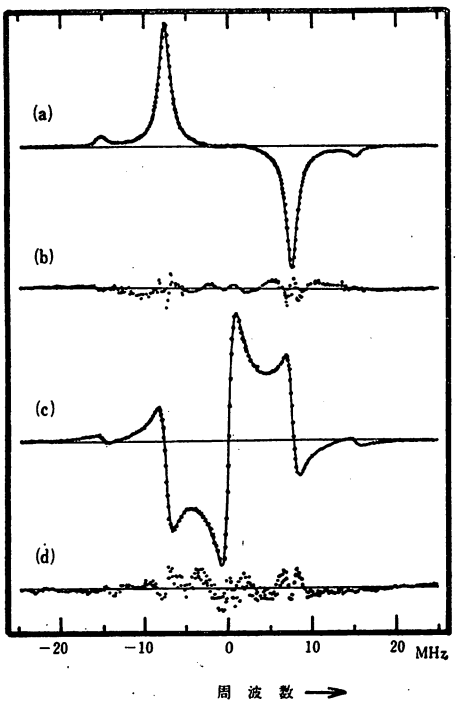

Fig. 11. Fig. 10 の実験装置による測定結果[2,30]
(a), (b)；飽和吸収，飽和分散のスペクトル．これらの図中，各点は測定値，実線は計算値である．
(b), (d)；(a), (c) 中の測定値に対する計算値のあてはめの際の残差．両図のたて軸は (a), (c) のたて軸の寸法の 5 倍に拡大されている．

ている．その装置を Fig. 10 に示す[2,30]．これもやはり色素レーザーを光源とし I_2 の飽和吸収，分散を測定するためのもので図中 I_2 の吸収セルを左方向に通過する光はポンプ光として働く．この光は周波数変調をうけていないが，この光がレーザー共振器に戻ってレーザー発振状態を乱すことを避けるために音響光学効果による周波数シフターにより周波数を一定の値 (80 MHz) だけずらしている．右向きの光はプローブ光として働き電気光学効果による変調器により周波変調されている．変調周波数値はレーザーAM雑音がショット雑音レベルまで低下するフーリエ周波数値より大きく設定して測定の高感度化をはかっている．ここではそれを 15 MHz としている．強いポンプ光によって生じた I_2 の飽和吸収，分散を，このプローブ光の搬送波，高周波側，低周波側側波帯の間のビート信号によって測定する．すなわち (7) 式と同じくビート信号の余弦成分が飽和吸収を，正弦成分が飽和分散を与える．Fig. 11 にその測定結果を示す．Fig. 9 の場合と異なり，ここでは搬送波周波数を広帯域掃引することによりプローブ光の搬送波，両側波帯のすべてを順次 I_2 スペクトルに同調させている．同図 (a) は飽和吸収の測定結果であり，吸収線中心より変調周波数の値の 1/2 はなれた位置，すなわち ±7.5 MHz のところに現われているピークはプローブ光の二つの側波帯を飽和吸収線にそれぞれ同調させ，これを測定した結果である．両ビートの位相差が π であるため，これらのスペクトルの符号も互いに逆になっている．プローブ光の搬送波が飽和吸収線に同調した場合，高周波，低周波側側波帯とのビート信号の余弦成分が打ち消し合うため図の中心周波数の位置には信号が現われていない．これは (7) 式で余弦成分の振幅が $\delta_{-1}-\delta_1$ になっていることに相当する．これに対し同図 (c) は飽和分散の測定結果であり，この場合にはプローブ光の搬送波，高周波，低周波側側波帯のそれぞれが順次 I_2 スペクトルに同調した場合，ビート信号の正弦成分が現われる．(7) 式の正弦成分の振幅が $\phi_1+\phi_{-1}-2\phi_0$ に比例しているのに相当し，図中 ±7.5 MHz における信号曲線の符号は等しく，

0 Hz におけるその符号はこれらとは逆で，かつこれらの値の2倍の値になっていることがわかる．また，これらの図中の各点は測定結果，実線はスペクトルをローレンツ形と仮定して実験値にあてはめたものである．(b) (d) はそれぞれ (a) (c) の曲線あてはめの際の残差を示したもので，これらの図のたて軸は (a) (c) のそれらの5倍に拡大されており，実験値と理論値とは高い精度で一致していることがわかる．この理由としては測定が高感度であると同時に，前述のように (7) 式の余弦，正弦成分を独立にとり出すためのマイクロ波移相器として高精度のものが容易に得られることが挙げられる．Fig. 11 (c) の信号を周波数弁別に用いれば真の共鳴周波数が精度よく求められる．さらにここで Fig. 9 の場合にくらべ有利な点としては前述のように飽和吸収の信号は中心周波数付近には現われないので，移相器による位相調整の精度が低下しても飽和分散の信号の中心周波数値が飽和吸収の影響により真の共鳴周波数からずれないことである．このようにして歪みの小さい周波数弁別特性を有する信号が得られ，共鳴周波数をこの飽和分散のスペクトル幅の値の 1/500 以内の精度で見出すことができて，これに安定化したレーザー周波数値の再現性を約 1 kHz 以内に抑えられることが実験的に確かめられている[2,30]．このヘテロダイン飽和分光法についての理論[20]，プローブ光のかわりにポンプ光を周波数変調する実験方法[31]，また，4波混合過程によりプローブ光，ポンプ光のうち一方の周波数変調をうけた光から他方の非変調の光への変調の移乗についての理論[32]が報告されており，周波数安定度，再現性の向上を目的とした研究とともに，高感度，高分解能の分光研究としての関心が高まっている．

4. スペクトルの狭帯域化による方法

原子・分子の共鳴周波数を精度よく見出す方法として **2.2**，**3.2** では Fig. 1 の方法 (I) についての試みが記述された．もう一つの方法 (II) として同図の (a) から (c) へと進む方向，すなわち，まず，より狭い幅のスペクトルを得ようとするやり方が考えられる．**2.2.**，**3.2.** の例ではスペクトルの幅を狭くする工夫はなされておらず，得られた最も狭い幅は飽和吸収によって実現しうる自然幅であった．従って自然幅の値以下の距離内で近接した二本以上のスペクトルを高分解能測定するための方法は何ら与えていない．すなわちスペクトル中心周波数の値が精度よく決定されたとしても分光的に興味ある情報（超微細構造の存在など）を何ら与えないという意味では分光研究上やや不満足な方法であるという感がある．これに対しさらに幅を狭くするための方法として近年超自然幅分光の報告がなされている．その一例として空間的に分離されたレーザー光束と原子・分子との相互作用を利用する光ラムゼイ分光が試みられており[33,34]，すでに多くの方法が提案され[35-37]，得られるスペクトル幅は可視域で数 10 kHz に達している[38]．このスペクトルを周波数安定化のための周波数基準として用いれば，安定度，再現性の向上が期待しうるのが明白であるが，現在のところ信号の S/N 値が小さく，平均化データ処理が必要であるため実時間測定がむずかしいこと，使用する光学素子の光軸調整ずれによりスペクトルの形が歪むことなどの欠点がある．これらの技術的問題を克服し，また現在多く用いられている原子・分子ビームの代りに吸収セル中の原子・分子を使うようにすれば[37,39]，長時間にわたっての高度な安定化も可能になろう．

この他に原子・分子の集団のうち励起準位に留まる寿命が集団の平均値より長いもののみをとり出しそのスペクトルを測定する測定する方法が試みられており，方法としては光の電場の位相のスイッチングを利用するもの[40]，偏光分光法を応用するもの[41]が報告されている．これらについても信号の S/N 値が向上すれば実時間測定が可能になり，安定化の有力な手法となりうる．

これ以外の方法として周波数安定度を飛躍的に向上させるために，高周波電磁場中にイオンを少数個とじこめてイオン間の衝突頻度を減少させることによりスペクトルを狭帯域化し，かつ第二次ドプラー効果を抑えて共鳴周波数のシフトをなくす方法が試みられつつあり[42-44]，これらの実現の際には周波数安定度，再現性は数ケタ向上することが期待される．

5. 結 言

レーザー周波数安定化の際，安定度，再現性を向上させるための方法として，まず，周波数基準として用いられるスペクトルの真の共鳴周波数を精度よく見出すために光学技術，マイクロ波技術を応用するいくつかの新しい手法を示した．周波数基準としてファブリ・ペロー干渉計，原子・分子の場合に分けて記したが，いずれの場合にも周波数弁別特性を有する波形歪の少ない分散形の信号を精度よく検出することが目標であり，これを達成するための各々の独特な技法を示した．光学技術を用いる場合は装置が簡単であり，マイクロ波技術を用いればさらに測定精度の向上が期待される．また，周波数基準としてファブリ・ペロー干渉計を用いる場合，装置が簡単であり波長可変レーザーに対して容易に用いることができる．原子・分子を用いる場合はさらに高い安定度，再現性が得られる．

一方，安定度，再現性向上のためのもう一つの方法として周波数基準スペクトルの幅を狭くするいくつかの技術についても最後に略記した．これらの方法はまだ信号の S/N 値は小さいが今後，安定度，再現性を飛躍的に向上させるための有力な手段となりうるであろう．

本稿がレーザー周波数安定化，分光技術の開発のための一助となれば幸いである．

文　献

1) A. Brillet and P. Cerez: Proceeding of Third Symposium on Frequency Standard and Metrology, J. de Physique Colloque **C-8**, supplement au no 12, pC 8-73, (1981).
2) J. L. Hall, L. Hollberg, Ma Long-sheng, T. Baer, and H. G. Robinson: ibid., pC 8-59.
3) T.W. Hänsch and B. Couillaud: Opt. Commun., **35**, 441 (1980).
4) R. V. Pound: Rev. Sci. Instrum., **17**, 490 (1946).
5) C. E. Wieman and S. L. Gilbert: Opt. Letters, **7**, 480 (1982).
6) G. Kramer, C. O. Weiss, and J. Helmcke: Z. Naturforsch., **30a**, 1128 (1975).
7) R. L. Barger and J. L. Hall: Phys. Rev. Lett., **22**, 4 (1969).
8) A. Titov: Opt. Commun., **43**, 419 (1982).
9) C. Wieman and T. W. Hänsch: Phys. Rev. Lett., **36**, 1170 (1976).
10) 中山　茂：応用物理 **50**, 943 (1981).
11) F. V. Kowalski, W. R. Hill and A. L. Schawlow: Opt. Letters, **2**, 122 (1978).
12) T. W. Hansch: D. R. Lyons, A. L. Schawlow, A. Siegel, Z. Y. Wang and G. Y. Yan: Opt. Commun., **37**, 87 (1981).
13) Ch. J. Bordé, G. Camy, B. Decomps, and J. P. Descoubes: J. Physique, **42**, 1393 (1981).
14) W. Radloff and H. H. Ritze: Appl. Phys. **20**, 247 (1979).
15) M. Ohtsu, S. Ohta and T. Tako: Jpn. J. Appl. Phys., **20**, 1701 (1981).
16) M. Ohtsu and T. Tako: Jpn. J. Appl. Phys., **20**, 2133 (1981).
17) M. Ohtsu and T. Tako: Jpn. J. Appl. Phys., **21**, 722 (1982).
18) Y. Iwai, M. Ohtsu and T. Tako: submitted to Jpn. J. Appl. phys.
19) G. A. Sanders, M. G. Prentiss and S. Ezekiel: Opt. Letters, **6**, 569 (1981).
20) A. Schenzle, R. G. DeVoe, and R. G. Brewer: Phys. Review A, **25**, 2606 (1982).
21) G. C. Bjorklund: Opt. Letters, **5**, 15 (1980).
22) M. Cardona: *Modulation Spectroscopy*, Supplement II of Solid State Physics, F. Seitz and D. Turnbull, eds., (Academic Press, New York, (1969).
23) W. Lenth, C. Ortiz, and G. C. Bjorklund: Opt. Letters, **6**, 351 (1981).
24) T. F. Gallagher, R. Kachru, F. Gonnand, G. C. Bjorklund, and W. Lenth: Opt. Letters, **7**, 28 (1982).
25) P. Pokrowsky, W. E. Moerner, F. Chu, and G. C. Bjorklund: Optics Letters, **8**, 280 (1983).
26) W. Zapka, M. D. Levension, F. M. Schellenberg, A. C. Tam, and G. C. Bjorklund: Opt. Letters, **8**, 27 (1983).
27) W. Lenth, C. Ortiz, and G. C. Bjorklund: Opt. Commun., **41**, 369 (1982).
28) P. Pokrowsky, W. Zapka, F. Chu, and G. C. Bjorklund: Opt. Commun., **44**, 175 (1983).
29) G. C. Bjorklund and M. D. Levenson: Phys. Rev. A, **24**, 166 (1981).
30) J. L. Hall, L. Hollberg, T. Baer and H. G. Robinson: Appl. Phys. Lett., **39**, 680 (1981).
31) G. Camy, C. J. Bordé, and M. Ducloy: Opt. Commun., **41**, 325 (1982).
32) J. H. Shirley: Opt. Letters, **7**, 537 (1982).
33) Y. V. Baklanov, B. Y. Dubetsuky, and V. P. Chebotayev: Appl. Phys., **9**, 171 (1976).
34) J. C. Bergquist, S. A. Lee, and J. L. Hall: Phys. Rev. Lett., **38**, 159 (1977).
35) G. Kramer: J. Opt. Soc. Am., **68**, 1634 (1978).
36) S. A. Lee, J. Helmcke, and J. L. Hall: *Laser Spectroscopy IV* ed. by H. Walther and K. W. Rothe (Springer Verlag, Berlin, Heidelberg, New York, 1979) p 130.
37) N. Hata and K. Shimoda: Appl. Phys., **22**, 1 (1980).
38) J. Helmcke, D. Zevgolis, and B. Ü. Yen: Appl. Phys. B, **28**, 83 (1982).
39) M. Baba and K. Shimoda: Appl. Phys., **24**, 11 (1981).
40) F. Shimizu, K. Umezu, and H. Takuma: Phys. Rev. Lett., **47**, 825 (1981).
41) W. Gawlik, J. Kowalski, F. Träger, and M. Vollmer: Appl. Phys. B, **28**, 84 (1982).
42) W. Neuhauser, M. Hohenstatt, P. Toschek, and H. Dehmelt: Phys. Rev. Lett., **41**, 233 (1978).
43) D. J. Wineland, R. E. Drullinger, and F. L. Walls: Phys. Rev. Lett., **40**, 1639 (1978).
44) D. J. Wineland, W. M. Itano, J. C. Bergquist, and F. L. Walls: *Proceediugs of 35th Annual Symposium on Frequency Control*, p 602 Ft. Monmouth, NJ, May 1981.

最近の展望 1

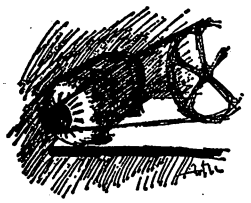

8.4, 10.4

半導体レーザーの周波数安定化

田幸敏治*・大津元一**
土田英実*

* 東京工業大学精密工学研究所　〒227　横浜市緑区長津田町 4259
** 東京工業大学理工学国際交流センター　〒152　東京都目黒区大岡山 2-12-1

(1982年12月22日　受理)

半導体レーザーの性能が，最近，著しく向上し，安定に単一モード発振し，数 MHz のスペクトル線幅をもつものが得られている．これとともに，その周波数制御技術も向上し，ファブリー・ペロー干渉計，原子・分子吸収線を基準として安定化することにより，10^{-11}～10^{-12} の高安定度が達成されている．本稿では，主として近赤外域の半導体レーザーについて，最近の周波数安定化の状況を紹介する．

1. まえがき

近年の半導体レーザーの性能向上はめざましく，発振モードの安定化と長寿命化が進み，0.7～0.9 μm 帯の AlGaAs レーザーと，1.1～1.6 μm 帯の InGaAsP レーザーはすでに実用化の段階に入っている．

これらの半導体レーザーは，主として光通信，光情報処理用光源として開発されたものであるが，半導体レーザーは，小型，高効率，波長可変，低価格，高速動作が可能などの利点があり，また，従来この波長域で発振するレーザーが少なかったことなどから，精密計測，高分解能分光などへの応用も期待されている．これらの応用に対して，半導体レーザーに要求される特性の中で，特に重要なものは，高いスペクトル純度と周波数の安定性で，この二つの要素は測定の感度や分解能に大きく影響する．また，これらは将来の通信システムとして，その可能性が検討されているコヒーレント光通信[1]においても，システムの性能を決定する重要な要素である．

スペクトル純度については，すでに縦・横単一モード発振が再現性よく得られており，AlGaAs レーザーでは，スペクトル線幅が数 MHz 程度と理論値[2~4]に近い測定結果[5~9]が得られている．これに対して半導体レーザーの周波数は，温度および電流の変化に対して非常に敏感で，例えば，AlGaAs レーザーの場合，温度に対して −20 GHz/K 程度，電流に対して −3～−7 GHz/mA の割合で周波数が変化する．このため，フリーランニング状態の半導体レーザーは周波数が大きく変動し，スペクトル線幅程度の安定度（数 MHz）を得るためには，周波数の安定化，すなわち外部からの周波数制御が必要になる．また，スペクトル線幅と周波数安定度との間には密接な関係があるが[10]，ここでは省略する．

半導体レーザーの周波数安定化の実験は，古くは 1970 年に Bykovskii ら[11]により，1975 年に Picque と Roizen[12]により，いずれも低温動作の GaAs レーザーを使い，ファブリー・ペロー干渉計を基準として行なわれ，10^{-7} 程度の安定度を得ている．最近では，特に日本において，性能のよい半導体レーザーが市販されるようになり，これらを使って周波数安定化の実験が行なわれ，10^{-11}～10^{-12} と気体レーザーに匹敵する高安定度も得られ，計測・分光に十分適用できる水準に達している[13]．

2. 半導体レーザーの周波数制御

半導体レーザーの周波数は，その共振器長，屈折率に依存するが，これらは温度および電流によって制御できる．温度による場合には，ペルチェ素子によりヒートシンク温度を制御する方法が用いられるが[14~16]，応答速度は遅く，制御帯域は 1 Hz 程度で[15]，この方式では短期安定度* は改善されない．

Frequency Stabilization of Semiconductor Lasers. Toshiharu TAKO*, Motoichi OHTSU** and Hidemi TSUCHIDA*. *Research Laboratory of Precision Machinery and Electronics, Tokyo Institute of Technology. 4259, Nagatsuta-cho, Midori-ku, Yokohama 227. **International Cooperation Center for Science and Technology, Tokyo Institute of Technology. 12-1, Ookayama 2 chome, Meguro-ku, Tokyo 152.

* ここでは，積分時間 1 秒以下の安定度を短期安定度，1 秒以上を長期安定度と呼ぶことにする．

これに対して電流による制御は[11,12,17-22]は，応答速度が速く，カットオフ周波数は約 1 MHz で[23,24]，温度の場合よりも広い帯域で高い安定度が得られる[18]．しかし，レーザーの光出力のドリフトが増加するという欠点もある[25,26]．

温度，電流による制御のほかに，波長可変範囲の拡大やスペクトル純度の改善を目的とした外部共振器型半導体レーザー[27-30]では，電歪素子 (PZT) を用いて外部共振器長を変えることにより周波数を制御できる[30]．

3. ファブリー・ペロー干渉計を基準とした周波数安定化——短期安定度の向上——

ファブリー・ペロー干渉計は，色素レーザーのような波長可変レーザーの周波数安定化の基準としてよく用いられる[31,32]．これは，ファブリー・ペロー干渉計が広い波長範囲で周波数弁別特性を有するためで，素子ごとに波長のばらつきが大きく，波長可変の半導体レーザーの周波数安定化にも適用できる[11,12,14-22]．

ファブリー・ペロー干渉計は短期安定度に優れ，レーザー周波数を無変調で安定化でき，制御帯域を広くとることができる．しかし，長期安定度は，主として干渉計の長さの熱的ドリフトにより制限され，線膨張係数の小さいインバーをスペーサーとして干渉計を構成した場合でも 10^{-8}〜10^{-9} である[15]．したがって，この方式は光通信のようなレーザーの高速動作が要求される応用に適している．

周波数安定化の例として，筆者らが行なった実験[19,25]を次に示す．**Fig. 1** は実験装置である．波長 823 nm の AlGaAs レーザー[33]を使用し，実験は特に温度安定 (0.1 K/週) な地下光学トンネル[34]内で行なった．レーザーの温度制御は特に行なっていないが，一般の実験室では 0.1 K 以内の温度制御が必要である．ファブリー・ペロー干渉計の端面や，その他の光学素子からの反射光がレーザーに戻ると，周波数安定度が低下する[35]ので，アイソレーターを使用するか，または光学素子を傾けて使用する必要がある．半導体レーザーは，その端面の反射率が低い (30% 程度) ので，戻り光の影響は気体レーザーに比べて大きい．誤差信号からレーザーの光出力変動成分を取り除くため，二つの光検出器の比で電流を制御する．干渉計の透過光強度が最大値の約 50% になるように制御点を設定した．比例 (P)，積分 (I)，微分 (D) 制御方式を用いた[18]．周波数安定度は 2 台の安定化レーザー間のビート信号より評価するのが望ましいが，測定系の容易さから制御系の誤差信号より評価した．

Fig. 2 に周波数安定度を表わすアラン分散[36]の平方根を示す．横軸 τ は積分時間，N はデータ数である．A(△) はフリーランニングレーザーの安定度で，1 ms≦τ≦150 s で，$3.8\times10^{-9}\leqq\sigma\leqq3.3\times10^{-8}$ である．$\tau>0.3$ s では温度変動によるドリフトにより，$\tau<0.3$ s では電流

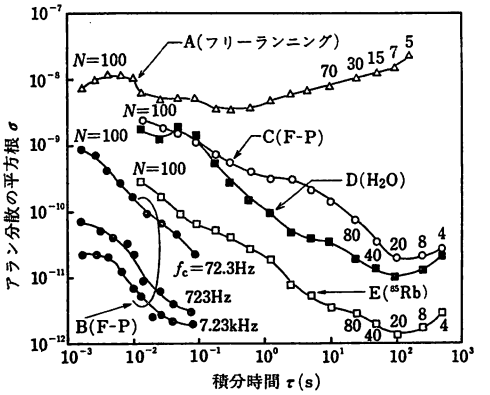

Fig. 2　周波数安定度を表わすアラン分散[36]の平方根．A：フリーランニングレーザーの周波数安定度，B〜E：安定化レーザーの周波数安定度．

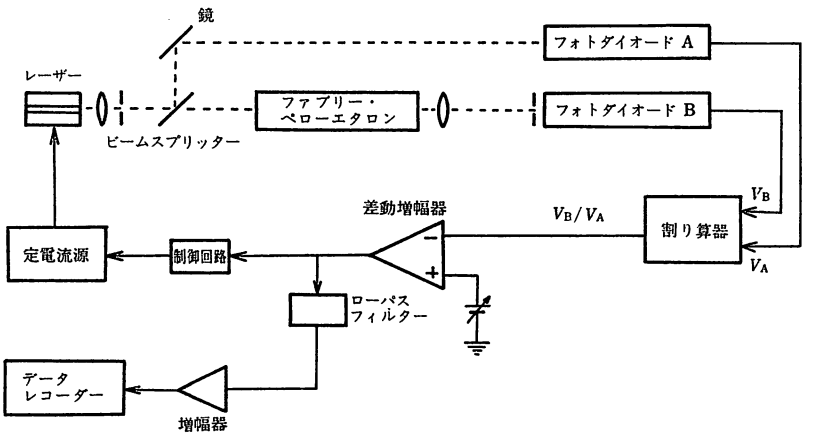

Fig. 1　ファブリー・ペロー干渉計を基準とした周波数安定化の実験装置．

Table 1 原子・分子吸収線を基準とした半導体レーザーの周波数安定化の例.

レーザー	波長 (μm)	基準	σ_{min} (積分時間)	文献
AlGaAs	0.824	H_2O の振動回転スペクトル	1.1×10^{-11} (100 s)	37)
AlGaAs	0.780	^{85}Rb-D_2 線	1.4×10^{-12} (100 s)	40)
AlGaAs	0.852	Cs-D_2 線	9×10^{-12} (0.2〜1 s)	41)
AlGaAs	0.841	Ar の光ガルバノスペクトル	4.0×10^{-11} (20 s)	42)
InGaAsP	1.28	HF の振動回転スペクトル	7.9×10^{-11} (240 s)	43)
InGaAsP	1.50	NH_3 の振動回転スペクトル	4.5×10^{-11} (200 s)	44)
PbSnTe	7.7	CH_4 の振動回転スペクトル	4.3×10^{-11} (15 s)	45)

源の雑音の影響により，安定度が低下している．B(●)は **Fig. 1** の装置で安定化されたレーザーの安定度で，f_c は制御系のカットオフ周波数である．f_c が増加すると安定度は向上し，f_c=7.23 kHz で最高の安定度 $\sigma=2.1\times10^{-12}(\tau=90$ ms) が得られ，フリーランニングレーザーに比較すると，短期安定度が約3桁向上している．これはレーザー周波数の電流に対する応答が速いためで，さらに制御帯域を 500 kHz 程度まで拡大すれば，積分時間 1 ms 以下の安定度も改善できる[22]．

ファブリー・ペロー干渉計を基準として長期安定度を向上させたい場合は，干渉計を長期安定度の優れた安定化レーザーで安定化すればよい[18,32]．筆者らは，ラムくぼみ安定化 He-Ne レーザー (λ=633 nm) により安定化された干渉計を基準として AlGaAs レーザーを安定化し，**Fig. 2** の C(○) に示すように，τ=100 s で $\sigma=2.0\times10^{-11}$ の安定度を得ている[18]．

4. 原子・分子吸収線を基準とした周波数安定化——長期安定度の向上——

気体レーザーで行なわれてきた原子・分子吸収線を基準とした周波数安定化は，長期安定度や再現性の向上に適している．半導体レーザーは，結晶成長時に発振波長を精密に制御することが技術的に難しく，また，素子ごとに波長のばらつきが大きいので，この方式で安定化を行なう場合，吸収線に近い波長のレーザー (±2 nm 以内) を選び出し，温度により波長同調しなければならない．吸収線に近い波長のレーザーでも，縦モードジャンプにより波長のとびが生じ，吸収線に同調できない場合もある．

安定化には，感度を上げるため吸収スペクトルの微分曲線を周波数弁別特性として使用するので，レーザーを電流により周波数変調し，原子・分子が封入されている吸収セルを透過したレーザー光強度をロックインアンプで同期検波する．変調周波数は 1 k〜100 kHz である．電流で周波数を制御した場合，制御帯域はロックインアンプの時定数により制限され，数 kHz 程度である．原子・分子の吸収が弱い場合，レーザーの電流-光出力特性のバックグラウンドにより，吸収スペクトルの一次微分曲線にオフセットが生じるので，これを除くため三次微分曲線を使用しなければならない[37]．

Fig. 2 に筆者らが行なった AlGaAs レーザーの周波数安定化の結果を示す．D(■) は，水分子の (2, 1, 1) バンドの振動回転スペクトル P (0-1_{-1}) に安定化されたレーザーの安定度である[37]．水分子は吸収は弱いが，815〜830 nm の波長域に多数の吸収線をもち[38]，この波長域のレーザーはほとんど安定化できる．現在，水分子に安定化したレーザーの波長を，基準の He-Ne レーザーと比較して測定し，分子定数を精密に求める実験を行なっている[39]．E(□) は ^{85}Rb-D_2 線に安定化したレーザーの安定度で[40]，フリーランニングレーザー (A) に比較して2〜4桁安定度が向上している．また，水分子の場合 (D) と比較して安定度が1桁高い．これは，^{85}Rb-D_2 線の吸収が水分子と比べて非常に強く，誤差信号の SN 比が大きいためである．

Table 1 に最近行なわれた周波数安定化の例と，得られた安定度の最小値を示す．これらの実験はすべて電流制御により行なわれている．藪崎ら[41]は，Cs-D_2 線の飽和吸収スペクトルに AlGaAs レーザーを安定化している．Rb, Cs に安定化されたレーザーは，原子周波数標準器のポンピング光源への応用が期待されている[46,47]．このほかに，アリカリ金属原子では，Rb-D_1 線 (794.8 nm), K-D 線 (766.5 nm, 766.9 nm) が利用できる．InGaAsP レーザーについては，山口と鈴木[43]が 1.3 μm 帯の HF に，筆者ら[44]が 1.5 μm 帯の NH_3 に安定化を行なっている．このほか，CO_2, HCN, H_2O, D_2O, CH_4 などの分子が利用できよう．大井[45]は，PbSnTe レーザーを CH_4 に安定化している．鉛化合物系の半導体レーザーは，赤外分光，汚染ガス検出の光源として重要である．

先にも述べたように，半導体レーザーは波長のばらつきが大きく，連続同調できないことが，原子・分子吸収線に安定化する場合の最大の障害である．これを解決す

る一つの方法が，外部共振器の利用による同調範囲の拡大（約5nm）である[30]．

5. 計算機制御

以上の周波数安定化では，制御回路の定数（利得，カットオフ周波数など）の設定は，周波数変動をオシロスコープで観測しながら手動で行なっており，必ずしも最適条件にあるとは限らない．そこで，マイクロコンピューターを利用し，実時間で周波数安定度を計算[48]するとともに，その値が最良値になるように制御回路の定数を自動的に制御する試みがなされている[49,50]．この方式では，レーザー素子や周波数基準が変わっても自動的に最適条件が得られるとともに，特定の積分時間域での安定度を最良にすること，あるいは外部からの異常雑音の侵入など環境条件が変化しても安定度が自動的に最適化されるなどの特色があり，綿密な手動による設定の場合に比べて，半桁から1桁の向上が見られた[49,50]．この方式はあらゆるレーザーの安定化に適用できる．

6. むすび

以上，最近の半導体レーザーの周波数安定化の状況について述べた．ここ数年で，半導体レーザーの周波数安定度は著しく向上し，10^{-11}～10^{-12}と気体レーザーに匹敵する高安定度が達成された．また，半導体レーザーの周波数安定度の理論的極限値の推定の研究も進められている[10,51]．今後は，安定化するだけでなく，高安定度を保ちながら周波数を広帯域に掃引する技術，波長を精密に設定できるレーザーの製作技術の開発が望まれる．これらを現在の周波数安定化技術と結びつければ，半導体レーザーは近赤外域できわめて有用な分光・計測用光源となることが期待される．

文　献

1) Y. Yamamoto and T. Kimura: IEEE J. Quantum Electron. **QE-17** (1981) 919.
2) A.L. Schawlow and C.H. Townes: Phys. Rev. **112** (1958) 1940.
3) A. Yariv and W.M. Caton: IEEE J. Quantum Electron. **QE-10** (1974) 509.
4) 山本喜久：電子通信学会技術研究報告 OQE 81-118 (1982).
5) T. Takakura, K. Iga and T. Tako: Jpn. J. Appl. Phys. **19** (1980) L 725.
6) 林　国康，根本和正，平野信夫：昭和55年度電子通信学会総合全国大会予稿集 (1980) 第4分冊, p. 56.
7) T. Okoshi, K. Kikuchi and A. Nakayama: Electron. Lett. **16** (1980) 630.
8) Y. Yamamoto, T. Mukai and S. Saito: Electron. Lett. **17** (1981) 327.
9) 山本喜久，斉藤　茂，向井孝彰：電子通信学会技術研究報告 OQE 81-119 (1982).
10) 大津元一：電子通信学会技術研究報告 OQE 82-100 (1983).
11) Yu.A. Bykovskii, V.L. Velichanskii, I.G. Goncharov and V.A. Masrov: Sov. Phys.-Semicond. **4** (1970) 580.
12) J.L. Picque and S. Roizen: Appl. Phys. Lett. **27** (1975) 573.
13) 田幸敏治：応用物理 **51** (1982) 465.
14) T. Okoshi and K. Kikuchi: Electron. Lett. **16** (1980) 179.
15) H. Tsuchida, S. Sanpei, M. Ohtsu and T. Tako: Jpn. J. Appl. Phys. **19** (1980) L 721.
16) K. Kikuchi, T. Okoshi and M. Kawanishi: Electron. Lett. **17** (1981) 515.
17) F. Favre and D. Le Guen: Electron. Lett. **16** (1980) 709.
18) H. Tsuchida, M. Ohtsu and T. Tako: Jpn. J. Appl. Phys. **20** (1981) L 403.
19) H. Tsuchida, M. Ohtsu and T. Tako: Trans. Inst. Electron. & Commun. Eng. Jpn. **E-65** (1982) 65.
20) A. Dandridge and A.B. Tveten: Electron. Lett. **17** (1981) 937.
21) K.W. Cobb and B. Culshaw: Electron. Lett. **18** (1982) 337.
22) 土田英実，田幸敏治，大津元一：第43回応用物理学会学術講演会予稿集 (1982) p. 126.
23) S. Kobayashi, Y. Yamamoto, M. Ito and T. Kimura: IEEE J. Quantum Electron. **QE-18** (1982) 582.
24) H. Tsuchida, T. Tako and M. Ohtsu: Jpn. J. Appl. Phys. **22** (1983) L 19.
25) 土田英実，大津元一，田幸敏治：電子通信学会技術研究報告 OQE 80-144 (1981).
26) 土田英実，田幸敏治，大津元一：第43回応用物理学会学術講演会予稿集 (1982) p. 126.
27) M. Ito and T. Kimura: IEEE J. Quantum Electron. **QE-16** (1980) 69.
28) K. Kikuchi and T. Okoshi: Electron. Lett. **18** (1982) 10.
29) S. Saito, O. Nilsson and Y. Yamamoto: IEEE J. Quantum Electron. **QE-18** (1982) 961.
30) 三瓶政一，土田英実，大津元一，田幸敏治：電子通信学会技術研究報告 OQE 81-137 (1982).
31) R.L. Barger, M.S. Sorem and J.L. Hall: Appl. Phys. Lett. **22** (1973) 573.
32) R.L. Barger, J.B. West and T.C. English: Appl. Phys. Lett. **27** (1975) 31.
33) K. Aiki, M. Nakamura, T. Kuroda, J. Umeda, R. Ito, N. Chinone and M. Maeda: IEEE J. Quantum Electron. **QE-14** (1978) 89.
34) 浅川賢一，田幸敏治，平田照二：応用物理 **48** (1979) 519.
35) 土田英実，大津元一，田幸敏治：第29回応用物理学関係連合講演会予稿集 (1982) p. 206.
36) D.W. Allan: Proc. IEEE **54** (1966) 221.

37) H. Tsuchida, M. Ohtsu and T. Tako: Jpn. J. Appl. Phys. **21** (1982) L 1.
38) W. Baumann and R. Mecke: Z. Phys. **81** (1933) 445.
39) 福岡和雄，土田英実，大津元一，田幸敏治：第 29 回応用物理学関係連合講演会予稿集 (1982) p. 238.
40) H. Tsuchida, M. Ohtsu, T. Tako, N. Kuramochi and N. Oura: Jpn. J. Appl. Phys. **21** (1982) L 561.
41) T. Yabuzaki, A. Ibaragi, H. Hori, M. Kitano and T. Ogawa: Jpn. J. Appl. Phys. **20** (1981) L 451.
42) S. Yamaguchi and M. Suzuki: Appl. Phys. Lett. **41** (1982) 597.
43) 山口静夫，鈴木正夫：電子通信学会技術研究報告 OQE 82-51 (1982).
44) 田川治男，小谷浩樹，大津元一：第 30 回応用物理学関係連合講演会予稿集 (1983) p. 190.
45) M. Ohi: Jpn. J. Appl. Phys. **19** (1980) L 541.
46) L. L. Lewis and M. Feldman: *Proc. 35th Annual Symp. Frequency Control, Ft. Monmouth, N. J., 1981* (Electronics Industries Association, Washington, D. C., 1981) p. 612.
47) M. Arditi: *Proc. 3rd Symp. Frequency Standards and Metrology, Aussois, France, 1981*, J. Phys. **42** (1981) Suppl. 12, p. C 8-261.
48) 椎尾一郎，大津元一，田幸敏治：電子通信学会論文誌 **64-C** (1981) 204.
49) 深田博之，大津元一，土田英実，田幸敏治：第 29 回応用物理学関係連合講演会予稿集 (1982) p. 207.
50) 深田博之，大津元一，土田英実，田幸敏治：第 43 回応用物理学会学術講演会予稿集 (1982) p. 150.
51) 土田英実，田幸敏治：電子通信学会技術研究報告 OQE 82-128 (1983).

7. レーザー

現在までに考案された数多くのレーザー装置のうち，応用上の目的から淘汰が行なわれて，そのうちの数種が生き残り実用化段階に達している現在，日本のレーザー研究動向に関しては半導体レーザー，およびその他のレーザーとに分けて考えるべきであろう．わが国のレーザーに関する全研究者のうち半導体レーザーに関与する人数の占める割合は大きく，それは米国での半導体レーザー以外のレーザーに関与する人数の割合と同等と思われる．このことはわが国における民生用の半導体レーザー研究の層の厚さと水準の高さを示すとともに，米国では他種レーザーがおもに軍事用，エネルギー産業への応用をめざして精力的に研究されていることを示している．

以下では応用物理学会講演会での発表状況を通じ，その動向を概観したい．昨年の応物学会では春秋合わせて約410件のレーザーに関する報告があり，実用化へ向けての研究の活発化がうかがえる．この数は一昨年の場合より約1割増加している．

7.1 半導体レーザー（LD）

半導体レーザー（LD）の研究の主眼はいかに素子を作るかに置かれており，その製法がレーザーの性能を決定するため結晶成長，光物性と深くかかわっている．これに対し他種レーザーは分光，波動光学など現象解析に関連し，これらの点で LD の研究手法と他種レーザーのそれとは相入れない部分が大きい．しかしながら近年，このギャップを埋めようとする努力が国内の LD 研究者の間でなされつつあることは喜ばしい（応物学会量エレ研 LD サブグループ，一昨年以降）．さらに LD 素子製造技術者の努力によりその発振特性が向上してくるとともに，他種レーザーの特性との類似，相違性が定量的に把握されるようになってきており，この点においても LD を他種レーザーと分けて考えることによりその研究動向がより的確に概観できると思われる．

前記発表件数のうち約170件（4割）を LD についての発表がしめている．さらにこのうち約110件は結晶成長技術に関するものであり，他種レーザーとの研究内容の相違がうかがえる．結晶成長技術については大面積結晶成長可能な MOCVD 法による AlGaAs レーザー製作（東芝・武藤ら）の実用化が試みられており，InGaAsP レーザーについてもこの方法が国内では初めて成功している（東工大・菅生ら）．また，光通信用1.3 μm レーザーの単一縦モード発振を得るための DFB や DBR の加工も各所で行なわれるようになり（日電・水戸ら，東芝・植村ら），また DFB 付きレーザーの単一縦モード発振条件の提案（東大・多田ら）も行なわれている．同じく，単一縦モード発振可能，かつ画像処理などに応用可能性を有する面発光型レーザー（東工大・茨木ら，電総研・幡ら）の開発が進められている．さらに MBE 技術により超薄膜を作り，発振特性の向上を目指した MQW レーザーの開発とその特性評価が活発になってきている（通研・岩村ら，東大・荒川ら）．また，ビデオディスクなどへの応用上，後述の雑音特性を改善

する目的で縦モードを多モード化する低コヒーレンスレーザーの実用化が進められている（シャープ・稲田ら）．さらにレーザーのアレイ化も試みられている（松下・浜田ら）．

以上の結晶成長技術とは別に，LD の発振特性についての報告のうち実用上重要なものは，戻り光誘起雑音とモードホッピング雑音であろう．これらの低周波雑音は民生用レーザーとして解決しなければならない問題であり，LD 固有の研究対象である．これらの雑音特性測定については多数報告があり（通研・河口ら，三菱・山下ら，東大・小笠原ら），高周波電流重畳による低減化（日立・大石ら），さらに上記の低コヒーレンスレーザー使用による低減化が試みられているが現在までのところこの雑音機構の理論的解明はなされていない．戻り光の効果を光ピックアップ用センサーに用いる試みとして SCOOP の開発が行なわれている（電総研・三橋ら）．このような戻り光誘起雑音解明の一つの手がかりとしてカオス現象の観測例が報告されている（阪大・張ら）．このカオスについては光通信用の増幅器に光双安定を応用する際に生ずることが報告され（通研・大塚），たんに応用数学上の問題のみでなく実用上の鍵となる様相を呈してきた．光双安定については増幅器，光ロジックなどへの応用から研究が進められている（日電・小田切ら，京大・矢野ら）．光ロジックや高速光現象研究に有用な光短パルス発生については AlGaAs レーザーにより 0.55 ps（電総研・鈴木ら），InGaAsP レーザーにより 34 ps（東北大・小野寺ら）の値が報告され transform-limited な光パルスが実現されつつあることを示している．

LD をコヒーレント光源として用いる際その周波数の安定性が重要である．周期 1 μs 以上のゆっくりした周波数変動を抑圧することは一昨年以前より継続して試みられ（工芸大・山口ら），また安定度の理論限界も解明された（東工大・大津ら）．今後は安定化技術そのものでなく，安定化レーザーを用いた光計測へと研究内容が推移すると考えられる．コヒーレンスの点でさらに重要な点としてスペクトル幅の値が挙げられる．戻り光を利用してその狭帯幅化が試みられている（日電・江村ら）が問題はその安定性にあり今後の研究が期待される．LD のコヒーレント光計測への応用例としてはドプラー流速計（三菱・久間ら），汚染ガス検出（東北大・陳ら，東工大・小谷ら），ライダー（公害研・竹内ら），ファイバジャイロ（東工大・大津），セシウムビーム標準器（電波研・梅津ら）などの報告があり，LD の実用化の時期の近いことがうかがえる．

7.2 他種レーザー

気体，色素，固体レーザーなどについては高出力化，短波長化，短パルス化，高コヒーレンス化などレーザーの極限状態を実現し，これを各種科学技術上の応用に用いる努力がすすめられており，巨大科学化の様相を呈しつつある．CO_2 レーザーでは高出力化をめざしたもの（慶大・小松ら，阪大・レーザー核融合グループ）や波長広帯域掃引可能で小型の導波路構造のもの（阪大・前田ら，東工大・中村ら）など多岐にわたる報告がある．またプラズマ診断などに用いる遠赤外レーザーの開発（阪大・山中ら，防大・平山ら）が行なわれている．高出力レーザーとして KrF，XeCl などのエキシマーレーザーの開発も活発である（電通大・草野ら，電総研・大和田野ら，九大・高橋ら，慶大・須田ら）．高利得レーザーとして有望な銅蒸気レーザーの発振特性が研究されている（近大・橋新ら，東大・黒田ら）．さらに画像処理用白色光 He-Cd II レーザーの実用化の試みがなされている（浜松・福満ら，同志社・佐々木ら）．

色素レーザーについては発振スペクトルの狭帯幅化のみでなく広帯域掃引可能であることも応用上重要で，1 回の掃引範囲 20 cm^{-1} 以上のものが開発された（慶大・上原ら）．また，モード同期色素レーザーにおけるパルス幅の拡がりに関する理論的考察が報告された（通研・宇理須）．

固体レーザーについてはガラスレーザーのモード同期に関する提案（阪大・藤本ら），YAG レーザーなどを用いた物性研究のための光短パルス発生（電総研・富江ら）が行なわれている．さらに核融合用として阪大では激光 XII 号ガラスレーザー装置を開発しその調整をしており今後の発展が期待される．

その他，赤外波長可変レーザーとしていくつかの応用が考えられるものに色中心レーザーがあり，波長選択のために DFB を用いる方式が提案された（金沢大・黒堀）．また，低損失のファイバを共振器中に含む YAG レーザーのラマン発振（通研・中沢ら），ファイバ・ラマン増幅（日電・青木ら）の報告があった．

以上のレーザーの応用例としてライダー（九大・前田ら，公害研・竹内ら，信大・藤本ら）などの分光分析をはじめ，レーザー顕微鏡（理研・村原ら，東北大・佐藤ら），ガンの診断（浜松・平野ら）など生体医用への応用などが報告された．

以上のように他種レーザーの研究としては極限的な性能を引き出し物理化学，エネルギー産業への高度な応用が試みられつつある．

以上，レーザー関係の研究動向につき概観したが複数の研究者，研究所で行なわれている内容についてはその名前を完全に列挙しえなかったことをおことわりしたい．

（東工大　大津元一）

UDC 621.375.826.018 : 621.373 : 535.33

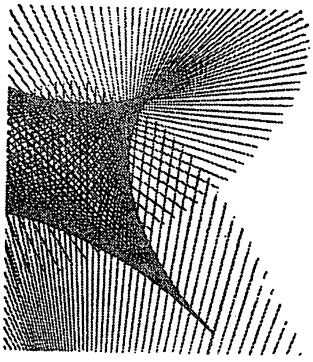

ミニ解説

レーザ周波数の安定化技術

正員 大津元一
東京工業大学理工学国際交流センター

1. はじめに

1940～50 年代の高安定マイクロ波発振器の開発，およびメーザの発明を技術的基盤として 1960 年にレーザが発明された。しかし，いかにレーザが原子，分子から発生する位相のそろった光* をもとにして作られた，周波数，振幅の安定な光源とはいっても，従来からあったマイクロ波発振器の安定性に比べ十分に優れているとはいえず，いろいろな応用に使うには特に周波数を更に高安定にすることが当時必要であった。本稿の主題であるレーザ周波数の安定化技術の研究はこのようにレーザの発明当初に端を発したといえる。以後 20 年以上の間に多種類のレーザが発明され，周波数の安定度も飛躍的に向上した。現在そのうちのあるものは既にマイクロ波発振器の周波数安定度をしのいでおり，いよいよこれらのレーザの性能は各種応用に使いうるようになってきた。そこで本稿ではこのような高度に周波数安定化されたレーザが必要とされる分野，周波数安定化の技術，安定度の現状と将来技術について述べる。図 1 には幾つかのマイクロ波発振器，レーザの周波数安定度の値を比較して示した[(1)~(3)]。ここで，縦軸，横軸の $\sigma_y(\tau)$，τ は第 3 章で示すアラン分数の平方根，およびその積分時間である。

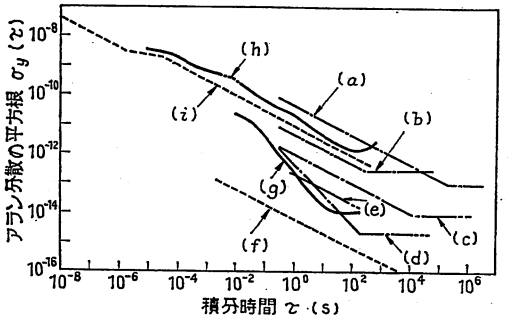

(a) 市販の Cs 原子発振器　(b) Rb 原子発振器
(c) 実験室形 Cs 原子発振器　(d) 水素メーザ
(e) CH_4 安定化 He-Ne レーザ　(f) (e)の理論限界値
(g) H_2CO 安定化 HeXe レーザ
(h) 周波数安定化 AlGaAs レーザ
(i) (h)の理論限界値

図 1 各種マイクロ波発振器，レーザの周波数安定度[(1)~(3)]

* 位相がそろっていることを時間的にコヒーレントであるということがある。また，この光は誘導放出という発光過程によって生ずる。

2. 周波数安定化レーザを必要とする応用分野

周波数安定化レーザ，更にマイクロ波発振器をも含めると，これらの高性能発振器は非常に多くのシステムに使われている。そこでまずはじめにこれらの発振器がどのような分野で使われているかを概観しよう。レーザのなかでも周波数の超高安定度を実現しうる気体レーザ，小形安価な半導体レーザの両者が実用上重要と思われるので，これらのレーザの関連した応用分野の代表的なものを表 1 (次ページ) に示した。次章以降ではレーザ周波数をこれらの応用に耐えうるほど高度に安定化するにはどのような技術を用いればよいかを述べる。

3. 気体レーザの周波数安定化技術

連続発振するレーザの中で気体レーザが最も低雑音で高い周波数安定度が得られるので表 1 の (5)，(6) などの応用に適している。レーザの周波数 ν は図 2 (a) に示すように発光物質 (ここでは放電気体) の発光スペクトル中心周波数 ν_0 には一致せず，発光物質を閉込めている空洞共振器 (通常は対向した 2 枚の鏡からなり，ファブリペロー共振器と呼ばれる) の寸法，すなわち 2 枚の鏡の距離 L で決る第 N 次の共振モード周波数 $\nu_N(=cN/2L$，c は光速度，N は整数) のうち，発光スペクトル幅内に入るものの一つのごく近くにある。従って周囲の温度変動や機械的な振動など

表 1　高安定周波数レーザ，マイクロ波発振器の応用分野の代表例

番号	応用分野	使用箇所	現在使われている発振器	将来使われると予想される発振器
(1)	ディジタル通信網 高度情報システム (INS)[4]	各中継局での PCM 情報のビット列送受のための時刻同期	Rb 原子発振器	半導体レーザ励起 Cs または Rb 原子発振器
(2)	光通信 (コヒーレントヘテロダイン方式)[5]	周波数または位相変調された送信用発振器，受信側でのヘテロダイン検波用局部発振器	(システム開発中)	高安定周波数半導体レーザ
(3)	人工衛星および衛星通信	慣性航法用ジャイロスコープ，衛星追尾用精密時刻保持，無線通信用同期	超小形気体リングレーザ，Rb または Cs 原子発振器	高安定周波数半導体レーザ（ファイバ・ジャイロスコープ），半導体レーザ励起 Cs または Rb 原子発振器
(4)	地球物理，天文，測距	超長基線電波干渉計 (VLBI)[6] 用精密時刻保持	小形の水素メーザ	半導体レーザ励起 Cs または Rb 原子発振器
(5)	時間標準および時刻保持	秒の一次標準	Cs 原子発振器	半導体レーザ励起 Cs 原子発振器またはレーザ冷却によるイオン捕獲を用いた超高安定周波数レーザ
(6)	長さ標準	光速度測定のための光波長および周波数の同時測定	気体レーザ，色素レーザ，色中心レーザ	左記のレーザに加え，更により短波長，高安定な新しいレーザ

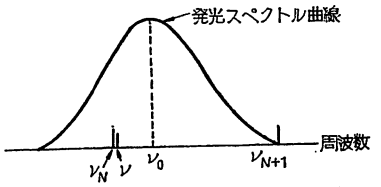

(a)　レーザ周波数 ν と共振周波数 ν_N，発光スペクトル中心周波数 ν_0 との関係

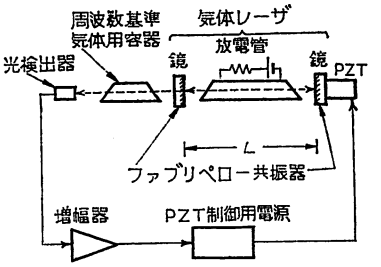

(b)　気体レーザの周波数安定化の原理

図 2

のために L が変動すると ν も変動する。更にまた ν は気体放電のための電流の変動によっても変動する。しかし負帰還技術を用いれば ν の変動をおさえることができる。よく用いられる方法は図 2 (b)のように鏡の一方を電わい素子 (PZT：電圧を加えると伸縮するセラミック) の上に固定し，これに加える電圧を制御するものである。PZT の応答周波数帯域は約 10 kHz 以下であり，低速であるが表 1 中(5)，(6)の応用のように 1 か月，1 年などの長期にわたる安定度を向上させるために用いる制御要素としては優れている。

さて，周波数を一定に保つ技術は制御工学の立場からみると定値制御にほかならない。そのためには安定な周波数基準をみつける必要があり，それは各レーザによって異なる。最も精度の高い基準は安定な原子，分子の吸収または発光スペクトルである。現在使われている原子，分子とレーザの波長の組合せの例を表 2 に示す。レーザ光をこれらの原子，分子に照射してそれらの吸収または発光スペクトルを測定し，レーザ周波数が常にそのスペクトルの中心周波数 ν_s に固定されるように PZT に加える電圧を自動制御すれば定値制御できる。但し ν_s は図 2 の発光スペクトル曲線の周波数幅内に入るような値であることが必要である。制御用電子回路は各レーザの雑音のフーリエ周波数特性をもとに最適設計される。

さてここで，特に強いレーザ光を原子，分子に照射すると非線形光学効果によってこれらの原子，分子の非常に幅の狭い吸収または発光スペクトル（飽和吸収または発光スペクトルと呼ばれる）が観測されることが知られている。例として表 2 中の H_2CO の飽和吸収スペクトルの三次微分波形を図 3 に示す[2]。これからわかるように，そのスペクトルは 1 MHz 以内の幅をもつ。波長 3.51 μm の He-Xe レーザの周波数が 86 THz であるから，これに比べるとこの幅は非常に狭いことがわかるであろう。このような狭い幅を有するスペクトルの中心周波数 ν_s に ν を定値制御すると

表 2　高安定周波数気体レーザと周波数基準用原子，分子の波長

気体レーザ	周波数基準用原子，分子	波長 (μm)
CO_2	CO_2, SF_6, OsO_4	10
He-Xe	H_2CO	3.5
He-Ne	CH_4	3.4
He-Ne	I_2	0.633, 0.612
Ar^+	I_2	0.515

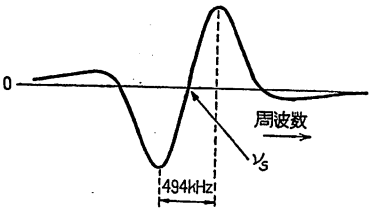

図 3 H_2COの飽和吸収スペクトルの三次微分波形[2]

10^{-12}～10^{-14}の安定度が得られる。

このようにして高度に安定化されたレーザ周波数の安定度を評価するには，同じ方法により同程度に安定化したもう1台のレーザとの間のビート信号の周波数変動の大きさを測定すればよい。周波数安定度を表わす一つの高精度な尺度はパワースペクトル密度であり，これは特定のフーリエ周波数値における安定度を知るのに便利なので，表1中(1)，(2)の通信関係ではよく用いられる。一方，同表中(3)～(6)の応用ではシステム全体が高域遮断周波数特性（その遮断時定数をτと書く）を有することが多く，そのシステムの中で発振器が発揮する周波数安定度を表わすには次式で定義される尺度，アラン分散[7]，を使う方が便利である。

$$\sigma_y^2(\tau)\equiv\lim_{N\to\infty}\frac{1}{N-1}\sum_{k=1}^{N-1}\frac{(\bar{y}_{k+1}-\bar{y}_k)^2}{2} \quad \cdots(1)$$

但し，

$$\left.\begin{aligned}&\bar{y}_k\equiv\frac{1}{\tau}\int_{t_k}^{t_{k+1}}y(t)\,dt\\&t_{k+1}\equiv t_k+\tau\\&t_k\text{は}k\text{回目の測定開始時間}\ (k=1,2,3,\cdots)\\&y(t)\equiv\delta\nu(t)/\nu\end{aligned}\right\}\quad\cdots\cdots\cdots\cdots\cdots\cdots(2)$$

である。ここで$\delta\nu(t)$は周波数変動量の瞬時値であり，$\bar{y}_k$は遮断時定数τの長さにわたりνに対する$\delta\nu(t)$の比$y(t)$を積分した値である。一般に発振器の周波数安定度は(1)式の平方根$\sigma_y(\tau)$とτ(積分時間と呼ぶことが多い）との関係で表わす。図1には図3のH_2COのスペクトルを用いて安定化された He-Xe レーザの周波数安定度も合せて示す[2]。τ=100 秒で $\sigma_y(\tau)=1\times10^{-14}$に達しており，1981年以来，レーザの世界最高値になっている[8]。

さて，定値制御技術を発展させて周波数高安定，かつ周波数掃引可能なレーザを作ることもできる。その原理を図4に示す。主発振器としてのレーザの周波数は上記の方法で定値制御しておき，従発振器との間のビート周波数ν_bが，あらかじめ用意されたマイクロ

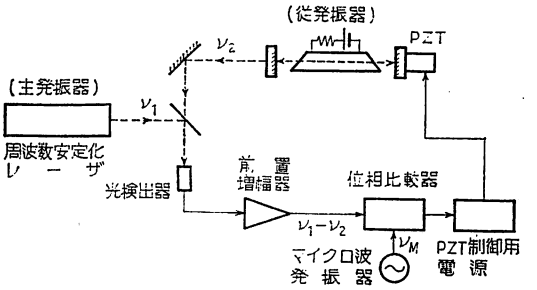

図 4 周波数オフセットロック法の原理図[2]

波発振器からの周波数ν_Mと等しくなるように従発振器の周波数を制御するものである。これは周波数オフセットロックと呼ばれる技術であり[2]，He-Xe レーザの場合，主発振器への従発振器の周波数追随度は10^{-14}に達しており，極めて高いことがわかる。これは表1中(2)の応用における光中継器や，ヘテロダイン検波に応用しうる高精度技術である。更にここでマイクロ波周波数ν_Mを掃引すると従発振器の周波数は主発振器と同程度の周波数安定度を保ちつつ掃引されるので，これは周波数高安定かつ掃引可能な発振器になる。掃引可能範囲はビート測定用の光検出器の周波数帯域に依存するが 1 GHz 程度は確保でき，物理，化学計測などに有力な光源となる。

レーザのスペクトル幅は究極的にはレーザ光とは独立に発光する位相のランダムな光，すなわち自然放出光によって決り，気体レーザの場合，その幅はわずか数 mHz と推定される。従って周波数が超高安定でスペクトル幅もこのように極めて狭い気体レーザは表1の各種の応用に使用可能な優れた能力を備えている。

4. 半導体レーザの周波数安定化

工業上重要なレーザである半導体レーザの周波数定値制御技術も気体レーザの場合と本質的に異なるところはない。

ビデオディスク，光通信などに用いられる波長 0.8 μm AlGaAs レーザ，1.3～1.5 μm InGaAsP レーザの周波数は温度，注入電流によって各々約 −10 GHz/K，−1 GHz/mA 変化するので周波数の制御には気体レーザの場合の PZT の代りに温度，または電流を調節して行なうことができる。但し，温度，電流の変化に対するレーザ周波数の応答帯域は各々約 10 MHz，1 GHz であるので制御帯域を広くとって高安定度を得るには電流調節によるのがよい。

さて，定値制御の際の周波数基準として最も安定なものは，やはり気体原子，分子の吸収または発光スペ

クトルであるが，半導体レーザは素子ごとの発振波長のばらつきが著しく，単一モード発振しにくく，更に温度や電流を広範囲にわたって掃引すると波長が数Åずつ何回か不連続に跳ぶ（モードホッピングと呼ばれる）こと，などの理由からレーザ波長を気体原子，分子のスペクトル波長に合せることが容易でない。従ってこれらのスペクトルは必ずしも常に周波数基準として使えない。更に 0.8～1.5μm の波長での原子，分子の吸収が微弱であるなどの問題もあるが，それでも現在までに H_2O, NH_3, Rb, Cs などの原子，分子が既に使われている[3]。

これよりも簡便な周波数基準として小形のファブリペロー干渉計の共振周波数が用いられることが多い。但しこの場合，干渉計の温度変化による伸縮，機械的振動のため長期にわたる高度安定化に用いるには不適当である。図1に 0.8μm AlGaAs レーザの周波数安定化の実験結果と理論限界とを合せて示した[3]。理論限界については自然放出光の強度によって決り，半導体レーザの場合はレーザ光強度に対する自然放出光の強度に対する自然放出光強度の比が気体レーザの場合に比べ大きく，従って周波数安定度の理論限界も気体レーザに比べ 10^3 以上悪いことが知られている[3]。

上記のように自然放出光の強度が大きいため発振スペクトルの幅も広く数 MHz～数 10 MHz の値をとる[3][9]。この値はコヒーレント光通信への応用には大きすぎるのでレーザ外部に反射鏡や回折格子を置いたり[10]，光ファイバを接続する[11]などして共振器寸法を増大し，スペクトル幅を狭くする工夫がなされており，30 kHz の値が得られた例がある[11]が，レーザ発振状態が不安定になることが問題である。

このほか半導体レーザの周波数安定化の際に問題となる現象として多モード発振時，各モード間の競合により各モード間でスイッチングを生ずること[12]，レーザ光がレーザに約 0.01% 以上再入射すると発振状態が不安定になること[13]などがあげられる。特に後者の場合，この戻り光の影響を避けるためにはファラデー効果を用いた光アイソレータが必要になる。光アイソレータには YIG 結晶，鉛ガラスなどが用いられるが，特に前者は温度特性が悪いため周波数安定化のような高精度の実験のときにはこれを直列に2，3段使わなければ十分でない。

5. 将来技術

5・1 レーザ冷却によるイオン捕獲

原子，分子の飽和吸収スペクトルを周波数基準として気体レーザの周波数を安定化する方法は得られる安定度の値が理論限界[3]に近づきつつある。その限界を決めている要因として，これらの原子，分子が真空中を熱運動でとびまわっているために光のドップラー効果でスペクトルの中心周波数がずれること（第二次ドップラー効果と呼ばれる）があげられる。この欠点を取り除くために真空中にマイクロ波電極を用意し，それに印加されるマイクロ波によってできる電磁ポテンシャルエネルギーの極小の位置に数個のイオン（Mg^+ または Hg^+）を閉込め（イオン捕獲と呼ばれる），同時にこのイオンにレーザ光を照射して熱運動エネルギーを奪い，静止させる（レーザ冷却と呼ばれる）技術が提唱され，その基礎実験が始められている[14]。このような静止イオンを周波数基準として用いると 10^{-15} より高い周波数安定度が得られることが試算されており，有望な技術である。但しこの方法を実現するにもレーザ冷却用のレーザとして 10^{-12}～10^{-14} 程度の高い周波数安定度をもつものが要求されるので第3章で述べた技術は将来，より一層重要性を増すことになろう。

5・2 半導体レーザ励起によるマイクロ波発振器

第4章で述べたように，半導体レーザの周波数安定度は気体レーザのそれに比べると劣るので，コヒーレント光通信への応用などを除いては高安定周波数光源として用いるには不利であり，何らかの補助的光源として用いる方がよい。そのなかで実用上有望な例として，ここでは，表1中にみられるマイクロ波領域での Cs や Rb 原子発振器の励起に半導体レーザを使うことを取りあげる。

周波数 9.2 GHz の Cs 原子発振器の場合，使用可能な Cs 原子を選別するのに，従来は磁界による偏向法が用いられていた。これに代り，波長 0.85μm の AlGaAs レーザの光吸収による方法を用いると使用可能な Cs 原子数が増し，マイクロ波周波数安定度が向上するはずである[15]。これは表1中の(5)に示す秒の一次標準の高精度化への要求から各国で研究が開始されつつある。

更に周波数 6.8 GHz の Rb 原子発振器においても

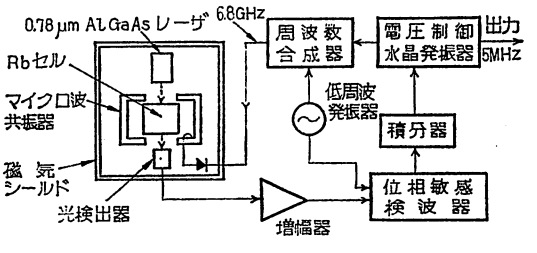

図 5　半導体レーザ励起 Rb 原子発振器の原理図[16]

波長 0.78 μm の AlGaAs レーザの光吸収により Rb 原子の選別ができる。その装置を図5に示す[16]。従来はこの選別に Rb ランプの光が使われていたがランプの寿命に問題があった。半導体レーザを用いれば長寿命化，短期安定度の向上，低価格化が可能となり，表1の多くの分野に使える高安定小形発振器が実現しうる。

以上の二つの例で必須なのは Cs, Rb の吸収スペクトル波長 0.85 μm, 0.78 μm に一致する発振波長をもつレーザ素子を見出すことであり，この点が素子ごとのばらつきの多い半導体レーザ使用の際の問題点である。現在のところビデオディスク用レーザとして波長 0.78 μm 付近のものが入手しやすく，Rb 原子発振器の励起のためには有利である。

6. おわりに

レーザ光の周波数安定化技術の現状と将来について簡単に述べた。この技術の応用分野は広く，周波数安定度も極めて高い値が得られているが，この技術はまだ初歩的な段階にあり，信頼性の向上など解決すべき点は多い。本稿が今後の発展の一助となれば幸いである。

(昭和59年6月26日受付)

文 献

(1) H. Hellwig: "A Review of Precision Oscillators" *NBS Tech. Note* 662, 1 (1975-2)

(2) M. Ohtsu, et al.: "Performances of a Frequency Offset Locked He-Xe Laser System at 3.51 μm" *IEEE J. Quantum Electron.* **QE-17**, 6, 1100 (1981-6)

(3) M. Ohtsu, et al.: "Estimation of the Ultimate Frequency Stability of Semiconductor Lasers" *Japan. J. Appl. Phys.* **22**, 7, 1157 (1984-7)

(4) 北原：「高度情報化社会へ向けての課題」信学誌 **65**, 7, 699 (昭 57-7)

(5) 大越・菊池：「ヘテロダイン型ならびにコヒーレント型光ファイバ通信」同上 **65**, 10, 1099 (昭 57-10)

(6) 川尻：「日米共同 VLBI 実験計画」同上 **65**, 10, 1046 (昭 57-10)

(7) D. Allan: "Statistics of atomic frequency standards" *Proc. IEEE* **54**, 2, 221 (1966-2)

(8) A. Brillet & P. Cerez: "Laser Frequency Stabilization by Saturated Absorption" *J. de Physique* **42**, 12, C8-73 (1981-12)

(9) M. Ohtsu & S. Kotajima: "Derivation of the Spectral Width of a 0.8 μm AlGaAs Laser Considering 1/f Noise" *Japan. J. Appl. Phys.* **23**, 6, 760 (1984-6)

(10) S. Sampei, et al.: "Frequency Stabilization of AlGaAs Semiconductor Lasers with External Grating Feedback" *ibid.* **22**, 4, L 258 (1983-4)

(11) F. Favre, et al.: "Optical Feedback Effects Upon Laser Diode Oscillation Field Spectrum" *IEEE J. Quantum Electron.* **QE-18**, 10, 1712 (1982-10)

(12) 大塚・大津・寺町：「1.5 μm InGaAsP レーザのモードホッピング雑音のパワースペクトル密度解析」信学技報 MW 84-23, p. 59 (昭 59-6)

(13) L. Goldberg, et al.: "Spectral Characteristics of Semiconductor Lasers with Optical Feedback" *IEEE J. Quantum Electron.* **QE-18**, 4, 555 (1982-4)

(14) D. J. Wineland & W. M. Itano: "Laser Cooling of Atoms" *Phys. Rev. A*, **20**, 4, 1521 (1979-10)

(15) J. L. Picque: "Hyperfine Optical Pumping of a Cesium Atomic Beam, and Applications" *Metrologia* **13**, 3, 115 (1977-3)

(16) M. Ohtsu: "Frequency Control of Semiconductor Lasers and its Application to Metrology" *Proceedings of Lasers '83 San Francisco, USA* (1983-12) (in press)

SYMPOSIUM

量子エレクトロニクス
—レーザー過程の物理学—／7

レーザーの雑音

大津元一
おおつ もといち
東京工業大学理工学国際交流センター 助教授

原稿受理：1984年10月17日(編集部)

レーザーの発振強度，周波数の変動，スペクトル幅，さらにモードホッピング雑音，戻り光誘起雑音とカオスにつき概説する．

1. はじめに

レーザーの光は周波数が 100 THz (10^{14} Hz) 前後の超高周波数電磁波であり，その波の振幅，周波数は種々の要因によって変動する．これらの変動がレーザーの雑音である．本稿ではこの雑音のうち自然放出過程により発生するレーザー光強度，周波数の変動，および発振している二モード間の競合によって生ずるレーザー光強度変動，戻り光によって生ずるレーザー光強度変動とカオスとの関係，について概説する．対象としては現存する各種レーザーのうちで最も低雑音化が実現できる気体レーザー，およびレーザー媒質が高密度であり共振器が小さいため多くの非線形光学現象を内在し，工業上にも重要なレーザーである半導体レーザーの二種類をとりあげる．

2. 自然放出による雑音

レーザー媒質からの光の放出過程としてレーザー発振に寄与する誘導放出の他に，位相のランダムな光を発生する自然放出が存在する．本節ではレーザー光に自然放出光が混入することにより発生する雑音の特性を議論し，実験結果との比較をする．そのための一つの有用なモデルとして，レーザー媒質の反転分布と誘起双極子モーメントの大きさを記述する密度行列の運動方程式およびレーザー光の電場の時間変化を記述する Maxwell の方程式を組合せて得られる van der Pol の方程式に，自然放出光の寄与を表わすランダムな擾乱項を付加項として加えた，Langevin の式が用いられる．これは半古典的なモデルであるが実験結果をよく説明する．これによると自然放出光によって生ずるレーザー光の強度雑音の特性を表わすパワースペクトル密度は高域遮断特性を有し，その遮断周波数はレーザー発振強度と共振器損失に比例する．そしてその雑音の大きさはレーザー発振強度の増加とともに減少する．一例として He-Ne レーザーの強度雑音のパワースペクトル密度を図 1 (a) に示す[1]．また，AlGaAs 半導体レーザーのそれを図 2 (a) に示す[2]．両図

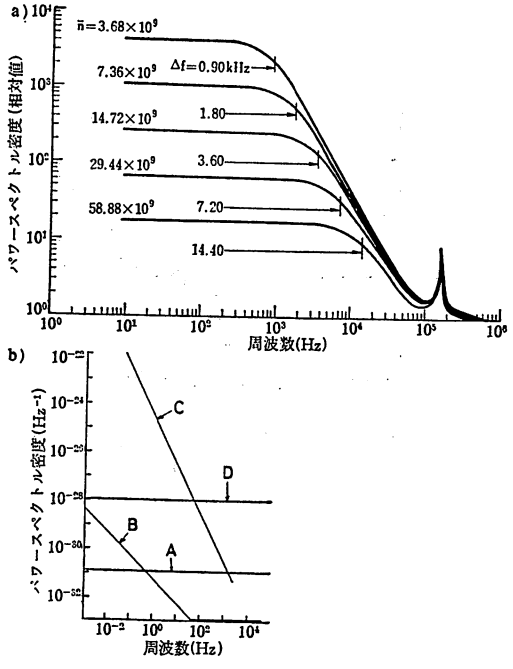

図 1 He-Ne レーザーの強度雑音[1] a) と周波数雑音 b) のパワースペクトル密度．a) $\bar{n}$ はレーザー光子数，Δf は遮断周波数，b) **A** が自然放出光による雑音成分．他は付加的雑音で，各々電源による雑音 **B**，温度ゆらぎによる雑音 **C**，および光検出器のショット雑音の大きさ **D**．

の実験結果とも上記の議論の結果とよく合っている．図 2(a) の半導体レーザーの場合約 1 GHz 付近にピークをもつのは半導体レーザー中の活性キャリヤの緩和振動による共鳴現象によるものであり，自然放出によるものとは異なるが，これを除くと高域遮断特性をもっていることがわかる．

一方，自然放出光によって生ずる周波数雑音は白色雑音であり，その大きさは強度雑音の場合と同様レーザー発振強度の増加とともに減少する．He-Ne レーザー，AlGaAs 半導体レーザーの周波数雑音のパワースペクトル密度の値を図 1 (b)，図 2 (b)[2] に示す．図 2 (b) でもやはり半導体中の活性キャリヤの緩和振動によるピークが現われているのが特徴である．

レーザーの発振スペクトルの形はレーザー光の瞬時電場の周波数分布である．従ってそのスペクトルの幅は周波数雑音によって支配される．周波数雑音が自然放出のみによって支配される白色雑音，すなわち位相雑音がランダムウォークのときスペクトルの形は Lorentz 形になり，スペクトルの半値全幅 $\Delta\nu$ は

$$\Delta\nu=\frac{h\nu}{8\pi P_0}\left(\frac{c}{nL}\right)^2\left(\alpha_l L+\ln\frac{1}{R}\right)\left(\ln\frac{1}{R}\right)n_{sp}(1+\beta^2) \quad (1)$$

で与えられる．ここで h はプランク定数，ν はレーザー周波数，P_0 はレーザー出力強度，c は光速度，n はレーザー媒質の屈折率，L は共振器長，R は共振器鏡の反射率，α_l は共振器内部損失，n_{sp} は自然放出光係数 (1～2 の値をとる) である．気体レーザーのように周波数雑音が究極的には自然放出のみで決まるときは (1) 式中の定数 $\beta=0$ であり，このときの (1) 式を Schawlow-Townes の式と呼ぶ．He-Ne レーザーの場合 (1) 式によると $\Delta\nu$ の値は数 mHz であると推定される．このレーザーの周波数は約 10^{14} Hz であるから，スペクトル幅が非常にせまいことがわかるであろう．これがレーザーがコヒーレントな光源であることの一つの理由である．半導体レーザーの場合周波数雑音は自然放出のみでなく，自然放出光によって誘起される活性キャリヤ密度変動，およびそれによりひきおこされる電流変動と温度変動にも依存する．このとき (1) 式の β の値は -1～-6 と推定されている．β はキャリヤ密度変動に伴なう半導体レーザー媒質の複素屈折率の実部と虚部の比である．半導体レーザーのスペクトル幅を議論するための β の項も含めた (1) 式を Modified Schawlow-Townes の式と呼ぶ．半導体レーザーでは共振器 Q 値が小さいことからスペクトル幅は数 MHz～100 MHz といった大きい値をとる．また，(1) 式はスペクトル幅がレーザー発振強度の値に反比例する特性を表わしているが半導体レーザーでは活性キャリヤ密度の変動[3]，活性キャリヤの易動度のゆらぎに依存する $1/f$ 周波数雑音などがさらに存在すること[4]により，レーザー強度には依存しないスペクトル幅が存在し，これは 1～10 MHz の値をもつことが測定されている[3]．半導体レーザーの場合は以上のように幅の広いスペクトルを有するためこのままではコヒーレント光通信などの応用には困難を有する．そこでスペクトル幅をせまくするために外部共振器を付加したり[5]，石英ファイバをレーザー端面に接続して[6]共振器 Q 値を増加させることが試みられ，30 kHz の値を得た例がある[6]．さらにまた次節で述べ

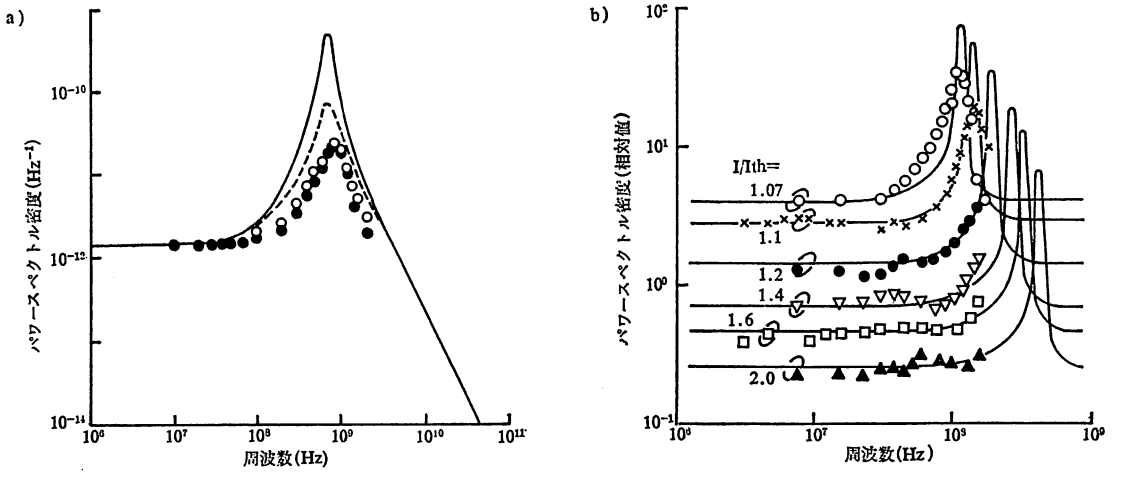

図 2 AlGaAs 半導体レーザーの強度雑音[2] a) と周波数雑音[2] b) のパワースペクトル密度．b) で I/I_{th} はしきい値電流に対する注入電流の比．

るような周波数雑音の抑圧のために 100 MHz 程度の広帯域制御を施す方法により，約 10 MHz のスペクトル幅を 1 MHz 以下にすることが可能である[7]．

3. 周波数雑音の抑圧

レーザーのコヒーレンスを向上させるためには前節で述べたように周波数雑音を抑圧してスペクトル幅を減少させる必要がある．本節ではこの周波数雑音の抑圧について述べる．

図 3(a)(b) に He-Ne レーザーと AlGaAs 半導体レーザーの周波数変動の大きさを示す[8]．ここで $\sigma_y(\tau)$ は周波数変動の分散値，すなわち二次モーメントの大きさを表わす Allan 分散[9] $\sigma_y^2(\tau)$ の平方根の値，τ はそれを測定するための積分時間（観測時間）である．ここで，$\sigma_y(\tau)$ とパワースペクトル密度とは一対一の対応がつけられることが知られている[9]．この図によると制御を施さない，すなわち Free Running の状態の He-Ne レーザー周波数は自然放出による量子雑音と周囲温度変動による温度ドリフトの影響をうけて変動している．この周波数を安定な原子分子のスペクトル線を周波数基準とし，電子回路を用いてレーザー共振器長を微調することにより制御すると，使用した光検出器のショット雑音で決まる値まで変動を抑圧でき，τ=100 秒で $\sigma_y(\tau)=7\times10^{-16}$ という非常

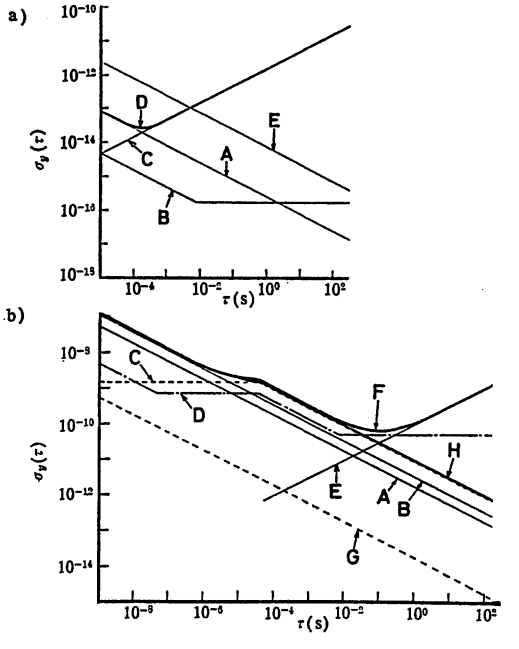

図 3 He-Ne レーザー a) と AlGaAs 半導体レーザー b) の周波数変動の Allan 分散の平方根[8]．a) A: 自然放出光による変動．B: 電源による変動．C: 温度ゆらぎによる変動．D: Free Running 状態での変動．E: 安定化を施した状態での変動．b) A: 自然放出光による変動．B: キャリヤ密度ゆらぎによる変動．C: 電流ゆらぎによる変動．D: 電源による変動．E: 温度ゆらぎによる変動．F: Free Running 状態での変動．G: 光検出器のショット雑音の大きさ．H: A～C の寄与の重ね合わせ．

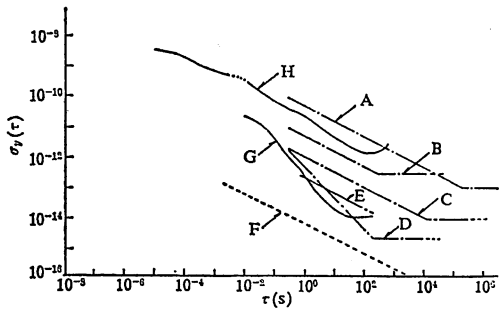

図 4 レーザー，各種マイクロ波発振器の周波数変動の大きさ[10]．A: 市販の Cs 原子発振器．B: Rb 原子発振器．C: 実験室形 Cs 原子発振器．D: 水素メーザ．E: CH_4 安定化 He-Ne レーザ．F: E の理論限界値．G: H_2CO 安定化 He-Xe レーザ．H: 周波数安定化 AlGaAs 半導体レーザ．

に小さな値，すなわち高度の周波数安定度が得られる．AlGaAs 半導体レーザーの場合図 3(b) によると Free Running 状態では自然放出のみでなく前節でも述べたように自然放出によって誘起される活性キャリヤ密度変動，電流変動の影響，さらに温度変動の影響をうけている．これを気体レーザーの場合と同様，安定な周波数基準を用いて抑圧すると τ=100 秒で $\sigma_y(\tau)=8\times10^{-13}$ の値になる．実験でもこの予測値に近い値が得られている．この値は上記の He-Ne レーザーの値にくらべ 1000 倍大きいが，これは半導体レーザーの共振器 Q 値が小さいことが原因である．図 4 には気体レーザー，半導体レーザーの周波数変動の値をマイクロ波領域の各種の高安定発振器の周波数変動量と合わせて示した[10]．これによると気体レーザーの周波数変動量は“秒の一次標準”をになう Cs ビーム標準器，VLBI（超長基線電波干渉計）の時刻保持などに使われる水素メーザーのそれにくらべて遜色がないことがわかる．これらの応用分野において超高安定マイクロ波発振器に代わり近い将来気体レーザーが使われる可能性が大きいと期待される．半導体レーザーはこれらにくらべ周波数変動が大きいが注意深く安定化すればコヒーレント光通信用信号源や Doppler-free の高分解能レーザー分光用光源として使用可能である．

4. レーザーのモードホッピング雑音

レーザーが多数のたてモードで発振しているとき，各たてモードがその発振に必要な利得を共通のレーザー媒質から得るために互いに競合し，各々のたてモードの発振強度は時間的に変動する．これはとくに多数のたてモードで発振しやすい半導体レーザーの場合についてよく見られる．このような強度変動をモードホッピング雑音という．これはとくに半導体レーザーをビデオディスク読み取り用ピックアップなどに用いるとき画質劣化の原因となる現象であり，その機構解明と雑音抑圧のための努力がなされている．本節ではこの現象について記述する．

波長 1.5 μm InGaAsP 半導体レーザーが二つのたてモードで発振しうるときの各々のモードの発振強度の時間的変化の実測値を図 5(a) に示す[11]．この図からわかるように一方のモードが発振を開始すると他方の発振が停止する．これがモードホッピング（モードの跳び）といわれる現象である．各々のモードの発振強度のゆらぎのパワースペクトル密度の測定結果を図 5(b) に示す[11]．この曲線は遮断周波数が約 1.4 MHz である Lorentz 形になっている．このことは出力の時間変化は確率過程として Poisson 過程に従うことを意味している．また，この遮断周波数はモードホッピングの平均くりかえし周期の逆数に対応している．次にこのような Poisson 過程が生ずる原因について考察しよう．

モードホッピングを発生させる主な原因は自然放出光であると考えることは妥当であろう．半導体レーザーの共振器の Q 値は小さいため共振器中での自然放出光の強度はレーザー光強度の約 0.001～0.01% にも達する[12]．自然放出光のうち図 5(a) に示したような二つのレーザー発振のたてモードの各々の波長と等しい波長をもつ成分は時間的に変動している．ある時刻において一方のたてモードの波長と等しい波長をもつ自然放出光の強度が増加すると，それが駆動力となってそのたてモードがレーザー発振を開始する．そのときレーザー発振に必要な利得をレーザー媒質である活性キャリヤから受けとるから他方のたてモードの発振に必要な利得が失なわれその発振が抑圧されると考えられる．このことを確認するために，二つのたてモードのレーザー光の電場に対する van der Pol の式と活性キャリヤ密度の時間変化を表わす式[13]とを連立させてアナログ計算機シミュレーションを行なうこと

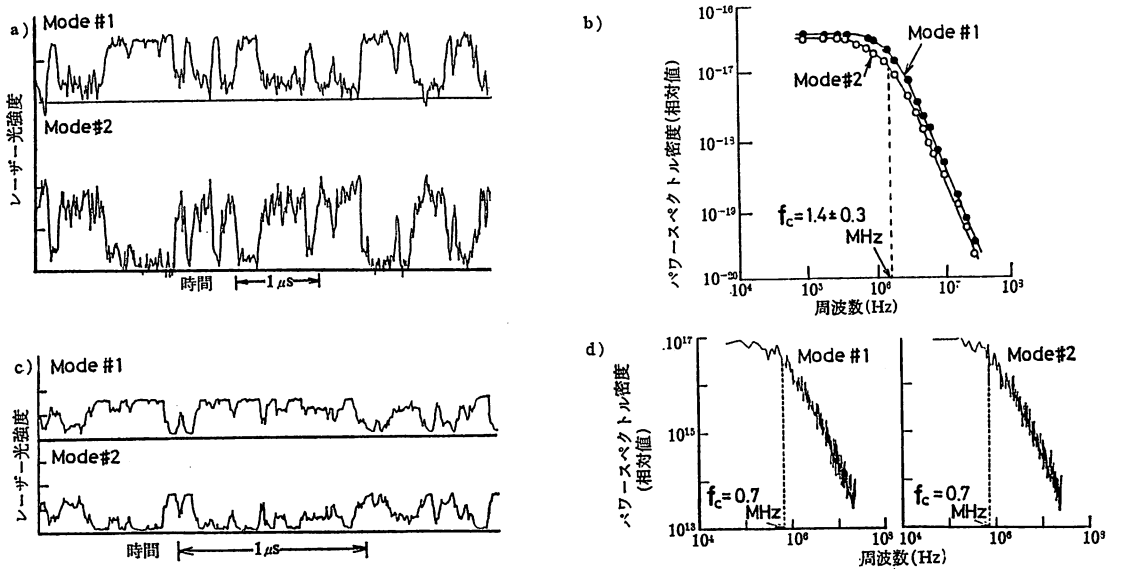

図 5 二モードで発振する InGaAs P 半導体レーザーのモードホッピング特性[11]. a): 各モードの発振強度の時間変化の実測値. b): a) のパワースペクトル密度. c): 各モードの発振強度の時間変化のシミュレーション結果. d): c) のパワースペクトル密度

ができる[11]. ただしこのとき自然放出の効果を与える項として強度分布が Gauss 分布, パワースペクトル密度は白色である二つの互いに無相関な雑音項を二モードの van der Pol の式に各々加える. このようにしてシミュレーションした結果得られた各モードの発振強度の時間変化のようすを図 5(c) に, そのパワースペクトル密度を図 5(d) に示すが, これらは図 5 (a), (b) とよく一致している. とくに図 5(d) の曲線はやはり Lorentz 形になっており, 自然放出光がモードホッピングをひきおこす駆動源になっていることが確認される.

このように自然放出光によって生ずるモードホッピングは半導体レーザーにとどまらず種々のレーザーでも見られることが知られている. たとえば Mandel のグループによりモード間の結合の弱い気体リングレーザー, 結合の強い色素リングレーザーの両方に対しそのホッピングの特性を記述するための四次元 Fokker-Planck の式をもとに確率密度関数, モードホッピングと第一次相転移とのアナロジー, などが議論されている[14]. 上記の半導体レーザーのモードホッピングについてはモード間の結合が強いため色素リングレーザーの場合に類似しており Mandel の手法が利用できる. これにより求められた First Passage Time の値から得られるモードホッピングのくりかえし周波数値, およびその Pump Parameter への依存性などは図 5 の実験値とよく一致していることも確かめられている[15].

5. 戻り光誘起雑音とカオス

レーザーの光が共振器外部の反射体で反射されレーザー共振器内に再入射するとレーザーの発振状態が著しく乱れ, 発振強度, 周波数がはげしく変動することが古くから実験的に知られている. これはしばしば戻り光誘起雑音と呼ばれる. このような不安定を避けるために通常は光アイソレータを使用する. 最近, 半導体レーザーをビデオディスク読み取り用ピックアップや光通信用光源として用いる応用が活発になり, ビデオディスク面や光ファイバ端面での反射による戻り光のために生ずる半導体レーザーの発振状態の著しい乱れがこれらのシステムの性能を制限する要因となることが明らかになった. また, これらのシステムでは全体の価格を低く保ったために高価な光アイソレータは使用しにくく, さらに半導体レーザーの共振器端面反射率は 30% 程度と低いために戻り光が容易に共振器内

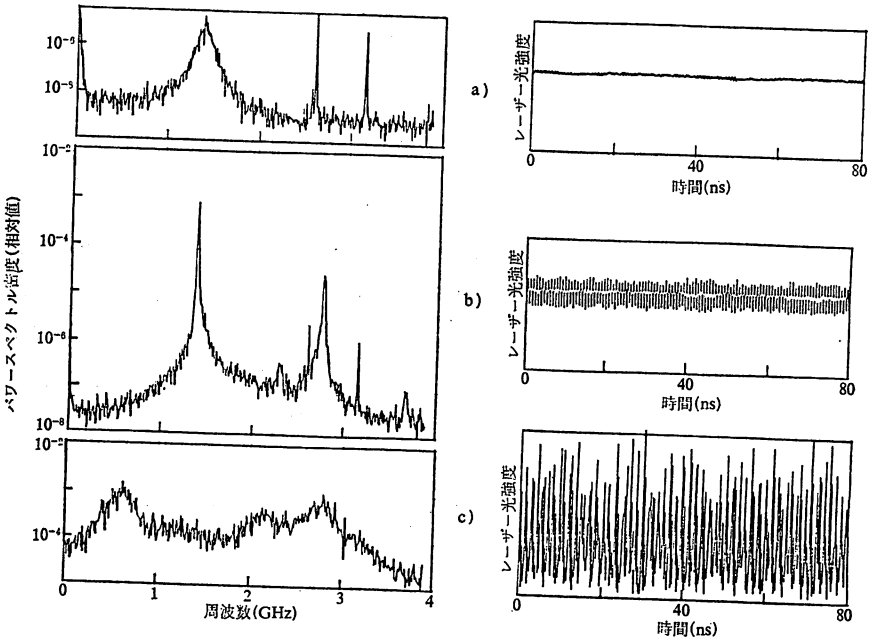

図 6 結合係数 κ とレーザー発振強度の時間変化(右図)，そのパワースペクトル密度(左図)との関係[17]． $T=0.33$ (ns). a): $\kappa=0$, b): $\kappa=1.5\times10^{9}$ (s^{-1}). c): $\kappa=3.8\times10^{10}$ (s^{-1}).

に入射しやすいこと，共振器Q値が小さいためにわずか 0.01% の強度の反射光が入射しても発振状態が不安定になり始めることなどの事情がある．これらを背景に最近，戻り光誘起雑音は主に半導体レーザーに関して研究が盛んになってきている．本節ではこれについて記述する．

半導体レーザーに戻り光が入射すると発振しきい値電流の変化，発振波長のシフト，発振たてモード数の変化，発振スペクトル幅の変化，緩和振動の抑制または助長などの多くの現象が見られることが報告されている[16]．これに対しレーザー共振器と反射体の間の光の往復時間に相当する位相遅れをもつ戻り光の電場を表わす項を加えた van der Pol の式と，活性キャリヤ密度変動の式とを連立させ，これらを線形化して計算が行なわれ，上記の特性がよく説明された[16]．ところで，そこで用いられたものよりさらにくわしくこの van der Pol の式を書くと次のようになる．

$$\frac{d^2}{dt^2}E=\frac{d}{dt}(\alpha E-\beta E^3)-\Omega^2E+\kappa\frac{d}{dt}E(t-T) \quad (2)$$

ここでEはレーザー光の電場であり光周波数で振動している．α, β, Ω はレーザーの発振に必要な線形利得，飽和利得係数，および共振器のたてモード角周波数であり，すべて活性キャリヤ密度に比例する．また (2) 式右辺の最後の項は戻り光を表わし，κ は戻り光電場がレーザー共振器に注入される量を表わす結合係数，Tはレーザー共振器と反射体との間の光の往復時間である．ここで半導体レーザーでは (2) 式中の α, β, Ω が活性キャリヤ密度の値n に比例し，nの値自身は $|E(t)|^2$ に比例するのでnの時間変化についての次式をも連立して (1) 式より $|E(t)|$ の値を求める必要がある．

$$\frac{d}{dt}n=-R(n-n_G)|E|^2+\frac{n_{th}}{\tau_s}\left(\frac{I}{I_{th}}-\frac{n}{n_{th}}\right) \quad (3)$$

ここでRは誘導放出に伴なうnの減少率を表わす定数，n_G は電流非注入時のnの値，n_{th} は発振に必要なnのしきい値，Iおよび I_{th} は注入電流とそのしきい値，τ_s は活性キャリヤが半導体レーザー中に注入されてから光子を放出するまでの時間である．(3) 式の存在のもとでの (2) 式は発振利得 α, β のみでなく光の位相を決める Ω もnに依存する非線形な差分微分方程式であり，時刻tにおける光の電場 $E(t)$ には時間 T だけ遅れたフィードバックがかかっているために $|E(t)|$ は時間的に不規則なふるまいをするようになる[17]．図6には結合係数 κ の値の増加とともにレー

ザー発振強度 $|E(t)|^2$ の変動のパワースペクトル密度が変化するようすを (2), (3) 式から求めて示した. この図によると κ の増加とともに活性キャリヤの緩和振動が助長されること, 緩和振動周波数 f_r 以上の高周波数領域での雑音レベルが増加してカオス (Chaos) 状態になること, 緩和振動周波数の高調波成分が発生すること, さらに緩和振動周波数以下の周波数領域での雑音レベルも増加することなどがわかる. これらの雑音増加の特性が上記の戻り光によるレーザー発振状態の変化についての多くの実験結果に対応していると考えられる.

さて, ここで現われたカオスはレーザーのみに限らず流体系をはじめ多くの非線形系で見られる現象で, 決定論的な法則に従う系が外部から確率論的な摂動を受けなくても不規則な変動を示す状態ということができる. 上の (2) 式のように戻り光の位相おくれ時間 T が τ_s などの系の特性時間より長いときに, 外部から加わる非線形系へのフィードバックの時間おくれがこのような不規則変動を与える原因となっている.

レーザー光学系でカオスが存在することの理論的予測はリング共振器中に置かれた非線形光学媒質の示す光双安定性に対するものが最初であった[18]. その後, 不均一拡がりの利得スペクトルをもつ三つのたてモードで発振する He-Ne レーザー[19], 単一たてモードの He-Xe レーザー[20]などでも観測された. さらに上記の半導体レーザーに関連したカオス現象として戻り光のある場合の共鳴型増幅器[21], 注入同期型増幅器[22]にも存在することが指摘されており, 現在光学系におけるカオスの研究は盛んである.

6. おわりに

気体レーザーと半導体レーザー, とくに本稿の後半では後者を主な対象としてレーザーの発振強度, 周波数の変動の原因と特性について記述した. このうちスペクトルの幅に関してはインコヒーレントな自然放出光に対するコヒーレント光の応答, モードホッピング雑音については自然放出光に対する二モードの非線形系の応答, と考えることができ, 非線形系の確率過程として興味深いトピックスである. また, 戻り光誘起雑音とカオスについては非線形系のダイナミックスとしてレーザーに留まらず広範な非線形物理現象とも深くかかわり, 現在注目を集めている問題である.

参考文献

[1] C. Freed and H. A. Haus: Appl. Phys. Lett., 6 (1965) 85
[2] Y. Yamamoto, S. Saito and T. Mukai: IEEE J. Quantum Electron., QE-19 (1983) 47
[3] D. Welford and A. Mooradian: Appl. Phys. Lett., 40 (1982) 560
[4] M. Ohtsu and S. Kotajima: Jpn. J. Appl. Phys., 23 (1984) 760
[5] S. Sampei, H. Tsuchida, M. Ohtsu and T. Tako: Jpn. J. Appl. Phys., 22 (1983) L258
[6] F. Fabre and D. Le Guen: Electron. Lett., 19 (1983) 663
[7] 古田島, 大津: 信学技報, OQE 84-130, 1985 年 3 月
[8] M. Ohtsu, H. Fukada, T. Tako and H. Tsuchida: Jpn. J. Appl. Phys., 22 (1983) 1157
[9] D. Allan: Proc. IEEE, 54 (1966) 221
[10] 大津元一: 電気学会雑誌, 104 (1984) 801
[11] M. Ohtsu, Y. Otsuka and Y. Teramachi: Appl. Phys. Lett., 46 (1985) 108
[12] Y. Suematsu, S. Akiba and T. Hong: IEEE J. Quantum Electron., QE-13 (1977) 596
[13] M. Yamada and Y. Suematsu: J. Appl. Phys., 52 (1981) 2653
[14] L. Mandel: Optics Communications, 42 (1982) 356
[15] 大塚, 大津, 寺町, 大崎: 信学技報, OQE 84-132, 1985 年 3 月
[16] R. Lang and K. Kobayashi: IEEE J. Quantum Electron., QE-16 (1980) 347
[17] Y. Teramachi and M. Ohtsu: Proc. of "US-Japan Seminar on Coherence, Incoherence, and Chaos in Quantum Electronics" Nara, August 1984, p. 63
[18] K. Ikeda: Optics Communications, 30 (1979) 257
[19] C. O. Weiss and H. King: Optics Communications, 44 (1982) 59
[20] J. Bentley and N. B. Abraham: Optics Communications, 41 (1982) 52
[21] K. Otsuka and H. Iwasawa: Phys. Rev. A, 28 (1983) 3153
[22] K. Otsuka and H. Kawaguchi: Phys. Rev. A., 29 (1984) 2953